80 years of building new worlds through knowledge

Programme and Book of Abstracts of the

CENTERA THz Days:

French-Polish Science & Technology Meeting

(October 15th-16th, 2019)

&

Annual Workshop of International Research Project (IRP) – TERAMIR

(October 17th-19th, 2019)

Venue: Centre for Advanced Materials and Technologies CEZAMAT

http://pirbinstytut.pl/index.php/centera-thz-days

Institute of High Pressure Physics
Polish Academy of Sciences

unipress

INSTYTUT

Warsaw, Poland

European Funds Smart Growth
Republic of Poland
FNP Foundation for Polish Science
European Union European Regional Development Fund

Our partners

National Center for Scientific Research, France
www.cnrs.fr/

Our sponsors

Polish Academy of Sciences
https://www.pan.pl/

Institut français de Pologne
https://www.institutfrancais.pl/

Ambassade de France à Varsovie
https://pl.ambafrance.org/2019-Annee-
-scientifique-franco-polonaise-8981

Industrial sponsors

TOPTICA Photonics AG
Graefelfing (Munich), Germany
https://www.toptica.com/

CENTERA

The „Center for Terahertz Research and Applications (CENTERA)" project is carried out within the „International Research Agendas" programme of the Foundation for Polish Science co-financed by the European Union under the European Regional Development Fund.
CENTERA is an international research center created in September 2018. Administratively CENTERA is attached to the Institute of High Pressure Physics of the Polish Academy of Sciences (IHPP PAS).
The main goal of CENTERA is to create in Warsaw a Central European Research Center stimulating research efforts in the domain of terahertz science and technology.
During October 15th-19th, 2019 CENTERA will organize the CENTERA THz Days, an international event of EU researchers active in the THz domain with the main purpose of building a basis for future strong scientific collaborations in the field.
CENTERA THz Days will consist of two main events: French-Polish Science & Technology Meeting and LIA TERAMIR Meeting.

French-Polish Science & Technology Meeting

The FRENCH-POLISH SCIENCE & TECHNOLOGY MEETING on 15–16 OCTOBER 2019 is a CNRS and Polish Academy of Sciences joint initiative having as a goal to reinforce existing French-Polish collaborations and to help create new links between teams active in different areas of terahertz science and technology.

LIA TERAMIR Meeting

The INTERNATIONAL RESEARCH PROJECT (IRP) – TERAMIR WORKSHOP (17-19 OCTOBER 2019) IRP is a natural continuation of the annual meetings of GDR and LIA programs of collaboration between France, Poland and Russia initiated by CNRS in 2010. Currently IRP–TERAMIR is directed not only to THz properties of solids but also to the dynamically developing research of different new states of the matter (Dirac matter, different topological states of 2D and 3D systems, Weyl semimetals, etc).
As usually, the TERAMIR meeting is devoted not only to the presentation of recent results of all participating laboratories (3 French, 2 Polish and 4 Russian) but invites also experts from the international scientific community. This October, we expect around 50 participants presenting their recent scientific results.

Symposium Chairs

Prof. Wojciech Knap (CENTERA, IHPP PAS, Poland & L2C, CNRS & Montpellier Univ., France)
Dr. Frederic Teppe (L2C, CNRS & Montpellier Univ., France)
Prof. Thomas Skotnicki (CENTERA, IHPP PAS, Poland)

Steering Committee

CENTERA THz Days will be conducted under supervision of CENTERA International Scientific Committee:
Prof. Tomasz Dietl - MagTop – IP PAS, Warsaw
Prof. Guillaume Ducournau - IEMN, CRNS, France
Prof. Sylvain Bollaert - IEMN, CRNS, France
Prof. Viktor Krozer - Goethe Universität Frankfurt am Main, Germany
Prof. Jean-Francois Lampin - IEMN, CNRS, France
Prof. Jerzy Łusakowski - University of Warsaw, Poland
Prof. Jacek Marczewski - ITE, Poland
Prof. Sylwester Porowski - IHPP PAS, Poland
Prof. Hartmut Roskos - Goethe Universität Frankfurt am Main, Germany
Prof. Gintaras Valušis - Center for Physical Sciences and Technology, Lithuania

Organizing Committee

Katarzyna Kołys
(CENTERA, Institute of High Pressure Physics, Polish Academy of Sciences)

Secretary

Elżbieta Krajewska
(Polski Instytut Rozwoju Biznesu)

Topics

THz physics:

- Carrier transport & quantum effects in devices,
- Nonequilibrium carrier dynamics,
- 2D materials & their heterostructures, Terahertz properties of Dirac matter.

THz devices & electronic/optical components:

- Sub-THz/THz transistors, mixers, etc.,
- Metamaterials, photonic crystals,
- Surface-plasmon-polaritons,
- Electronic/photonic/plasmonic devices,
- Nonlinear optics based devices,
- Superconductors, bolometers, etc.

THz applications:

- Wireless communications,
- Imaging Spectroscopy,
- Astronomy

Conference venue

Centre for Advanced Materials and Technologies CEZAMAT
19 Poleczki Street, Warsaw, Poland
Conference Room 1.50 / Aula

http://www.cezamat.eu/pl/
http://pirbinstytut.pl/index.php/centera-thz-days

Transportation from Airport Chopin – Warsaw Okęcie to CEZAMAT:
buses No 148 & 331 (from bus stop „Przyloty 02")
to bus stop „Poloneza 01" in the vicinity of CEZAMAT

more info about public transport in Warsaw: https://www.ztm.waw.pl/index.php?l=2

Programme

CENTERA THz DAYS

French-Polish THz Science and Technology Meeting

October 15th- 16th, 2019

Venue: Centre for Advanced Materials and Technologies CEZAMAT,
19 Poleczki Street
Conference Room 1.50/Aula

October 15th - Tuesday

Conference room 1.50

October 15th - Tuesday			
	11:00	**Registration**	
	13:20-13:40	**Welcome Coffee** (canteen)	
	13:40-15:10	**Session A** (conference room 1.50)	Tue-A
	13:40-14:10	Idelfonso Tafur Monroy (Eindhoven University of Technology) *Towards Terahertz Systems on chip*	Tue-A-1
	14:10-14:25	Cezary Kołaciński (Institute of Electron Technology, Warsaw) *THz technology at ITE: detectors and readouts*	Tue-A-2
	14:25-14:40	Marcin Wojciechowski (GUM, Warsaw) *The Use of Spectrum Analyzer to Measure Beat Waves of Terahertz Sources*	Tue-A-3
	14:40-14:55	Przemyslaw Zagrajek (Military University of Technology, Warsaw) *Nonlinear THz response of silicon based devices*	Tue-A-4
	14:55-15:10	Sylvain Bollaert (IEMN, Lille, CENTERA ISC MEMBER) *75 nm gate length and asymmetric gate recess InGaAs/InAlAs HEMT with THz f_{max}*	Tue-A-5
	15:10-15:30	**Coffee break (canteen)**	
	15:30-16:45	**Session B** (conference room 1.50)	Tue-B
	15:30-15:45	Emilie Hérault (LAHC, Chambéry) *Development of new tools to characterize materials and devices in the terahertz domain*	Tue-B-1
	15:45-16:00	Sergey Rumyantsev (CENTERA, IHPP PAS) *Negative Photoconductivity and low frequency noise in HgTe Quantum Wells*	Tue-B-2
	16:00-16:15	Dmytro But (CENTERA, IHPP PAS) *Landau levels terahertz emission from HgCdTe bulk films*	Tue-B-3
	16:15-16:30	Grzegorz Cywinski (TEAM, IHPP PAS) *THz Detectors Based on GaN/AlGaN Lateral Schottky Barrier Diodes*	Tue-B-4
	16:30-16:45	Pavlo Sai (CENTERA, IHPP PAS) *Noise Characterization of GaN/AlGaN High Electron Mobility Transistors*	Tue-B-5
	16:45	**Closing of Day 1**	
	18:00	**Dinner,** Restaurant Gościniec, Piwna St 14	

October 16th - Wednesday

Aula

October 16th			
	8:00	**Registration**	
	9:00-9:30	**Welcome session** (Aula)	
		Welcome from the Chairmen - Prof. Wojciech Knap (CENTERA LABORATORIES IHPP-PAS & L2C Laboratory CNRS and University of Montpellier) / Dr. Frédéric Teppe (L2C, CNRS & Montpellier University) Welcome from PAS - Dr Anna Plater-Zyberk (Polish Academy of Sciences) Welcome from CNRS - Prof. Niels Keller (CNRS-INP) Welcome from the French Embassy - Mr. Christophe Paoli (attaché de coopération scientifique et universitaire) Welcome from Foundation for Polish Science - Prof. Maciej Żylicz Welcome from the Director of IHPP PAS - Prof. Izabella Grzegory Welcome from the Rector of Warsaw University of Technology - Prof. Jan Szmit Welcome from Cezamat - Prof. Thomas Skotnicki	
	9:30-10:50	**Session C** (Aula)	
	9:30-9:45	Wojciech Knap (CENTERA LABORATORIES IHPP-PAS & L2C Laboratory CNRS and University of Montpellier) *Presentation of IRAP CENTERA*	Wed-C-1
	9:45-10:00	Tomasz Wojtowicz (MagTop, Warsaw) *Developing, Understanding and Functionalizing Topological Materials at MagTop*	Wed-C-2

October 16th -Wednesday	10:00-10:20	Robert Nietubyć / Karolina Szamota-Leandersson (National Centre for Nuclear Research, Świerk) *PolFEL – a tunable source of THz radiation*	Wed-C-3
	10:20-10:35	Juliette Mangeney (LPENS) *THz excited state level spacing in encapsulated graphene quantum dots*	Wed-C-4
	10:35-10:50	Sukhdeep Dhillon (LPENS, Paris) *Quantum Cascade Lasers: From Modelocking to THz non-linear optics*	Wed-C-5
	10:50-11:05	**Coffee break (canteen)**	
	11:05-12:20	**Session D** (Aula)	
	11:05-11:20	Frédéric Teppe (L2C, Montpellier) *Fine study of zero-mode Landau levels in HgTe quantum wells*	Wed-D-1
	11:20-11:35	Jérémie Torres (IES, Montpellier) *Toward a new scheme of communications between proteins*	Wed-D-2
	11:35-11:50	Yevhen Yashchyshyn (Warsaw University of Technology, CENTERA IHPP PAS) *Reconfigurable Antennas based on S-PIN diodes*	Wed-D-3
	11:50-12:05	Agnieszka Siemion (Warsaw University of Technology, Faculty of Physics, Warsaw) *Terahertz Diffractive Structures in Application for Skin Cancer Diagnosis*	Wed-D-4
	12:05-12:20	Norbert Palka (Military University of Technology, Warsaw) *Security applications of terahertz radiation*	Wed-D-5
	12:20-13:15	**Lunch** (canteen)	
	13:15-14:00	**Session E** (Aula)	
	13:15-13:30	Yanko Todorov (LPENS) *Ultrastrong light-matter coupling in deeply subwavelength THz LC resonators*	Wed-E-1
	13:30-13:45	Jerzy Lusakowski (University of Warsaw) *THz laboratory at the University of Warsaw*	Wed-E-2
	13:45-14:00	Gaël Mouret (LPCA, Dunkerque) *Broadband terahertz heterodyne spectrometer exploiting synchrotron radiation at sub--megahertz resolution*	Wed-E-3
	14:00-14:15	**Coffee break** (canteen)	
	14:15-15:45	**Session F** (Aula)	
	14:15-14:30	Jean-François Lampin (IEMN, Lille) *A new approach for THz molecular lasers*	Wed-F-1
	14:30-14:45	Stefano Barbieri (IEMN, Lille) *Observation of self-mode-locked pulses in terahertz quantum cascade lasers through intra-cavity self-detection*	Wed-F-2
	14:45-15:00	Alvydas Lisauskas (CENTERA, IHPP PAS) *Active THz devices*	Wed-F-3
	15:00-15:15	Jérôme Lesueur (ESPCI, Paris) *Superconducting THz devices*	Wed-F-4
	15:15-15:30	Pawel Kopyt (Warsaw University of Technology) *Measurements of low-loss dielectrics with a Fabry-Pérot Open Resonator up to the W-band*	Wed-F-5
	15:30-15:45	El Mustapha Feddi (Ecole Normale Supérieure de l'Enseignement Technique Université Mohamed V Rabat) *Optical and magneto optical responses assigned to probable processes of formation of exciton bound to an ionized donor in quantum dot and their involvements in THz*	Wed-F-6
	15:45-18:30	**Coffee break** (canteen) **and CEZAMAT Lab Tour**	

October 16th -Wednesday	**18:30-19:30**	**Session G** (Aula)	
	18:30-18:45	Jerome Degert (LOMA, Bordeaux) *Intense pulsed THz source: 2D spectroscopy, wavefront measurement and structuration*	Wed-G-1
	18:45-19:00	Patrick Mounaix (IMS, Bordeaux) *Deep data processing for multilayered material characterized by terahertz spectroscopy*	Wed-G-2
	19:00-19:15	Alexandre Locquet (Georgia Tech, Metz) *Terahertz pulsed imaging for nondestructive evaluation*	Wed-G-3
	19:15-19:30	Yannick De Wilde (ESPCI, Paris) *Sub-wavelength studies of plasmonic devices and thermal sources*	Wed-G-4
	19:30	**Closing Session** (Aula)	
	20:30-22:30	**Gala Dinner** (Restaurant Dom Polski, Francuska St 11) Host of the the social event: Institut français de Pologne à Varsovie CENTERA THz Days conference has been granted the title of official event of French-Polish Year of Science. The French Institute in Poland has honor to host the Gala Dinner on 16th October 2019.	

80 years of building new worlds through knowledge

Programme

CENTERA THz DAYS

IRP TERAMIR Meeting

October 17th- 19th, 2019

Venue: Centre for Advanced Materials and Technologies CEZAMAT,
19 Poleczki Street
Conference room 1.50

October 17th - Thursday Conference room 1.50			
	11:00	**Registration**	
October 17th - Thursday	**13:00-13:40**	**Welcome Coffee** (canteen)	
	13:40-14:00	Frédéric Teppe (L2C, CNRS & Montpellier University)/Wojciech Knap (CENTERA, IHPP PAS & L2C, CNRS & Montpellier University) *Opening of the International Research Project (IRP) – TERAMIR WORKSHOP*	
	14:00-16:00	**Session A** (conference room 1.50)	
	14:00-14:40	Sergey Ganichev (THz Center Regensburg/CENTERA, IHPP PAS) *Tutorial: Overview on Spin photogalvanics induced by terahertz radiation*	Thu-A-1
	14:40-15:00	Guillaume Ducournau (IEMN-Lille/CENTERA, ISC MEMBER) *Terahertz communications using photonics based emitters for 300 GHz band*	Thu-A-2
	15:00-15:20	Zhaofeng Li (Chinese Academy of Sciences CAN) *Investigations of the Receiving Antennas Designed for FET THz Detectors*	Thu-A-3
	15:20-15:40	Valentin Kachorovski (Ioffe, Saint Petersburg/ CENTERA, IHPP PAS) *Current-driven optical response of plasmonic crystal: From dissipation to amplification*	Thu-A-4
	15:40-16:00	Katja Dutzi/Andreas Isemann (Toptica)	
	16:00-16:20	**Coffee break** (canteen)	
	16:20-19:00	**Session B** (conference room 1.50)	
	16:20-17:00	Hartmut Roskos (Goethe Universität Frankfurt am Main/CENTERA ISC MEMBER) *Tutorial: Light-matter interaction in a 1D THz photonic crystal cavity: Ultrastrong co-upling and nonlinear optics*	Thu-B-1
	17:00-17:20	Patrick Mounaix (IMS, Bordeaux) *Deep data processing for multilayered material characterized by terahertz spectroscopy*	Thu-B-2
	17:20-17:40	Olivier Pirali (Soleil, Gif-sur-Yvette) *High Resolution Spectroscopy in the THz using synchrotron radiation source*	Thu-B-3
	17:40-18:00	Alvydas Lisauskas (CENTERA, IHPP PAS) *High-performance THz detectors in CMOS technologies*	Thu-B-4
	18:00-18:20	Gintaras Valusis (CENTERA ISC Member) *Advantages of extended focus in THz imaging*	Thu-B-5
	18:20-18:40	Mikhail Khodzitsky (ITMO University, Saint Petersburg) *THz time-domain spectroscopy of bismuth films*	Thu-B-6
	18:40-19:00	Jean-Francois Lampin (IEMN, CNRS) *A new approach for THz molecular lasers*	Thu-B-7
	19:30	**Dinner** (Restaurant Gaumarjos, Al. KEN 47)	

October 18th - Friday

October 18th - Friday	**8:00**	**Registration**	
	9:00-10:40	**Session C** (conference room 1.50)	
	9:00-9:40	Mikhail Belkin (Walter Schottky Institute, Germany) *Plenary: Room-temperature terahertz quantum cascade laser sources based on intra-cavity difference frequency generation*	Fri-C-1
	9:40-10:00	Jerome Degert (LOMA, Bordeaux) *Conical vs Gaussian Terahertz Emission from Two-Color Laser-Induced Air Plasma Filaments*	Fri-C-2
	10:00-10:40	Viktor Krozer (Goethe Universität Frankfurt am Main, Germany/CENTERA ISC MEMBER) *Tutorial: Higher frequency electronics and sub-terahertz diabetes detection*	Fri-C-3
	10:40-11:00	**Coffee break** (canteen)	
	11:00-12:20	**Session D** (conference room 1.50)	
	11.00-11.20	Abdel El-Fatimy (Centrale Casablanca, Morocco. CEITEC, Brno University, Brno, Czech Republic) *Defect-induced cooling effect on graphene hot-electron bolometers*	Fri-D-1
	11:20-11:40	Georgy Fedorov (Moscow Institute of Physics and Technology (State University), Russia) *Detection of terahertz radiation with graphene-based field effect transistors*	Fri-D-2
	11:40-12:00	Andrey Generalov (Aalto University) *Graphene in FET THz detectors*	Fri-D-3
	12.00-12.20	Maciej Sakowicz (CENTERA, IHPP PAS) *AlGaN/GaN Heterostructures for Plasma Wave Detection and Emission in THz Regime*	Fri-D-4
	12:20:13:20	**Lunch** (canteen)	
	13:20-15:40	**Session E** (conference room 1.50)	
	13:20-14:00	Tomasz Dietl (MagTop-IP PAS) *Tutorial: Point-contact spectroscopy of topological materials*	Fri-E-1
	14:00-14.20	Benoit Jouault (Laboratoire Charles Coulomb, Montpellier University) *Quantum Hall states in HgTe topological quantum wells probed by transconductance fluctuations*	Fri-E-2
	14:20-14:40	Yvan Yahniuk (CENTERA, IHPP PAS) *Topological phase transition in HgTe quantum wells induced by hydrostatic pressure*	Fri-E-3
	14:40-15:00	Milan Orlita (LNCMI-Grenoble) *Auger scattering and cyclotron emission of massless electrons*	Fri-E-4
	15:00-15:20	Sergey Krishtopenko (L2C-Montpellier) *Fingerprints of topological Anderson insulator in HgTe quantum well*	Fri-E-5
	15:20-15:40	Michael Feiginov (TU, Vienna) *THz resonant-tunneling diodes*	Fri-E-6
	17:00-22:00	**Social event and dinner** Chopin Music Concert - Nowy Świat St 63 at 5 pm, dinner at 6.30 pm - Restaurant Kompania Piwna, Podwale St 25	

October 19th - Saturday			
October 19th - Saturday	9:00-10:40	**Session F** (conference room 1.50)	
	9:00-9:20	Vladimir Gavrilenko (IPM Nizhnij Novgorod) *Long wavelength stimulated emission from HgCdTe quantum wells: overcoming the Auger recombination*	Sat-F-1
	9:20-9:40	Nikolay Mikhailov (Novosybirsk-RAS) *The growth and characterization HgTe/CdHgTe quantum wells*	Sat-F-2
	9:40-10:00	Dmitry Khokhlov (M.V. Lomonosov Moscow state University, Russia) - *Nonlocal Terahertz Photoconductivity in the Topological Phase of $Hg_{1-x}Cd_xTe$ Semiconductors*	Sat-F-3
	10:00-10:20	Dmitry Yavorskiy (TEAM, IHPP PAS, Warsaw) *THz magnetospectroscopy of a HgCdTe epitaxial layer under hydrostatic pressure*	Sat-F-4
	10:20-10:40	Frédéric Teppe (L2C, CNRS & Montpellier University) *Fine study of zero-mode Landau levels in HgTe quantum wells*	Sat-F-5
	10:40-10:50	**Closing ceremony**	
	10:50-12:00	**Farewell coffee** (canteen)	

Abstracts

Title: **Emerging Applications for Terahertz Photonic Systems on Chip**
by **Idelfonso Tafur Monroy**, Professor Terahertz Systems, Eindhoven University of Technology

The goal of the talk is to introduce the merging new area of products and solutions where photonic integration, and THz photonics on chip technologies are very well suited such as in agro-food technologies, infrastructural monitoring, THz detection of fake medicines, safe medical scanning and beyond 5G wireless communications.

Thereafter, the talk explains why and how photonic -electronic co-integration is essential for bringing to the mass market these new technologies. Finally, the talk makes a bridge between the research trends, the product development, and the potential and opportunities for the Dutch photonic integration eco-system.

Title:
THz technology at ITE: detectors and readouts

Speaker:
Cezary Kołaciński

Abstract:
This presentation is a brief review of achieved results and current activity in the field of THz technology at ITE (Institute of Electron Technology, Poland). The speaker will focus on two main areas: THz detectors development and integrated readouts design.

The first topic concerns fabrication of transistor-based detectors and their integration with silicon lenses. The THz detection mechanism occurs for the frequency range that is appreciably higher than the device cut-off frequency — and this fact enables the manufacturing of detecting transistors in not expensive, legacy silicon processes. Additional integration with dedicated silicon lens significantly increases the sensitivity of this type of devices.

The second part of presentation deals with the low noise readout design, targeted for low-frequency applications (spectroscopy, imaging). In the vast majority of laboratory studies, the lock-in amplifier is used as an essential component of test set-up and is required for proper readout operation. At ITE we developed the unique integrated readout circuit, intended to operate with transistor-based THz detectors. It has been experimentally proven that this solution can successfully replace the lock-in equipment, offering comparable parameters but without the necessity of modulating the THz wave and using complex and expensive measurement equipment.

The Use of the Spectrum Analyzer to Measure Beat Waves of Terahertz Sources

M. Wojciechowski
Central Office of Measures (GUM), Electricity and Magnetism Laboratory, Warsaw, Poland

E-mail: marcin.wojciechowski@gum.gov.pl

Abstract — The article describes an attempt to use spectrum analyzer to measure beating of electromagnetic waves obtained from sources whose frequencies are outside the analyzer's operating range, with a view to using them for measurements in the T-band. The test used an anechoic chamber, a set of broadband antennas, precision electromagnetic wave generators and a radio frequency (RF) receiver with spectrum analysis function. A system for measuring terahertz beats and comparing the power of their sources as well as the use of a resonance antenna and Ultra-Low-Noise Amplifier (Ultra-LNA) were proposed.

Keywords — terahertz beat, CW THz setups, Ultra-LNA, resonate antenna, power measurement

I. Introduction

In our country more and more scientific centers have equipment operating in the terahertz frequency band. Currently there is no measuring consistency both in terms of frequency and power measurements in this band. This applies to our country as well as to the whole of Europe and the whole world. GUM strives to ensure measurement traceability for all measurements in Poland, hence the Laboratory of Electricity and Magnetism attempts to recognize the problem and presents a number of proposals for detailed and system solutions.

Also, the European Association of National Metrology Institutes (EURAMET), of which GUM is also a member, in its guidelines in the field of electricity and magnetism mainly indicates quantum standards, but also measurements in the T-band and only projects in this these areas are currently financed. GUM joined The European Metrology Programme for Innovation and Research (EMPIR) s02 TEMMT "Traceability for electrical measurements at millimetre-wave and terahertz frequencies for communications and electronics technologies" project provided by EURAMET. In preparation for the project, two terahertz frequency standards were designed and a measurement setup for frequency and power measurement using terahertz beats was proposed.

The first design involves a terahertz generator with a frequency of 1.0125 THz and output power of 5 µW (ultimately 1 mW), in which the reference frequency is obtained by multiplication of frequency of the national atomic caesium time and frequency standard. Cooperating with a stable quartz standard with 10^{-10} relative accuracy, whose signal of a voltage approx. 1 V_{RSM} and a frequency of 10 MHz, is fed to the Laboratory of Microwave, Electromagnetic Field and Electromagnetic Compatibility GUM, where works related to the T band are carried out. The reference frequency is multiplied in three blocks. In the first active megahertz multiplier up to 625 MHz, then in the active microwave multiplier x20 to 12.5 GHz and then in terahertz x81 passive multiplier terminated with a diagonal horn antenna [1].

In the second design, in order to generate a terahertz wave, it was proposed to beat laser beams and generate a terahertz wave by a photomixer. Using the measuring capabilities of GUM laboratories, it is possible to make a generator that according to the design would have a frequency of 1.0119 THz with a theoretically maximum relative accuracy of 3 * 10^{-5} [2].

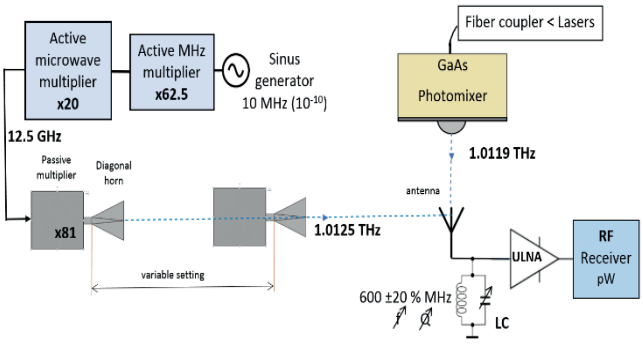

Fig. 1. Setup for measuring the power and frequency of terahertz beat [3].

Fig. 1 is a schematic diagram for comparing the power of two terahertz generators made according to the aforementioned designs [3]. A generator with greater stability and more power was considered a standard and placed on a bench with the possibility of changing the position in relation to the axis of the tested generator. Description of measurement and calibration of the measuring setup with the antenna is presented below.

II. Description of the Experiment

For the experiment, an anechoic chamber was used, in which three broadband antennas were set up. Two of the antennas worked as transmitters and their axes were at right angles. The third antenna worked as a receiving antenna and was set at the intersection of the transmitting antennas axes at an angle of 45 degrees to these axes. Outside the chamber, there are two precise generators, whose outputs are attached to transmitting antennas and a precise radio receiver with the possibility of spectrum analysis. The photo of the measuring stand is shown in Fig. 2.

The first test was conducted to check whether it is possible to receive the beat signal in case of two electromagnetic waves

outside the receiver's operating frequency range. The antennas sent waveforms above 3 GHz, i.e. above the operating range of the receiver.

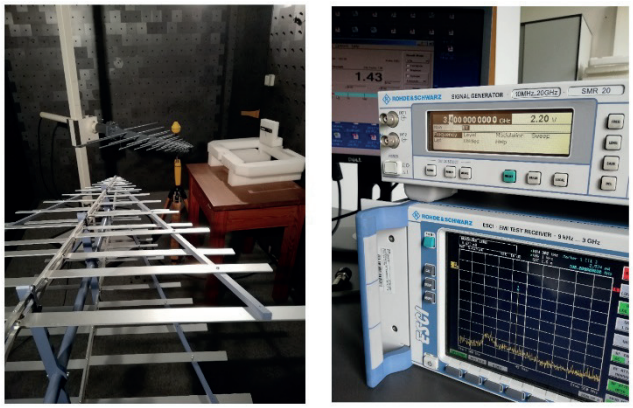

Fig. 2. Anechoic chamber with put on broadband antennas, and a set of electronic equipment for measuring electromagnetic beating in GUM.

Fig. 3 presents the spectrum of frequencies received by the antenna, where the beat signal with an amplitude of approx. 5 pW and a frequency equal to the frequency difference of the transmitting antennas, equals to 300 MHz is clearly visible.

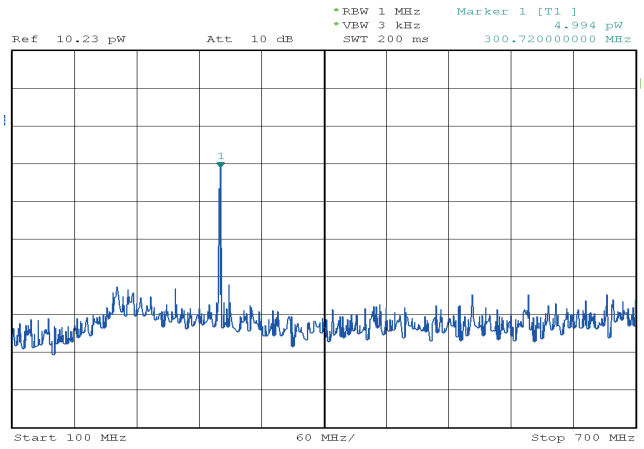

Fig. 3. Measurement of beat signal received by the broadband antenna appeared on the radio wave receiver.

In order to capture the relationship between the beat amplitude and excitation waveforms amplitudes, all waveforms frequencies were selected so that they were all within the receiver's range of operation. For two 850 and 950 MHz waves with approximately the same 8.5 µW power, the beat has a frequency of 100 MHz and a power of approx. 109 pW. The result of this measurement is presented in Fig. 4. The same phenomenon was also observed in such a way that the beat frequency should be between the frequencies causing them [3]. In both cases, the difference between the amplitudes is of the order of 50 dB and at lower powers is a few dB smaller. It has also been observed that the greatest beat-to-noise amplitude ratio is when both waveforms causing a beat are the same amplitude.

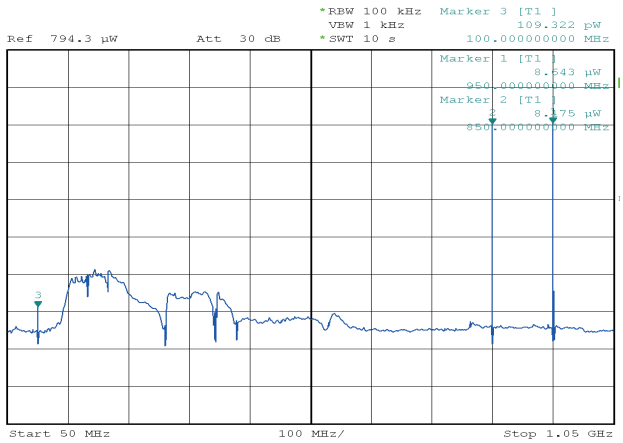

Fig. 4. Measurement of waves sent by transmitting antennas and the beat wave illustrated on a radio wave receiver.

For measuring the 600 MHz beat, in accordance with the project assumptions, a resonant circular antenna with 445 nH inductance and 0.158 pF capacitance was proposed, as well as an ULNA amplifier capable of operating in the frequency range from 450 MHz to 2.5 GHz with an input noise level of 0.5 dB (NF) and total gain of 45 dB for 600 MHz What with the power signal from both generators at the level of 0.1 µW should enable measurement of beating parameters and visualize them on the spectrum analyzer screen, as for the 95 dBµV signals visible in Fig. 4, and the beat signal should be larger than the 41 dBµV (250 pW) signal visible in the same figure.

III. Conclusion

The ideal spectrum analyzer cannot receive the envelope of electromagnetic superposition. Because in reality there are no perfectly linear elements and even the wave paths and antennas show some non-linearity not noticeable in most measurements, it is possible to receive waveforms on the spectrum analyzer.

Preliminary measurements and analysis of the results allow stating that it is possible to compare the power of terahertz sources with the help of spectrum analyzers.

References

[1] J. L. Hesler, T. W. Crowe et al: High-power solid-state terahertz sources. SPIE Newsroom, 2015.

[2] M.Wojciechowski: 2 THz Frequency Standard Project, Quantum and Precision Metrology Conference, QPM Cracow 2019.

[3] M.Wojciechowski: Setups for measuring the beat of two 1 THz waves, EMC Europe Symposium, Barcelona 2019.

Nonlinear THz response of silicon based devices

P. Zagrajek[1], J.Marczewski[2], D. Obrebski[2], C. Kolacinski[2], P. Kopyt[3], S.N. Danilov[4], S.D. Ganichev[4]

[1] Institute of Optoelectronics, Military University of Technology, Warsaw, Poland
[2] Institute of Electron Technology, Warsaw, Poland
[3] Inst. of Radioelectronics and Multimedia Technology, Warsaw University of Technology, Warsaw, Poland
[4] Regensburg Terahertz Center (TerZ), University of Regensburg, Regensburg, Germany

E-mail: przemyslaw.zagrajek@wat.edu.pl

Abstract – In this paper a terahertz detectors based on silicon transistors are described. Measurements for frequency dependence and time resolution are presented. Presented results suggest possible application of such kind of devices.

Keywords –terahertz, detectors, silicon

I. Introduction

Field effect transistors (FETs) have been used for many years as low cost detectors of THz radiation[1,2]. They are very reproducible, easy to integrate with monolithic antennas and read-out circuits. Mainly it is a truth for silicon structures. Depending on a possible application a different property of the detector is important. For fast communication purposes short response time as well as linearity of the responsivity seems to be crucial. For identification applications a spectral selectivity is the most important feature. Both cases was implemented in silicon technology and are presented in two sections below.

The detection process, described by Dyakonov and Shur[3], generates a DC voltage between drain and source electrodes. To enhance the deposition of electromagnetic (EM) wave energy in the transistor channel antennas connected to gate and source electrodes are used. The type of antenna defines the detection band of the device.

II. Narrowband detectors

The first type of detectors were developed for identification purposes. To achieve a given detection frequency they were equipped with patch antennas deposited in the top metallization layer. The details were described in Ref. 4. The transistors were fabricated in CMOS technology with some non-standard steps of the process. The EM waves tend to propagate in a substrate part of detector. To avoid such an effect the area below detector was thinned. The decrease in the sensitivity of the detector with respect to the thickness of the substrate can be found in Ref. 5. A sensitivity of the detectors was increased additionally by using wafers with high resistivity silicon.

Spectral dependence of detectors responsivity were measured with narrowband, widely tunable source of radiation. As a source a frequency multiplier made by

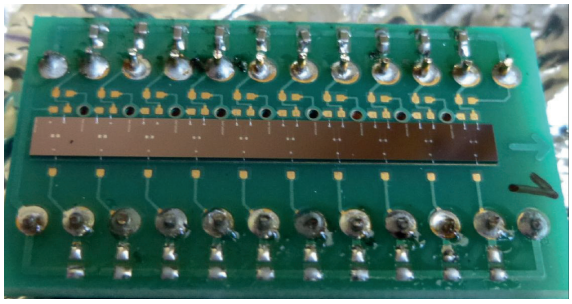

Fig. 1. Ten pixel array of NMOS detectors equipped with patch antennas. Each detector was designed for different frequency.

Virginia Diodes, Inc. was used. Measurements were performed with a lock-in technique. A results for chosen detectors are presented in Fig.2.

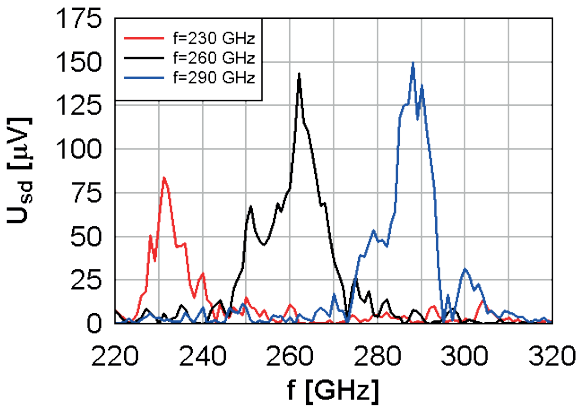

Fig. 2. Frequency dependence of the photoresponses of the detectors. Designed center frequency is shown in a box.

For material identification process data in given frequencies are necessary. The monolithic array of the detectors was fabricated. It contained 10 pixels connected with a readout system. Frequencies of their maximal photoresponse were chosen for material identification, based on spectral properties of various substances. A detailed description of identification with a detector array one can find in Ref. 6

III. WIDEBAND DETECTOR

The second type were n-type silicon transistors fabricated in CMOS technology integrated with wide-band log-periodic antennas and mounted on a Si lens. The devices under consideration had 6µm/3µm channel width

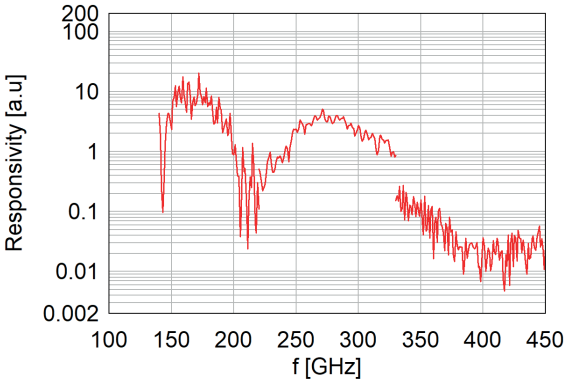

Fig. 3. Frequency dependence of the photorespons of the MOSFET detector equipped with wideband log-periodic antenna.

and length, respectively. The transistor was fabricated on a high resistivity Si bulk substrate. As it was described in ref. 7 a so-called channel stopper was removed from the area below antenna to increase detector responsivity. Detector was connected with two types of readouts. One was voltage amplifier (VA) with 450kΩ input resistance and second was transimpedance amplifier (TIA) with input resistance below 1Ω.

Frequency dependence of detector responsivity for

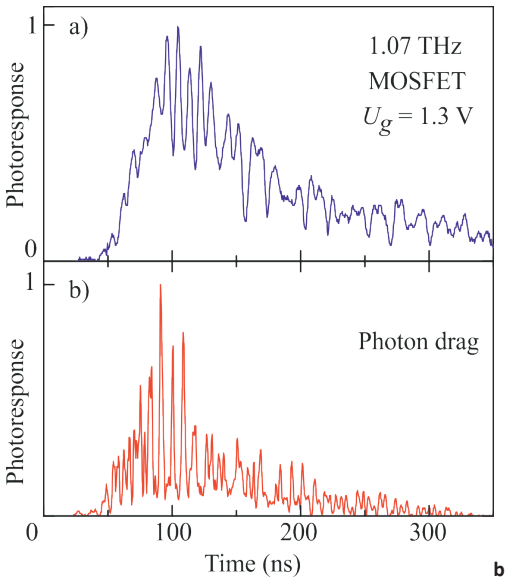

Fig. 4. Normalized photoresponses of the MOSFET detector (a) and photon drag detector showing laser pulse shape (b) for radiation frequency 1.07THz.

f<1THz was measured with the same source and method as described in Sec. II. For time and power dependent measurements a line-tunable pulsed molecular THz laser was used. This source based on a pump CO_2 laser were using CH_3F and NH_3 gases as active media for frequencies 0.6, 1.07 and 2.02THz.

The principal description of such source can be found in Ref 8. The laser works in single pulse regime with the pulse duration of about 100 ns and the repetition frequency 1 Hz. The photoresponses of detectors were measured with a fast digital oscilloscope. A photon drag detector was used as a reference detector.

Described devices detected radiation for frequencies as high as 2.02 THz. Due to the spontaneous mode-locking the laser pulses consisted of spikes with time duration of about 4 ns, what allowed us obtaining time constants of the studied detectors. Comparing signals from our detectors and photon drag reference detector - Fig. 4 shows result for MOSFET, we noticed that all detectors operating with TIA had time resolution of couple of nanoseconds. For VA response slows to hundreds of ns. The more accurate description can be found in 9.

SUMMARY

Silicon based field effect transistors were used as THz detectors working in a range 0.1-2THz. When equipped with various antennas they can work as narrow- or wideband devices.

ACKNOWLEDGMENTS

This work was financially supported by the Deutsche Forschungsgemeinschaft (DFG) and the Volkswagen Stiftung Program (90298). This study was partially supported by the National Center for Research and Development in Poland grants PBS1/A9/11/2012, PBS3/B3/30/2015, LIDER/020/319/L-5/13/NCBR/2014.

REFERENCES

[1] A. Lisauskas, U. Pfeiffer, E. O. Ojefors, P. H. Bolivar, D. Glaab, and H. G. Roskos, “Rational design of high-responsivity detectors of terahertz radiation based on distributed self-mixing in silicon field-effect transistors”, J. Appl. Phys. 105 (11), 114511, 2009.

[2] F. Schuster, H. Videlier, A. Dupret, D. Coquillat, M. Sakowicz, J. Rostaing, M. Tchagaspanian, B. Giffard, and W. Knap, “A broadband THz imager in a low-cost CMOS technology,” IEEE International Solid State Circuits Conference Digest of Technical Papers (ISSCC), San Francisco, CA (IEEE, 2011), p. 42.

[3] M. I. Dyakonov and M. S. Shur, “Plasma wave electronics: novel terahertz devices using two dimensional electron fluid”, IEEE T. Electron Dev. 43 (10), pp. 1640-1645, 1996.

[4] P. Kopyt, J. Marczewski, K. Kucharski, J. Lusakowski and W. Gwarek, “Planar Antennas for THz Radiation Detector Based on a MOSFET,” 36th International Conference on Infrared, Millimeter, and Terahertz Waves (IRMMW-THz), Houston (USA), 2-7 Oct. 2011.

[5] D. Coquillat, J. Marczewski, P. Kopyt, N. Dyakonova, B. Giffard, W. Knap, “Improvement of Terahertz Field Effect Transistor Detectors by Substrate Thinning and Radiation Losses Reduction”, Opt. Express, 24, (1), pp. 272-281, 2016.
[6] J. Marczewski, et al. "THz detectors based on Si-CMOS technology field effect transistors–advantages, limitations and perspectives for THz imaging and spectroscopy." Opto-Electronics Review 26.4, 261-269,2018.
[7] K. Kucharski, et al. „Application of High-Resistivity Silicon Substrate for Fabrication of MOSFET-Based THz Radiation Detectors”. Acta Physica Polonica, A., 134.4, 2018.
[8] S.D. Ganichev and W. Prettl, Intense Terahertz Excitation of Semiconductors (Oxford Univ. Press 2006).
[9] P. Zagrajek, et al. "Time Resolution and Dynamic Range of Field-Effect Transistor–Based Terahertz Detectors." Journal of Infrared, Millimeter, and Terahertz Waves, 40, 703-719, 2019.

75 nm gate length and asymmetric gate recess InGaAs/InAlAs HEMT with THz f_{max}

S. Bollaert, N. Wichmann, X. Wallart, C. Coinion, S. Lepilliet, M. Samnouni.
IEMN, University of Lille, CNRS, Centrale Lille, ISEN, Univ. Valenciennes, UMR 8520 - IEMN
UMR 8520 - IEMN
59000 Lille, France
E-mail: sylvain.bollaert@univ-lille.fr

Abstract – We report a high maximum frequency of oscillation (f_{max}) and a current-gain cutoff frequency (f_T). f_{max} / f_T = 1.2 THz / 220 GHz at V_{DS} = 1V with pseudomorphic high-electron mobility transistor (PHEMT), using a composite, InGaAs/InAs channel and an asymmetric gate recess. This result was achieved with long gate length L_G=75nm. The device was optimized based on another transistor operating at f_{max} = 800 GHz. Moreover, the noise measurment of 800 GHz transistor has been characterized until 110GHz, noise extraction gives a minimum noise figure (NF_{min}) of 0.8 dB (with associated gain G_{ass} = 16 dB) and 1.8 dB (with associated gain G_{ass} = 11.6 dB) at 40 GHz and 94 GHz respectively.

Keywords High-Electron Mobility Transistor (HEMT), Asymmetric Gate Recess, Noise Figure

I. Introduction

High Electron-Mobility Transistors (HEMTs) technology is the best candidate for low noise amplifier and Terahertz applications. Due to their superior high-frequency characteristics InP-based HEMTs are very promising for millimeter-wave applications and image sensor systems [1]. Currently, the record for f_T is 688GHz (f_{max} = 800 GHz) with metamorphic-HEMTs (MHEMTs) on GaAs substrate [2], and f_{max} is 1.5 THz (f_T = 610 GHz) with pseudomorphic-HEMTs (PHEMTs) on InP substrate [3]. In fact, for the last 10 years, the strategy used to improve electrical performance of HEMT was to reduce the gate length below 50 nm combined with epilayer engineering. This approach allows high cutoff frequencies and excellent transconductance with a record g_m of 3.45 mS/µm, recently published papers report high f_{max} while keeping longer gate length L_G = 75 nm [4].

II. Fabrication and Result of Characterization

Pseudomorphic HEMT (PHEMT) epitaxial layers were grown on semi-insulating InP substrate by gas source molecular beam epitaxy (MBE). The layer structure (figure 1), from bottom to top, consist of an

$In_{0.52}Al_{0.48}As$ buffer layer, a bottom silicon-delta doped plane, an $In_{0.52}Al_{0.48}As$ first spacer, an $In_{0.53}Ga_{0.47}As$ /InAs/$In_{0.53}Ga_{0.47}As$ composite channel, an

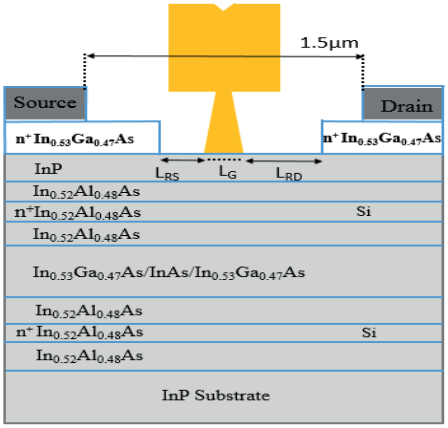

Fig. 1. Cross-section schematic of epitaxial layer structure.

$In_{0.52}Al_{0.48}As$ second spacer, a top silicon-delta doped plane, an $In_{0.52}Al_{0.48}As$ barrier, an InP etch-stop layer, and finally a thick $In_{0.53}Ga_{0.47}As$ cap layer. The epilayer structure was optimized for high electron density and mobility in the channel. To achieve high channel mobility, strained pure InAs layer was inserted in InGaAs channel. A highly doped thick cap layer was used to ensure low access resistance. For PHEMT fabrication, electron beam lithography was used except for the mesa isolation, where standard optical lithography is sufficient. The first step of the fabrication was mesa isolation by wet chemical etching. The InGaAs cap layer was removed by Orthophosphoric acid based solution (H_3PO_4-solution). InP layer was then suppressed by Hydrochloric acid based solution (HCL-solution) followed by a second etching with H_3PO_4-solution to finish the mesa down to the InAlAs buffer layer. Next, Ohmic contact was realized as follow: after defining the Drain-Source with 1.5µm distance by e-beam lithography (Figure 1), Ti/Pt/Au metals was evaporated followed by thermal annealing. TLM measurement reports a low contact resistance (R_c) of 30 Ω.µm. The gate was then formed on InP layer by e-beam lithography evaporation of Ti/Pt/Au metals.

III. Characterization

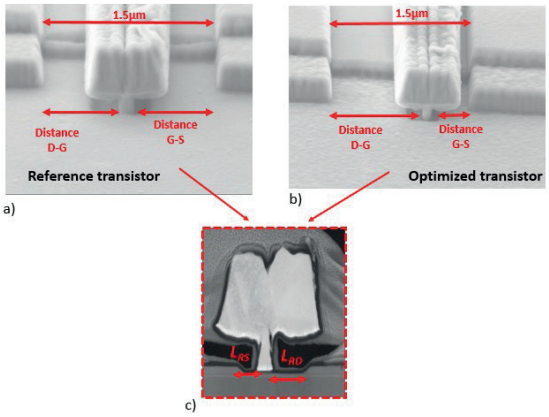

Fig. 2. a) and b) Images of SEM c) FIB STEM of 75 nm Gate length

THz applications requires high oscillation frequency f_{max}, which is one relevant parameter for analog circuits as Low Noise Amplifier. Epilayer and topology of the transistor were then optimized. Hall measurements report sheet electron density n_H=2.9×10^{12}/cm^2 and a high Hall mobility μ_H=11000cm^2/Vs. Composite InGaAs/InAs channel has been used and layer thicknesses, delta-doped have been optimized. For the transistor topology, an asymmetric recess (figure 3) was adopted to reduce short channel effect and to improve intrinsic voltage gain gm/g_d and the ratio C_{GS}/C_{GD}. For the reference transistor, the gate was kept in the same distance 0.7µm to the drain and to the source contacts (see figure 2a). Furthermore, f_{max} can be achieve THz frequency with extending more the distance L_{RD}. The optimized transistor has L_{RD} of 225 nm and the gate source distance was reduced from 0.7 µm to 0.5 µm (see figure 2b) in order to further improve f_{max}.

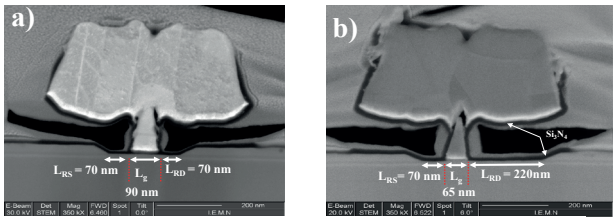

Fig. 3. Cross section of HEMT with a) symmetric and b) asymmetric recess

DC results of PHEMT with 75 nm gate length and an asymmetric recess are given in figure 4. High current of I_D = 800 mA/mm and I_D = 1000 mA/mm respectively for reference and optimized PHEMT. The extrinsic peak transconductance gm of 1400 mS/mm was obtained at V_{DS} = 0.8 V for both transistors.

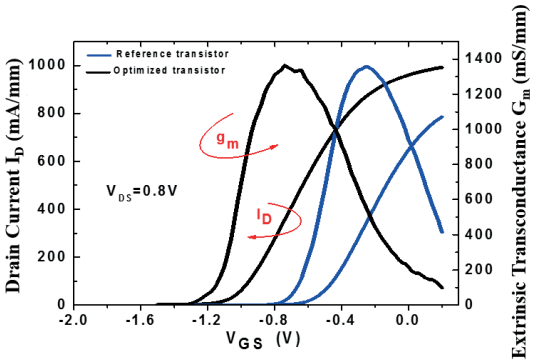

Fig. 4. a) and b) Images of SEM c) FIB STEM of 75 nm Gate length

S-parameters measurements on a Vector Network Analyser was achieved up to 110 GHz . The extrapolation by (20 dB/decade) of U gives f_{max} = 800 GHz and f_{max} = 1.2 THz at V_{DS} = 1 V for reference and optimized transistor respectively (figure 5).

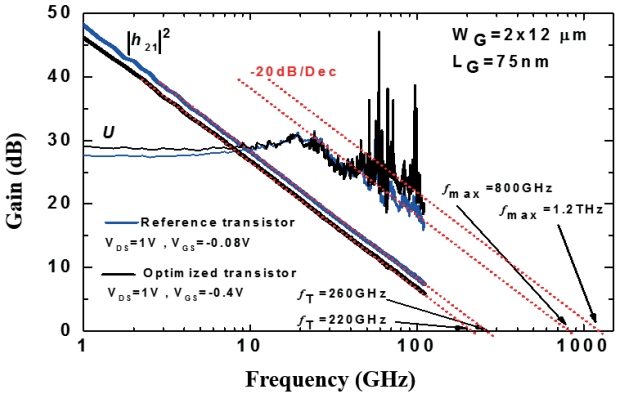

Fig. 5. Measured comparison $U/|h_{21}|^2$ of reference and optimized HEMTs (L_G = 75nm and W_G = 2x12 µm)

In order to extract the four noise parameters of the transistor, NF_{50} method [5] has been used. The method consists in fitting a noise model (figure 6) with two uncorrelated noise source with noise temperatures at the input T_{in} and at the output T_{out} to the noise figure measured on 50 impedance (*NF50*) up to 110GHz.

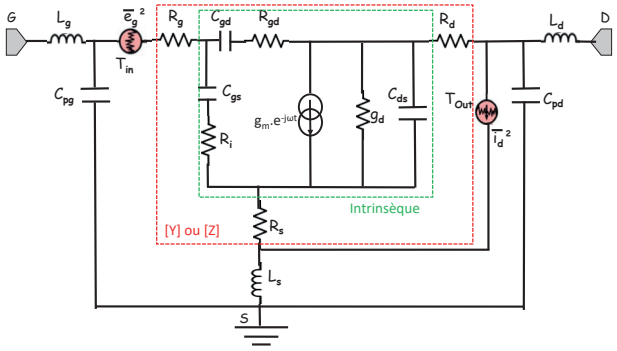

Fig. 6. Noise model used in *NF50* method [5]

Tin was fixed at room temperature T_{in}=293K and the fitting method gave a T_{out}=1350K. The results achieved at 94 GHz were NF_{min} of 1.8 dB (with associated gain of 11.6 dB) for an optimal gate voltage V_{GS_Opt} = - 0.3 V and the reference transistor (figure 7).

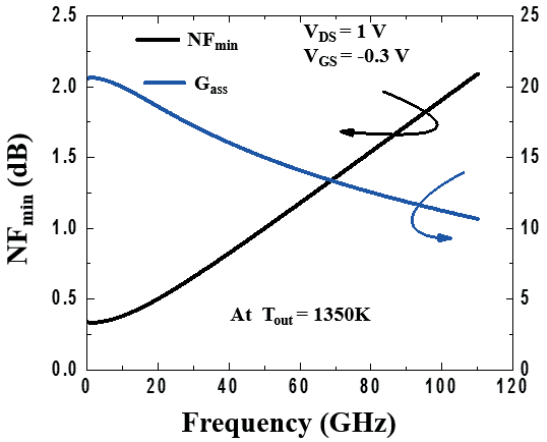

Fig. 7. NF_{min} and G_{ass} at T_{out}=1350K Up to 110GHz of HEMT reference

ACKNOWLEDGMENTS

This work was developed in IEMN's cleanroom, a part of the French National Fabrication Network (RENATECH).

REFERENCES

[1] M. Sato *et al. Antennas Propag. IET Microw.*, vol. 2, no. 8, pp. 848–853, Dec. 2008.
[2] D. H. Kim, *et al*. in *2011 International Electron Devices Meeting*, 2011, pp. 13.6.1-13.6.4.
[3] X. Mei *et al. IEEE Electron Device Lett.*, vol. 36, no. 4, pp. 327–329, Apr. 2015.
[4] T. Takahashi *et al. Appl. Phys. Express*, vol. 10, no. 2, p. 024102, Jan. 2017.
[5] F. Danneville *et al. Int. J. Numer. Model. Electron. Netw. Devices Fields*, vol. 27, no. 5–6, pp. 736–747, Sep. 2014

Development of new tools to characterize materials and devices in the terahertz domain

Emilie Herault, Maxime Bernier, Frederic Garet and Jean-Louis Coutaz
IMEP-LAHC, UMR 5130 CNRS, University Savoie Mont-Blanc
73376 Le Bourget du Lac Cedex, France

The main expertise of our laboratory lies in material and device characterization in the THz range as well as in optoelectronic generation and detection of THz signals. This will be illustrated through two activities. In a first part, we'll describe a new microscopy technique: optical rectification THz imaging (ORTI). Thanks to optical rectification, THz signal is generated by focusing a femtosecond laser pulse onto the surface of a sample and detected by a photoconductive antenna. By moving the sample in the laser beam, an image of the sample non linearities can be recorded. In this configuration, the spatial resolution of the image is fixed by the laser spot size and not by the THz wavelength. Image of a sugar grain, ZnTe slivers and domains of a ppKTP were then obtained with resolution up to 11 μm (λ/185 at 0.15 THz).
In a second part, we'll present the design and characterization of THID tags for identification or authentication of manufactured products. In order to take into account of the advantages of the THz domain compared to the optical and RF ones, more precisely the transparency of most of dielectrics and the short corresponding wavelengths, we develop original methods to fight against counterfeiting. For example, we propose a tag structure based on a diffraction grating engraved on a plastic substrate whose transmission or reflection signature exhibits sharp lines constituting the main information. Using statistical methods to process the tags signatures, we demonstrate the potentialities of such tags to be used for authentication of products.
The talk will be concluded on the presentation of the lab new THz characterization platform and its equipment.

Negative Photoconductivity and low frequency noise in HgTe Quantum Wells

S. Rumyantsev[1], I. Yahniuk[1], D. B. But[1,2], G. Cywinski[1,2], N. N. Mikhailov[3], S. A. Dvoretsky[3], J. Łusakowski[4], W. Knap[1,2,5]

[1]Center for Terahertz Research and Applications (CENTERA), Institute of High Pressure Physics, Polish Academy of Sciences, Warsaw, Poland

[2]CEZAMAT, Warsaw University of Technology, 02-822, Warsaw, Poland

[3]Rzhanov Institute of Semiconductor Physics Siberian Branch of Russian Academy of Sciences, Novosibirsk, Russia

[4]Faculty of Physics, University of Warsaw, Warsaw, Poland

[5]Laboratoire Charles Coulomb, University of Montpellier & CNRS, Montpellier, 34095, France

E-mail: roumis4@gmail.com

Abstract –Photoconductivity and low frequency noise were studied in HgTe/CdHgTe quantum wells with electron dominated conductivity. Decrease of the conductivity under illumination (negative photoconductivity) was observed and explained by four steps process: i) generation of electron-hole pairs outside the quantum well, ii) their separation by built in electric field, iii) drift of holes inside the quantum well, and iv) recombination of holes with electrons leading to reduction of the electron density, hence the conductivity. The amplitude of the noise in HgTe quantum wells was also studied and found within the range which is typical for Si MOSFETs.

Keywords – HgTe, negative photoconductivity, noise, noise reduction.

I. Introduction

The band structure of CdHgTe can be tuned by composition, temperature and hydrostatic pressure within the range from zero to a few tens of meV. HgTe/CdHgTe quantum wells (QWs) of different thicknesses provide one more mechanism to tune the band structure. These make HgTe/CdHgTe quantum wells (QWs) structures promising for different infrared and terahertz applications.

Detection and emission by different mechanisms in the terahertz frequency range were already demonstrated in several publications (see [1] and references therein). The knowledge of electrical properties of HgTe QWs, including effect of illumination and noise is important for the understanding of the current flow mechanisms and judgement about possible applications.

II. Results and Discussions

The HgTe/CdHgTe QW structures, studied in this work, were grown by molecular beam epitaxy (MBE) on GaAs substrate (013) with the thickness of d = 7 – 7.5 nm. This thickness corresponds to inverted band structure at 4 K and normal band ordering at 300 K [2]. Fig. 1 shows the composition profile of the studied structures. Hall measurements at 4K indicated the electron mobility and concertation of $\mu = (4 - 70) \cdot 10^3$ cm^2/Vs, $n = (2 - 10) \cdot 10^{11}$ cm^{-2}, respectively.

The resistance of the structures was measured in 4-probe configuration in the dark and under illumination.

Usually illumination leads to increase of density of conducting carriers and therefore decrease of the resistance. Surprisingly all investigated HgTe/CdHgTe QW structures demonstrated negative photoconductivity under ambient visible light illumination at 300 K, i.e. the resistance increased under illumination (this kind of negative "persistent" photoconductivity is known for other types of heterostructures [3]). Figure 2 shows the characteristic times of the transient processes with light on and off. As seen from Fig. 2, the transient processes are non-exponential and include characteristic time of a few tens on seconds. The non-exponential kinetics of the photoconductivity is an indication of the wide spectrum of deep traps with small capture cross section, which also could contribute to the low frequency noise.

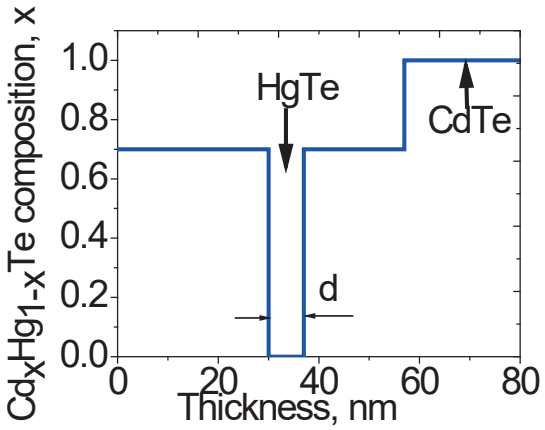

Fig. 1. Composition profile of the studied structures. Quantum well width d =7 nm.

In quantum well structures the most realistic mechanism of negative photoconductivity is the separation of electrons and holes generated in the barrier layer ($Cd_{0.7}Hg_{0.3}Te$ in our case) by built in electric field. As a result, electrons move to the surface and are trapped

by the deep states. Holes move towards the quantum well where they recombine with electrons reducing their concentration and, therefore the conductivity.

The low frequency noise was measured at room temperature in the dark and under illumination. The spectral noise density of the current fluctuation was always proportional to the current squared. This confirms that the noise is due to the resistance fluctuations and the current does not affect these fluctuations.

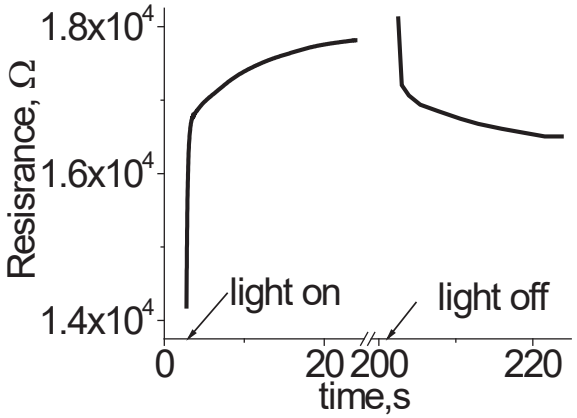

Fig. 2. Transient processes of the resistance change under illumination.

Figure 3 shows examples of the noise spectra of current fluctuations in the dark and under illumination. The noise spectra in the dark had the form of the 1/*f*-like noise. Illumination led to overall reduction of the noise at frequencies 1 Hz < *f* < 100 Hz and to the change of the spectra shape.

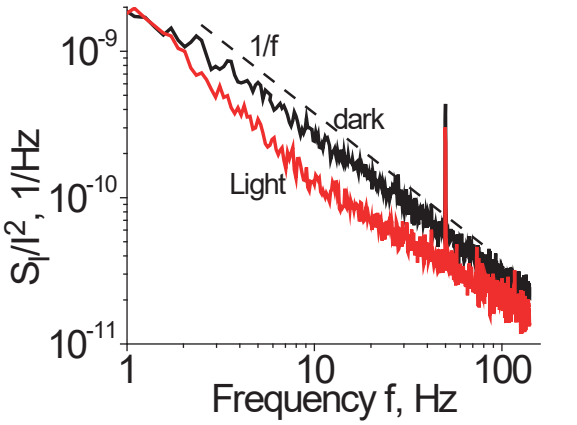

Fig.3. Noise spectra of CdHgTe quantum well structure in the dark and under illumination. V=10mV, *T* = 300 K.

One of the common way to characterize the amplitude of noise is based on the McWhorter model [4,5]. The model allows to calculate the effective trap density responsible for noise as:

$$\frac{S_I}{I^2} = \frac{kTN_t}{\gamma f W L n_s^2}, \qquad (1)$$

where k is the Boltzmann constant, T is the temperature, N_t is the effective trap density f is the frequency, WL is the channel area, n_s is the concentration and γ is the attenuation coefficient of the electron wave function under the barrier. The McWhorter model is widely used to analyze the 1/f noise in MOSFETs.

With known amplitude of noise and electron concentration from the Hall measurements, trap density estimated based on McWhorter model for different samples was found within the range $N_t = 10^{18} – 10^{20}$ cm^{-3}eV^{-1}. These are the typical values for the state of the art Si MOSFETs with high-k dielectric.

Reduction of noise under illumination in semiconductors is known for GaAs, Si, and SiC [6]. It is explained by the model which includes the capture of the minority carriers by the traps responsible for the carriers' number fluctuations [6]. Similar mechanism could be responsible for the noise reduction in HgTe QWs as well.

III. CONCLUSIONS

In conclusion, negative photoconductivity and noise reduction under illumination were found in HgTe/CdHgTe QW structures. These effects are explained by electrons and holes generation in the $Cd_{0.7}Hg_{0.3}Te$ layer followed by hole's recombination in quantum wells. The amplitude of the noise in HgTe quantum wells was found to be within the range typical for Si MOSFETs.

ACKNOWLEDGMENTS

The work at *CENTERA* was supported by the Center for Terahertz Research and Applications project carried out within the 'International Research Agendas program of the Foundation for Polish Science co-financed by the European Union under the European Regional Development Fund, by the Foundation for Polish Science through the grant TEAM/2016-3/25 and by the National Science Centre, Poland allocated on the basis of the decision No. UMO-2017/25/N/ST3/00408.

REFERENCES

[1] Yu. B. Vasilyev, *et al.,* "Terahertz Emission from CdHgTe/HgTe Quantum Wells with an Inverted Band Structure," Semiconductors, Vol. 50, pp. 915–919, 2016.
[2] M. König, et al. "The Quantum Spin Hall Effect: Theory and Experiment." J. Phys. Soc. Jpn. Vol. 77, p. 031007, 2008.
[3] A. S. Chaves and H. Chacham, Appl. Phys. Lett., vol. 66, p. 727, 1995.
[4] A. L. McWhorter, in *Semiconductor Surface Physics*, edited by R. H. Kingston, University of Pennsylvania Press, Philadelphia, 1957.
[5] S. Christensson, I. Lundstrom and C. Svensson, "Low frequency noise in MOS transistors", Solid-State Electr., vol. 11, pp. 797-812, 1968.
[6] N.V. D'yakonova, M.E.Levinshtein, S.L.Rumyantsev, "Nature of the bulk 1/f noise in GaAs and Si," Sov. Phys. Semicond. vol.25, pp. 1241-1265 1991.

Landau levels terahertz emission from HgCdTe bulk films

D.B. But[1,2], C. Consejo[2], S.S. Krishtopenko[2], N. Dyakonova[2], N.N. Michailov[4], S.A. Dvoretskii[4], V. I. Gavrilenko[3], F. Teppe[2] and W. Knap[1,2]

[1]CENTERA Lab, Institute of High Pressure Physics, PAS, 02346 Warsaw, Poland
[2] Laboratoire Charles Coulomb, CNRS 5221, University of Montpellier & CNRS, 34095, Montpellier, France
[3]Institute for Physics of Microstructures RAS, GSP-105, 603950, Nizhny Novgorod, Russia
[4]Institute of Semiconductor Physics, Siberian Branch RAS, 630090, Novosibirsk, Russia.

We report on THz emission from HgCdTe bulk films. Our experiments clearly show magnetically tunable THz emission that can be attributed to electron radiative recombination between the Landau levels (cyclotron emission). Energy band structure theoretical calculations using Kane Hamiltonian are performed. They allow identification of observed resonances as related to transitions between two lowest conduction band Landau levels.

Keywords – *terahertz, emission, Landau levels*

SEMICONDUCTOR based THz/Far IR magnetically tunable emission was a subject of the intense studies for decades [1, 2]. Impressive results have been obtained in GaAs and InSb semiconductors leading to construction of cyclotron emission based THz/Far IR spectrometers [3]. The magnetically tunable THz sources regained its interest with appearance of narrow gap and/or gapless semiconductor materials with linear band dispersion, like graphene or specific HgCdTe alloys [4]. This is because of two main reasons: i) first - the splitting of LLs is inversely proportional to the effective electron mass that decreases with the bandgap. Therefore, semiconductors with band gap, smaller than in InSb, should have significantly higher magnitude of cyclotron emission tunability. Thanks to the technological progress, HgCdTe conduction electron masses lower than $10^{-3}m_0$ (m_0 is a free electron mass) could be realized [5]. ii) second - strongly non-equidistant Landau levels (LLs) are necessary to cancel self-absorption losses. Indeed, in the case of parabolic band dispersion, emitted THz photons can be reabsorbed by whole family of equidistant LLs. The latter is avoided in the case of narrow gap semiconductors with strong band nonparabolicity leading to non-equidistant LLs fan.

The first cyclotron emission of electrons ('Landau emission') was observed in InSb [1]. However, as mentioned above, semiconductors with band gap, smaller than in InSb, should have significantly higher magnitude of cyclotron emission tunability. One of few gapless semiconductors, well-known for ages, is $Hg_{1-x}Cd_xTe$ alloy. At critical cadmium concentration $x \approx 0.17$, the bandgap shrinks to zero and the electronic dispersion has linear dependence on quasimomentum [4, 6].

So far, there is only a single work [7], in which cyclotron emission from $Hg_{0.8}Cd_{0.2}Te$ film with was reported. However, the range of tunability was not demonstrated therein. The main factor, limited the radiative properties of $Hg_{1-x}Cd_xTe$ alloy at $x < 0.2$ was the material quality, because the growth of $Hg_{1-x}Cd_xTe$ films ($x < 0.2$) with low inhomogeneity and impurity/defect concentration used to involve certain technological problems [8]. The quality of such structures has significantly increased in the last 2-3 decades due to progress made in the molecular-beam epitaxy (MBE) technique [5].

In this work we present the first experimental results on magnetically tunable THz emission from $Hg_{1-x}Cd_xTe$ films with $x < 0.2$. Our sample of $Hg_{0.808}Cd_{0.192}Te$ with the band gap of about 40 meV at 4.2 K was grown on (013) semi-insulating GaAs substrate covered by thick CdTe buffer [9]. The film was sufficiently thick (≈ 3.2 μm) to be considered as a bulk material.

The 4.2 K carrier density n_V and mobility μ were determined by standard magneto transport measurements to be $2.5 \cdot 10^{14}$ cm^{-3} and $3 \cdot m^2 \cdot V/s$ respectively [10].

Our experimental setup contained two independent 8 T and 14 T superconducting coils placed in a one cryostat. The sample was inserted in the first coil, while a magnetically tunable InSb photoconductive detector [11] was in the second one. The measurements were performed at 4.2 K. THz radiation from the sample was guided into detector by a copper light pipe. System operated in modes than the emitter magnetic field was tuned and the detector is kept at constant field.

The electrons were heated with electric field pulses leading to the Fermi distribution is distortion and population of higher levels. In our experiments, the pulsed electric fields had peak-to-peak values up to 12V/cm. The pulse duration was 7 ms and the duty circle was tuned in such a way that the average power consumption of emitter did not exceed 12 mW (to avoid sample heating). Figure 1 shows photoconductive signals of InSb detector at different magnetic (step 0.1 T) fields as a function of the magnetic field of HgCdTe sample.

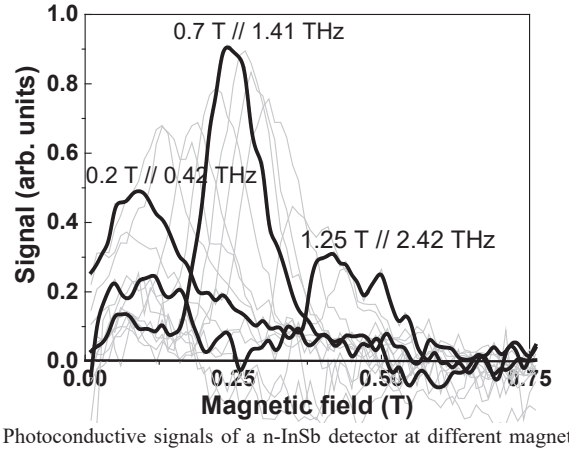

Fig. 1. Photoconductive signals of a n-InSb detector at different magnetic fields as a function of the magnetic field of cyclotron terahertz $Hg_{0.808}Cd_{0.192}Te$ emitter. The black solid lines are three selected results for detector at 0.2T, 0.7T, 1.25T corresponding to resonant detection at 0.42 THz, 1.41THz, 1.25THz. Gray lines in the background show results for intermediate magnetic fields/frequencies.

Figure 2 shows calculated, conduction band LLs energies for quasimomentum $k_z=0$ as a function of magnetic field. The calculations were done using Kane Hamiltonian as described in Ref. [12]. The z axis coincides with the growth direction and orientation of magnetic field. The arrows indicate cyclotron resonance (CR) transitions from two lowest LLs.

For details of LLs notations see [12].

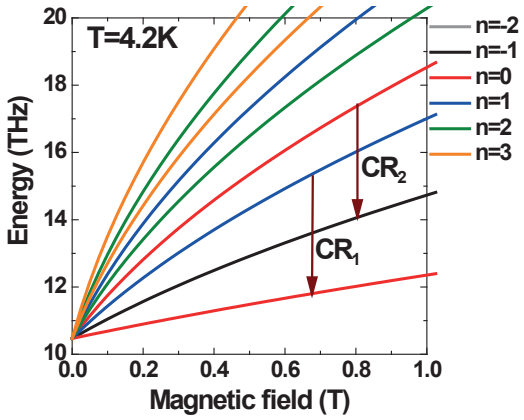

Fig. 2. Landau levels fan chart at k_z =0 in conduction band of $Hg_{0.808}Cd_{0.192}Te$ sample. Magnetic field is oriented along the growth direction. Zero energy corresponds to the top of valence band. For details of LLs notations see [12].

As mentioned above non-equidistance of LLs in given magnetic field is attributed to the nonparabolicity of conduction band. One can see in Fig.2 that nonparabolicity leads to a deviation from the linear dependence of the LLs splitting. Also a decrease of spacing between LLs (cyclotron energy) with increasing energy for a given *B* maybe observed. This results in an emission line broadening at the low frequency side and in a split of the emission spectrum into several lines if transition from several LLs are present [12].

Figure 3 presents the comparison between theoretical and experimental results. It shows emission spectra at different values of magnetic field plotted as a color map. The open symbols correspond to the maximum intensity in a given magnetic field. Dashed color curves describe theoretical CR energies from the two lowest LLs (see Fig. 2). A good agreement between theoretical curves and experimental results demonstrates that emission from our sample is indeed attributed to the CR excitations from LLs in conduction band.

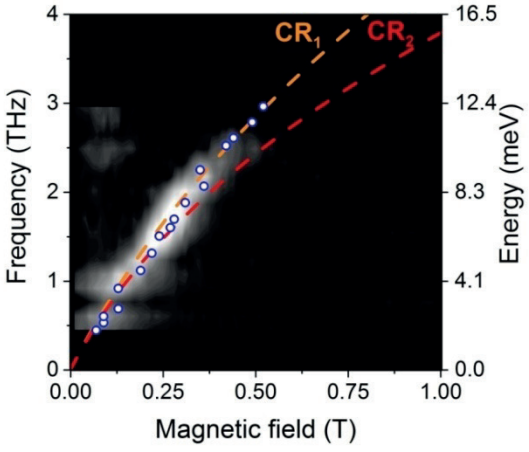

Fig. 3. Color map for cyclotron emission spectra as a function of magnetic fields for $Hg_{0.808}Cd_{0.192}Te$ film. The white region corresponds to the maximum intensity of THz emission.

In conclusion: our results pave the way towards new cyclotron emission THz spectrometers based on HgCdTe films sources. The observed intensities are well described by radiative transitions between LLs. Still higher tunability may be obtained by exploring HgCdTe layers with narrower bandgap. This may lead to emitters with lower effective masses (higher tunability) and lower self-absorption losses (higher intensity).

ACKOWLEDGEMENT

This work was supported by the CNRS through LIA TeraMIR project, by the Languedoc-Roussillon region via the Gepetto Terahertz platform and by the Russian Foundation for Basic Research (Grant Nos. 15-02-08274, 15-52-16012 and 16-02-00672). This work was partially supported by the National Centre for Research and Development in Poland (grant no. PBS1/A9/11/2012), by the National Science Centre in Poland (DEC-2013/10/M/ST3/00705).
The „Center for Terahertz Research and Applications (CENTERA)" project is carried out within the 'International Research Agendas' programme of the Foundation for Polish Science co-financed by the European Union under the European Regional Development Fund.

REFERENCES

[1] W. Müller, F. Kohl, and E. Gornik, "Tunable far-infrared radiation with subnanosecond risetime from Landau-emission sources," (en), *Infrared Physics*, vol. 18, no. 5-6, pp. 691–696, 1978.

[2] W. Zawadzki, C. Chaubet, D. Dur, W. Knap, and A. Raymond, "Cyclotron FIR emission from hot electrons in GaAs/GaAlAs heterostructures," (en), *Solid-State Electronics*, vol. 37, no. 4-6, pp. 1213–1216, 1994.

[3] W. Knap *et al,* "A far-infrared spectrometer based on cyclotron resonance emission sources," (en), *Rev. Sci. Instrum,* vol. 63, no. 6, p. 3293, 1992.

[4] F. Teppe et al., "Temperature-driven massless Kane fermions in HgCdTe crystals: verification of universal velocity and rest-mass description," *arXiv:* 1602.05999.

[5] V.S. Varavin *et al,* "HgCdTe epilayers on GaAs: growth and devices". Opto-Electron. Rev. 11 (2), pp. 99-111, 2003.

[6] M. Orlita *et al,* "Observation of three-dimensional massless Kane fermions in a zinc-blende crystal," (en), *Nat Phys*, vol. 10, no. 3, pp. 233–238, 2014.

[7] E. Gornik, "Far infrared cyclotron emission in semiconductors," (en), *Journal of Magnetism and Magnetic Materials*, vol. 11, no. 1-3, pp. 39–46, 1979.

[8] A. Rogalski, "HgCdTe infrared detector material: History, status and outlook," (en), *Rep. Prog. Phys,* vol. 68, no. 10, pp. 2267–2336, 2005.

[9] S. Dvoretsky *et al,* "Growth of HgTe Quantum Wells for IR to THz Detectors," (en), *Journal of Elec Materi*, vol. 39, no. 7, pp. 918–923, 2010.

[10] A. V. Ikonnikov, M. S. Zholudev, V. I. Gavrilenko, N. N. Mikhailov, and S. A. Dvoretskii, "Magnetoabsorption in narrow-gap HgCdTe epitaxial layers in the terahertz range," (en), *Semiconductors*, vol. 47, no. 12, pp. 1545–1550, 2013.

[11] L. Dmowski, M. Cheremisin, C. Skierbiszewski, and W. Knap, "Far-Infrared Narrow-Band Photodetector Based on Magnetically Tunable Cyclotron Resonance-Assisted Transitions in Pure n-Type InSb," (en), *Acta Physica Polonica A*, vol. 92, no. 4, pp. 733–736, 1997.

[12] M. Zholudev *et al,* "Magnetospectroscopy of two-dimensional HgTe-based topological insulators around the critical thickness," (en), *Phys. Rev. B*, vol. 86, no. 20, 2012.

THz Detectors Based on GaN/AlGaN Lateral Schottky Barrier Diodes

G. Cywiński[1,2], P. Sai[1,3], M. Dub[1,3], M. Sakowicz[1], D. B. But[1,2,3], P. Prystawko[4], W. Knap[1,2,5], and S. Rumyantsev[1]

[1] CENTERA Laboratories, IHPP PAS, ul. Sokołowska 29/37, 01-142, Warsaw, Poland

[2] CEZAMAT, Warsaw University of Technology, 02-822, Warsaw, Poland

[3] V. Ye. Lashkaryov Institute of Semiconductor Physics, National Academy of Sciences of Ukraine, 41 pr. Nauki, 03680, Kyiv, Ukraine

[4] Institute of High Pressure Physics PAS, ul. Sokołowska 29/37, 01-142, Warsaw, Poland

[5] Laboratoire Charles Coulomb, University of Montpellier and CNRS UMR 5221, 34950, Montpellier, France

E-mail: gc@unipress.waw.pl

Abstract— This work presents results of investigations of lateral and vertical Schottky diodes based on Molecular Beam Epitaxy (MBE) grown GaN/AlGaN heterostructures. We have used plasma assisted molecular beam epitaxy in metal rich conditions on freestanding GaN commercial substrates and GaN/sapphire heterosubstrates. The optimized technological procedures have been used to avoid parasitic conduction channels through adjacent epitaxial layers, regrowth interface (RI) or conductive substrates. The investigated 2 dimensional electron gas (2DEG) epistructures were characterized using room temperature Hall measurements. The device processing was performed by using the laser writer technique and shallow mesa etching for electrical insulation of Schottky barrier diodes (SBDs). Our electrical measurements and first detection experiments performed in sub-THz confirm high quality of epitaxial layers, processing and possibility to use lateral SBD as high frequency (HF) detectors.

Keywords – lateral Schottky diode, GaN, AlGaN, 2DEG, Schottky barrier diode, THz, sub-THz, THz detection

I. Introduction

High breakdown voltage, high thermal conductivity and high carrier mobility makes GaN a very attractive semiconductor for high power, high voltage applications. For example GaN-based Schottky barrier diodes were already demonstrated as efficient devices for high power and high voltage applications [1, 2]. Moreover, high electron mobility saoistnyand high concentration of 2DEG, in AlGaN/GaN heterostructures makes them attractive also for HF applications. While AlGaN/GaN high electron mobility transistors (HEMTs) are well developed and commercially available, GaN-based Schottky diodes are still under development. For HF applications the Schottky diodes with the Schottky contact along the edge of 2DEG is of special interest. This kind of structure was first proposed in ref. [3] and experimentally demonstrated for GaN/AlGaN system in [4]. The advantage of this structure is small junction capacitance and small series resistance, which result in cut-off frequency fc=1/(2πCR) exceeding 1 THz.

The schematic picture of lateral and vertical SBD presented in Fig. 1 below.

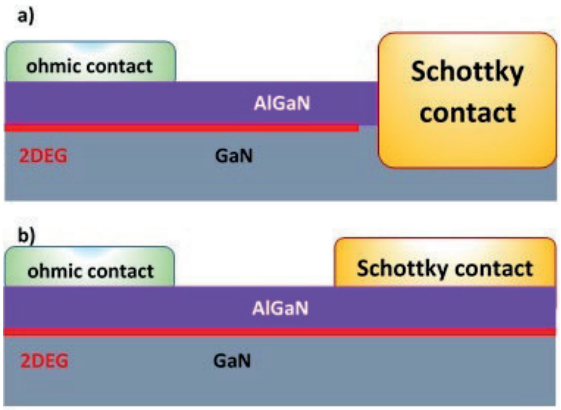

Fig. 1. Schematic of lateral (a) and vertical (b) Schottky diodes under study.

We report on fabrication, characterization and first sub-THz detection experiments performed on lateral GaN/AlGaN Schottky barrier diodes. We present epitaxy technology, processing, electrical characterization and detection at sub-THz range performed on lateral SBDs.

Experiment

The epitaxial growth was performed by Plasma Assisted Molecular Beam Epitaxy (PAMBE) in metal rich conditions on different types of gallium polar (0001) GaN substrates. For the optimization of PAMBE growth procedures the (0001) GaN/sapphire heterosubstrates prepared by Metalorganic Vapour Phase Epitaxy (MOVPE), which are commonly used for such purposes. The main purpose of optimization of epitaxy was fabrication of high quality of 2DEG it means, which contains high mobility 2DEG and where parasitic conduction channels are eliminated. The high quality of 2DEG epistructures were performed keeping gallium rich

conditions during all time during growth and ensuring the appropriate conditions for step-flow mode growth. To the best of our knowledge these result in the lowest residual doping incorporation and elimination of point defects. Such epitaxy, together with high purity of epitaxial materials and outgassing procedures, leads to the highest resistances of epitaxial layers of intrinsic GaN. To separate the epitaxial structure from regrowth interface impurities and semiconducting substrates we have used 0.5 µm Thick GaN:Mg startup layer followed by 0.8 µm GaN intentionally undoped buffer layer. The concentration of magnesium and layer thickness of GaN:Mg were optimized to provide very good electrical insulation. In this paper, we report device characterization performed on two different 2DEG epitaxial layers: epistructure A and epistructure B with different aluminum content in AlGaN layer. Both epistructures were grown on freestanding (0001) GaN substrate with dislocation density of ~10^7 cm^{-2}. The growth was started with 0.5 µm thick GaN:Mg, followed with 0.8 µm GaN buffer, and 25 nm AlGaN with 15% and 25% aluminum for epistructure A and B, respectively. In both cases the AlGaN layer was capped by 2 nm GaN layer. The electron sheet density and mobility in the 2DEG channel have been obtained from Hall experiment taken at room temperature and were: $N_{2DEG} = 4.6 \cdot 10^{12}$ cm^{-2}, $\mu_{2DEG} = 1925$ cm^2/Vs and $N_{2DEG} = 1 \cdot 10^{13}$ cm^{-2}, $\mu_{2DEG} = 1760$ cm^2/Vs, for structures A and B, respectively.

For the purposes of THz wave detection experiments, a test epistructure C on gallium polar GaN/sapphire, with 2D electron concentration $N_{2DEG} = 4.6 \cdot 10^{12}$ cm^{-2}, and slightly lower RT mobility $\mu_{2DEG} = 1840$ cm^2/Vs, has been fabricated as well. The epitaxial growth was performed on commonly used in PAMBE (0001) GaN/sapphire MOVPE heterosubstrates. The epistructure C was very similar to epistructure A grown on freestanding (0001) GaN, it means it contained 25 nm AlGaN layer with 15% aluminum. However, due to higher threading dislocation density, of the order of $5 \cdot 10^8$ cm^{-2}, the value of normalized leakage current measured at -1 V was more than three orders of magnitude higher in comparison to similar devices fabricated on freestanding GaN.

The comparison of current-voltage characteristics of both types of diodes is presented in Fig. 2. In comparison to vertical diodes, lateral Schottky barrier diodes have lower turn-on voltage due to the lower barrier height. At high forward voltage the current voltage characteristics are linear with the differential resistance determined by the resistance of the ohmic contacts. It was found that the contact resistance increased with the increase of the Al mole fraction in the AlGaN layer. As a result epistructure B with higher Al mole fraction had higher series resistance in spite of higher electron sheet concentration in it. An appropriate solution of this issue could be the regrown n+ GaN ohmic contact [5], which is commonly used for RF transistors nowadays.

The resistance measurements between ohmic contacts of two isolated devices and measurements of subthreshold characteristics of transistors on the same structures showed that the resistance of the insulating GaN layer is very high (see Table I). This led us to the conclusion that GaN layer does not contribute to the characteristics of lateral Schottky diodes.

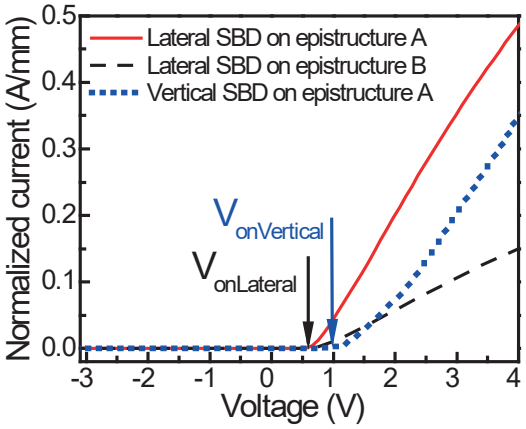

Fig. 2. (Color online) Current-voltage characteristics of lateral and vertical Schottky diodes fabricated on MBE grown 2DEG epitaxial structures. Solid lines show data for lateral devices fabricated on the base of epistructure A (red solid line) and B (black dashed line) with $N_{2DEG} = 4.6 \cdot 10^{12}$ cm^{-2} and $N_{2DEG} = 1 \cdot 10^{13}$ cm^{-2}, respectively. The blue dotted line shows data for the vertical Schottky diode fabricated on epistructure A. Arrows show how the turn-on voltages $V_{onLateral}$ and $V_{onVertical}$ were defined.

The reverse current-voltage characteristics for two different devices fabricated on two epistructures A and B are presented in Fig. 3. Despite of the significant differences in electron sheet concentrations in both structures, the reverse currents ≤ 1 µA/mm have been measured. This very small reverse leakage current at RT indicates a high quality of the Schottky contact, proper device geometry, high quality processing and low defect concentration in the active part of the device.

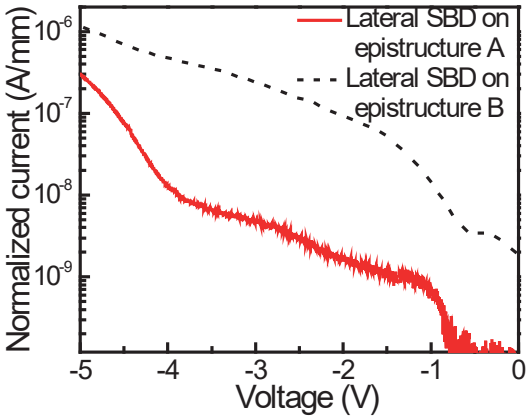

Fig. 3. (Color online) Normalized reverse current-voltage characteristics of lateral Schottky barrier diodes fabricated on two different epitaxial structures (epistructure A and epistructure B, with electron sheet concentration $N_{2DEG} = 4.6 \cdot 10^{12}$ cm^{-2} and $N_{2DEG} = 1 \cdot 10^{13}$ cm^{-2}, respectively).

The results of the measurements at high revers voltage are presented in Fig. 4. As seen, for both lateral

and vertical devices, the breakdown voltage reaches ~-90 V which is five times higher than 18 V reported in ref. [6] The compared in Fig. 4 lateral and vertical devices were fabricated in the same processing and using very similar layouts. We believe that non passivated surface between contacts limited the breakdown voltage for both structures (see Fig. 1).

The detection experiment was performed using a 140 GHz Aerfortis IMPATT source modulated by TTL signal from the lock-in amplifier SR830. The detected signal was amplified by the EG&G5113 low noise preamplifier, which was set to gain 5. The 140 GHz source was equipped with a horn antenna and a lens, which focused the ~ 40 mW signal down to the spot size ~ 0.25 cm^2. During our measurements, the estimated power density was 150 mW/cm^2 at the plane of device. The detection measurements were performed on the wafer using probe station Cascade EPS150CoaxPlus and Keithley SMU 2400 at room temperature. Our preliminary results of the detection on lateral Schottky diodes are presented in Fig. 4. The maximum of the detected signal is for the voltage V = 0.05-0.2 V, which corresponds to the exponential part of the current-voltage characteristic (see Fig. 4). We suppose that small forward voltage decreases the input capacitance and therefore enhances the response. This detection experiment, which was done on the detector sample grown by MBE on the GaN/sapphire substrate, showed surprisingly high responsivity of detected signal. We still expect even better THz detector properties, in a case of devices grown on freestanding substrates. Further THz detection and low frequency noise analysis will be the subject of forthcoming future works.

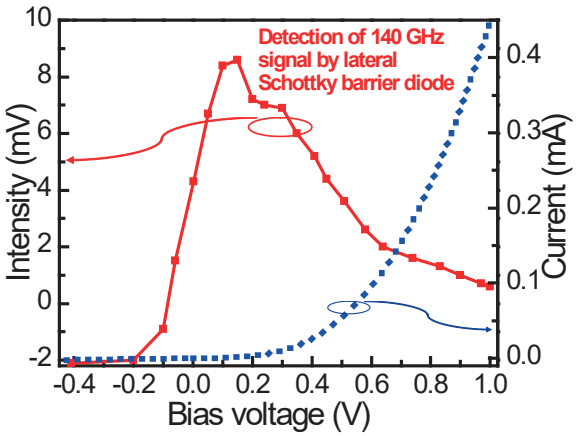

Fig. 4. (Color online) The example of detection performed on lateral Schottky diode (epistructure C) at 140 GHz. The signal was acquired as the function of DC biasing of the diode. The blue dotted line shows the corresponding current-voltage characteristic of this lateral SBD.

The selected SBD devices were bonded into holders and measured in an open space sub-THz setup equipped with the tunable VDI source. The spectral range of this measurement was 110-170 GHz. Our typical photoresponse of lateral SBDs is presented in Fig. 5. The spectral photoresponse for lateral SBD detectors exhibits characteristic spectral pattern for this type of experiments, which is related to the signal reflections and standing wave phenomena in the device substrate.

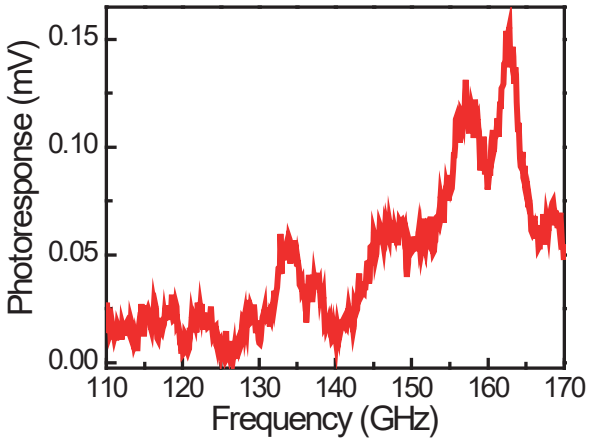

Fig. 5. The example of detection performed on lateral Schottky diode (epistructure C) bonded into a holder. The signal was acquired at 0.4 V forward bias of the lateral SBD.

Because of the layout geometry of lateral SBD and geometry of bond connectors one can expect significant angular dependence of its photoresponse. Our measurements at selected frequencies confirm strong angular dependence of photoresponse, which seems to be related to the elongated Schottky contact to 2DEG at the edge of the device mesa. The example of results of the angular dependence taken at 156 GHz is presented in Fig. 6. The results of this measurements are in good agreement with simulations done for the linear polarization.

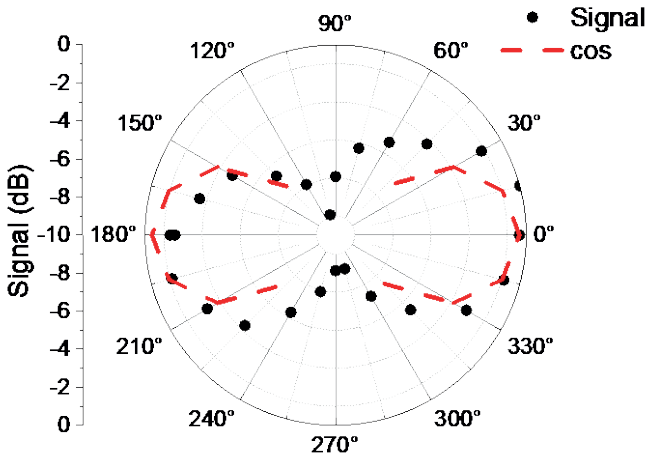

Fig. 6. The angular dependence of the 156 GHz signal detected using lateral Schottky diode bonded into holder. Dots and dash line correspond to experimental results and prediction for the linear polarization, respectively.

SUMMARY AND CONCLUSIONS

We report successful fabrication of lateral Schottky diodes based on MBE epistructures. Our approach was to use high quality 2DEG epilayers, with highly resistive

adjacent layers. The high quality epistructures were grown on freestanding gallium polar GaN substrates. The performed DC test measurements, breakdown voltage, and low frequency noise investigations confirm high quality of epitaxial material and processing. In the case of SBD devices, which contained 25% of aluminum in epilayer, we found significant increase of differential resistance at on-state, which is attributed to the dependence of ohmic contact resistance on the Al mole fraction. The obtained normalized reverse currents did not exceed 1 μA/mm and breakdown voltage was around -90 V. Extremely low reverse leakage currents, for devices grown on freestanding GaN, is the fingerprint of high quality of adjacent layers and very good insulation to the RI and to the substrate. As expected in the lateral Schottky diode case the turn-on voltage, in the lateral Schottky diodes was lower than in vertical ones due to the lower barrier height. These parameters are of high importance for future nitride device development. The first trial of detection experiment at 140 GHz, which was performed on the test detector device on GaN/sapphire, showed very high responsivity of detected signal. The bonded lateral SBD were measured at 110-170 GHz and experiments showed typical photoresponse and its angular dependence. These results show high potential of GaN/AlGaN lateral Schottky diodes for sub-THz and THz detectors.

ACKNOWLEDGMENTS

This project was partially supported by the National Science Centre, Poland allocated on the basis of Grant No. 2016/22/ E/ST7/00526, by the ERANET RUS PLUS–TERASENS project, and by the Foundation for Polish Science through grants TEAM/2016-3/25, TEAM/2016-3/26 and MAB/2018/9 (the latter for ‘Center for Terahertz Research and Applications (CENTERA)’ project, carried out within the ‘International Research Agendas’ programme co-financed by the European Union under the European Regional Development Fund.)

REFERENCES

[1] Y. Saitoh et al., Applied Physics Express 3 (2010) 081001
[2] M. Zhu, et al., IEEE ELECTRON DEVICE LETTERS, 36, NO. 4, APRIL 2015
[3] W. C. Peatman, et al., EEE Electron Device Lett., vol. 13, no. 1, pp. 11–13, Jan. 1992.
[4] D. Veksler, et al., GaN Heterodimensional Schottky Diode for THz Detection, The 5th IEEE conference on sensors, Oct.20-25, 2006, Daegu, Korea.
[5] F. A. Faria, J. Guo, P. Zhao, G. Li, P. K. Kandaswamy, M. Wistey, H. Xing, and D. Jena, Appl. Phys. 101, 032109 (2012).
[6]K. Shinohara, D. C. Regan, Y. Tang, A. L., D. F. Brown, J. C. Wong, J. F. Robinson, H. H. Fung, A. Schmitz, T. C. Oh, S. J. Kim, P. S. Chen, and R. G. Nagele, A. D. Margomenos, M. Micovic, IEEE Transactions on Electron Devices 60, 2982 (2013).

Noise Characterization of GaN/AlGaN High Electron Mobility Transistors

P. Sai[1,2], J. Jorudas[3], M. Dub[2,4], M. Sakowicz[4], D. B. But[1,2], P. Prystawko[4], G. Cywinski[1,5], I. Kašalynas[3], W. Knap[1,5,6], and S. Rumyantsev[1]

[1] CENTERA Laboratories, Institute of High Pressure Physics PAS, ul. Sokołowska 29/37, 01-142, Warsaw, Poland

[2] V. Ye. Lashkaryov Institute of Semiconductor Physics, National Academy of Sciences of Ukraine, 41 pr. Nauki, 03680, Kyiv, Ukraine

[3] Terahertz Photonics Laboratory, Center for Physical Sciences and Technology (FTMC), Saulėtekio al. 3, LT-10257 Vilnius, Lithuania

[4] Institute of High Pressure Physics PAS, ul. Sokołowska 29/37, 01-142, Warsaw, Poland

[5] CEZAMAT, Warsaw University of Technology, 02-822, Warsaw, Poland

[6] Laboratoire Charles Coulomb, University of Montpellier and CNRS UMR 5221, 34950, Montpellier, France

E-mail: psai@unipress.waw.pl

Abstract – We report experimental results on the low-frequency noise in high electron mobility transistors with different channel geometry fabricated based on GaN/AlGaN heterostructure. The effective density of traps responsible for noise is found to be below 10^{19}cm^{-3} for some of the wafers. This trap density is of the same order of magnitude as that reported in Si MOSFETs with high-k dielectric.

Keywords – GaN/AlGaN, HEMT, FinFET, EdgeFET, effective trap density

I. Introduction

High electron mobility transistors (HEMTs) are the key elements of high frequency electronics. The operation frequency of these devices extends up to a terahertz frequency range. GaN/AlGaN devices are attractive for these high frequency applications because of their excellent material properties: high breakdown robustness, radiation hardness and ability to form a very high concentration two dimensional electron gas (2DEG) with high mobility at the GaN/AlGaN interface [1]. High electron concentration, exceeding 10^{13} cm^{-2} on the GaN/AlGaN interface provides very small series resistance in these structures.

In this work we studied electrical and noise properties of three different kinds of transistors: i) regular top gate HEMTs, ii) FinFets, and iii) EdgeFETs.

FinFET design provides high cut-off frequency and suppressed short channel effects [2,3]. The design of the channel in the form of fin allows also to fabricate gate with the Schottky barrier formed only on the edges of the 2DEG channel (EdgeFET). This approach has an advantage of extremely small gate capacitance $C < 0.2$ fF/μm [4,5]. The design of the lateral Schottky contact directly to the edge of the 2DEG channel was proposed and studied based on AlGaAs/InGaAs/GaAs system in 1990s [6-9].

This kind of GaN/AlGaN field effect transistors with two gates formed only on the edges of the 2DEG channel (EdgeFET) were studied recently in a few publications [5,10,11]. EdgeFET geometry allows to form wire channel transistor by applying gate voltage which is beneficial for the purpose of terahertz applications.

The level of the low-frequency noise is one of the important parameters, which determines whether the devices are suitable for high frequency application.

II. Experimental details

The GaN/AlGaN structures were grown by the Metalorganic Vapour Phase Epitaxy (MOVPE) method in a closed coupled showerhead 3x2 inch Aixtron reactor on sapphire and SiC substrates. The epistructures were grown on high-resistivity GaN:C buffer formed either on c-axis sapphire (Al_2O_3) or on semi-insulating (SI) 6H poly-type SiC substrate by the metalorganic chemical vapor deposition (MOCVD) method. The sequence of layers and their parameters are shown in Table 1. The molar fraction, x, of Al content and the thickness of the $Al_xGa_{1-x}N$ barrier were obtained from X-ray diffraction measurements.

The shallow mesas were etched down to 150 nm to separate devices in cases of FinFETs and EdgeFETs.

For HEMTs a specific transistor design was chosen in order to avoid the mesa etching step and minimize the process flow to two photo-lithography procedures. In this design, a square-shaped drain contact is surrounded by rectangular double gate and double source electrodes. Optical microscope pictures of the transistor and its main dimensions are shown in the insert in Fig.1. The Ohmic and Schottky contacts were fabricated using the Ti/Al/Ni/Au and Ni/Au metal stacks, respectively.

The noise spectra were measured as a function of the applied voltage at room temperature on wafer using a probe station. The voltage fluctuations, S_v, from load resistance $R_L = 1\text{-}10$ kΩ were analyzed with a dynamic signal analyzer. The short-circuit current fluctuations were calculated in the usual way as $S_I = S_v[(R_L+R_D)/(R_L R_D)]^2$,

where R_D is the differential diode resistance obtained from the experimental current-voltage characteristic.

Table 1. Nominal thickness and some other parameters of epilayers.

Wafer Layer	#TG2196	#Hx2688	#Hx2991	#Hx3875
GaN cap	no	2 nm	2 nm	2 nm
$Al_xGa_{1-x}N$	25 nm	19 nm	25 nm	25 nm
barrier	x = 0.20	x = 0.25	x = 0.15	x = 0.15
UID-GaN	500 nm	1000 nm	700 nm	1250 nm
GaN:C	1000 nm	1300 nm	1000 nm	650 nm
Substrate	Al_2O_3	SiC	Al_2O_3	SiC

III. RESULTS AND DISCUSSIONS

A. HEMTs

GaN/AlGaN HEMTs were characterized by ~6 orders of magnitude on/off ratio and small gate leakage current. The subthreshold slope was within the range of $\eta = 1.5$-2. The noise spectra had the form of $1/f^{\alpha}$ noise with $\alpha = 0.95$-1.05 without noticeable contribution of the generation-recombination noise. In the linear regime the spectral noise density of the drain current fluctuations, S_I, was always proportional to current squared. The dependences of noise on the gate voltage swing $(V_g - V_t)$ in the linear regime at frequency $f = 10$ Hz for the representative devices are shown in Fig.1 (V_t and V_g are the threshold voltage and gate voltage, respectively). They have the usual shape for FETs. At high gate voltage, noise slightly increases with the gate voltage increase manifesting the contribution of the contact noise. At lower gate voltage, noise decreases with the gate voltage increase steeper than $1/(V_g - V_t)^2$. Although McWhorter model predicts the $1/(V_g - V_t)^2$ slope, the steeper dependences are often observed. There are several possible reasons for that. First, is the influence of the drain and source access resistances. Second, is the dependence of the trap density on energy. Correlated mobility fluctuations might also contribute to noise and change the slope.

In the McWhorter model, the spectral noise density of the drain current fluctuations S_I/I^2 is given by [12]

$$S_V = \frac{kTN_t q^2}{\gamma f W L_g C^2}, \qquad (1)$$

where $S_V = (S_I/I^2)/(g_m/I)^2$, k is the Boltzmann constant, T is the temperature, q is the electron charge, N_t is the effective trap density, f is the frequency, WL_g is the channel area, C is the gate capacitance per unit area, g_m is the external transconductance, and γ is the attenuation coefficient of the electron wave function under the barrier, usually taken equal to 10^8 cm^{-1}.

Figure 2 shows the gate voltage dependence of the effective trap density for the HEMTs fabricated on different epitaxial structures and calculated using Eq. (1). At high gate voltage, the trap density in studied GaN/AlGaN HEMTs is below 10^{19} eV^{-1}cm^{-3} (see Fig.2). Similar or higher values of the effective trap density are often found in Si MOSFETs with high-k dielectric [14,15].

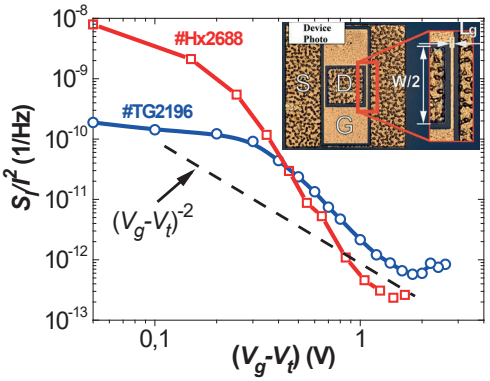

Fig. 1. Dependences of noise on the gate voltage swing $(V_g - V_t)$ for the representative HEMTs; $f = 10$ Hz; device photo is present on the insert, where S – sourse, D – drain, G – gate, $W = 200$ μm – channel width, $L_g = 2$ μm – gate length.

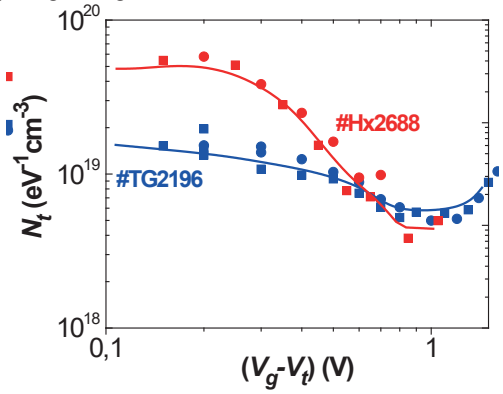

Fig. 2. Effective trap density N_t as a function of the gate voltage swing $(V_g - V_t)$ for HEMTs.

B. FinFETs

Figure 3 compares the dependence of noise on the gate voltage for FinFETs fabricated on sapphire and SiC substrates.

FinFETs on SiC substrate are characterized by the smaller noise level (Fig.3). For all devices, the relative spectral noise density of the drain current fluctuations decreases with gate voltage increase with the slope close to $1/(V_g - V_t)^2$. It is known that at high gate voltage this dependence in some cases may become flat. Absence of this behavior in the studied devices indicates negligible contribution of the contact noise.

Following the same algorithm, that was done for HEMTs, we extracted the effective trap density in FinFETs (Fig.4). As seen, the effective trap density for the device on SiC substrate is smaller than that for sapphire substrate. The trap density in SiC substrate device is below 10^{19} eV^{-1}cm^{-3} that indicates high quality of FinFETs. In the case of sapphire substrate two reasons might cause the dependence of noise on the gate voltage: contribution of the mobility fluctuations or dependence of the trap density in the barrier layer on energy.

C. EdgeFETs

Overall, FinFETs and EdgeFETs demonstrated similar current-voltage characteristics, in spite of different physics of their operation: above threshold, gate voltage in FinFETs drives the channel concentration; in EdgeFETs gate voltage affects the channel thickness keeping the

concentration virtually constant [10]. This allows forming a nanowire, which should be beneficial for resonant terahertz detection.

Figure 5 shows the dependence of the relative spectral noise density on the gate voltage for two EdgeFETs on sapphire and SiC substrates. As seen from the comparison with Fig.4, EdgeFETs are characterized by higher noise level than FinFETs. Interface state on the open (not covered with the metal) surface of the fin may contribute to the noise in these devices.

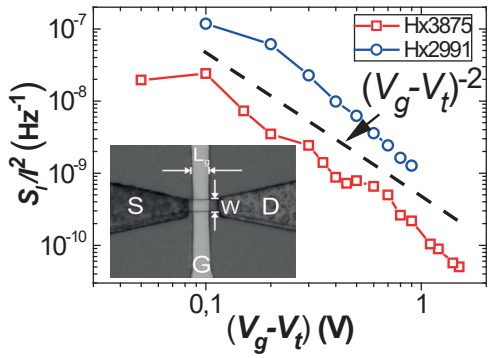

Fig. 3. Dependences of noise on the gate voltage swing ($V_g - V_t$) for the FinFETs; f = 10Hz; device photo is present on the insert, where S – sourse, D – drain, G – gate, W = 4 μm – channel width, L_g = 4 μm – gate length.

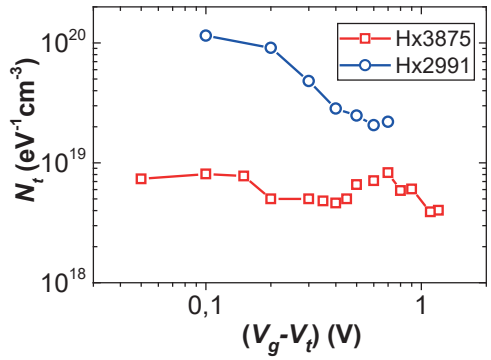

Fig. 4. Effective trap density N_t as a function of the gate voltage swing ($V_g - V_t$) for FinFETs.

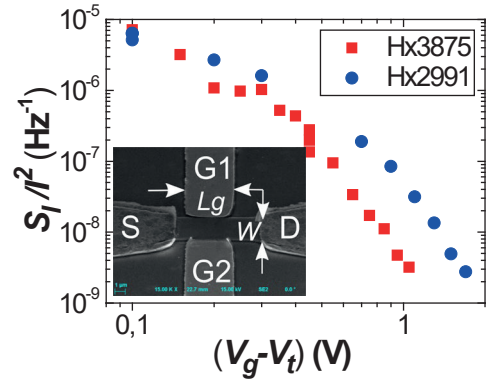

Fig. 5. Dependences of noise on the gate voltage swing ($V_g - V_t$) for the EdgeFETs; f = 10 Hz; device photo is present on the insert, where S – sourse, D – drain, G1 and G2 – first and second gates, W = 4 μm – channel width, L_g = 4 μm – gate length.

IV. Conclusions

We conducted low frequency noise investigation of different types of GaN/AlGaN transistors with two dimensional electron gas in the channel. The effective trap density was extracted from low frequency noise measurement.

The effective trap density in GaN/AlGaN HEMTs and FinFETs can be below 10^{19} eV^{-1}cm^{-3}, which is of the same order of magnitude as in Si MOSFETs with high-k dielectric.

Only EdgeFETs are characterized by considerably higher noise level. Interface state on the open (not covered with the metal) surface of the fin may contribute to the noise in these devices.

Acknowledgments

The work was supported by the 'International Research Agendas' program of the Foundation for Polish Science co-financed by the European Union under the European Regional Development Fund (MAB/2018/9) and by the National Science Centre, Poland allocated on the basis of Grants Nos. 2016/22/E/ST7/00526 and UMO-2017/27/L/ST7/03283. The research at the Terahertz Photonics Laboratory at Vilnius was supported by the Research Council of Lithuania (Lietuvos mokslo taryba) under the "TERAGANWIRE" project (Grant no. S-LL-19-1).

References

[1] L. M. Tolbert, B. Ozpineci, S. K. Islam, and M. S. Chinthavali, *Semiconductors* **1**, 3 (2003).
[2] W. Xing, Z. Liu, H. Qiu, G. I. Ng, and T. Palacios, *IEEE Electron Device Letters* **38**, 619-622 (2017).
[3] Y. He, C. Wang, M. Mi, M. Zhang, Q. Zhu, P. Zhang, *et al.*, *Applied Physics Express* **10**, 056502 (2017).
[4] S. Petrosyan and A. Y. Shik, *Zh. Eksp. Teor. Fiz* **69**, 1261 (1989).
[5] K. Shinohara, D. C. Regan, Y. Tang, A. L. Corrion, D. F. Brown, J. C. Wong, *et al.*, *IEEE Transactions on Electron Devices* **60**, 2982-2996 (2013).
[6] W. C. B. Peatman, T. W. Crowe, and M. Shur, *IEEE Electron Device Letters* **13**, 11-13 (1992).
[7] M. Shur, W. Peatman, H. Park, W. Grimm, and M. Hurt, *Solid-state electronics* **38**, 1727-1730 (1995).
[8] M. Levinshtein, S. L. Rumyantsev, G. Simin, H. Park, W. Peatman, and M. Shur, *Applied physics letters* **68**, 3138-3140 (1996).
[9] B. Gelmont, W. Peatman, and M. Shur, *Journal of Vacuum Science & Technology B* **11**, 1670-1674 (1993).
[10] G. Cywiński, I. Yahniuk, P. Kruszewski, M. Grabowski, K. Nowakowski-Szkudlarek, P. Prystawko, *et al.*, *Applied Physics Letters* **112**, 133502 (2018).
[11] P. Sai, D. But, I. Yahniuk, M. Grabowski, M. Sakowicz, P. Kruszewski, *et al.*, *Semiconductor Science and Technology* **34**, 024002 (2018).
[12] A. McWhorter, *Semiconductor surface physics* (Univerisity of Pennsylvania Press, Philadelphia, 1957).
[13] M. Shur, *Physics of Semiconductor Devices*, (Inc., Englewood Cliffs, New Jersey, 1990).
[14] E. Simoen, A. Mercha, L. Pantisano, C. Claeys, and E. Young, *IEEE transactions on electron devices* **51**, 780-784 (2004).
[15] P. Magnone, F. Crupi, G. Giusi, C. Pace, E. Simoen, C. Claeys, *et al.*, *IEEE Transactions on Device and Materials Reliability* **9**, 180-189 (2009).

W.Knap

CENTERA Laboratories – International Research Agenda 2018-2023

The enormous potential carried by both the basic science and applications identified and already partially exploited in the THz field during the last 20 years, has established a Terahertz-related science and technology as an important axis unifying efforts of a large scientific community, similarly to Quantum Computing and Spintronics, bridging the optronics and electronics communities.

The main goal of CENTERA project is to create a specialized, world-class, interdisciplinary research unit in Poland, a Center for Terahertz Research and Applications (CENTERA). CENTERA offers an original inter-disciplinary approach to implement Terahertz science and technology to the benefit of the society. The activity of CENTERA is carried out by 5 interacting groups working in the following domains: i) Solid State Physics (THz plasma instabilities in semiconductor-based low dimensional systems and topological insulators – WG1); ii) Biology and Medicine (Terahertz signatures of the proteins binding heavy metals in plants and food and THz spectroscopy for diagnosis of cancerous and burned tissue - WG2); iii) Electronics (exploration of high-frequency limits of Field Effect Transistors (FETs), Heterojunction Bipolar Transistors (HBTs) and nano-antennas towards THz-Integrated-Circuit Electronics - WG3 and WG4) and iv) THz applications (patents, demonstrators, technology drivers, and technology transfer - WG5). CENTERA is a unique research agenda in bringing inter-disciplinary research teams into a single center with a main objective to promote and incorporate THz science and applications in the society. It will gain from the synergy between the mentioned working groups, which will generate breakthrough scientific results not possible to obtain in a single laboratory or scientific group. This presentation will present basic ideas and achievements of CENTERA.

Developing, Understanding and Functionalizing Topological Materials at MagTop

T. Wojtowicz[1], T. Story[1,2], A. Wiśniewski[1,2], T. Dietl[1]
[1] International Research Centre MagTop, Institute of Physics, Polish Academy of Sciences, Warsaw, Poland
[2] Institute of Physics, Polish Academy of Sciences, Warsaw, Poland

E-mail: wojto@MagTop.ifpan.edu.pl

After presenting the project goals in the context of the outstanding and surprising properties of topological matter, we will outline the way we pursue in order to develop new material systems, assess their structural and chemical characteristics, fabricate functional nanostructures, and perform experimental studies under extreme conditions, such as measurements at temperatures below 1 K. The particular steps involve the methods of molecular beam epitaxy, various forms of nanolithography, advanced electron microscopy and synchrotron radiation studies revealing details of atom arrangements and corresponding spectra of electron energies, and electrical transport studies at low temperatures and high magnetic fields. We will then show some examples of progress achieved so far including results indication emergence of topological signatures in our topological materials.

Keywords – topological materials, molecular beam epitaxy

PolFEL – a tunable source of THz radiation

K. Szamota- Leandersson[1], R. Nietubyć[1], P. Czuma[1], P. Krawczyk[1], J. Lorkiewicz[1], N. Pałka[2], J. Sekutowicz[1,3], M. Staszczak[1], J. Szewiński[1], P. Zagrajek[2]
[1] National Centre for Nuclear Research, Świerk, Otwock, Poland
[2] Institute of Optoelectronics, Military University of Technology, Warsaw, Poland
[3] Deutsches Elektronen Synchrotron, Hamburg, Germany

E-mail: r.nietubycs@ncbj.gov.pl

Abstract – Preparation to a construction of PolFEL free electron laser facility was launched in 2018 at NCBJ Świerk. It will be furnished with continues wave operating linear accelerator based on TESLA type superconducting resonant cavities and fully superconducting electron injector. The use of such an injector pertains to the flexible time pulse pattern and constitutes a novelty desired by the experimentalists. PolFEL will be a tunable source of electromagnetic radiation ranged from THz to VUV. THz radiation will be generated in a superradiant undulator settled behind the IR undulators. Preliminary evaluations showed that radiation in the range from 0.5 to 3 THz will be emitted in about 3 µJ pulses with 50 kHz repetition rate. The beam will be delivered to the dedicated laboratory consisted of diagnostic, spectroscopic and imaging sections, to where an auxiliary laser beam will be brought for pump and probe experiments with few picoseconds jitter. Pulse after pulse beam diagnostics and measurements in cryogenic temperatures and high magnetic field will be enabled.

Keywords – free electron laser, terahertz sources, time domain spectroscopy, wavelength tunability

I. Introduction

A desirability of free electron lasers as sources of THz radiation comes from its ability to generate radiation in the so called THz gap region of the electromagnetic spectrum. Radiation emission from the free relativistic electrons for which a continuum energy states is available makes FELs tunable emit radiation in the range between 0.5 THz and 3 THz, unreachable for optically pumped lasers.

II. PolFEL overview

In PolFEL Electrons will be emitted from all superconducting RF electron gun and accelerated in 8 superconducting PolFEL linear accelerator will provide electron beam with the energy ranging up to 200 MeV [1].

TESLA – type resonators structures installed in 4 cryomodules (Fig.1). The beam is shaped as a continues train of bunches with repetition rate tuned from single shot up to 50 kHz. Electromagnetic field frequency will on line tuned over the mentioned range. Next to the second section the linac splits in VUV and THz-IR branches, each furnished with a dedicated undulators. Maximal electrons energy in THz-IR branch will be 80 MeV. Electron will be led to the IR and THz undulators alternatively. IR undulators are settled prior to THz one. They will be retracted out of the beam tract while THz operation. THz undulators will be built based on permanent magnet Bazin design [2]. Two modules will be installed, each having 4 periods of 17.5 cm length.

Beam dynamical calculations allow to assume the electron bunch charge up to 250 pC and length 100 µm. For long wavelength part of the energy range that allows for a superradiant mode of operation in which the bunch length is significantly shorter than the emitted radiation and behaves similarly to the single multiply charged electron. That radically boosts the pulse energy as the intensity of emitted radiation depends on charge square. Preliminary evaluation of radiation properties has been performed based on analytical for formulas. Results are presented in Tab. 1

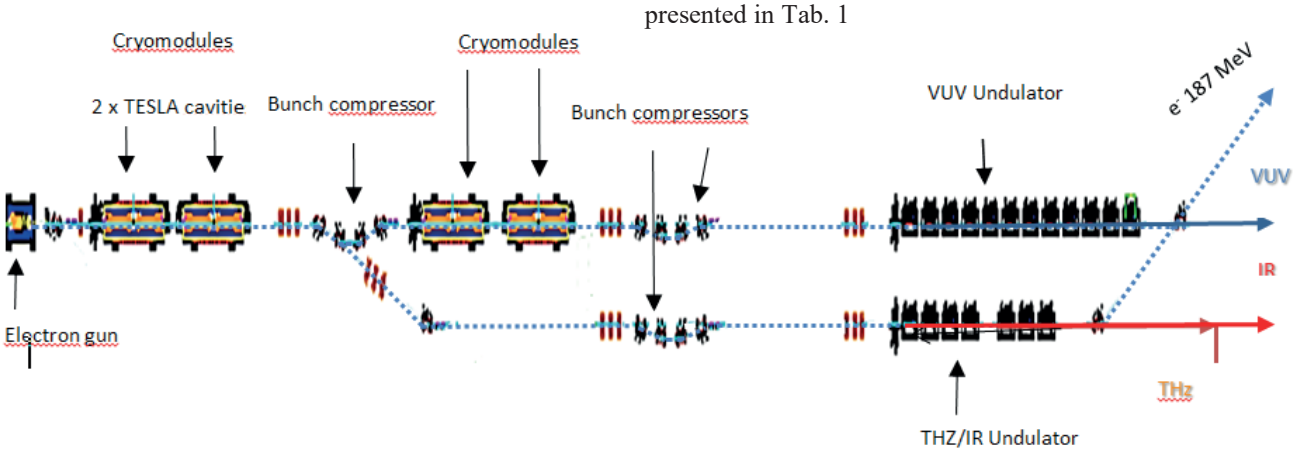

Fig. 1. PolFEL layout

Table 1.Preliminarly evaluated beam parameters pulse energy E_p, divergence Θ and pulse duration τ for various electromagnetic field frequencies f

f [THz]	E_p[μJ]	Θ [mrad]	τ [ps]
0.5	3.0	40	24
1.0	3.4	30	16
2.0	3.0	20	4
3.0	2.1	16	2.5

III. THz LINE

Terahertz radiation beam will be decoupled from the electron one and transmitted in nitrogen environment to the laboratory hall by means of a system om toroidal, golden, 6 inches, mirrors. On-line diagnostics will be performed with probe beam split out at a diamond Brewster mirror. Pulse energy, energy density profile, pulse duration and wavelength will be recorded for consecutive pulses (Fig. 2).

Measurement setups dedicated for pump and probe, spectroscopic and imaging experiments will be built. FEL beam will be crossed with a beam from an axillary solid state laser. On line jitter correction scheme will be applied to facilitate time domain spectroscopic measurements (Fig. 3). THz laboratory will be furnished with a instrumentation essential for beam interaction with sample registration: beam path optics, detectors, cameras, spectrometers, experimental chamber and gases distribution system.

Sample will be installed in dry nitrogen environment at a liquid helium cooled holder which enables temperature control down to few Kelvins. Superconducting magnet will be used to apply magnetic field up to 9 T.

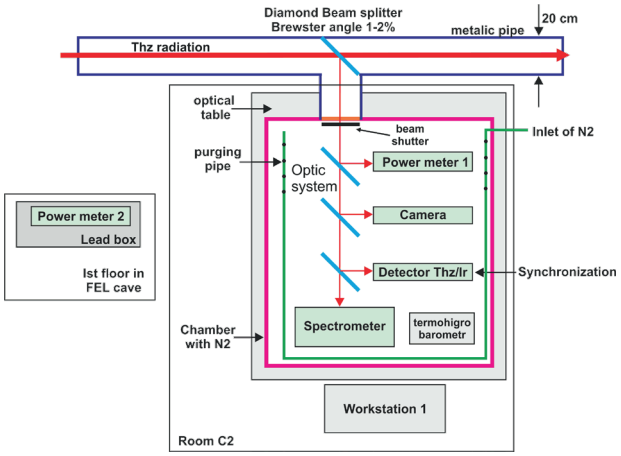

Fig. 2. Scheme of the THz diagnostic station

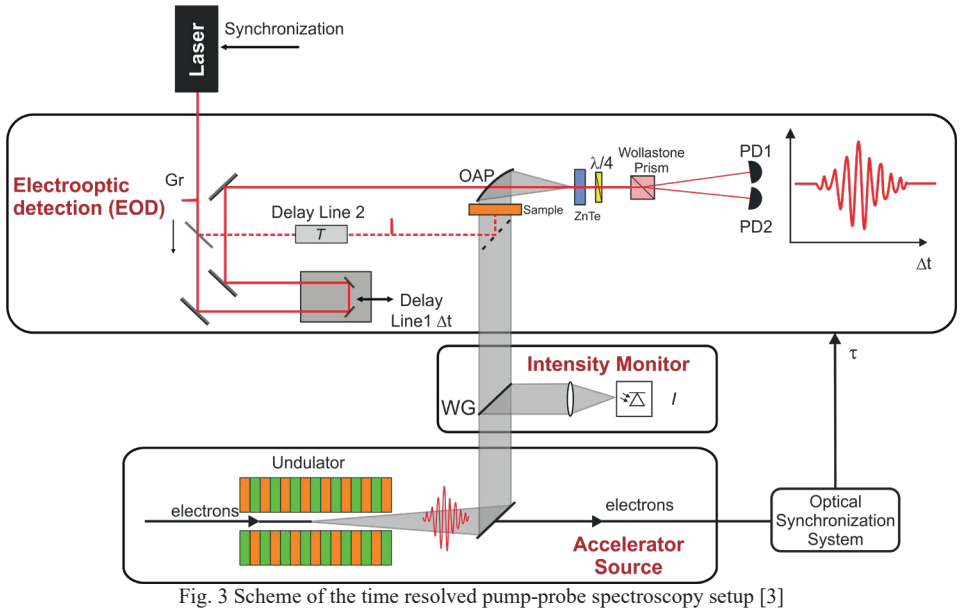

Fig. 3 Scheme of the time resolved pump-probe spectroscopy setup [3]

IV. SUMMARY

Further development of the experimental setup is foreseen adequately to the scientific case proposed by the users. A wide range of topics is expected from fundamental issues of radiation interaction with matter, through solid state physics to applied materials science. Separate optical laboratories will be established for the use of VUV radiation and for biological studies. Electron beam will be used for neutrons and femtosecond pulses of x-ray generation.

PolFEL will be an user facility, access to which is open for Polish and overseas scientists and granted based on scientific criteria. A part of beam time is dedicated for industrial applications. Besides radiation physics users operation, PolFEL constitutes an accelerator physics laboratory and combines the wide experience of Polish laboratories gained in large international particles acceleration and synchrotron radiation projects. It will be furnished with a number of worldwide unique solutions

developed thereby mostly associated with continues wave operation of RF linac.

REFERENCES

[1] J. Sekutowicz, P. Czuma; P. Krawczyk; K. Kurek; J. Lorkiewicz; R. Nietubyć; J. Poliński; M. Staszczak; K. Szamota-Leandersson; J. Szewiński, „Polish free electron laser: short technical description" Proc. SPIE 11054, Superconductivity and Particle Accelerators 2018, 1105405 (2019).

[2] M. Pedrozzi, M. Calvi, R. Ischebeck, S. Reiche, C. Vicario, B. D. Fell, N. Thompson, „The Laser Heater System Of SwissFEL, Proceedings of FEL 2014 Conference THP059.

[3] S. Kovalev, B. Green, T. Golz, S. Maehrlein, N. Stojanovic, A. S. Fisher, T. Kampfrath, and M. Gensch, "Probing ultra-fast processes with high dynamic range at 4th-generation light sources: Arrival time and intensity binning at unprecedented repetition rates", Structural Dynamics 4, 024301 (2017).

Juliette Mangeney (LPA-Paris)

Title: THz excited state level spacing in encapsulated graphene quantum dots

Abstract : We report a high-quality encapsulated graphene quantum dot that exhibits stable Coulomb diamonds and excited states with a spacing of 0.4 THz. We performed the first transport spectroscopy measurement under THz illumination of a large quantum dot. The photocurrent map allows to measure with high precision a non-linear chemical potential renormalization of the graphene electrodes via the interaction with the quantum dot states.

Dr. Sukhdeep Dhillon
Laboratoire de Physique de l'Ecole Normale Supérieure
24 rue Lhomond
75231 Paris Cedex 05, France
Sukhdeep Dhillon <Sukhdeep.Dhillon@lpa.ens.fr>

Quantum Cascade Lasers: From Modelocking to THz non-linear optics

The Quantum Cascade Laser is the semiconductor solution to realise laser action over the entire mid-infrared to the terahertz (THz) regions of the electromagnetic spectrum. This has led to a mini-revolution in these spectral domains with novel and new applications, such as highly sensitive spectroscopy and non-destructive imaging. In this work I will present how new and recent functionalities that can be introduced using the inherent properties of QCLs i) Ultrashort pulse generation via active and passive modelocking of THz QCLs [1,2], illustrating how the ultrafast dynamics are not a hindrance for the generation of short THz pulses; and ii) Up-conversion of MIR and THz QCL emission into the telecom range without consideration of phase matching [3,4], opening up perspectives in a sensitive probe of complex THz bandstructures, as well as QCL stabilization and locking using telecom technology.

[1] F. Wang, H. Nong, T. Fobbe, V. Pistore, S. Houver, S. Markmann, N. Jukam, M. Amanti, C. Sirtori, S. Moumdji, R. Colombelli, L. Li, E. Linfield, G. Davies, J. Mangeney, J. Tignon, and S. Dhillon, "Short Terahertz Pulse Generation from a Dispersion Compensated Modelocked Semiconductor Laser", Laser Photonics Rev. **11**, 1700013 (2017).
[2] F. Wang, V. Pistore, M. Riesch, H. Nong, P-B. Vigneron, R. Colombelli, O. Parillaud, J. Mangeney, J. Tignon, C. Jirauschek, and S. S. Dhillon " Ultrafast Response of Active and Self-starting Harmonic Modelocked THz Laser", submitted (2019).
[3] S. Houver, A. Lebreton, A. Mottaghizadeh, M. I. Amanti, C. Sirtori, G. Beaudoin, I. Sagnes, O. Parillaud, R. Colombelli, J. Mangeney, R. Ferreira, J. Tignon, and S. S. Dhillon, ACS Photonics **5**, 890 (2018).
[4] S. Houver, A. Lebreton, T. A. S. Pereira, G. Xu, R. Colombelli, I. Kundu, L. H. Li, E. H. Linfield, A. G. Davies, J. Mangeney, J. Tignon, R. Ferreira, S. S. Dhillon, " Giant optical nonlinearity interferences in quantum structures" Science Advances (accepted).

Fine study of zero-mode Landau levels in HgTe quantum wells

Frederic Teppe

Laboratoire Charles Coulomb (L2C), UMR CNRS 5221, GIS-TERALAB, Université de Montpellier, 34095, Montpellier, France

(e-mail: frederic.teppe@umontpellier.fr)

The most efficient way to discriminate trivial and inverted band ordering in HgTe/CdHgTe QWs is to probe evolution of a particular pair of zero-mode Landau levels (LLs) under applied magnetic field [1]. These zero-mode LLs split from the edges of $E1$ and $H1$ subbands and have pure electron-like and hole-like origin, respectively. The electron-like LL always tends toward high energies, while the energy of the zero-mode LL from the $H1$ subband decreases with magnetic field. In inverted HgTe QWs, the zero-mode LLs cross at a critical magnetic field B_c, above which the inverted band ordering transforms into the trivial one [1].

The presence of bulk inversion asymmetry (BIA) [2] in the unit cell of zinc-blend materials and interface inversion asymmetry (IIA) at the HgTe/CdHgTe heterojunction [3] induces the anticrossing of zero-mode LLs in the vicinity of B_c. So far, experimental values of anticrossing gap Δ arising in the vicinity of B_c obtained by different techniques differ significantly from each others. Particularly, the measurements of magnetotransport [4,5] performed with the gated Hall bars show that the anticrossing gap is small. On the contrary, far-infrared magnetospectroscopy reveals a fine structure of the strong absorption lines, corresponding to the α and β transitions from the zero-mode LLs [6,7]. Analysis of this fine structure in the vicinity of B_c within the Dirac-like model including BIA and IIA gives Δ~5 meV for the joint effect. Thus, the controversial experimental values of the anticrossing gap obtained in magnetotransport and magnetospectroscopy produce a lot of speculations on the actual strength of BIA and IIA in HgTe QWs.

In my talk, I will present recent experimental results obtained by far-infrared magnetospectroscopy in Montpellier. Particularly, we focused on the evolution of optical transitions from the zero-mode LLs in inverted HgTe QWs at different electron concentration varied by persistent photoconductivity effect. By fitting the difference in the transition energies in the vicinity of critical magnetic field B_c with an analytical expression including BIA and IIA, we extract the band-gap and anticrossing gap Δ from our experimental data. Unexpected strong dependence of the band-gap and Δ on the electron concentration clearly evidences that electron-electron interaction affects the LL transitions beyond the single-particle picture. This paves the way towards clarifying the key reason for controversial conclusions on the strength of BIA and IIA in HgTe QWs obtained by magnetotransport and magnetospectroscopy.

[1] M. Konig et al., Science **318**, 766 (2007).

[2] C. Liu et al., Phys. Rev. Lett. **100**, 236601 (2008).

[3] M. V. Durnev and S. A. Tarasenko, Phys. Rev. B **93**, 075434 (2016).

[4] B. Buttner et al., Nat. Phys. **7**, 418 (2011).

[5] A. M. Kadykov et al., Phys. Rev. Lett. **120**, 086401 (2018).
[6] M. Orlita et al., Phys. Rev. B **83**, 115307 (2011).
[7] M. Zholudev et al., Phys. Rev. B **86**, 205420 (2012).

From: Jeremie Torres <jeremie.torres@umontpellier.fr>

Title: Toward a new scheme of communications between proteins

Abstract: Self-organization of living organisms presents an astonishing complexity and efficiency. More specifically, biological systems are the site of a huge number of very specific reactions that require the right biomolecule to be at the right place, in the right order and in a reasonably short time to sustain cellular function and ultimately cellular life. This efficiency could be explained by the possibility that biomolecules interact through long-range electromagnetic interactions resulting in oscillations of the total electric dipole moment. In this presentation, after an overview of the main characteristics and applications of terahertz waves, we will discuss about the possibility of detection of long-range electromagnetic interactions between proteins.

Reconfigurable Antennas based on S-PIN diodes

Y. Yashchyshyn[1,2]

[1] Institute of Radioelectronics and Multimedia Technology, Warsaw University of Technology, Warsaw, Poland
E-mail: e.jaszczyszyn@ire.pw.edu.pl
[2] CENTERA, Institute of High Pressure Physics PAS, Warsaw, Poland

Abstract – Reconfiguration of the antenna's aperture can be achieved in many ways including mechanical, electronical, optical or magnetical methods. Electrical methods are typically based on PIN diodes, however, surface PIN (S-PIN) diodes have recently attracted a lot of attention in the scientific community. S-PIN diodes can be used to achieve a discrete reconfiguration of: frequency, polarization, or radiation pattern of the antenna. This communication discusses parameters of S-PIN diodes and their suitability for reconfigurable antennas operating in millimeter wave band.

Keywords – adaptive beamswitching, surface P-i-N diodes

I. Introduction

The beamforming is the main function of smart antenna system. In general, a smart antenna system may make use a fixed beamforming network, an adaptive array antenna, or both [1]. Adaptive array antennas can adjust their pattern to enhance the desired signal, reduce interference, and collect correlated multipath power. In smart antenna systems which use only the fixed beamforming network, a switch is used to select the best beam to receive a particular signal. The switched beamforming is relatively simple to implement, requiring only a beamforming network, an RF switch, and control logic to select a particular beam.

Beamforming increases antenna gain in the direction of a desired transmitter, simultaneously placing a null in the direction of interfering sources. Fundamental concepts, functionality, and design applications at the system level may be divided into three types of antenna beamforming types.

The first type is a baseband beamforming. One of the biggest challenges of this approach is utilization of power-hungry converters (both analog to digital and digital to analog). This high-power requirement will increase hardware complexity and power consumption of the system and makes this architecture impractical for these types of designs. Digital beamforming is used in expensive military equipment and base station.

The second type is an RF beamforming. This concept is based on modification of phase and amplitude of RF signals at the antenna level. The main problem with this type is a limited performance of phase shifters, especially variation of amplitude and phase versus frequency, and variation of phase versus the control voltage.

The third type is a hybrid beamforming. which combines advantages of both analog and digital beamforming systems. The total number of RF chains with power consuming ADC/DAC converters is reduced by incorporation of phase-shifters. Hybrid beamforming is a tradeoff between the baseband beamforming and the RF beamforming.

II. Beam-steering by Reconfiguration

Reconfiguration is another approach for beamforming. Instead of employing a complex system composed of an antenna array and phase shifters or ADCs, only one aperture is used and can be modified to obtain required frequency, gain, direction of radiation, or polarization. In general, reconfiguration of the antenna is achieved by dynamic modification of surface currents of an aperture. The most common techniques are based on switching, structural modifications or material tuning.

The reconfiguration of the aperture may be used in some applications, especially in low cost solutions. There are four main methods of changing the antenna's beam in reconfiguration systems: electronic, e.g. by using PIN diodes, or surface PIN (S-PIN) diodes; mechanical/electromechanical, e.g. by using micro-electro-mechanical systems (MEMS) switches; optical, e.g. by using photosensitive devices; electrical/magnetic, e.g. by using special substrate media such as controllable materials (ferroelectrics, liquid crystal and ferrite).

Moreover, a hybrid approach combining two or more of mechanisms is also very useful. Considering the properties of a base design, reconfigurable antennas can be classified according to the continuity of reconfiguration, which is defined by the reconfiguration mechanism:

- continuous reconfiguration within a range of parameters,
- discrete - a finite number of reconfigured states.

Different types of reconfigurable antennas employ a distinct mechanism e.g. photonic, MEMS or solid state switches; although the most popular technique for antenna reconfiguration is a discrete reconfiguration based on switchable elements. It relies on switches embedded in the antenna's aperture that are controlled by DC bias signals. The main role of the switch is to short or break an electrical connection between conductive parts of the antenna. In this way switches can be used to control flow of the RF power over different parts of the aperture. Typically, this may include changing arrangement of paths in a feeding network, closing and opening slots in a waveguide, or changing shape or radiating elements. Electronic switches are usually PIN diodes, S-PIN diodes or GaAs FET switches. Selection of the switching element used in the

reconfigurable antenna should consider electrical parameters such as rise/fall time of the RF signal, isolation, input impedance, losses and maximum input power. Other characteristics as control mechanism, packaging, and cost should be considers as well. Even if it is not relevant at low frequencies, it very important at the RF frequency to consider parasitic capacitance and inductance introduced by switches. which may severely affect performance of the antenna. The aperture can be reconfigured to alter operating parameters, e.g. impedance bandwidth, , polarization, radiation pattern. as well as the antenna feed and, in the case of arrays, any power distribution network.

III. S-PIN Diodes for Silicon Monolithic Reconfigurable Antennas

Conventional method of the aperture reconfiguration can be achieved by the opening or closing different connections between some or all conductive areas on the aperture by means of many switches [2]. The most advanced method of the aperture reconfiguration consist in temporary formation of plasma regions with fairly high electrical conductivity placed at the surface of the silicon device. In this case, the key reconfigurable element is a surface PIN diode (S-PIN, [3]). Such a semiconductor device, when activated, should limit the carrier injection into a small volume near the surface of the device. Then, in the ON state, the S-PIN diode represents a layer of highly conductive material. The resistance of an activated S-PIN device depends on a level of the forward current and the carrier lifetime at the plasma region. The long lifetime can be easily achieved in the highly resistive floating zone (FZ) silicon wafer. The reason for using silicon substrates is that silicon has good temperature and mechanical properties, and there are several foundries offering customized silicon technology.

Contrary to a conventional PIN diode an S-PIN diode structure is lateral. It is a very simple semiconductor device. Similarly to the bulk PIN, it requires only two regions: n^+ and p^+ embedded in a highly resistive substrate with metal contacts. A silicon dioxide layer passivates silicon surface and a phosphorous-doped silica glass (PSG) layer has been used in our case to protect ready device from moisture. The technological process is fairly uncomplicated. Most of the technological operations are the same as in the case of a standard silicon technology.

In the OFF state, i.e. not biased, the S-PIN device offers a high resistance of the area between the doped regions. Contrary, it is characterized by a low resistance of the plasma of injected carriers in the surface area, when the diode is strongly biased in the forward direction. At the forward bias a ΔW wide slot in metallization is short-circuited by the conducting plasma of carriers.

The plasma should be conductive enough that it becomes equivalent to a quasi-metallic layer. It is also required, in many applications, that the metal contacts, used for biasing the diode, should be as small as possible. In order to be used at microwave and millimeter wave ranges, the S-PIN diode has to provide a possibility of the dynamic switching between OFF and ON states.

For the application under consideration, the injected carriers should be sufficiently confined to a zone between the anode and cathode of the S-PIN. The size of the conducting plasma area and the concentration of carriers have to be optimized for keeping the carriers in the defined volume with a sufficiently high concentration, while the supplied current should be reasonably minimized. Essentially, the thickness of the plasma region must not be smaller than 2-3 skin depths [4]. It was mentioned that the conductivity of the activated S-PIN diode depends on the lifetime of the carriers, which, in turn, depends on its initial value (order of a millisecond for FZ high resistivity silicon substrates) and usually it is considerably degraded during the process of fabrication. Some literature studies [4] showed that for a forward current of 20 mA a carrier concentration of 10^{18}-10^{19}/cm^3 might be achieved for a 50 μm wide diode.

As it was proved, taking into consideration the microwave losses, SOI substrates should behave much better. An SOI wafer consists of a monocrystalline Si film over an insulating layer of SiO_2 (called buried oxide layer) on a Si substrate (called sometimes a handle wafer since for most of the applications it plays only a mechanical role). The buried oxide (BOX) entirely isolates the lower part of the SOI wafer from the carriers injected by the S-PIN diode. Therefore, the bottom silicon layer, if the SOI substrate has been fabricated from high-resistive silicon, behaves like a dielectric, while the upper layer conductivity depends on the bias of S-PINs. Such a device is shown in Fig. 1. In this case, all injected carriers are confined into the top silicon layer, and their density is higher than in the case of their bulk counterparts and the DC current to get similar carrier density is significantly lower.

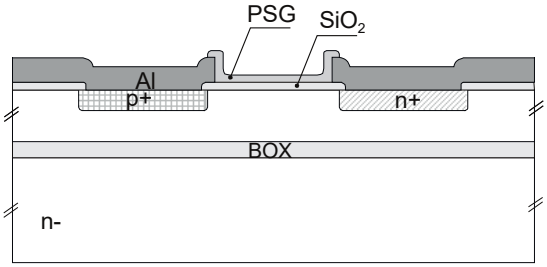

Fig. 1. S-PIN diode realized on SOI

In the case of the SOI S-PIN diode the BOX layer is a barrier for the injected carriers. Hence the carrier density above the BOX is high (even slightly higher than in the bulk device), while the carrier density below the BOX, at a depth of 5 μm, results only from the field effect and is much lower. As a consequence, the Si area below the BOX behaves like an insulating, low-loss medium [5].

IV. Reconfigurable Antennas Based on S-PIN Diodes

First antenna based on the reconfigurable aperture with S-PIN diodes for 17-34 GHz range was presented in [6]. The aperture is consisted of 64 inclined slots with embedded surface diodes (Fig. 2). Each element can be excited by means of an electromagnetic field existing in a waveguide, therefore generation of many different radiation patterns is possible. Additionally, operating frequency can also be selected remaining radiation in the same or similar direction. The main disadvantage of the proposed antenna is relatively low maximum efficiency. For the center frequency efficiency is approximately 20%.

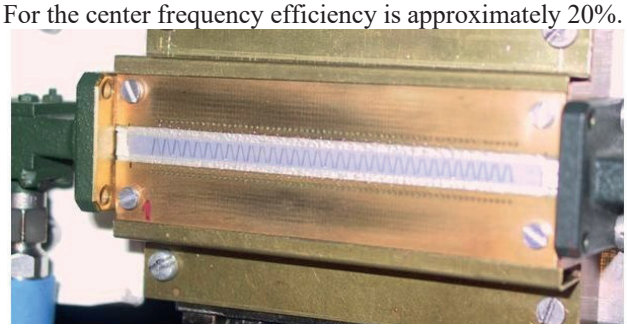

Fig. 2. Example of reconfigurable antenna with 64 inclined slots

Another application of the waveguide slot antenna with semiconductor reconfigurable structure was described in [7]. The antenna was designed for implementing a spatial multiplexing of local element (SMILE) technique. Thus, only four independent slots (or pair of slots) were used. In this case all slots are arranged in a row along the SOI device as presented in Fig. 3. By switching the states of the antenna and combining the phase-shifted signals received during particular states, baseband beamforming was achieved. It was also shown that the antenna can be used to increase the signal-to-noise-and-interference ratio (SINR) in the mm-wave communication system.

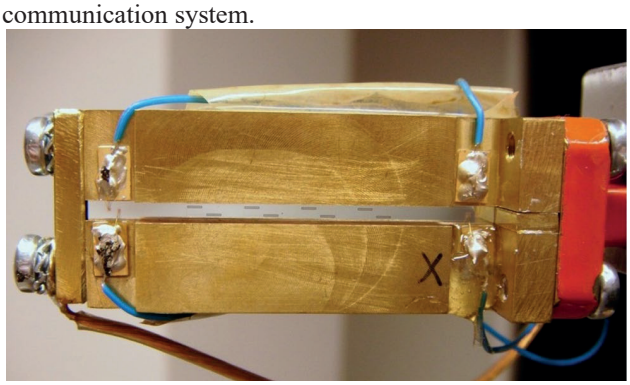

Fig. 3. Reconfigurable antenna based on a spatial multiplexing of local elements for 36 GHz

However, the performance of the system is limited because only one slot (or one pair) radiates during each state.

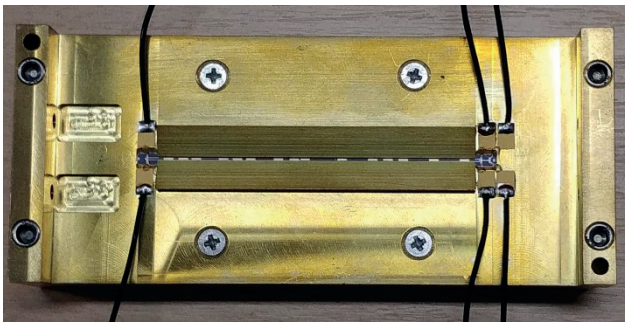

Fig. 4. 28 GHz switched-beam antenna for 5G mobile communications

The reconfigurable semiconductor circuit with S-PIN diodes is presented in Fig. 4 and can also be used to develop a switched-beam antenna. Example of such antenna was presented in [8]. The reconfigurable semiconductor circuit has fifteen slots. Slots are grouped to achieve three configurations. Three, five, and nine slots are used to generate beams directed towards 0º, 30º, and 45º, respectively.

REFERENCES

[1] J.-F. Kiang, Novel Technologies for Microwave and Millimeter-Wave Applications, Springer, 2013.

[2] L. N. Pringle, P. H. Harms, S. P. Blalock, and all, “A Reconfigurable Aperture Antenna Based on Switched Links Between Electrically Small Metallic Patches”, *IEEE Trans. Antenna and Propag*., vol. AP-52, no. 6, pp. 1434 – 1445, June, 2004.

[3] G. C. Taylor, A. Rosen, E. Fathy, P. K. Swain, S. M. Perlow, “Surface PIN device”, U. S. Patent no.: US 6,617,670 B2, Sep., 9, 2003.

[4] A. Fathy, A. Rosen, H. Owen, F. McGinty and all, “Silicon-based Reconfigurable Antennas - Concepts, Analysis, Implementation, and Feasibility”, *IEEE Trans. Microwave Theory and Thech.*, vol. 51, no. 6, pp.1650 – 1661, June, 2003.

[5] Y. Yashchyshyn, J. Marczewski, and D. Tomaszewski, “Investigation of the S-PIN Diodes for Silicon Monolithic Antennas With Reconfigurable Aperture,” *IEEE Transactions on Microwave Theory and Techniques*, vol. 58, no. 5, pp. 1100–1106, May 2010.

[6] Y. Yashchyshyn, J. Marczewski, K. Derzakowski, J. W. Modelski, and P. B. Grabiec, “Development and Investigation of an antenna system with reconfigurable aperture,” *IEEE Trans. Antennas Propag*, vol. 57, no. 1, pp. 2–8, Jan. 2009.

[7] Y. Yashchyshyn, K. Derzakowski, P. R. Bajurko, J. Marczewski, and S. Kozłowski, “Time-Modulated Reconfigurable Antenna Based on Integrated S-PIN Diodes for mm-Wave Communication Systems,” *IEEE Trans. Antennas Propag.*, vol. 63, no. 9, pp. 4121–4131, Sep. 2015.

[8] Y. Yashchyshyn, K. Derzakowski, G. Bogdan, K. Godziszewski, D. Nyzovets, C. H. Kim, and B. Park, “28 GHz Switched-Beam Antenna Based on S-PIN Diodes for 5G Mobile Communications,” *IEEE Antennas Wireless Propag. Lett.*, vol. 16, 2017. Accepted for publication.

Terahertz Diffractive Structures in Application for Skin Cancer Diagnosis

A. Siemion[1], P. Komorowski[2], M. Surma[1], I. Ducin[1], P. Sobotka[1], M. Walczakowski[3], M. Sypek[4], E. Czerwińska[3],

[1] Faculty of Physics, Warsaw University of Technology, Warsaw, Poland
[2] Institute of Microelectronics and Optoelectronics, Warsaw University of Technology, Warsaw, Poland
[3] Institute of Optoelectronics, Military University of Technology, Warsaw, Poland
[4] Orteh Company, Warsaw, Poland

E-mail: agnieszka.siemion@pw.edu.pl

Abstract – This work is aimed at designing, manufacturing and implementing of diffractive optical element, which illuminates sample with terahertz beam and focuses the reflected radiation on the detector. Structures are designed to be universal and work with most of available THz sources. The ultimate goal is to non-invasively detect tumorous changes on human skin. First, elements have been designed, manufactured and evaluated. Obtained results prove the concept and effectiveness of the method and will be preliminary verified by measuring simple samples.

Keywords – terahertz radiation, diffractive optical element, cancer detection

I. Introduction

Every year in Europe thousands of people die from diagnosed melanoma and therefore quick and early detection becomes crucial [1]. The aim of the T-SKIN project (Project financed by the National Center for Research and Development under the Lider programme) is to create diffraction based optical structures for examination of reflection from healthy skin and cancer tissues for effective detection of skin cancer.

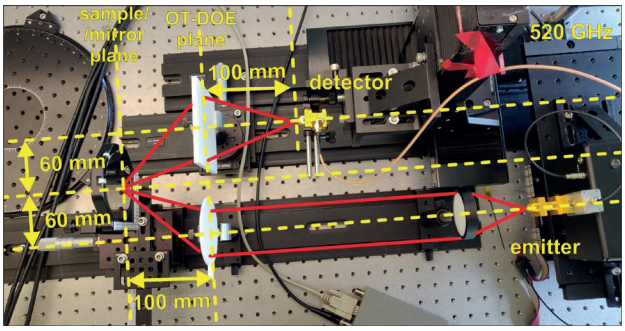

Figure 1 The experimental setup with marked optical paths, used elements and distances (OT-DOE – Optimized THz DOE). Structures were designed for 520 GHz.

II. Setup configuration

Proposed diffractive structures have been designed to work in the setup presented in Figure 1. Quasi-point terahertz radiation source is placed 200 mm before the collimating lens, which results with the beam of Gaussian shape in the amplitude but constant phase (quasi-plane wave). The designed structure can be found afterwards, focusing the radiation on the sample in off-axis configuration as well as gathering back the reflected radiation and focusing it on the detector.

III. Design algorithm

A set of diffractive optical elements has been numerically calculated by means of light propagation in the Fresnel region [3] and the Gerchberg-Saxton algorithm [4]. The optimized THz diffractive optical element (OT-DOE) consists of two parts: emitter lens and detector lens, realizing the optical setup illustrated in Figure 1. Initial field is assumed as quasi-plane wave - a THz source is located at a distance f before the collimating lens (having the focal length f = 75 mm and diameter d = 50 mm). These two elements are additionally shifted 60 mm from the main optical axis of the setup in order to obtain off-axis focusing with respect to the center of the first lens (and source of the radiation). Next, the iterative part of algorithm begins. In each step four main operations are performed: (1) propagation from the OT-DOE plane to the focal point, (2) overwriting amplitude with desired, (3) back-propagation to the plane of the OT-DOE, (4) overwriting amplitude with amplitude of the input light field distribution. Final phase distribution defines diffractive lens, capable of off-axis focusing at designed distance and wavelength (called emitter lens). Detector lens is designed simply by a mirror reflection of emitter lens, summed with on-axis converging lens to perform additional focusing.

The design frequency was chosen to be 520 GHz to be able to work within the regime of detecting difference between healthy and cancer skin tissues [5-6]. While the absorption coefficient is linearly increasing with the frequency (from approx. 0.3 THz) for healthy and cancerous skin, the refractive index value differs. The biggest difference was denoted for 500 GHz [5], where it was equal almost to 3%. Frequencies from the 350-550 GHz range have very similar and high difference. Moreover, 520 GHz was one of the emission peaks for

the used source (VDI WM-380 (WR-1.5) – working in the 500-750 GHz range) and thus was chosen as design frequency.

The sampling was 117 µm x 117 µm to assure good manufacturing resolution. The calculation matrix size was 4096 x 4096 pixels, which corresponded to the area of approximately 480 mm x 480 mm.

Numerical simulations were carried out in the LightSword 6.0 software accessible in the Laboratory of Optical Information Processing at the Faculty of Physics in Warsaw University of Technology.

IV. EVALUATION

Designed DOEs have been manufactured using additive manufacturing (3D printing) by selective laser sintering (SLS) method. The performance of the whole OT-DOE has been evaluated experimentally in the setup presented in Figure 1 with Schottky diodes with frequency multipliers used as a source and as a detector of terahertz radiation. A refractive HDPE lens (f = 75 mm, d = 50 mm) was used to form a quasi-plane wave. After verifying spot sizes at sample and detector planes two simple samples were examined.

The first sample was a flat polyamide plate with aluminum foil on its surface divided into two half planes placed 1, 3 and 6 mm apart from each other. The values registered on the detector while scanning along direction perpendicular to the slit is shown in Figure 2.

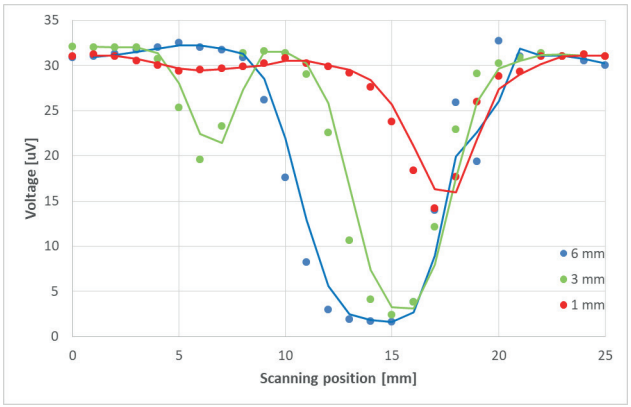

Figure 2 The voltage values corresponding to the power registered by the detector in relation to the position in sample plane (perpendicular to the mail optical axis of the system). The sample was a flat polyamide plate with aluminum foil on its surface divided into two half planes placed 1, 3 and 6 mm apart from each other.

The signal from the aluminum foil is at the same level as for the reference mirror. When slit is 6 mm wide, the signal reflected from the sample (Fig. 2 – marked with blue) decreases significantly to approx. 4-5% of the initial signal. It is consistent with the theory, because polyamide has the refractive index value around 1.5, and then Fresnel losses (which means the reflection from the polyamide surface) are around 4-5%. In case of the smallest slit (1 mm) it is seen that the signal does not decrease to the desired value. This limits the resolution of such system to 2-3 mm. In the simplest case it can be reduced by minimizing the focal length of emitter and detector lenses.

The second sample consisted a block of PMMA with 5-mm-thick stripe of PA12 material. Both these materials have the refractive indices close to 1.6 and they vary less than 1.5%, which is approx. 2 times smaller than the difference between healthy and cancer skin tissues. The result of scanning 20-mm-wide block with 5-mm-thick stripe is shown in Figure 3. In the inset a photo of the sample is given. We can see small changes between these two materials, which allows to conclude that measurements carried out on skin tissues will also give good results. Here, the spot size is around 2 mm diameter, but can be minimized to assure better spatial resolution of scanned sample.

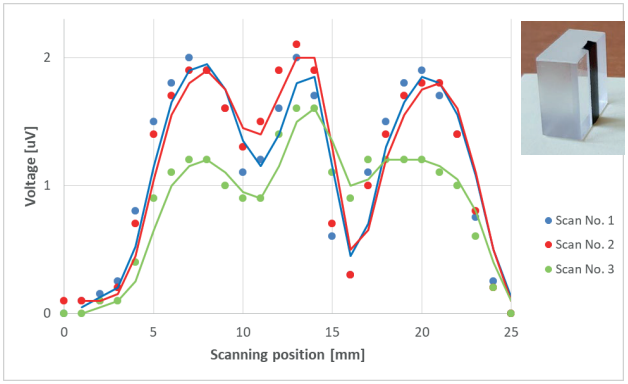

Figure 3 The voltage values corresponding to the power registered by the detector in relation to the position in sample plane (perpendicular to the mail optical axis of the system). The sample was a block of PMMA with 5-mm-thick stripe of PA12 material.

V. CONCLUSIONS

We have designed, manufactured and tested diffractive off-axis optical elements, capable of focusing THz radiation on the sample, as well as gathering the reflected radiation and focusing it back on the detector. The scans of simple samples allowed to determine the basic optical parameters that will allow to prepare a device able to non-invasively monitor human skin tissues. Plans for farther work include but are not limited to point by point scanning of wider samples and usage of detector matrix.

ACKNOWLEDGMENTS

Project financed by the National Center for Research and Development under the LIDER program - LIDER / 11/0036 / L-9/17 / NCBR / 2018.

The Authors would like to thank Orteh Company for providing LS 6.0 software used for designing and

modelling of diffractive optical elements and for enabling access to THz detector matrix.

REFERENCES

[1]. The Melanoma, a white paper: Reshaping EU Healthcare for Melanoma Patients (Brussels, 2012)

[2]. A. J. Fitzgerald, E. Pickwell-MacPherson and V. P. Wallace, "Use of finite difference time domain simulations and Debye theory for modelling the terahertz reflection response of normal and tumour breast tissue", PLoS One, 9(7), e99291 (2014).

[3] M. Sypek, "Light propagation in the Fresnel region. New numerical approach," Optics communications, 116(1-3), 43-48 (1995).

[4] R. W. Gerchberg and W. O. Saxton, "A practical algorithm for the determination of the phase from image and diffraction plane pictures," Optik 35, 237 (1972).

[5] V. Wallace, A. Fitzgerald, E. Pickwell, R. Pye, P. Taday, N. Flanagan, T. Ha, "Terahertz pulsed spectroscopy of human basal cell carcinoma". Applied spectroscopy 60(10), 1127-1133 (2006).

[6] E. Pickwell, A. Fitzgerald, B. Cole, P. Taday, R. Pye, T. Ha, M. Pepper, V. Wallace, "Simulating the response of terahertz radiation to basal cell carcinoma using ex vivo spectroscopy measurements," Journal of Biomedical Optics, 10(6), 064021 (2005).

Security applications of terahertz radiation

N. Palka
Institute of Optoelectronics, Military University of Technology, Warsaw, Poland

E-mail: norbert.palka@wat.edu.pl

Abstract – The exceptional properties of terahertz waves create hope of developing novel technologies to respond to security threats associated with the wave of terrorism. In this presentation, at the beginning results of general studies on interaction of THz waves with explosive and explosive related materials using Time Domain Spectroscopy technique. We investigated transmission and reflection spectral characteristic of commonly used explosives, insensitive explosives, perspective explosives as well as influence of a sample surface and its shape on the reflectance and the phase difference. We show the p-spectrum method which was developed for identification of materials covered with a few layers of semi-transparent materials like paper, polyethylene foils etc. Last part of the presentation focuses on detection of dangerous body born IEDs by means of terahertz cameras and portals.

Keywords – security, terahertz radiation, spectroscopy

I. INTRODUCTION

Due to low photon energy, terahertz radiation is non-ionising and, therefore, is safe for humans, which is crucial for development of any security system. THz radiation penetrates through most non-metallic and non-polar substances such as paper, cardboard, plastic, clothes and ceramics. Attenuation of these materials increases for higher frequencies (1). Many substances, including explosive materials (such as Hexogen (RDX), Octogen (HMX), Trinitrotoluene (TNT) and Penthrite (PETN)) have characteristic absorption features above 0.5 THz. These "spectral fingerprints" result from vibrations and interactions between molecules (2–3). So, the operation range for the identification of concealed explosives should be between 0.7 (first peak of RDX) and 2.5 THz.

The basis of operation of active body scanners detecting suspicious objects (e.g. weapons, bombs) under clothing is the fact, that THz waves perfectly reflect from metal objects with reflectivity above 0.995 (4–5). However, the fact that the human body is usually hotter than the hidden items and has different emissivity is the basis of passive screening systems [5]. The very high attenuation of the atmosphere related to the presence of many absorption lines for water vapour presents a serious limitation for THz wave propagation over long distances (6). Some narrowband THz systems operates in transmission windows in the vicinity of: 100, 250, 340, 420, 670, 850 GHz and higher (7).

There are three main terahertz security system groups designed for identification of dangerous materials, detection of dangerous objects hidden under clothing on the human body as well as detection of these objects inside mail and baggage.

The first group consists of solutions for the identification of hazardous materials. The explosives and drugs can be hidden in letters or packages. The process of assigning an unknown substance to individual classes (e.g. dangerous, non-dangerous) or even indication of a specific material from the database is known as identification. Consequently, a powder in an envelope can be distinguished a dangerous material or a harmless substance. The identification process is usually based on the spectral characteristic of materials, signal conditioning and processing, as well as advanced algorithms for identification (8–9). The identification can be performed in situ, when a suspicious sample is placed inside the scanner and is analysed both in transmission and in reflection configurations. More interesting, but also challenging, is the stand-off detection case with a few metres' distance between the scanner and the object, where water vapour highly attenuates the radiation (10–11). Although there is a need for the ready-to-use systems, there are few in situ solutions, which work in limited scenarios (12–14).

The security scanners present regions with higher/lower attenuation in the transmission image of the examined mail or baggage. Currently, a few companies offers ready-to use security scanners [15–17]. The image can reveal the shape of a hidden element like a knife, scissors, wires connected to a small bomb. Obviously, to identify the threat further examination is needed. Similar shape-based principle of operation is applied in x-ray scanners.

The people screening technology (body scanners), due to strong demand from airport and critical infrastructure operators as well as military needs, has been successfully developed and has many implementations (18–22). Body scanners examine people and reveal objects hidden under clothing. Further analysis is also required to confirm a threat. This group consists of portals and short-range systems, where a traveller is scanned from both or one sides, respectively, as well as stand-off cameras, which can analyse people in motion from one side from the distance of up to 25 m (18, 23).

II. P-SPECTRUM METHOD

Time Domain Spectroscopy (TDS) is a commonly used technique for spectral characterization of materials. It bases on analysis of a very short (~1ps) impulses of electromagnetic radiation, which have very broad useful

bandwidth, usually 0.1-3.0 THz, and high sensitivity (up to 70 dB) [24].

Reflectance of the sample can be experimentally determined by division of the measured power spectrum, by a power spectrum from a gold mirror reference, measured in an otherwise identical fashion. The above mentioned explosives have rather small reflectance, about 2-10%, and the change in the reflectance in the regions of their spectral feature is about 5-10% [25] and decreases when the sample is not smooth (in case of pellets) or the grain of the powder is bigger than about 50-100 μm.

THz radiation can transmit through most of covering materials like plastic foils, paper, clothes, etc. If the covering layer is far from the sample (more than about 2 mm) it slightly modifies the reflectance of the measured materials. However, if the material is closer, we obtain two impulses – one reflected from the layer and the second – from the sample. In this case, spectrum of the impulse is heavily deformed and the spectral features of explosives are hard or impossible to identify. We report on a simple method which can identify hidden RDX-based explosives (pure and plastic ones). The method takes into account only part of the impulse reflected from the sample, which is next analyzed in frequency domain by Fast Fourier Transform.

III. Experiment

For the investigations we applied TPS 3000 Spectrometer (range 0.1-3.0 THz, dynamic 70 dB, 30 scans/second Fig. 1b) from Teraview in reflection configuration - so-called Stand-off unit. The measurements were carried out in an external free standing module with a fiber-fed emitter and detector (Fig. 1). THz beam by means of a set of mirrors was focused on the sample and after specular reflection was collected and focused on the detector. Samples were measured in the compartment purged with dry air (humidity about 1%) in the distance 30 cm between the sample and the mirrors. Incident angle was 7 degrees. The samples were placed on a horizontal stage with a micrometer screw. The measurement time was about one minute depending on averaging and length of the scan.

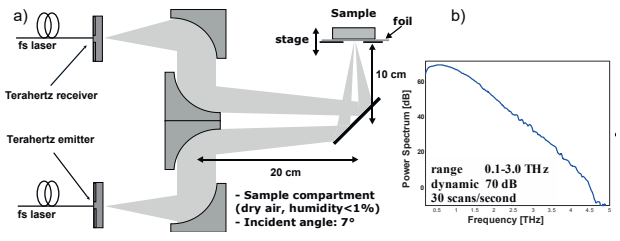

Fig. 1. Layout of the Stand-off unit (a) and power spectrum of the spectrometer (b)

For investigations, we used various samples with smooth surfaces: a pellet made of the pure RDX, a flat sample of a RDX-based plastic explosive and samples made of lactose and tartaric acid. The plastic explosive consists of RDX mixed with some plastic binder and plasticizer (similar to C4), which is easy to shape. The samples were covered with a thin Polyethylene (PE) foil.

III. Results and Discussion

The proposed method of identification of covered materials based on the fact that the TDS signal reflected from a covered sample consists of two peaks and some "waves" after the second peak, which carry the spectral information about the sample. FFT analysis of this part of the signal reveals spectral features of the sample. Figure 2a, b present the signal reflected from the smooth RDX sample (pellet) covered with the thin PE foil. The solid line represents part of the THz impulse (dashed line) which was analysis by FFT. The normalized power spectrum of this part of the impulse is shown in Fig. 2c. For comparison, we also present absorbance of the RDX, which was measured in a transmission TDS setup and has a maximum at 0.84 THz [4]. The agreement of the peak frequencies is very good.

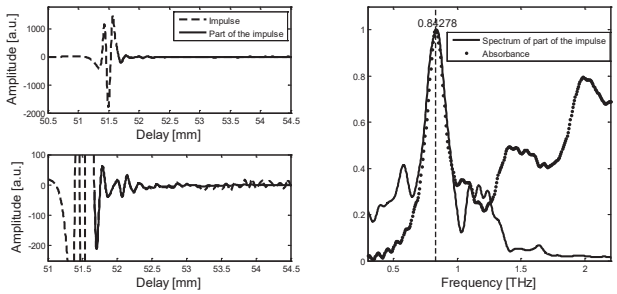

Fig. 2. THz impulse reflected from the RDX sample covered with the PE foil (a), zoom-in part of the Fig. 2b (b), and power spectrum of the part of the impulse compared to absorbance (c).

Figure 3 present the same analysis for the smooth uncovered RDX sample. Peak position is also in accordance with the transmission results.

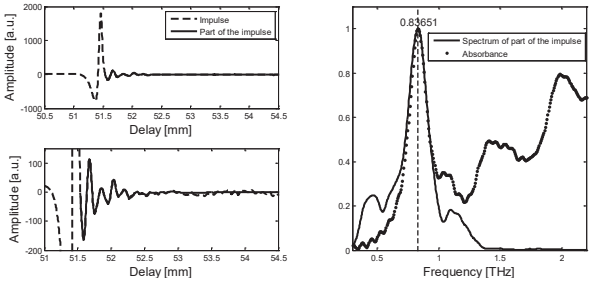

Fig. 3. THz impulse reflected from the uncovered RDX sample (a), zoom-in of the Fig. 2b (b), and power spectrum of the part of the impulse compared to absorbance (c).

In the same manner we analyzed the sample of the RDX-based plastic explosive which was covered with the thin foil. For various ten arrangements foil-sample we obtained different shapes of impulses (Fig. 4) and maxima of the peaks are in the range 0.835-0.865THz.

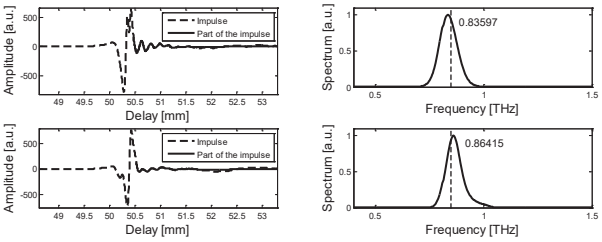

Fig. 4. THz impulses reflected from the RDX-based plastic explosive covered with the PE foil (left) and normalized power spectra of the part of the impulses (right).

Moreover, we applied sandpaper sheets with grit 120, 80 and 40 to extrude random rough surfaces on the samples. In this case, we also observed the right positions of the peaks with frequency fluctuation of about ±0.03 THz. The presented method is reference-free and it bases only on analysis of the signal reflected from the sample. The method is sensitive to atmospheric water vapour. Humidity of above 5% manifests as increase in level of "waves" after the main impulse and results in additional water peaks, which suppress the sample-related peaks. The method is restricted to frequencies of about 1.5 THz and other explosive materials with characteristic features in the THz range cannot be analyzed.

IV. People Scrrening

Terahertz systems for people screening have been strongly developing during the last 20 years. To provide a full image of a person, their desired field of view should be 1×2 m. The existing systems can be divided into three main groups: portals, short range and stand-off systems. Detection of small objects requires a resolution of about 1-2 cm. Portals detect mostly non-metallic weapons and suspicious packages concealed under clothing on a person and are commonly used at airports and critical infrastructure objects. The passenger is scanned for a few seconds with high resolution while he stands motionlessly on the designated spot with his hands raised up. The most widely deployed system is the L-3 ProVision portal (26). Other known systems include Rohde&Schwarz QPS (28) and Smiths eqo (27). Such systems usually operate below 94 GHz (29). Security imagers can be divided into active and passive systems. In active devices, an object is artificially illuminated by an emitter and the system measures a reflected radiation. Passive imagers are easier societally acceptable as noninvasive because they use natural radiation emitted by observed objects.

IV. Conclusions

Twenty years ago, it seemed that terahertz radiation would be easily applied for identification of concealed explosive materials.

However, both technical limitations and physical constraints critically verified this initial enthusiasm. Currently, the existing short-range systems can identify small quantities of dangerous materials in thin low-attenuating packages. However, the main challenge - stand-off operation, is still far away despite significant development of technology and new detection methods. Nevertheless, there is a hope that this goal will be implemented someday taking into account huge progress especially in tuneable QCL lasers (30).

On the other side, several companies have been offering relatively matured terahertz body scanners by for at least 15 years. Passive systems, especially with cooled FPA, have been growing tremendously over the past 10 years. It is believed, that someday current bulky deeply cooled systems will evolve into very sensitive portable palm-size devices.

References

[1] Gatesmana, A. J., Danylova, A., Goyettea, T. M., Dickinsona J. C., Gilesa, R. H., Goodhuea W., Waldmana J., Nixonb, W. E., Hoenc, W. (2006). Terahertz Behavior of Optical Components and Common Materials, Proc. SPIE., 6212, pp. 62120E-1- 62120E-12.

[2] Chen, J., Chen, Y., Znao, H., Bastiaans, G. J., Zhang, X. C. (2007). Absorption coefficients of selected explosives and related compounds in the range of 0.1-2.8 THz, Opt. Express, 15, pp. 12060-12067.

[3] Kemp, M. C., Taday, P., Cole, B. E., Cluff, J. A., Fitzgerald, A.J., Tribe, W.R. (2003). Security applications of terahertz technology, Proc. SPIE., pp. 44-52.

[4] Kemp, M. C. (2006). Millimetre Wave and Terahertz Technology for the Detection of Concealed Threats – A Review, Proc. SPIE, pp. 64020D 1-19.

[5] Petkie, D. T., Casto, C., De Lucia, F. C., Murrill, S. R., Redman, B., Espinola, R. L., Franck, C. C., Jacobs, E. L., Griffin, S. T., Halford, C. E., Reynolds, J., O'Brien, S., Tofsted, D. (2008). Active and passive imaging in the THz spectral region: phenomenology, dynamic range, modes, and illumination, J. Opt. Soc. Am. B, 25, pp. 1523-1531.

[6] Yang, Y., Shutler, A., Grischkowsky, D. (2011). Measurement of the transmission of the atmosphere from 0.2 to 2 THz, Opt. Express, 19, pp. 8830-8838.

[7] Melinger, J. S., Yang, Y., Mandehgar, M., Grischkowsky, D. (2012). THz detection of small molecule vapors in the atmospheric transmission windows, Opt. Express, 20, pp. 6788-6807.

[8] Nystad, H. E. (2015) Comparison of Principal Component Analysis and Spectral Angle Mapping for Identification of Materials in Terahertz Transmission Measurements, (Trondheim Norwegian University of Science).

[9] van Rheenen, A., Haakestad, M. W. (2015). Robust Identification of Concealed Dangerous Substances by Spectral Correlation of Terahertz Transmission Images, IEEE Trans. Terahertz Sci. Technol., 5, pp. 438- 444.

[10] Skvortsov, L. A. (2014). Standoff detection of hidden explosives and cold and fire arms by terahertz time-domain spectroscopy and active spectral imaging (review), Appl. Spectrosc., 81, pp. 725-749.

[11] Clough B., Dai J., Zhang, X. C. (2013). Laser air photonics: beyond the terahertz gap, Mater. Today., 15, pp. 50-58.
[12] https://www.hubner-photonics.com/products/terahertz-technology/terahertz-spectrometers/t-cognition/
[13] Mikiya, K., Tripathi, S. R., Murate, K., Imayama, K., Kodo, K. (2016). Non-destructive drug inspection in covering materials using a terahertz spectral imaging system with injection-seeded terahertz parametric generation and detection, Opt. Express, 24, pp. 6425-6432.
[14] Kawase, K., Ogawa, Y., Watanabe, Y. (2003). Non-destructive terahertz imaging of illicit drugs using spectral fingerprints, Opt. Express, 11, pp. 2549-2554.
[15] Suszek, J., Siemion, A. M., Bieda, M. S. et al. (2015). 3-D-Printed Flat Optics for THz Linear Scanners, IEEE Trans. Terahertz Sci. Technol., 5, pp. 314-316.
[16] https://www.orteh.pl.
[17] http://terasense.com/products/thz-scanner.
[18] http://thruvision.com.
[19] http://www.brijot.com.
[20] http://www.millivision.com.
[21] http://www.trexenterprises.com.
[22] https://asqella.com.
[23] Cooper, K. B., Dengler, R. J. et al. (2008). Penetrating 3-D Imaging at 4- and 25-m Range Using a Submillimeter-Wave Radar, IEEE Trans. Microw. Theory Tech., 56, pp. 2771 – 2778.
[24] L. Yun-Shik, Principles of Terahertz Science and Technology, Springer, (2008).
[25] N. Palka, THz Reflection Spectroscopy of Explosives Measured by Time Domain Spectroscopy, Acta Physica Polonica A, Vol. 120, 713-715 (2011).
[26] https://www.sds.l3t.com/advancedimaging/provision-at.htm.
[27] https://www.smithsdetection.com/products/eqo.
[28] https://www.rohde-schwarz.com/us/product/qps-productstartpage_63493-332676.html.
[29] Luukanen, A., Appleby, R., Kemp, M., Salmon, N. (2012) Millimeter-Wave and Terahertz Imaging in Security Applications, Chapter 19, (Springer Series in Optical Sciences).
[30] Dhillon, S.S., et al. (2017). The 2017 terahertz science and technology roadmap, J. Phys. D: Appl. Phys., 50, pp. 1-49.

Ultrastrong light-matter coupling in deeply subwavelength THz LC resonators

Mathieu Jeannin[1], Djamal Gacemi[1], Angela Vasanelli[1], Lianhe Li[2], Edmund Linfield[2], Carlo Sirtori[1] and Yanko Todorov[1]

[1]Laboratoire de Physique de l'Ecole Normale Supérieure ENS, Université PSL, CNRS, Sorbonne Université, Université Paris Diderot, Sorbonne Paris Cité, Paris, France

[2]School of Electronic and Electrical Engineering, University of Leeds, LS2 9JT Leeds, United Kingdom

E-mail: yanko.todorov@ens.fr

We present a novel architecture for THz metamaterials relying on three-dimensional meta-atoms embedding a semiconductor active region. The meta-atoms behave as inductor-capacitive (LC) resonators with nano-scale capacitive parts, and they have extremely sub-wavelength mode volume ($10^{-6}\lambda_0^3$) and footprint ($10^{-3}\lambda_0^2$). When the LC resonators are coupled to a two-dimensional electron gas confined inside the capacitive elements the ultra-strong light-matter coupling regime is achieved. We also discuss the potential of such structures for ultra-low dark current THz quantum well photodetectors

Keywords – metamaterials, strong light-matter coupling, quantum wells

I. Introduction

Metamaterials consisting in the periodic repetition of artificially designed meta-atoms with dimensions much smaller than the wavelength of interest λ_0, are often described as high frequency inductor-capacitor (LC) resonators sustaining a resonance at $\lambda_0/c=(LC)^{1/2}$. Their peculiar ability to confine the electromagnetic field on a subwavelength scale opens new prospects for optoelectronic devices [1,2]. The LC circuit concentrates the electric field in an extremely small effective volume V_{eff} linked to its capacitive parts. Light-matter interaction occurring in the coupling between an absorber/emitter and the electric field inside the capacitors scales as $1/V_{eff}^{1/2}$, and is thus strongly enhanced. Here, we demonstrate a novel, three-dimensional architecture realizing a LC resonator with semiconductor material inserted in its capacitive elements. This architecture makes use of a novel processing technique that permits to define metal patterns on both sides of the semiconductor layer.

II. Results

The meta-atom which defines the unit cell of our metamaterial is shown in Fig. 1 (a). Its bottom part is formed by two square metallic pads connected by a straight wire. Its top part is formed by two rectangular metallic pads connected by a bent wire in the form of a squared coil. The metallic pads define two ultra-subwavelength parallel-plate capacitors embedding a semiconductor region. This resonator sustains a LC-circuit-like mode, in which the electric field is perpendicular to the metallic plates and strongly confined inside the capacitive elements, while the magnetic field loops around the top and bottom wires. The three-dimensional architecture results in a highly subwavelength lateral dimension ($\lambda_0/20$), allowing to reach the quasi-static regime.

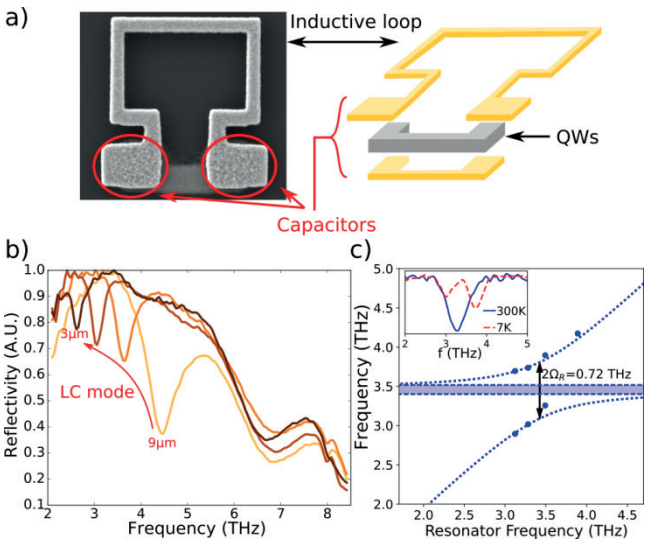

Fig. 1: a) Electron microscope picture and sketch of a LC meta-atom. b) Room-temperature reflectivity of the metamaterial, tuning the inductive loop length from 9µm to 3µm. c) Dispersion relation of the intersubband polaritons showing a Rabi splitting of 0.72 THz. Inset: 300K (blue) and 7K (red) reflectivity of the metamaterial showing the polariton splitting.

We fabricate arrays of ~5.10^4 meta-atoms, keeping the capacitive elements identical but increasing the dimension of the top wire loop. As shown in Fig. 1 b), room-temperature reflectivity experiments reveal the tuning the resonance through independent change of the capacitive and inductive parts, maintaining good resonances quality factors even semiconductor structures as thin as 300 nm.

We insert inside the capacitive elements an active region composed of 5 delta-doped GaAs/AlGaAs quantum wells embedding a two-dimensional electron gas sustaining an intersubband plasmon at 3.3 THz. Reflectivity experiments at 4K show the polariton splitting owe to the ultra-strong light matter coupling between the plasmon and the LC mode (Fig. 1c). Using the experimental

polariton dispersion curves, we can derive precisely the effective mode volume of our resonators, $V_{eff}=10^{-6}\lambda_0^3$, as well as the total number of electrons involved in the light-matter interaction, $n_e=2.4x10^3$ $e^-/capa$, a record low number in intersubband systems.

In these device architectures, the top and bottom parts of the metaatoms can be contacted with electrical leads. We will discuss preliminary results on the realization of a metamaterial enhanced quantum well infrared photodetector (QWIP) in the THz region. As the resonators allow reducing dramatically the electrical area of the device while maintaining a large optical cross-section, we expect a large improvement of the QWIP temperature performance, as previously demonstrated in the mid-infrared spectral range [2].

ACKNOWLEDGMENTS

This work was financially supported by the French National Research Agency under the contract ANR-16-CE24-0020.

REFERENCES

[1] M. Jeannin et al., *ACS Photonics*, **6**, 1207-1215 (2019)
[2] D. Palaferri et al., *Nature,* vol. 556, (2018).

Broadband terahertz heterodyne spectrometer exploiting synchrotron radiation at sub-megahertz resolution

O. Pirali[1,2], Z. Buchanan[3], S. Eliet[4], M.-A. Martin-Drumel[1], J. Turut[4], F. Hindle[5], P. Roy[2], J.-F. Lampin[4], and G. Mouret[5]
[1]Institut des Sciences Moléculaires d'Orsay, Orsay, 91405, France
[2]SOLEIL synchrotron, AILES beamline, Saint-Aubin, F-91190 Gif-sur-Yvette, France
[3]Department of Chemistry, University of California, Davis, CA 95616, USA
[4]Institut d'Electronique Microélectronique et Nanotechnologie, Villeneuve d'Ascq, F-59652, France
[5]Laboratoire de Physico-Chimie de l'Atmosphère, Dunkerque, F-59140, France

Abstract – A new spectrometer on the AILES beamline of the SOLEIL synchrotron facility to achieve sub-MHz resolution in the THz and far-IR regions is currently developed. Thanks to a dedicated heterodyne detection by use of a new kind of molecular laser as local oscillator along with a Fast Fourier Transform Spectrometer, several pure rotation absorption lines of H_2S and CH_3OH around 1.073 THz have been recorded.

Molecular laser, Heterodyne detection

I. Introduction

The AILES beamline extracts synchrotron radiation emitted by various operating modes of the SOLEIL machine in a broad spectral range covering the THz and far-IR regions. As every synchrotron-based far-IR spectroscopy stations over the world, the AILES beamline makes use of Fourier Transform (FT) interferometry to acquire high resolution absorption spectra. FT instruments have an inherently limited spectral resolution; the highest spectral resolution presently attainable with this technique being about 0,0009 cm^{-1} (around 27 MHz) which corresponds to an optical path difference of 11 meters. This limit the spectroscopic studies in terms of molecular sizes, frequency accuracy, and detection of weak but important couplings between angular momenta.

To reach higher spectral resolution, we have developed a dedicated heterodyne detection based onto a new kind of molecular laser as local oscillator (LO), a Hot Electron Bolometer (HEB) as high efficiency mixer, and a Fast Fourier Transform Spectrometer allowing a multiplex spectral analysis of 2,5 GHz around the OL frequency. The figure 1 give a global overview of the new high-resolution spectrometer station based on heterodyne detection of synchrotron radiation (SR). In this demonstration, a 1073049.6 MHz LO frequency was generated using a new generation optically pumped far-IR molecular laser developed by the IEMN laboratory [1].

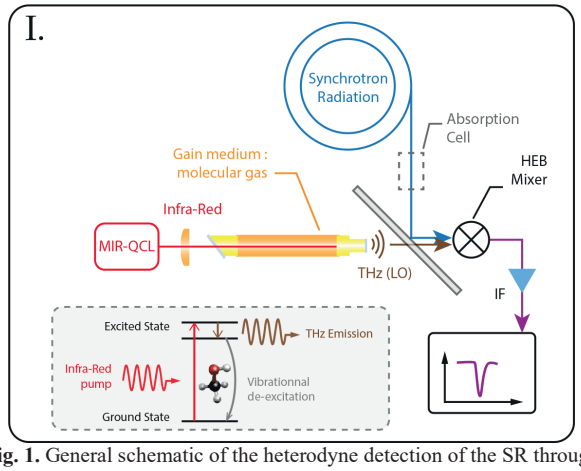

Fig. 1. General schematic of the heterodyne detection of the SR through an absorption cell, $f_{IF} = f_{SR} - f_{LO}$ is called Intermediate Frequency. In the dash box, energy levels scheme enabling the THz stimulated emission radiation. The far-IR continuum of the SR is optically filtered to be collimated through a 55 cm long single-pass absorption cell equipped polytetrafluoroethylene windows. A wire grids polarizer is used to overlap SR and LO radiation to be collected by the He liquid cooled HEB mixer.

II. Results

To record the absorption lines of H2S, we injected 30 µbar of gas in cell. Small portions of the IF spectrum are shown on Figure 2. This observed absorption line fitted by using a Gaussian profile is centered at 1735.202 MHz on the FI scale and has a FWHM of 2.9 MHz. We deduce a central frequency at 1 071 314,4 MHz taking into account the OL frequency, that being a deviation of 0.6 MHz compared to expected value. The line position accuracy is limited by the width of the absorption lines, the S/N ration of the line, and the LO frequency accuracy and stability. From those first measurement, a higher control should lead to better frequency accuracy.

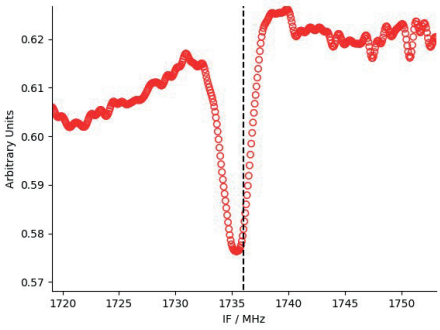

Fig. 2 A Small portion of the IF spectrum extracted from the 2.5 GHz full bandwidth recorded simultaneously, in which the $8_{6,3} \leftarrow 8_{5,4}$ H_2S transition is clearly observed

ACKNOWLEDGMENTS

Funding. This project received fundings from the Agence Nationale de la Recherche (ANR) (HEROES, ANR-16-CE30-0020-03); partial fundings from the LABoratoire d'EXcellence PALM (University Paris-Saclay) and from the SATT-Nord "TER- APOMPE" project.

Acknowledgment. The authors acknowledge SOLEIL for provision of synchrotron radiation under beamtime proposal 20180684 and we would like to thank J.-B. Brubach and K. Rad- dler for technical assistance. ZSB acknowledges support from the Chateaubriand Fellowship of the Office for Science & Tech- nology of the Embassy of France in the United States

REFERENCES

[1] A. Pagies, G. Ducournau, and J. F. Lampin, "Low-threshold terahertz molecular laser optically pumped by a quantum cascade laser," APL PHOTONICS 1 (2016).

.

A new approach for THz molecular lasers

S. Barbieri[1], J. Turut[1], A. Pagies[1], J.-F. Lampin[1]
[1] Institute of Electronics Microelectronics and Nanotechnology, UMR CNRS 8520, Lille University, Villeneuve d'Ascq, France
E-mail: jean-francois.lampin@univ-lille.fr

Abstract – Despite several progress generation of electromagnetic power in the THz range is still underdeveloped compared to the other frequency bands. Direct THz generation poses fundamental and practical problems very difficult to solve. Generating THz using sources from lower or higher frequencies is an alternative way. We will discuss our recent results about a new approach for continuous wave THz molecular lasers. Traditionally these lasers were pumped by CO_2 lasers that have several drawbacks. We have demonstrated that mid-infrared quantum cascade lasers can be used as pump lasers to invert the population of polar molecules. Here we demonstrate an efficient laser based on ammonia (NH_3).

Keywords – Terahertz, Laser, Ammonia

I. Introduction

Using optical sources for generating submillimeter or THz waves was proposed in the 1960's consecutively to the demonstration of the first optical oscillator (laser)[1]. Two approaches were investigated: the photoelectric mixing (or photomixing) and the difference frequency generation (DFG) in nonlinear crystals. But in 1970 the first optically-pumped THz laser (OPTL) was demonstrated at Bell Telephone Labs[2]. It was powerful and was adopted quickly as a replacement for the discharge-pumped molecular laser which was difficult to operate and less efficient. These sources were (and still are) the most powerful in the THz range for narrow band emission but they are also bulky and expensive. We have proposed to pump a molecular laser with a quantum cascade laser (QCL) instead of a CO_2 laser[3]. Since their demonstration in 1994 the performance of the QCLs has increased significantly and it is possible to consider their use for pumping other lasers.

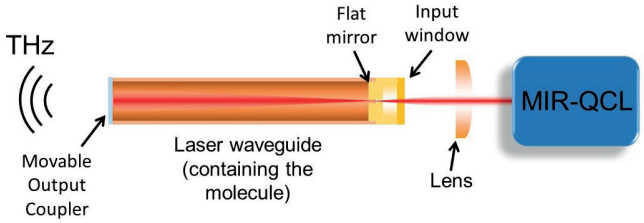

Fig. 1. Simplified schematic of the mid-IR (MIR) QCL-pumped THz molecular laser.

II. QCL-Pumped Molecular Laser

Fig. 1 displays a typical schematic of this kind of laser. The reduced size of the QCL compared to a typical CO_2 laser is welcome but the main advantage of the QCL is its continuous tunability. The tunability of CW CO_2 lasers is generally less than 1 GHz around each CO_2 line but QCLs can reach a tunability of few 100's GHz or more. The molecule and the transition can then be chosen to optimize some parameters of the molecular laser like the frequency, the gain or the efficiency.

The THz cavity is made of a hollow metallic waveguide closed by to flat mirrors. One of them has a hole in the center to allow the pumping beam to enter into the cavity. The other mirror is the output coupler and transmit partially the THz beam. This mirror is mounted on a translation and piezo stage to allow the fine adjustment of the cavity length.

We have demonstrated the first QCL-pumped molecular laser by choosing the NH_3 (ammonia) molecule. It is a light molecule that exhibits a strong permanent electric dipole and that strongly absorbs infrared. Its equilibrium configuration is a pyramidal symmetric top and the various quantum levels are dictated by the J and K quantum numbers. But this molecule has also a large amplitude internal motion due to the tunnel effect of the nitrogen atom through the potential created by the three hydrogen atoms. This effect splits the NH_3 levels in symmetric (s) and anti-symmetric levels (a). They are separated by about 0.8 cm^{-1} when the molecule is its fundamental vibrational state. Inversion of population between these levels was achieved in the first maser[7] demonstration around 24 GHz. In the first vibrational state (v_2=1), a and s levels are separated by about 36 cm^{-1} corresponding to about 1 THz. Inversion of population between these levels and CW THz oscillation are possible by pumping the molecule with a MIR-QCL[3-5].

III. Experiments

A laser such as that described in Fig. 1 was realized, filled with NH_3 and optimized.

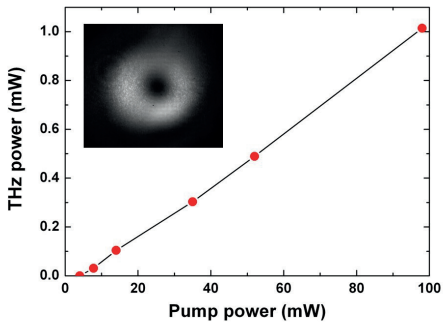

Fig. 2. THz power versus mid-IR pump power (inset: image of the beam)[9].

Fig. 2 shows the highest measured THz power at 1073 GHz versus the 10.3 µm pump power. The threshold is very low (few mW) and the conversion efficiency is close to 1 mW/W. The maximum theoretical efficiency of this kind of laser is given by: $\frac{1}{2}(\nu_{THz}/\nu_{pump})$ = 1.8 mW/W. The measured efficiency is equal to 55% of the maximum theoretical efficiency. The inset in Fig. 2 shows the beam pattern of the most powerful mode: it corresponds to the TE_{01} mode of the metallic circular waveguide which has very low losses.

The THz gain has been measured in a single pass cell[8]. The maximum measured value is 10.1 dB/m at 1073 GHz for a pumping power of 40 mW. This value is the highest measured in a CW-MIR-pumped gas in the THz range. It explains why the threshold of the laser is very low.

Fig. 3 shows the different laser transitions obtained with the QCL-pumped laser. All these laser lines are pure inversion transitions of NH_3 in the ν_2=1 excited state labelled by their (J,K) quantum numbers. The spectra were measured using a subharmonic mixer.

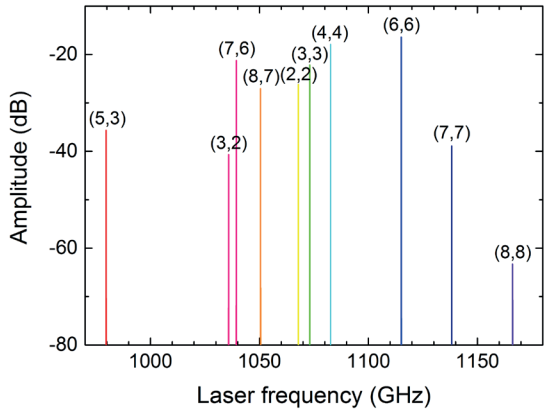

Fig. 3. Spectra of the different laser transitions obtained with the QCL-pumped NH_3 laser labelled by their (J,K) numbers.

We have also investigated recently the frequency noise of this laser[6,9]. It has been measured by beating the laser frequency with the 1080th harmonic of the repetition rate of a 1 GHz, 1560 nm frequency comb as a reference. We find a frequency noise power spectral density lower than 10 Hz^2/Hz (-95 dBc/Hz) at 100 kHz from the carrier. If we equal this value with the phase noise of a ×108 multiplied source it would require a 10 GHz oscillator with a phase noise of -135 dBc/Hz (100 kHz from the carrier) which is a low value comparable to the best commercial synthesized sources. We have also showed that the laser can be phase-locked to a frequency reference by controlling the QCL drive current down to a sub-Hz linewidth[9].

IV. Applications

We have investigated some possible applications of this kind of laser. The first application concerns the THz imaging: as showed in Fig. 2, the output power is sufficient to illuminate the sensor of a THz microbolometer camera at 25 frame/s with a good signal/noise ratio. The laser can also be used as a local oscillator. We have demonstrated that it can pump efficiently a NbN hot electron bolometer (HEB) mixer. The noise temperature was sufficiently low to detect the radiation produced around 1 THz by a Hg lamp. In a second experiment we have detected the synchrotron radiation from the AILES beamline at Soleil synchrotron[10]. Thanks to the excellent frequency resolution of this heterodyne receiver, it was possible to demonstrate molecular spectroscopy around 1 THz with MHz resolution[10]. Finally, as it was demonstrated in the past, the OPTL can also be used to build a magneto-conducted spectrometer. We have used it to investigate the effective mass of electrons in an InAs quantum well thanks to cyclotron resonance[11].

In this work we have demonstrated that a CW THz laser source can be built from a MIR QCL and a THz cavity filled with polar molecules. This source operates at room-temperature, does not need high voltage or water cooling. With ammonia its efficiency and its phase noise are comparable to state-of-the-art multiplication source at 1 THz. At higher frequencies, better efficiencies are expected. At frequencies higher than 1 THz and/or with more powerful QCL we can expect CW output powers in the 10 mW range.

Acknowledgments

We acknowledge the members of the IEMN Terahertz Photonics Group. This work has benefited from the facilities of the EQUIPEX ExCELSiOR Nanoscience Characterization Center and the RENATECH network. This work was supported by the SATT-Nord project TERAPOMPE, the ANR project HEROES (ANR-16-CE30-0020) and the LABEX Cluster of Excellence FIRST-TF (ANR-10-LABX-48-01). We also acknowledge financial support from the region Hauts-de-France and the 'Fonds Européen de Développement Régional' (FEDER) through the 'Contrat de Projets Etat Région (CPER)' "Photonics for Society".

REFERENCES

[1]. J.C. Bass, "Generation of millimetre and submillimetre waves by frequency mixing of laser beams", *Millimetre and submillimetre waves*, Ed. F. A. Benson, Chap. 8, Iliffe, London, 1969.

[2] T.Y. Chang and T.J. Bridges, "Laser action at 452, 496, and 541 μm in optically pumped CH_3F," *Optics Communications,* **1**, 423 (1970).

[3] A. Pagies, G. Ducournau, and J.-F. Lampin, "Low-threshold terahertz molecular laser optically pumped by a quantum cascade laser," *APL Photonics,* **1**, 031302 (2016).

[4] A. Pagies, G. Ducournau, and J.-F. Lampin, "Continuous wave terahertz molecular laser optically pumped by a quantum cascade laser," *41st International Conference on Infrared, Millimeter, and Terahertz waves (IRMMW-THz)*, Copenhagen, Denmark, 2016.

[5] A. Pagies, G. Ducournau, and J.-F. Lampin, "Progress in continuous wave THz molecular laser optically pumped by a quantum cascade laser," *42nd International Conference on Infrared, Millimeter, and Terahertz waves (IRMMW-THz)*, Cancun, Mexico, 2017.

[6] A. Pagies, S. Eliet, J.-F. Lampin, G. Santarelli, W. Hansel, R. Holzwarth, and S. Barbieri, "Frequency noise power spectral density of a molecular THz-laser using a fs-fibre laser comb with 1 GHz repetition rate," *43rd International Conference on Infrared, Millimeter, and Terahertz waves (IRMMW-THz)*, Nagoya, Japan, 2018.

[7] J.P. Gordon, H. J. Zeiger, and C.H. Townes, "The maser-new type of microwave amplifier, frequency standard, and spectrometer," *Physical Review,* **99**, 1264 (1955).

[8] M. Micica, S. Eliet, M. Vanwolleghem, R. Motiyenko, A. Pienkina, L. Margulès, K. Postava, J. Pistora, and J.-F. Lampin, "High-resolution THz gain measurements in optically pumped ammonia," *Optics Express,* **26**, 212242 (2018).

[9] J.-F. Lampin, A. Pagies, G. Santarelli, J. Hesler, W. Hänsel, R. Holzwarth, and S. Barbieri, "Quantum cascade laser-pumped terahertz molecular lasers: frequency noise and stabilization using a 1560 nm frequency comb," submitted.

[10] J.-F. Lampin, O. Pirali, Z.S. Buchanan, S. Eliet, M.-A. Martin-Drumel, J. Turut, P. Roy, F. Hindle, and G. Mouret, "Broadband terahertz heterodyne spectrometer exploiting synchrotron radiation at megahertz resolution," Optics Letters, in press.

[11] J.-F. Lampin, A. Pagies, S. Barbieri, L. Desplanque, X. Wallart, J. Hesler, O. Drachenko, and J. Leotin, "Terahertz pulsed-field magneto-spectrometer at room-temperature," *44th International Conference on Infrared, Millimeter, and Terahertz waves (IRMMW-THz)*, Paris, France, 2019.

Observation of self mode-locking in terahertz quantum cascade lasers through intra-cavity self-detection

H. Li,[1] W. Wan,[1] Z. Li,[1] J. C. Cao,[1] S. Lepillet,[2] J-F. Lampin,[2] and S. Barbieri[2]

1. Key Laboratory of Terahertz Solid State Technology, Shanghai Institute of Microsystem and Information Technology, Chinese Academy of Sciences, Shanghai, 200050, China

2. Laboratoire IEMN, CNRS and Université de Lille, Villeneuve d'Ascq, 59652, France
Email. Stefano.barbieri@iemn.fr

We report an experimental study of terahertz (THz) quantum cascade lasers (QCLs) exploiting an intra-cavity self-detection process, where we demonstrate the generation of trains of self-mode-locked pulses. The detection technique is based on a well-known property of these devices, namely the fact that their gain dynamics unfolds on an ultra-fast time scale, in the order of tens of ps (for THz QCLs), determined by intersubband relaxation [1]. The resulting modulation of the population inversion can therefore be observed as a function of time over very large bandwidths, in the ~10-100GHz range, simply by monitoring the QCL current [2]. To fully exploit this possibility, in this work we processed an exceptionally long single-plasmon ridge waveguide of 15mm, based on an ultra-low threshold, 4.2THz active-region design [3,4]. The resulting multimode emission spectrum consists of ~60 longitudinal modes with a free spectral range (FSR) of ~2.4GHz. The QCL was driven in free-running in continuous wave (CW) at a temperature of 30K, and we monitored the *ac* current gain-induced modulation with the help of a microwave probe connected to a real-time oscilloscope with and overall 3-dB measurement-system

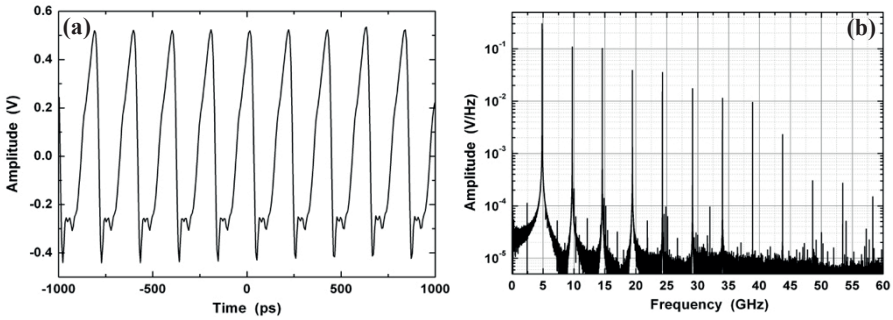

Fig. 1(a) Oscilloscope trace of the measured current pulse train (35dB amplification). The QCL was driven in CW at 7V and 2.1A. **(b)** Fourier transform of the time trace of panel (a) recorded over a time window of 2μs.

bandwidth >45GHz [2]. In Fig.1(a) we report an example of measured time-trace, showing a train of ~85-ps long pulses separated by T = 205ps =1/(2xFSR) (not corrected by the measurement-system frequency response). The corresponding Fourier transform on the right shows that at least up to 25 modes (~60GHz/2.4GHz) are coherently coupled and participate to the pulse train. This number is limited by the bandwidth of our system. Another striking finding is that the inter-mode beatings in Fig.1(b) are extremely narrow (<30kHz at 4.8GHz), leading to a very stable measured pulse train over time scales of tens of μs (not shown), a clear signature of self-mode locking operation. Despite several demonstrations of spontaneous inter-mode beat-note narrowing and active mode-locking [3-6], to the best of our knowledge this is the first time that self-mode-locked pulses are reported for a THz QCL. This finding contradicts the presently established theory according to which an unfavourable ratio "gain-recovery time/roundtrip time" prevents spontaneous mode-locking in QCLs (although this conclusion is somewhat relaxed for THz QCLs) [7]. Depending on the drive current, the regime of stable self-mode locking with two pulses per roundtrip (Fig.1), alternates with wider current regions characterised by a more unstable regime, with one pulse per roundtrip, and more pronounced amplitude noise and timing jitter. A complete analysis of the laser dynamics *vs* drive current will be given, allowing to discriminate between amplitude and phase noise.

References

[1] C. G. Derntl, G. Scalari, D. Bachmann, M. Beck, J. Faist, K. Unterrainer, and J. Darmo, "Gain dynamics in a heterogeneous terahertz quantum cascade laser" Appl. Phys. Lett. **113**, 181102 (2018).
[2] P. Gellie, S. Barbieri, J-F. Lampin, P. Filloux, C. Manquest, C. Sirtori, I. Sagnes, S. P. Khanna, E. H. Linfield, A. G. Davies, H. Beere, D. Ritchie, "Injection−locking of terahertz quantum cascade lasers up to 35GHz using RF amplitude modulation", Opt. Expr. **18**, 20816 (2010)
[3] M. Wienold, B. Röben, L. Schrottke, and H. T. Grahn, "Evidence for frequency comb emission from a Fabry-Perot terahertz quantum-cascade laser", Opt. Expr. **22**, 30411 (2014)
[4] W. J. Wan, H. Li, T. Zhou, and J. C. Cao, "Homogeneous spectral spanning of terahertz semiconductor lasers with radio frequency modulation", Sci. Rep. **7**, 44109 (2017).
[5] M. Rösch, G. Scalari, M. Beck, and J. Faist, "Octave spanning semiconductor laser," Nat. Photonics **9**, 42 (2014).
[6] A Mottaghizadeh, D. Gacemi, P. Laffaille, H. Li, M. Amanti, C. Sirtori, G. Santarelli, W. Hansel, R. Holzwart, L. H. Li, E. H. Linfield, and S. Barbieri "5ps-long terahertz pulses from an active-mode locked quantum cascade laser," Optica 4, 170 (2017).

[7] J B. Khurgin, Y. Dikmelik, A. Hugi, and J. Faist “Coherent frequency combs produced by self-frequency modulation in quantum cascade lasers,”Appl. Phys. Lett. **104**, 081118 (2014)

Superconducting THz devices

F. Couëdo[1], Y. Srivastava[2], P. Pitchappa[2], C. Ulysse[3], E. Recoba-Pawlowski[1-4], C. Feuillet-Palma[1], N. Bergeal[1], R. Singh[2] and J. Lesueur[1]

[1] Laboratoire de Physique et d'Etude des Matériaux (LPEM), ESPCI-Paris/CNRS, PSL, Paris, France
[2] Centre de Nanosciences et de Nanotechnologies (C2N), Université Paris-Saclay, Palaiseau, France
[3] Center for Disruptive Photonic Technologies, SPMS, Nanyang Technological University, Singapore
[4] Unité Mixte de Physique CNRS, Thales, Université Paris-Sud, Université Paris-Saclay, Palaiseau, France

E-mail: Jerome.lesueur@espci.fr

Abstract – We present our recent work on ion irradiated superconducting high-frequency devices made with High Temperature Superconductors. Using a new type of Josephson nano-junctions, we made very efficient mixers in the low THz frequency range, and developed highly sensitive RF magnetometers. We also fabricated tunable superconducting THz meta-materials, which can be optically switched on the ps time scale with a very low IR energy density pulse. Future developments of this emerging technology will be sketched as well.

Keywords – THz detector, Superconductor, Josephson junctions, Meta-materials

I. Introduction

In the quest for efficient detectors and more generally devices working in the THz range of the electromagnetic spectrum, superconductors appear as interesting candidates for advanced applications, especially cuprate compounds such as $YBa_2Cu_3O_7$ (YBCO). Not only their critical temperature T_c in the 90 K range allows operation with rather simple and cost-effective cryogenic systems, but also their cut-off frequency reaches 5 to 10 THz, an order of magnitude larger than the conventional superconductors'one.

To fully benefit from the quantum nature of superconductivity and make highly efficient devices, one needs to fabricate Josephson Junctions (JJ), which are weak links between two superconductors with a typical size in the nano-meter range. While a mature technology has been developed for superconductors working at low temperature (4K), there is no equivalent with High Tc Superconductors (HTS) yet. We invented a special way of making HTS Josephson Junctions based on an ion irradiation technique [1], which have good properties and can be made from commercial YBCO thin films at a very large scale. Since then, we are developing several applications at GHz and THz frequencies.

II. Superconducting Josephson junctions

A superconductor has a complex conductivity, with a dissipative part starting from zero in DC and increasing up to a cut-off frequency corresponding to the binding energy of Cooper pairs (20 meV for HTS, 7 THz), and an inductive one, which diverges at the critical temperature. Below the cut-off frequency, a superconductor therefore displays very low losses together with a temperature dependent "kinetic inductance", which are two main ingredients to make highly efficient and versatile high frequency circuit elements. In addition, one can use lumped elements, the Josephson junctions, whose peculiar dynamics offers unique and powerful high frequency operations.

The electrodynamics of a JJ is ruled by two coupled equations :

$$I = I_c \sin(\varphi) \quad (1)$$

$$V = \frac{\Phi_0}{2\pi}\frac{\partial \varphi}{\partial t} \quad (2)$$

where φ is the phase difference between the quantum phase functions of the two coupled superconductors, Φ_0 the flux quantum ($\Phi_0 = h/2e$), I_c, the critical current, I the current and V the voltage across the JJ. At finite voltage V, an alternative current at frequency $\nu = V/\Phi_0$ is generated within the JJ ($\nu \sim 500$ GHz/mV). Conversely, when a JJ is irradiated with an electromagnetic wave at frequency ν, quantized steps appear in the I-V characteristics, called Shapiro steps. JJ can therefore be used as emitters and detectors up to a cut-off frequency $\nu_c = I_c R_n/\Phi_0$, R_n being the normal state resistance of the JJ, which can reach several THz. Moreover, since equations (1) and (2) define a non-linear I-V characteristic, JJs are suitable to fabricate high-frequency mixers. The phase difference φ can be tuned by a small magnetic field, and so all the properties of the JJs. This property is used to make highly sensitive magnetometers made of two JJs in parallel, called Superconducting Quantum Interference Devices (SQUIDs), and new tunable THz devices.

III. Superconducting high frequency devices

HTS materials are very sensitive to disorder which one can introduce on purpose by high-energy (~100 keV) oxygen ion irradiation for instance. At low ion dose, T_c decreases till becoming null at a critical dose ; beyond it, the material becomes insulating. To make circuits, we pattern an e-beam resist to protect the superconducting parts from high dose irradiation. In a second step, the whole structure is protected, except 20-40 nm wide slits, where a low dose irradiation creates JJ by locally lower T_c between two superconducting reservoirs [1]. Such a process is highly scalable ; up to

hundred thousands of JJ can be made. Arrays of SQUIDs were successfully made [2,3], which provide highly sensitive RF magnetometers [4].

We used the strong non-linearity of JJ to make HTS mixers in the low THz range working in the 50-70 K temperature range [5-6]. We inserted a JJ in a wide-band spiral antenna, connected to a transmission line adapted for microwaves. Both Local Oscillator (LO) and high-frequency signal were coupled from free space to the antenna, and the signal at the intermediate frequency (around 6 GHz) was measured. We could detect electromagnetic waves beyond 0.4 THz, with a spectral resolution limited by the LO one (instrumentation limited at ~1 MHz), and using extremely low LO power, in the nW range, as compared to mW in conventional mixers. A complete modelling of the Josephson mixer was undertaken, based on the standard Resistively-Shunted-Junction (RSJ) model [5,6]. The noise of the JJ has been measured to be only two times the thermal noise [7]. Moreover, since a DC biased JJ is an emitter whose frequency is simply proportional to the applied voltage, we are working on a fully integrated mixer, with on-chip tunable LO made of an array of JJ. This requires a full synchronization of the JJs that we studied [8].

As stated above, HTS superconductors display low losses up to a few THz. We fabricated HTS meta-surfaces based on Split Ring Resonators, with resonance frequencies in the THz range, showing very appealing properties [9]. For comparable geometries, the Q-factor of the resonances is higher for superconducting materials than for metals [10]. The frequency can be tuned, thanks to the change in the kinetic inductance of the superconductor with temperature [11].

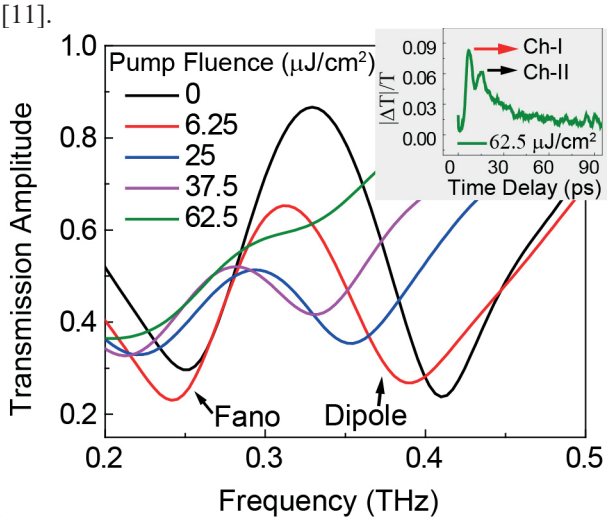

Figure 1 : Transmission of a 50 nm thick asymmetric meta-material with two resonances as a function of frequency upon IR pump. Inset : change in the transmission in the time domain

We also reported ultra-fast optical switching of such meta-surfaces using pump-probe experiments. A 800 nm wavelength fs laser pulse excites the meta-material, which is then probed by a delayed THz one. The transmission measured in the frequency domain shows resonances whose amplitude is modulated with the energy density of the pulse [12]. For a 50 nm thick YBCO film on sapphire, a modulation of 90% of the transmission on a ps time scale is measured, for a fluence of 900 μJ/cm^2 [13]. We made similar structures using the ion irradiation technique described above. The quality factor of the resonance is enhanced by a factor 2 to 3 with respect to the original meta-surfaces made by etching, and a 100 % modulation is obtained for only 65 μJ/cm^2, on the same time scale (Figure 1). This paves the way of ultra-fast low energy optical switching of THz meta-materials. In the future, we will incorporate JJ within the meta-surface to tune the resonance frequency by mean of a weak magnetic field, thanks to the field dependent Josephson inductance.

We recently started to make a new type of HTS JJ, based on direct irradiation of a YBCO thin film by a He Focused Ion Beam whose diameter is only 0.5 nm. Their dynamic properties in the RF frequency range are fully understood within the RSJ model, and their noise level is exactly what is expected from thermal fluctuations in a wide range of parameters and temperature [14]. These new HTS nano-junctions look very promising for future applications in the THz frequency range as well.

IV. Conclusions

We fabricated HTS circuits and Josephson junctions, which show very interesting high frequency properties. These devices are highly sensitive, and their properties can be tuned with very low energy density and on a very short time. These achievements pave the way of new cryogenics THz devices.

Acknowledgments

This work has been supported by the QUANTUMET ANR PRCI program, the T-SUN ANR ASTRID program, the Emergence Program from Ville de Paris and by the Région Ile-de-France in the framework of the DIM Nano-K and Sesame programs.

References

[1] N. Bergeal et al, Applied Physics Letters 87, 102502 (2005)
[2] S. Ouanani et al, Sup. Sc. and Techn. 29, 094002 (2016)
[3] E. Recoba et al, Sup. Sc. and Techn. 31, 5005 (2018)
[4] F. Couëdo et al, App. Physics Letters 114, 192602 (2019)
[5] M. Malnou et al, App. Physics Letters 101, 233505 (2012)
[6] M. Malnou et al, J. of Applied Physics 116, 074505 (2014)
[7] A. Sharafiev et al, Sup. Sc. and Techn. 29, 074001 (2016)
[8] A. Sharafiev et al, Sup. Sc. and Techn. 31, 035003 (2018)
[9] R. Singh and N. Zheludev, Nat. Photonics 8, 679 (2014)
[10] Y. K. Srivastava et al, Ad. Opt. Materials 4, 1875 (2016)
[11] H. T. Chen et al, Phys. Rev. Lett. 105, 247402 (2010)
[12] R. Singh et al, Nanophotonics 1, 117 (2012)
[13] Y. K. Srivastava, Adv. Mat. 30, 1801257 (2018)
[14] F. Couëdo et al, arXiv:1908.11163 (2019)

Recent Activities of the Electromagnetic Measurements and Modeling of Material Properties Group located at WUT

P. Kopyt[1], B. Salski[1], T. Karpisz[1], A. Pacewicz[1], M. Krysicki[1], J. Cuper[1], M. Rytel[1], J. Krupka[2]

[1] Warsaw Univ. of Technology, Institute of Radioelectronics and Multimedia Technology, Warsaw, Poland
[2] Warsaw Univ. of Technology, Institute of Micro- and Optoelectronics, Warsaw, Poland

E-mail: pkopyt@ire.pw.edu.pl, bsalski@ire.pw.edu.pl

Abstract – This paper presents a brief description of the activities of the Electromagnetic Measurements of Material Properties Group located at Warsaw University of Technology. The group is mainly active in the area of development of novel methods and instruments for characterization of materials in a broad frequency spectrum.

Keywords – Permittivity, Fabry-Pérot

I. Introduction

Precise electromagnetic (EM) characterization and modeling of various materials is of interest in a number of research areas and industries. The Electromagnetic Measurements and Modeling of Material Properties Group located at the Institute of Radioelectronics and Multimedia Technology (a part of Warsaw University of Technology) is working to answer these diverse requirements by providing tailored modeling approaches and specialized, custom-made methods and equipment for material characterization.

II. Research areas

In this short paper a brief description of activities of the group is given with a list of topics that the Electromagnetic Measurements and Modeling of Material Properties Group has been working on recently.

A. Ferrite characterization and linewidth measurement

The formulation of characteristic equations for ferromagnetic materials of particular geometries has brought about a major shift in the understanding of the nature of their resonances (1)-(4) and opened up new ways for more accurate characterization of their physical properties, such as ferromagnetic linewidth (ΔH), saturation magnetization (M_s) or effective g-factor (5)-(8).

B. Material characterization using the Fabry-Pérot open resonator

As an answer to low-loss material characterization needs of the microelectronics industry as well as the scientific community a method based on Fabry-Pérot open resonators (FPORs) with con-focal cavities has been proposed. First, it has been developed to cover the band from 20 up to 50 GHz, as presented in (9). Then, the approach has been extended to work up to 110 GHz, towards the sub-THz band, as presented in (10). The main advantage of the FPOR in applications where measuring dielectric properties (the dielectric constant and the dielectric loss of low-loss materials) is needed, as compared to alternatives, is that it operates in a broad frequency spectrum using consecutive $TEM_{0,0,q}$ (q – longitudinal mode order) Gaussian odd modes with the Q-factor exceeding 10^5. Thus, the material under test can be measured at each of the resonant frequencies with unparalleled accuracy.

As a major development stage of the broadening the frequency band of operation of the FPOR and using the method to measurements well in the sub-THz band, an effort is being taken to couple the resonator with a time-domain THz spectrometer (THz-TDS), which would combine the broad operation range of the spectrometer with high accuracy of the resonator. The work in this area of research is currently in progress.

C. Design of VNA replacements for material characterization in the mm-wave bands

In order to replace expensive VNA, used together with the FPOR, we proposed an alternative setup – a scalar network analyzer dedicated for measurements of resonators. As presented in (11), the constructed device consists of two separate frequency synthesizers similar to those shown in (12), which are synchronously swept in the frequency domain. The signals generated with these sources feed a frequency multiplier and a sub-harmonic mixer connected to a resonator under test. A sensitive narrow-band detector records the transmission signal detection. A dedicated software enables a user to extract dielectric properties of a sample in an automated way.

D. Design of FET-based THz radiation detectors

As a part of our interests in the applications located in the sub-THz frequency band we have been working on efficient modeling of antennas dedicated for detectors of the sub-THz radiation that are realized using processes typical for microelectronics and using Field Effect Transistors (FETs). The recent developments in this area, in particular efficient modeling of silicon-based

substrates, are shown in (13). The other area of our research are trustworthy methods to verify responsivity of such structures. Existing approaches are often burdened with large systematic errors resulting from arbitrary coefficients (e.g. arbitrarily assumed effective aperture of an antenna) needed in the procedure. Alternatives based on on-wafer measurements as well as a comparative method are presented in (14).

E. Modeling in non-linear optics

A major hurdle in the development of accurate material characterization tools is a lack of high-power THz-radiation sources known as the terahertz gap. A part of an effort to bridge this gap is our research into efficient design of a microstructural fiber, where efficient conversion of energy of optical pulses into terahertz pulses could take place within finite (but large as compared to the volume of a typical Schottky junction) volume of the structure, as described in (15)-(18).

F. EM modelling of QCL cavities

Being EM numerical modeling specialists we have also developed novel computationally-efficient full-wave fully-numerical approach to the electromagnetic modeling of quantum cascade laser (QCL) structures based on metal-clad dielectric waveguides with the aid of a three-dimensional electromagnetic solver with no need (in practical cases) for separate analyses of propagation within the waveguide. The method described in (19) enables to calculate the resonant frequencies of an electrically long Fabry-Pérot cavity and to link them to particular propagating (transverse) modes of the waveguide. As an extension of the method, a new approach to passive electromagnetic modelling of coupled–cavity quantum cascade lasers has been developed and is presented in (20). Thanks to the novel approach, passive analysis of an electrically long laser can be split into a cascade of relatively short sections having low quality factor, thus, substantially speeding up rigorous EM analysis of the QCL structure. Eventually, the proposed method is used to elaborate basic synthesis rules of coupled–cavity quantum cascade lasers.

G. Coupled modelling of semiconductors

Yet another field of interest of the group are methods to model whole laser devices, and not just cavities. Coherent radiation in semiconductor lasers can be computed using the Maxwell curl equations coupled with drift-diffusion (DD) equations. DD simulation allows calculating spatial distribution of electron and hole density profiles, which in turn is used to calculate gain spectral characteristic within each cell of the model. Subsequently, EM simulation of a four-level two-electron atomic system with a Pauli exclusion principle is undertaken to obtain radiation gain of the laser. A description of the approach has been presented in (21).

IV. Conclusions

A brief description of research interests and activities of the Electromagnetic Measurements and Modeling of Material Properties Group has been presented with references to recent publications authored and coauthored by the members of the group containing details of developed solutions.

Acknowledgments

The activities of the Electromagnetic Measurements and Modeling of Material Properties Group was partly funded from the project “High-precision techniques of millimeter and sub-THz band characterization of materials for microelectronics” operated within the Foundation for Polish Science TEAM-TECH Programme co-financed by the European Regional Development Fund, Operational Programme Smart Growth 2014-2020.

References

[1] J. Krupka, B. Salski, P. Kopyt, and W. Gwarek, “Electrodynamic study of YIG filters and resonators,” *Sci. Rep*., vol. 6, no. 1, p. 34739, Dec. 2016.

[2] J. Krupka, P. Aleshkevych, B. Salski, and P. Kopyt, “Magnetodynamic Study of Spin Resonances in Cylindrical and Spherical YIG Samples,” *IEEE Trans. Microw. Theory Tech*., vol. 66, no. 2, pp. 803–812, Feb. 2018.

[3] A. Pacewicz, J. Krupka, B. Salski, P. Kopyt, and P. Aleshkevych, “Rigorous Electrodynamic Approach to Ferromagnetic Resonance in Cavity-Coupled Ferrimagnetic Films,” *Phys. Status Solidi - Rapid Res.* Lett., vol. 12, no. 7, p. 1800144, Jul. 2018.

[4] J. Krupka, P. Aleshkevych, B. Salski, P. Kopyt, and A. Pacewicz, “Ferromagnetic Resonance Revised-Electrodynamic Approach,” *Sci. Rep.*, vol. 7, no. 1, p. 5750, Dec. 2017.

[5] J. Krupka, P. Aleshkevych, B. Salski, and P. Kopyt, “Ferromagnetic linewidth measurements employing electrodynamic model of the magnetic plasmon resonance,” *Meas. Sci. Technol.*, vol. 29, no. 2, p. 025501, Feb. 2018.

[6] J. Krupka, “Measurement of the complex permittivity, initial permeability, permeability tensor and ferromagnetic linewidth of gyromagnetic materials,” *Meas. Sci. Technol.*, vol. 29, no. 9, p. 092001, Sep. 2018.

[7] A. Pacewicz, J. Krupka, B. Salski, P. Aleshkevych, and P. Kopyt, “Rigorous broadband study of the intrinsic ferromagnetic linewidth of monocrystalline garnet spheres,” *Sci. Rep.*, 2019.

[8] J. Krupka et al., “Electrodynamic improvements to the theory of magnetostatic modes in ferrimagnetic spheres and their applications to saturation magnetization measurements,” *J. Magn. Magn. Mater.*, 2019.

[9] T. Karpisz, B. Salski, P. Kopyt, J. Krupka, "Measurement of Dielectrics from 20 to 50 GHz with a Fabry–Pérot Open Resonator", *IEEE Trans. on MTT*, vol. 67, no. 5, pp. 1901-1908, 2019.

[10] T. Karpisz, B. Salski, P. Kopyt, J. Krupka, “W-band measurements of low-loss dielectrics with a Fabry-Perot Open Resonator,” *Proc. Intl. Microwave Symp. (IMS 2019)*, Boston, Jun. 2019.

[11] J. Cuper, M. Rytel, T. Karpisz, A. Pacewicz, B. Salski, P. Kopyt, "Ka-band Compact Scalar Network Analyzer Dedicated to Resonator based Measurements of Material Properties," *2019 IEEE/MTT-S International Microwave Symposium*

[12] M. Rytel, P. Kopyt, B. Salski, "Phase Locked Loop Ku-Band Frequency Synthesizer Based on a Tuned YIG Oscillator," *Proc. 22nd Intl. Conf. on Microwaves, Radar and Wireless Comm*. (MIKON-2016),. pp. 604-607, May 2018.

[13] P. Kopyt, B. Salski, P. Zagrajek, D. Obrębski, J Marczewski, "Modeling of Silicon-Based Substrates of Patch Antennas Operating in the Sub-THz Range," *IEEE Trans. on Terahertz Science and Technology*, Vol. 7, No 4, Jul 2017, pp 424 – 432.

[14] P. Kopyt, B. Salski, A. Pacewicz, P. Zagrajek, J. Marczewski, "Measurements of the responsivity of FET-based detectors of sub-THz radiation," *Opto-Electronics Review*, Vol. 27, No 2, Jun 2019, pp. 123-129.

[15] [1] T. Karpisz, B. Salski, R. Buczynski, P. Kopyt, and A. Pacewicz, "Computationally-efficient FDTD modeling of supercontinuum generation in photonic crystal fibers," *Opt. Quantum Electron*., 2016.

[16] [2] B. Salski, P. Kopyt, and A. Pacewicz, "On bridging the terahertz gap using four-wave mixing in photonic crystal fibers," in *2016 Conference on Lasers and Electro-Optics*, CLEO 2016, 2016.

[17] [3] A. Pacewicz et al., "Characterization of Linear Properties of Nonlinear Soft Glasses at Terahertz and Infrared Frequencies," in *2nd International Conference on Optics, Photonics and Lasers* (OPAL), 2019, pp. 85–86.

[18] [4] A. Barh, R. K. Varshney, G. P. Agrawal, B. M. A. Rahman, and B. P. Pal, "Plastic fiber design for THz generation through wavelength translation," *Opt. Lett.*, 2015.

[19] P. Kopyt, B. Salski, M. Sakowicz, Efficient Three-Dimensional Electromagnetic Modeling of Metal–Metal Waveguides Employed for Quantum Cascade Lasers Operating in the THz Band," *IEEE Journal of Lightwave Technology*, Vol. 36 , No 9, May. 2018, pp. 1721-1729.

[20] M. Krysicki, B.Salski, P. Kopyt, "Passive synthesis rules of coupled-cavity quantum cascade lasers," *Opto-Electronics Review*, Vol. 27, No 3, Sep. 2019, pp. 268-274.

[21] M. Krysicki, B. Salski, "Hybrid electromagnetic modelling of coherent radiation in electrically-pumped semiconductor lasers," *Proc. 2019 Intl. Conf. on Numerical Simulation of Optoelectronic Devices (NUSOD)*, 2019, pp. 33-34.

Prof. Jerôme Degert (LOMA)
Title : Intense pulsed THz source: 2D spectroscopy, wavefront measurement and structuration
Abstract :
In LOMA, we developed intense THz sources (air plasma, optical rectification in ZnTe and LiNbO3) on the COLA platform (amplified Ti:Sa laser). We were able to generate sub-picosecond THz pulses with broadband spectral range (0-8 THz) and high electric field (up to 200 kV/cm).

The first part of the communication will concern the use of this source for time-resolved 1D and 2D THz spectroscopy applied to the study of the optical and electrical properties of new materials of interest. First, we study the mechanisms of conduction in thin films (few hundreds of nm) of a new conducting polymer derived from the well-know PEDOT/PPS complex, widely used in OLED or photovoltaic cells, and which makes it possible to get reed of some drawbacks (acidity, hygroscopic character, etc.) of the later. This study is performed in the stationnary and the transient regime through THz-TDS and optical pump-THz probe spectroscopies, respectively. We also apply these two techniques to the characterization of the optoelectronical properties of heterostructures made of 2D conductors or semiconductors, namely graphene and MoS2/MoSe2. The idea is to get some new functionalities in the field of ultrafast optoelectronics by combining the exceptional properties of both compounds.
The second part of the communication will report on the development of a wavefront sensor for THz pulses using a direct two-dimensional electro-optic imaging system. By measuring the phase variation of the THz electric field, one can reconstruct the THz wavefront and determine the aberrations of the optical system. Associated with deformable mirrors or specifically designed optics, the sensor will open the route to terahertz adaptive optics. Another application of THz phase structuration concerns topological beam-shaping of THz beams using geometric phase elements. THz vortex beams can be produced and characterized both in amplitude and phase from the reconstructed realtime two-dimensional imaging of the THz electric field. The results emphasize the versatility of the spin-orbit electromagnetic toolbox to prepare on-demand structured light endowed with polarization-controlled orbital angular momentum content in the THz domain, which should find many uses in future THz technologies.

Deep data processing for multilayered material characterized by terahertz spectroscopy

Q. Cassar,[1] A. Chopard,[1] F. Fauquet,[1] J.P. Guillet,[1] M. Pan,[1] J.B. Perraud,[1] M. Roux,[2] and P. Mounaix[1,3]
[1)] *University of Bordeaux, IMS UMR CNRS 5218 351 cours de la Libération, 33405 Talence, France*
[2)] *L'Atelier des Renaissances, 1 allée de Gieu, 33650 Saucats, France*
[3)] *Corresponding author: patrick.mounaix@u-bordeaux.fr*

Abstract – We report on further numerical developments for the analysis of multilayered structures and the extraction of individual layer properties. An iterative algorithm implements a connected propagation tree which denotes the occurrence of the incident pulse division. Each subpulse is individually monitored and its carried proportion of the incident power is extracted. Such a process allows to extract the specific dielectric properties of each layer but additionally permits to derive a parametric transfer function describing the whole interaction with an incident beam. The procedure was tested both for the art science and the aeronautic industry. Results on an XVIIth century painting and on aeronautics multilayered samples are reported.

Key Words: data processing, multilayered structures, terahertz spectroscopy.

I. INTRODUCTION

Terahertz radiations offer the opportunity to carry out contactless and non-destructive sensing of materials. As a consequence, the technique has legitimately been deployed to control layer thicknesses inside dielectric paint stacks for automotive and aeronautic industries and art science, for instance[1,2]. However, the wave propagation model commonly used to extract layer thicknesses computes indistinguishably the contribution of all the possible propagation routes. The number of calculated paths could be gigantic while a precise knowledge of the most contributing optical paths would awfully minimize the quantity of computed routes and clarify the involved propagation processes. Furthermore, the derivation of a parametric transfer function would drastically reduce the required computation power to minimize the objective function of an inverse electromagnetic formulation. A new algorithm monitoring the pulse subdivisions at dielectric interfaces has been developed[3]. The algorithm classifies each portion of the signal as a function of the number of encountered dielectric interfaces. Additionally, it identifies the various optical paths involved in these signal portions. The optical routes that contribute the most to the power are labeled and used to derive a parametric transfer function. The effectiveness of the algorithm is demonstrated by analyzing the principle optical paths and by deriving the appropriate parametric transfer function of a painting stack made of layers of several tens of microns.

II. RESULTS

The central principle for the algorithm is to increment, at each encountered dielectric interface, a parameter k denoting the pulse subdivision (Fig. 1). Each propagating signal is thus

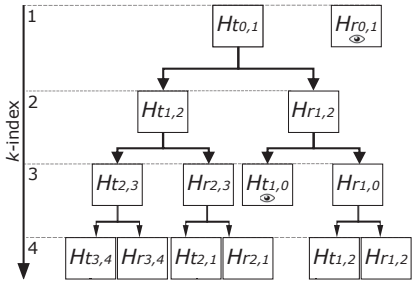

FIG. 1. Scheme of the iterative tree algorithm procedure. Each k-incrementation gives access to further possible events based on the previous ones at $k-1$. Detected pulses have been marked with an eye in the node box.

the sum of reflection and transmission processes occurring at the k-1 algorithm step, involving surrounding dielectric layers and verifying propagation continuity:

$$E^k_{r_{i,i+1}} = H_{r_{i,i+1}}(E^{k-1}_{r_{i,i-1}} + E^{k-1}_{t_{i-1,i}}) \quad (1a)$$

$$E^k_{r_{i,i-1}} = H_{r_{i,i-1}}(E^{k-1}_{r_{i,i+1}} + E^{k-1}_{t_{i+1,i}}) \quad (1b)$$

$$E^k_{t_{i,i+1}} = H_{t_{i,i+1}}(E^{k-1}_{r_{i,i-1}} + E^{k-1}_{t_{i-1,i}}) \quad (1c)$$

$$E^k_{t_{i,i-1}} = H_{t_{i,i-1}}(E^{k-1}_{r_{i,i+1}} + E^{k-1}_{t_{i+1,i}}) \quad (1d)$$

All optical paths are theoretically recorded by the detector among which, a handful is importantly contributing to the 4 layers stack signal. The numerical procedure saved a total of 33 different optical paths (Fig. 2). The correlation coefficient between the real and the optimized transfer function leading to the temporal signal measured is greater than 0.999. This new algorithm is used to understand a stratified material response by terahertz time domain characterization. The identification of the main optical paths responsible of the reflected signal led to an optimized signal reconstruction.

To achieve the simulations and the characterization, we carefully extracted the dielectric properties of each painting layer (see table 1). Both the real and the imaginary part of the dielectric function are fitted with a first order Debye relaxation model. Debye model's parameters are determined by an inverse algorithm and used to reconstruct the obtained signals.

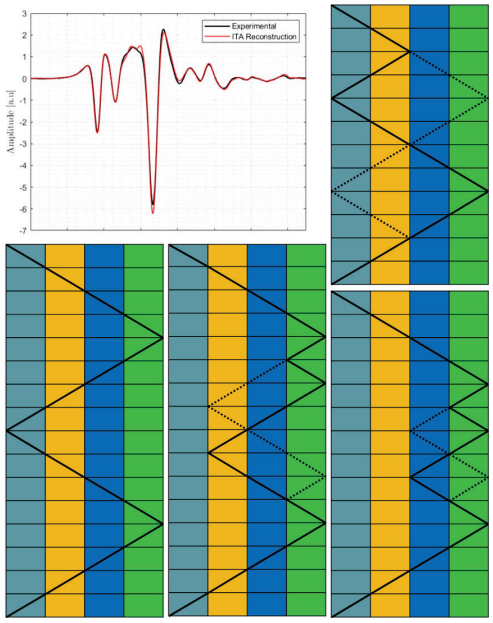

FIG. 2. Identification of some optical paths contributing to the recorded signal. The shape is mainly recovered for k-value spanning from 13 to 17. Dashed paths represent symmetric routes, providing the exact same intensity to the signal.

TABLE I. Fitting Debye parameters for the four coatings of the aeronautic painting stack extracted from a Levenberg-Marquadt algorithm.

	ε_∞	$\Delta\varepsilon$	τ [fs]	d^{IEP} [μm]	$d^{Optical}$ [μm]
Primer	3.7151	0.8461	83.038	32.2	33.1 $\pm$1
Sub-layer	3.2290	0.7095	72.074	72.7	78.6 $\pm$1
Top-layer	4.2586	0.9150	83.733	88.0	83.8 $\pm$1
Varnish	2.47834	0.3890	70.823	64.5	68.8 $\pm$1

THz pulses are generated by focusing ultrafast (100 fs) pulses of near infrared light onto the gap between two electrodes (TPS 4000 Teraview). A signal-to-noise ratio (SNR) of around 4000:1, limited by the thermal noise of the antenna, is achieved.

For the painting on copper substrate, the situation is quite different because we have only few information about the used materials and the different thicknesses. Then, THz properties of varnish layers are extracted through a specific custom-made algorithm for describing ultrathin multilayered materials. The algorithm is planned to generate a wide set of combinations between the dielectric properties and the thickness. Then, it extracts the trio minimizing the quadratic error amplitude between the simulated signal and the measured one. The Fig. 3. reports the recorded signals from the copper substrate, a pigment-copper location and a varnish-pigment-copper multi structure.

Furthermore, we extracted the thickness of the varnish by means of terahertz time-domain spectroscopy and we compared it with the data obtained by a profilometer from an area

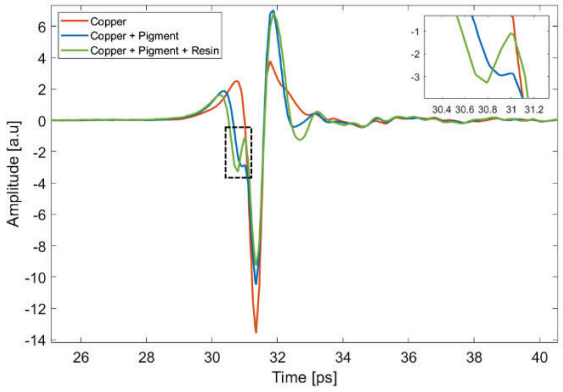

FIG. 3. THz time-domain signal for the different structures. Through these signals the dielectric properties of each layers have been extracted using a specific algorithm. A slight detection-time difference is recorded between the peak arising from the reflection on pigment and the one from the varnish.

of the sample where the varnish was partially missing. We found that the painting layer is about 40 m thick, the varnish around 20 m thick with an optical index in the range of 2.2. This information is very precious within the conservation field, considering that, once that the varnish layer has lost its optical performances, it has to be removed and replaced. The evaluation of the amount of varnish removed from a painted surface is particularly important during a cleaning operation. In fact, since this removal and replacement is not always desirable as it can lead to the damaging of the painting, it is sometime prescribed not to remove the varnish in its full thickness. Thus, the cleaning operation requires a straight control for which THz may provide a non-invasively and contactless solution.

III. CONCLUSION

We use a combination of numerical simulation to find parameters that best describe reflections from a given multilayered paint sample. The reflected terahertz time-domain waveform is simulated using a Fresnel's equations, where each paint layer is represented by a set of numerical parameters that describe both the thickness and the optical response. Numerical optimization is then employed to find a set of values for those parameters that best fits the measurements.

[1]S. Krimi, J. Klier, J. Jonuscheit, G. von Freymann, R. Urbansky, and R. Beigang, "Highly accurate thickness measurement of multi-layered automotive paints using terahertz technology," Applied Physics Letters **109**, 021105 (2016).

[2]J. Van Mechelen, A. Kuzmenko, and H. Merbold, "Stratified dispersive model for material characterization using terahertz time-domain spectroscopy," Optics letters **39**, 3853–3856 (2014).

[3]Q. Cassar, A. Chopard, F. Fauquet, J.-P. Guillet, M. Pan, J.-B. Perraud, and P. Mounaix, "Iterative tree algorithm to evaluate terahertz signal contribution of specific optical paths within multi-layered materials," IEEE Transactions on Terahertz Science and Technology (2019).

Terahertz Pulsed Imaging for Nondestructive Evaluation

A. Locquet[1,2], J.Dong[1,2], M. Zhai[1,2], and D.S. Citrin[1,2]
[1]UMI 2958 Georgia Tech-CNRS UMI2958, Georgia Tech Lorraine, 2 Rue Marconi, 57070 Metz, France
[2] School of Electrical and Computer Engineering, Georgia Institute of Technology, Atlanta, Georgia 30332-0250 USA

E-mail: alocquet@georgiatech-metz.fr

Abstract – Terahertz time-domain spectroscopy has proven to be a useful tool for the nondestructive evaluation of several non-conductive materials. We demonstrate how the combination of a good understanding of the material response with signal processing techniques can lead to significant improvement in terms of resolution and dynamic range.

Keywords – nondestructive evaluation, THz-TDS

We review recent results from our group on the application of THz time-domain spectroscopy, often in combination with signal processing techniques, to samples of different nature.

Signal processing techniques based on time-domain sparse deconvolution [1] and on spectral-domain autoregressive extrapolation [2] will be demonstrated.

In terms of applications, results in fiber-reinforced composites of different types (glass, carbon, mixed-type) [3,4,5], on optically thin layers of paint or oxides on a metal substrate [6], and on various works of art [7,8], will be presented.

ACKNOWLEDGMENTS

This work was financially supported by the Conseil Régional Grand Est, Arcelor Mittal Maizières Research, and CPER SusChemProc.

REFERENCES

[1] J. Dong, X. Wu, A. Locquet, and D.S. Citrin, "Teraherthz super-resolution stratigraphic characterization of multi-layered structures using sparse deconvolution", IEEE Trans. THz Sci. Technol. 3, 260 (2017).

[2] J. Dong, A. Locquet, and D. S. Citrin, "Depth-resolution enhancement of terahertz deconvolution by autoregressive spectral extrapolation", Optics Letters 42, 1828 (2017).

[3] J. Dong, B. Kim, A. Locquet, P. McKeon, N. Declerq, D. Citrin, "Nondestructive evaluation of forced delamination in glass fiber-reinforced composites by terahertz and ultrasonic waves", Compos. Part B 79, 667(2015).

[4] J. Dong, A.Locquet. N. Declerq, and D.S. Citrin, "Polarization-resolved terahertz imaging of intra- and inter-laminar damages in hybrid fiber-reinforced composite laminate subject to low-velocity impact", Compos. Part. B 92, 167 (2016).

[5] J. Dong, P. Pomerade, L. Chemami, A. Locquet, F. Meraghni, N. Declercq, D.S. Citrin, "Visualization of carbon fiber-reinforced composites using polarization-sensitive terahertz imaging", NDT&E Int. 99, 72 (2018).

[6] J. Dong, A. Locquet, and D. S. Citrin, "Terahertz Quantitative Nondestructive Evaluation of Failure Modes in Polymer-Coated Steel.", IEEE J. Sel. Top. Quantum Electron. 23, 8400207 (2017).

[7] J. Dong, J. Bianca Jackson, M. Melis, D. Giovannacci, G.C. Walker, A. Locquet, J.W. Bowen, and D. S. Citrin, "Terahertz Frequency-Wavelet Domain Deconvolution for Stratigraphic and Subsurface Investigation of Art Painting", Opt. Express 24, 26972 (2016).

[8] J. Dong, A. Locquet, M. Melis, and D. S. Citrin, « Global mapping of stratigraphy of an old-master painting using sparsity-based terahertz reflectometry", Sci. Rep. 7, 15098 (2017).

Yannick De Wilde (ESPCI-Paris)

Title: Sub-wavelength studies of plasmonic devices and thermal sources

Abstract: In this presentation, I will first show how the use of scattering-type near-field scanning optical microscopy (sNSOM) allows one to go beyond the diffraction limit by capturing the contribution of evanescent waves. While sNSOM generally requires the use of an external source, we will first show its adaptation to the detection of the field produced on active plasmonic devices based on quantum cascade lasers [1], and then using the sole thermal radiation of a sample in a mode called thermal radiation scanning tunneling microscopy (TRSTM). The TRSTM method allows one to perform both infrared imaging and Fourier transform infrared (FTIR) spectroscopy at the nanoscale, and produces a signal which is closely related to the local density of electromagnetic states. Probing the thermal radiation in the near field has allowed one to reveal extraordinary coherence effects associated with surface polaritons, with strong deviation from Planck blackbody spectrum [2, 3].

Besides investigating surface polaritons, we have recently used the TRSTM to probe the near-field at the surface of single metal-insulator-metal plasmonic antennas (MIM) made of a 2 x 2 microns square patch of gold separated from a gold mirror by a silica spacer layer. Using a spatial modulation spectroscopy scheme modified to detect the far-field thermal radiation from single MIMs, we manage to suppress the background radiation from the substrate, which is an important problem when measuring the FTIR spectrum from subwavelength objects. We then measure the spectrum of the emissivity of a single MIM, which is equal to the absorptivity according to Kirchhoff's law [4].

[1] A. Babuty, A. Bousseksou, J.−P. Tetienne, I. Moldovan Doyen, C. Sirtori, G. Beaudoin, I. Sagnes, Y. De Wilde, R. Colombelli, Semiconductor Surface Plasmon Sources, PHYSICAL REVIEW LETTERS, 104, 226806 (2010).

[2] A. Babuty, K. Joulain, P.-O. Chapuis, J.-J. Greffet, Y. De Wilde, Blackbody spectrum revisited in the near-field, PHYSICAL REVIEW LETTERS, 110, 146103 (2013).

[3] F. Peragut, L. Cerutti, A. Baranov, J.-P. Hugonin, T. Taliercio, Y. De Wilde, J.-J. Greffet, Hyperbolic metamaterials and surface plasmon polaritons, OPTICA, 4, 1409-1415 (2017).

[4] C. Li, V. Krachmalnicoff, P. Bouchon, J. Jaeck, N. Bardou, R. Haïdar, Y. De Wilde, Near-Field and Far-Field Thermal Emission of an Individual Patch Nanoantenna, PHYSICAL REVIEW LETTERS, 121, 243901 (2018).

Overview on Spin Photogalvanics Induced by Terahertz Radiation

S. D. Ganichev[1,2]
[1] Terahertz Center TerZ, University of Regensburg, Regensburg, Germany
[2] Department of CENTERA, CENTERA University, Warsaw, Poland

E-mail: sergey.ganichev@physik.uni-regensburg.de

Abstract – In this tutorial talk we introduce theoretical and experimental studies on spin-related photogalvanic effects.

Keywords – terahertz, spin, photogalvanics

The paper overviews theoretical and experimental studies on spin-related photogalvanic effects, for recent review see [1]. A short phenomenological introduction is followed by the discussion of the circular photogalvanic effect (CPGE) and the direct (inverse) spin-galvanic effect. Then we consider the pure spin currents and magneto-gyrotropic photocurrents. Finally, we briefly discuss the spin-dependent photogalvanics in topological insulators. Various aspects of these phenomena will be addressed including experimental achievements, phenomenological description, models visualizing physics of nonlinear responses, and microscopic theory of individual effects.

Circular photogalvanic effect and the spin-galvanic have in common, that the current flow is driven by an asymmetric distribution of carriers in $\boldsymbol{k}$-space in gyrotropic systems with lifted spin degeneracy due to k-linear terms in the Hamiltonian. CPGE requires excitation with circularly polarized radiation which yields optical spin orientation. It is the result of selective photoexcitation of carriers in $\boldsymbol{k}$-space with circularly polarized light due to optical selection rules. The spin-galvanic effect is caused by asymmetric spin-flip scattering of spin polarized carriers. It is determined by the process of spin relaxation and may be generated by any means of spin injection. The inverse spin-galvanic effect has also been detecting demonstrating that electric current in non-magnetic but gyrotropic materials results in a non-equilibrium spin orientation. In some optical experiments the photocurrent may represent a sum of spin-galvanic and circular photogalvanic effects effects. Both effects provide methods to determine spin relaxation times. Furthermore, the relative strengths of Rashba and Dresselhaus terms describing the spin-orbit coupling in semiconductor quantum well structures can be extracted from spin photocurrent measurements, opening a way to determine the different contributions to spin-orbit coupling. While for the spin-galvanic and the CPGE photocurrents spin orientation is needed pure spin currents and the magneto-gyrotropic effect can be generated even by unpolarized radiation. Microscopically it is caused by electron gas heating followed by spin-dependent relaxation.

In last several years it has been demonstrated that photogalvanics and magneto-photogalvanics can also be efficiently use for probing topological surface and edge states. It is shown that THz radiation results in spin-polarized *dc* electric current, which is sensitive to the radiation polarization and may have a component changing the sign by reversing the radiation helicity. An important advantage of photogalvanic effects is that, due to symmetry arguments, they can be used to excite selectively the surface states of most 3D TIs. A possibility to selectively probe the surface states even at room temperature is particularly helpful in the search for novel 3D TIs in which transport experiments are often handicapped by a residual bulk charge carrier density.

REFERENCES

[1] E.L. Ivchenko and S.D. Ganichev, *Spin Photogalvanics, in Spin Physics in Semiconductors*, ed. M.I. Dyakonov (2nd edition, Springer 2016).

.

Terahertz communications using photonics based emitters for 300 GHz band

C. Belem-Goncalves[1,2,3], E. Lacombe[2], V. Gidel[2], C. Durand[2], F. Gianesello[2], D. Gloria[2], C. Luxey[3], V.K. Chinni[1], P. Latzel1, M. Zégaoui[1], C. Coinon[1], X. Wallart[1], E. Peytavit[1], J.F. Lampin[1], K. Engenhardt, P. Szriftgiser[4], M. Zaknoune[1]and G. Ducournau[1]

[1] Institut d'Electronique, de Microélectronique et de Nanotechnologie, Univ. Lille, CNRS, Centrale Lille, ISEN, Univ. Valenciennes, UMR 8520 - IEMN, F-59652 Villeneuve d'Ascq, France.

[2]STMicroelectronics, 850 rue Jean Monnet | 38926 Crolles | France

[3]Polytech'Lab, Université Nice-Sophia, 06560 Valbonne, France.

[4]Laboratoire de Physique des Lasers Atomes et Molécules (PhLAM), UMR CNRS 8523, Université de Lille, F-59655 Villeneuve d'Ascq Cedex, France.

E-mail: guillaume.ducournau@univ-lille.fr

Abstract – This paper will present the context of THz communications and results of THz link enabled by photonics-based emitters in the 300 GHz band.

Keywords – terahertz, components, wireless

I. Introduction

Data traffic is increasing exponentially, with internet protocol traffic expected soon to reach over 100 exabytes per month. Since the fastest-growing part of data traffic is related to wireless channels, such an increase in network capacity requires much higher wireless transmission data rate links. Beyond the E-band (71-76 GHz and 81-86 GHz) that will be rapidly saturated, the millimeter (D-band; 110 GHz-170 GHz) and sub-millimeter range, between 275 GHz and 400 GHz have strong potential to enable these applications. Among potential solutions is to use high data rate terahertz links using photonics-based terahertz emitters (UTC-PD) to downconvert optical fluxes to mmWaves [1]. Recent development uses III-V photonics as well as silicon photonics [2] has been demonstrated as enabling technology to achieve mmWave and terahertz links with up to 100 Gbit/s data rates utilizing the recently released frequencies of the IEEE 802.15.3d standard for 100G wireless links. Indoor and outdoor field trial will be presented at the workshop as well as ongoing projects.

Acknowledgments

This work was supported by the CNRS, IEMN, University of Lille. The presented results have also been supported by ST-IEMN common laboratory, Nano 2017 and IPCEI program/Nano 2022, Equipex programs 'FLUX', 'EXCELSIOR', ANR 'COM'TONIQ', Era-net Chist-Era'TERALINKS', by CPER 'Photonics for society', IRCICA and PhLAM, and contribute the "digital world" Hub 3 of the I-Site Université de Lille. Part of the work was realized under an academic collaboration with Tektronix, were a 50GS/s arbitrary waveform generator AWG70001A and 200GS/s real-time oscilloscope DPO77002SX were used.

References

[1] T. Nagatsuma et al., "Advances in terahertz communications accelerated by photonics", Nature Photon., vol. 10, pp. 371–379, 2016, doi: 10.1038/nphoton.2016.65.

[2] E. Lacombe et al. "10 Gbps indoor THz communications using Industrial Si Photonics Technology", IEEE Microwave and Wireless Components Letters, Vol. 28, No. 4, pp. 362-364, 2018.

.

Investigations of the Receiving Antennas Designed for FET THz Detectors

Zhaofeng Li[1,2,3], Wei Yan[1], Bowen Zhang[1,3], Zhen Huang[1,3], Xiaodong Wang[1,2,3], and Fuhua Yang [1,2,3,4]

[1]Engineering Research Center for Semiconductor Integrated Technology, Institute of Semiconductors, Chinese Academy of Sciences, Beijing 100083, China

[2]Center of Materials Science and Optoelectronics Engineering, University of Chinese Academy of Sciences, Beijing 100049, People's Republic of China

[3]School of Microelectronics, University of Chinese Academy of Sciences, Beijing 100049, China

[4]State Key Laboratory of Superlattices and Microstructures, Institute of Semiconductors, Chinese Academy of Sciences, Beijing 100083, China

E-mail: yanwei@semi.ac.cn

Abstract –The development of terahertz (THz) detectors based on field effect transistors (FETs) with planar antennas requires improving the detector responsivity, thus it needs higher coupling efficiency between the antenna and THz radiation. The impact of substrate effect and channel electric field at the gate edge of FET on the detector responsivity have been investigated for the case of semi-infinite substrate. The simulation results show that the thickness of substrate and the electric field in the channel have a significant impact on the detector responsivity. The simulation results are also confirmed by experiments.

Keywords – terahertz detectors, planar antenna, channel electric field, antenna efficiency, FET

I. INTRODUCTION

Field effect transistors have been used as terahertz detectors for nearly 30 years. There are many successful methods to improve the responsivity. The most popular one is to integrate some kind of planar antennas to FET THz detectors. It has been proven that the integration of planar antenna could improve the responsivity of FET THz detectors significantly[1-3]. Depending on the materials and devices being used, various types of planar antenna and structures could be integrated with the FET THz detectors, such as patch antenna [4], bowtie antenna [5], trip resonant antenna [6], floating antenna [7], novel nanoantennas [8], etc.

Despite the progress in the research of field effect transistor terahertz detectors with integrated planar antennas, the responsivity of FET THz detectors are still far from theoretically predicted level due to the limitation in several aspects: First, the limitation of the substrate effect. Because the semiconductor device needs to be fabricated on a semiconductor wafer substrate, the presence of the substrate causes a lot of terahertz radiation to be not coupled by the antenna, thereby greatly reducing the performance of the antenna; second, the impedance matching problem between the antenna and the transistor. Because the input impedance of the transistor in the terahertz band is difficult to extract by actual testing. Therefore, the impedance matching between the antenna and the transistor is difficult to accurately perform; finally, a proper model to design the antenna and optimize its receiving characteristics at desired frequency is still lacking.

In this paper, the impact of Substrate effect and channel electric field at the gate edge of FET on the detector responsivity have been investigated for the case of semi-infinite substrate. The simulation research of responsivity versus substrate thickness has been performed. Then, we present a further analysis of the substrate effect with different thickness and its relationship with the detector responsivity. What's more, we propose a method to design the planar antenna, which is based on the simulation of channel electric field at the gate edge of FET. This method is especially suitable for the situation where the FET input impedances may not be conveniently determined, which is often the case in the THz range. We hope all of the results will be enlightening for future design of FET THz detectors.

II. SIMULATION DESCRIPTION

The simulation firstly considered here is a simplified model of THz detector based on GaN HEMT (high electron mobility transistor) which can be fabricated in the experiment. The simulated structure consists of a grounded infinite slab substrate with a planar antenna printed on the top surface. The substrate with metalized back-plane contains several layers as shown in Fig. 1 which refers to the substrate structure of the real GaN HEMT in the experiment. In our simulation, the substrate is extending towards infinity in the direction of length and width, but with finite thickness. We mainly change the thickness of sapphire layer for variation and set the thickness of other layers as constant. As for the planar antenna, we choose four different types for comparison in our simulation. Those four types are: single-dipole, dual-dipole, four-leaf-clover, and bow-tie antenna. The

dimensions of four antennas are all designed for 900GHz as shown in Fig. 2 and they are made of two metal layers (200nm Au layer on the top and 20nm Ni layer on the bottom). In the simulation, the conductivity of Au and Ni is set as 4.1×107 S/m and 1.45×107 S/m. We choose the commercial program COMSOL using the FEM algorithm due to the ability to simulate the infinite substrate.

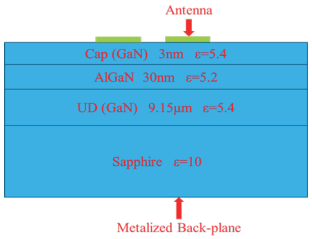

Fig. 1. The structure of substrate in the simulation. The relative dielectric constant of each layer is represented by ε.

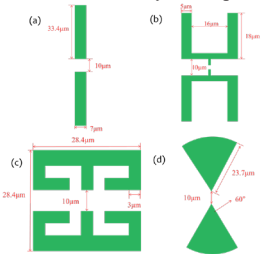

Fig. 2. Schematic of four antennas in the model: (a) single-dipole antenna (b) dual-dipole antenna (c) four-leaf-clover antenna (d) bow-tie antenna.

III. RESULTS AND DISCUSSION

A. Substrate Effect

The substrate effect resulting from the inside propagation of electromagnetic wave could be analyzed by a simplified 1-dimensional model in the waveguide theory [9]. As the substrate becomes electrically thicker, more substrate modes would be generated. In the meantime, the ratio of mode's power propagating in the substrate to the total power for each mode would become larger [10].

The power radiated by planar antenna printed on the dielectric substrate can be divided into two parts: one part propagating away from the antenna in the air, the other part radiated into the substrate. The ratio R of the power radiated into the air to the total power radiated by the planar antenna can be numerically calculated. It can be defined as:

$$R = \frac{P_{rad}}{P_{rad} + P_{sub}} \tag{1}$$

where P_{rad} is the power radiated into the air by the antenna, P_{sub} represent the radiated power confined to the substrate. The simulation results of substrate effect are presented in Fig. 3-4.

From simulation results, we can obtain that the ratio (R) of the power radiated into the air to the total power radiated by planar antenna shows several peaks when the substrate thickness increases. Independent of antenna structure and source impedance, the ratio R would only depend on the substrate thickness, the dielectric constant of substrate, and the operation frequency.

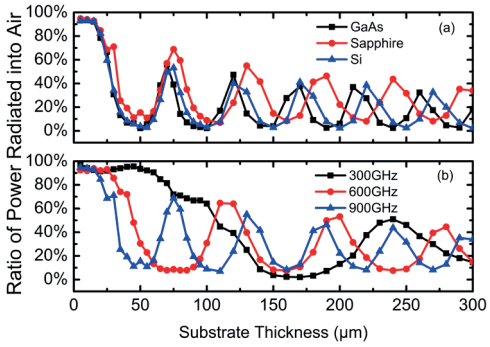

Fig. 3. (a) The radiation power ratio R versus substrate thickness of single dipole antenna at 900GHz (using Sapphire, GaAs, Si as substrate). (b) The radiation power ratio R versus substrate thickness of single dipole antenna at 300, 600, 900GHz (using Sapphire as substrate).

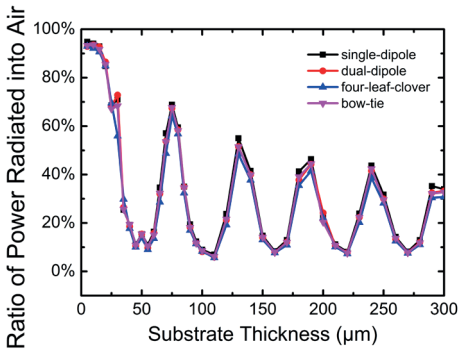

Fig. 4. The radiation power ratio R of four antennas versus substrate thickness at 900GHz (using sapphire as substrate).

The responsivity of the detector can be defined as[11]:

$$R_u = \frac{e|Z_T|^2 \lambda^2 U}{2K_B T S_{ant} \mathrm{Re}(Z_T) P_0} \tag{2}$$

where e is the electron charge, K_B is the Boltzmann constant, and T is the temperature of the detector, λ is the wavelength of THz wave, Re is taking the real part of the complex variable, Z_T is the input impedance between the gate and source electrode of the transistor channel, S_{ant} is the pixel area of the THz detector, U is the radiation intensity in the direction and P_0 is the power delivered to the terminals of antenna.

The values of U can be extracted from the simulation of the planar antenna in the radiating mode. Based on the positive correlation between radiation intensity U and responsivity R_u, we could improve the corresponding responsivity by increasing the radiation intensity in the direction of interest. Based on (2), one can obtain the correlation between responsivity R_u and the ratio R as shown in Fig. 5.

Because the radiation power ratio R is independent of the planar antenna structure and source impedance, R can

be a very useful parameter to choose proper substrate thickness under certain substrate material and operation frequency. This substrate effect theory has already been confirmed by experiments[12].

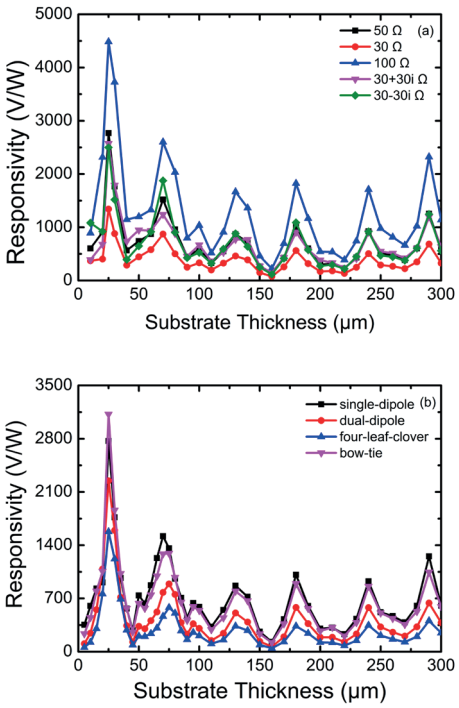

Fig. 5. (a) The simulated responsivity of different FET input impedances versus substrate thickness at 900GHz (using single dipole antenna). (b) The simulated responsivity of four types of antennas versus substrate thickness at 900GHz. (The FET impedance is set as 50Ω.)

B. Channel Electric Field at the Gate Edge of FET

The application of the antenna in FET THz detectors involves a two-part theory: the first part of the theory is the antenna theory. This part of the theory is mainly used to explain how the antenna couples and emits electromagnetic waves. This part of the theory is quite mature. The antenna integration in FET THz detectors is basically the conventional application of the mature antenna theory. The second part of the theory is the terahertz detection theory of FET THz detectors. Through this part of theory, we study how the antenna interacts with the transistor and how it enhances the detector's detection performance. This part of the theory still needs to be investigated and has possibility to be improved.

At present, there are two main theoretical terahertz detection theory of FET THz detectors: plasma wave theory and self-mixing theory. In the plasma wave theory, the role of the antenna is mainly energy transfer: the antenna is connected to the electrodes of the transistor (gate-source or source-drain), couples the THz waves in the space and transfers the energy of the electromagnetic waves to the load (transistor). While in self-mixing theory, the main role of the antenna is electric field enhancement[13]: the antenna couples the THz waves in the space and enhances the electric field in the channel of the transistor. In this theory, the antenna and the electrodes of the transistors do not have to be connected, nor do they have to involve energy transfer. According to two different detection theories, we have two different antenna simulation models: energy transfer model and electric field enhancement mode. The first one will focus on antenna parameters and impedence matching; for the second model, we mainly cencerns about the electric field enhancement in the channel of the transistor.

At present, both models can guide the antenna design in the FET THz detectors. However, whether these two theories can be achieved in the same way or which one is more advantageous remains to be studied.

In this work, we try to identify the resonant frequencies of different antennas in terms of the maximum channel electric field at the gate edge of HEMT in the receiving mode. The simulation and experiment results show in Fig. 6-7.

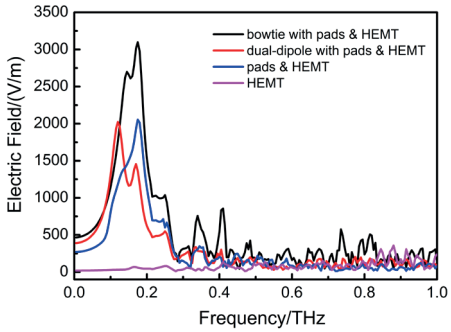

Fig. 6. The simulated electric field of several structures versus frequency.

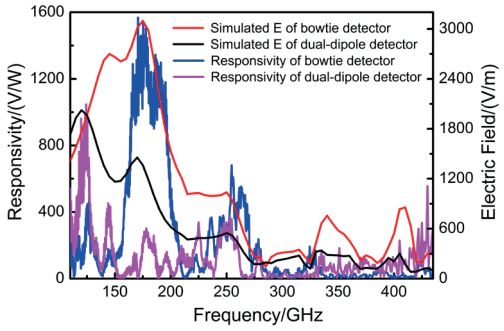

Fig. 7. The measured responsivities as a function of frequency for THz detectors integrated with bowtie and dual-dipole antennas.

We can see that the experimental results and the simulation results are in good agreement. It means that in the case when the transistor impedance cannot be accurately extracted, we can use electric field enhancement mode to design the antenna of FET THz detectors.

IV. Conclusions

In this paper, we carried out a study of substrate effect in FET THz detectors integrated with four different

planar dipole antennas. It is shown that both the substrate effect and antenna design would play important roles in improving the responsivity of THz detectors. When the substrate material and operation frequency are decided, the method to choose proper substrate thickness has been suggested. What's more, we have proposed a method to identify the resonant frequencies and evaluate the performances of different antennas for FET THz detectors on the basis of the simulated channel electric field at the gate edge. This method is especially suitable for the situation where the input impedances of FETs cannot be conveniently obtained in the THz regime. We hope these results would be enlightening for the future design of THz detectors based on FETs.

ACKNOWLEDGMENTS

This work was financially supported by the National Natural Science Foundation of China (61971395).

REFERENCES

[1] Sun, Y.F., et al., Room temperature GaN/AlGaN self-mixing terahertz detector enhanced by resonant antennas. Applied Physics Letters, 2011. 98(25).

[2] Bauer, M., et al. Bow-tie-antenna-coupled terahertz detectors using AlGaN/GaN field-effect transistors with 0.25 micrometer gate length. in Microwave Integrated Circuits Conference (EuMIC), 2013 European. 2013. IEEE.

[3] Boppel, S., et al., CMOS Integrated Antenna-Coupled Field-Effect Transistors for the Detection of Radiation From 0.2 to 4.3 THz. Ieee Transactions on Microwave Theory and Techniques, 2012. 60(12): p. 3834-3843.

[4] Ojefors, E., et al., A 0.65 THz focal-plane array in a quarter-micron CMOS process technology. Solid-State Circuits, IEEE Journal of, 2009. 44(7): p. 1968-1976.

[5] Schuster, F., et al., Broadband terahertz imaging with highly sensitive silicon CMOS detectors. Optics Express, 2011. 19(8): p. 7827-7832.

[6] Sun, Y., et al., Room temperature GaN/AlGaN self-mixing terahertz detector enhanced by resonant antennas. Applied Physics Letters, 2011. 98(25): p. 252103.

[7] Sun, J., et al., High-responsivity, low-noise, room-temperature, self-mixing terahertz detector realized using floating antennas on a GaN-based field-effect transistor. Applied Physics Letters, 2012. 100(1): p. 013506.

[8] Hou, H., et al., A sub-terahertz broadband detector based on a GaN high-electron-mobility transistor with nanoantennas. Applied Physics Express, 2016. 10(1): p. 014101.

[9] Pozar, D., Considerations for millimeter wave printed antennas. IEEE Transactions on antennas and propagation, 1983. 31(5): p. 740-747.

[10] Coquillat, D., et al., Improvement of terahertz field effect transistor detectors by substrate thinning and radiation losses reduction. Optics Express, 2016. 24(1): p. 272-281.

[11] Zhang, B., et al., Analysis of Substrate Effect in Field Effect Transistor Terahertz Detectors. Ieee Journal of Selected Topics in Quantum Electronics, 2017. 23(4).

[12] Tu, X., et al., Investigation of antenna-coupled Nb5N6 microbolometer THz detector with substrate resonant cavity. Optics Express, 2018. 26(7): p. 8990-8997.

[13] Sun, J.D., et al., Probing and modelling the localized self-mixing in a GaN/AlGaN field-effect terahertz detector. Applied Physics Letters, 2012. 100(17).

Current-driven optical response of plasmonic crystal: From dissipation to amplification

I.V. Gorbenko[1], V.Yu. Kachorovskii[1,2], W. Knap[2]
[1] Ioffe Institute, St. Petersburg, Russia
[2] CENTERA Laboratories, Institute of High Pressure Physics, Warsaw, Poland, Warsaw, Poland

E-mail: kachor.valentin@gmail.com

Abstract –We study optical response of a plasmonic crystal based on multi-gated 2D structure with periodic modulation of the electron density in the device channel. In such a structure, the plasma wave velocity is periodically modulated as well. We consider the simplest model of periodically alternating stripes of the electron density and plasma wave velocity: active regions with high plasma wave velocity and passive regions with low plasma wave velocity. Terahertz radiation applied to such a structure excites plasmonic resonances both in the active and passive stripes. The width of the resonances is determined by the momentum relaxation rate. For sufficiently large relaxation rates, the resonances in the passive regions strongly overlap and only "active resonances" survive. In this regime, the plasmonic oscillations in the active regions rapidly decay into the passive regions, so that different active regions are disconnected at plasmonic frequencies but connected at zero dc frequency. We assume that dc current is applied to this plasmonic crystal and calculate radiation-induced correction to the dissipation in the channel. We demonstrate that with increasing the dc current this correction changes sign, which results in amplification of the optical signal.

Keywords – plasma waves, plasmonic crystal, optical response, amplification of terahertz radiation

I. INTRODUCTION

As was shown about 25 years ago[1], a direct current (dc) in the channel of a field effect transistor (FET) might become unstable. The instability results in the generation of plasma oscillations, whose frequency can be tuned by the gate voltage. As a consequence, FET should emit a THz radiation. Nonlinear properties of the plasma waves in a FET channel may be also used for detection of THz radiation[2].

The plasma wave approach to THz electronics was strongly supported by observation of both detection (resonant and broadband) and emission of sub-THz and THz radiation by nanoscale FETs based on different materials (see review in Refs. 3-4). Plasmonic THz detectors are tunable by varying the gate voltage and the drain current, with fast response time and demonstrate relatively low noise equivalent power up to room temperature. Hence, they are promising candidates for THz systems applications. However, responsivity of THz detectors based on single FETs is still quite low due to weak coupling to the THZ radiation.

A possible way to improve the responsivity and emission power is to use periodic structures (such as FET arrays, grating structures, and multi-gate structures) instead of single FETs. Such structures already demonstrated excellent performance as THz detectors and first observations of THz emission were also reported (see discussion in Ref. 5 and references therein).

The periodic plasmonic structures can be considered as one-dimensional (1D) plasmonic crystals[6]. Here we discuss an optical response of such a 1D plasmonic crystal to THz radiation in the presence of driving dc electric current. This theoretical study is motivated by preliminary experiments[5], where transmission of THz radiation through multifinger-gated structure was studied and current-driven amplification of the optical signal was observed. Here we assume that electron-electron collisions are very fast, turning the system into the hydrodynamics regime and study optical response within hydrodynamical approximation.

II. MODEL

We consider the plasma crystal (see Fig. 1) consisting of strips of length L with high plasma wave velocity S (active regions) separated by strips having length L' with much smaller velocity $s' \ll s$ (passive regions).

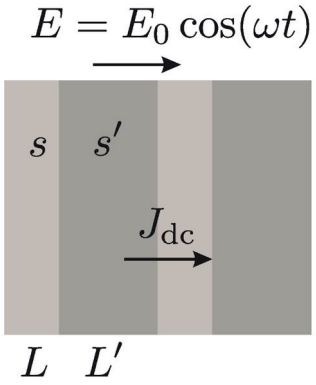

Fig.1 1D plasmonic crystal driven by dc current J_{dc} in the oscillating field of THz radiation.

Such a structure can be realized in a device with floating interdigitated gates or with multiple gates that are biased individually in such a way that the potential difference between the gate and channel has translational symmetry even when current flows in the device channel. The structure is illuminated by radiation with the large wavelength, $\lambda \gg L, \lambda \gg L'$, so that the electric field of radiation is approximately homogeneous. This field excites plasmonic oscillations in the active regions with the fundamental frequency $\omega_0 = \pi s / L$ and in the passive regions with the frequency $\omega'_0 = \pi s'/ L' \ll \omega_0$ (see Fig. 2). In this work, we

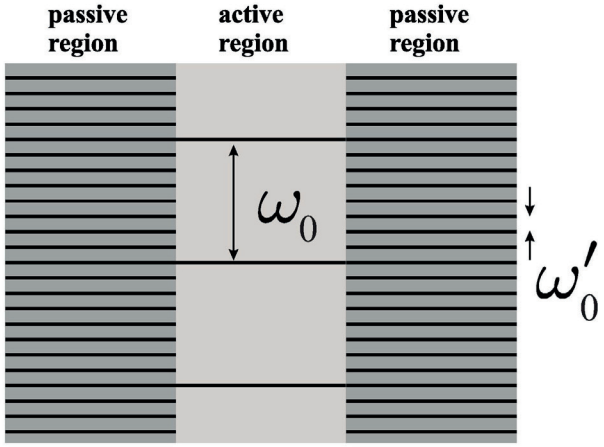

Fig 2. Active regions of the plasmonic crystal with large fundamental frequency are separated by passive regions with small frequency.

assume that momentum relaxation rate, γ, obeys the following inequalities

$$\omega_0 \gg \gamma \gg \omega'_0 . \qquad (1)$$

In this case, resonances in the passive region strongly overlap and plasmonic oscillations in the active region decay due to emission of the plasmons into the passive regions. This leads to renormalization of the effective damping rate of the "active" plasmonic resonances

$$\gamma \to \gamma_{\text{eff}} = \gamma + \frac{4s'}{L}. \qquad (2)$$

The condition $\gamma \gg \omega'_0$ also implies that plasma waves strongly decay along the passive region. This means that different active regions are disconnected at plasmonic frequencies (but connected at zero dc frequency).

We solve the standard set of hydrodynamic equations[1,2] and calculate dissipation in the channel $P = \int dx\, N\, m v^2 / \tau$, where $N = N_0 + \delta N$, and $v = V + \delta v$ are concentration and velocity in the channel including radiation-induced corrections δN and δV. Most importantly, the radiation-induced correction to dissipation

$$\delta P = \int dx \frac{m}{\tau}\left(N_0\, \delta v^2 + V \delta N \delta v \right), \qquad (3)$$

is not positively-defined (!!!) for non-zero dc current $J_{\text{dc}} = eN_0 V \neq 0$ in the channel. For $\delta P < 0$ the incoming radiation gains energy from the dc current that corresponds to amplification of the THz signal.

III. Results

In the absence of the driving current ($V = 0$) dissipation is positively defined and shows sharp plasmonic resonances with the width γ_{eff} (see Fig. 3)

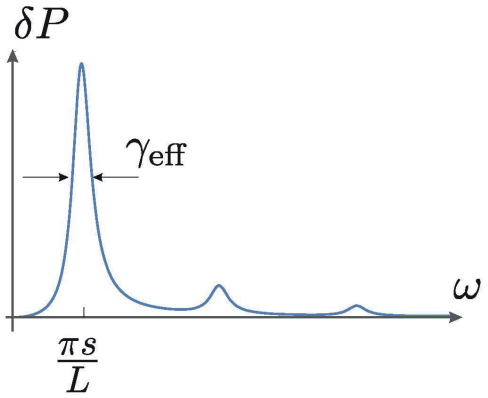

Fig. 3 Resonances in the dissipation in the absence of dc current

Next, we consider resonance corresponding to fundamental frequency $\omega_0 = \pi s / L$ and study what happens with increasing the dc current. The result is plotted in Fig. 4 (using different scale). As seen, with increasing the drift velocity in the channel the resonance is red-shifted and its amplitude decreases. For certain value of drift velocity, δP changes sign.

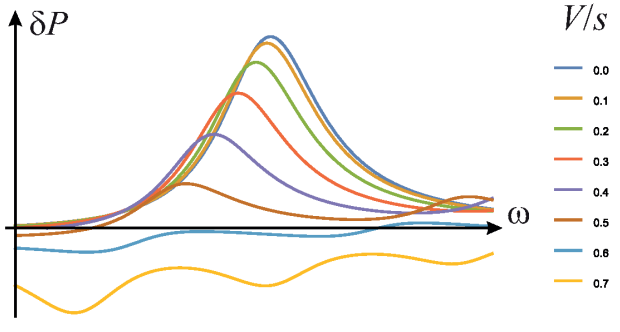

Fig 4. Dependence of dissipation in the channel on the frequency for different values of the drift velocity in the channel (only resonance corresponding to the fundamental harmonic is shown). With increasing drift velocity, δP changes sign, which implies amplification

Simple analytical expression for δP can be found in the resonant approximation, when $\omega \gg \gamma_{\text{eff}}$. In this case dissipation is given by

$$\delta P = \frac{L N_0 \left(eE_0\right)^2}{\pi^2 m} \frac{\gamma_{\text{eff}}}{\delta\omega^2 + (\gamma_{\text{eff}}/2)^2} A(x), \quad (4)$$

where $\delta\omega = \omega - \omega_0(x)$ is deviation of the radiation frequency ω from the Doppler shifted frequency of the fundamental harmonic,

$$\omega_0(x) = \frac{\pi}{L}\frac{s^2 - V^2}{s} = \frac{\pi s}{L}(1 - x^2), \quad (5)$$

and

$$A(x) = \frac{(1 - 3x^2)[1 + \cos(\pi x)]}{2(1 - x^2)^2} \quad (6)$$

is the numerical coefficient which depends on the ratio of the drift velocity to the plasma wave velocity: $x = V / s$. As seen, function $A(x)$ turns to zero at $x = x_0 = 1/\sqrt{3}$ (see Fig. 5).

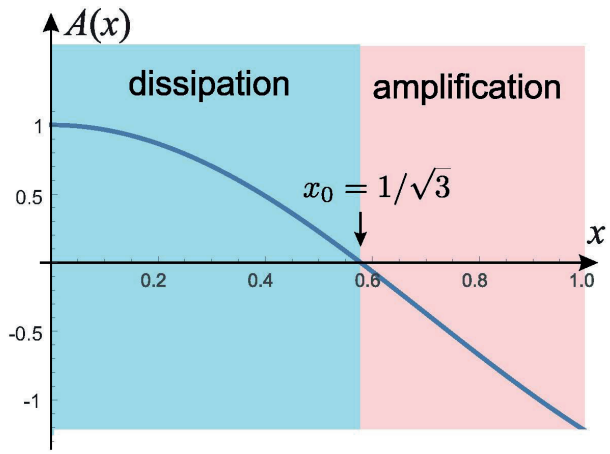

Fig. 5 Dependence of the dimensionless amplitude $A(x)$ on x.

IV. Conclusions

We discussed optical response of a 1D plasmonic crystal to the THZ radiation. We found analytical expression for dissipation power δP in the channel and demonstrated that at certain value of the current in the channel, δP changes sign. Hence, we predict amplification of electromagnetic radiation in a good qualitative agreement with recent experimental observations [5].

Acknowledgments

This work was financially supported by . was supported by RFBR (Grant No. 17-02-00217), by Foundation for the Advancement of Theoretical Physics and mathematics "BASIS", and by the Foundation for Polish Science through the grant MAB/2018/9 for CENTERA.

.....

References

[1] M.I. Dyakonov and M. S. Shur, Phys. Rev. Lett. **71**, 2465 (1993).
[2] M. I. Dyakonov and M. S. Shur, IEEE Trans. on Elec. Dev. **43**, 380 (1996).
[3] M. Shur, "Plasma Wave Terahertz Electronics", Electronics Letters **46**. 18 (2010).
[4] W. Knap, M. Dyakonov, D. Coquillat, F. Teppe, N. Dyakonova, J.Lusakowski, K. Karpierz, M. Sakowicz, G. Valusis, D. Seliuta, I.Kasalynas, A. El Fatimy, Y. M. Meziani, and T. Otsuji, "Field effect transistors for terahertz detection: physics and first imaging applications,"J. Infrared Milli. Terahz Waves **30**, 1319 (2009).
[5] Stephane Boubanga-Tombet, W. Knap, D. Yadav, A. Satou, D. B. But, V. V. Popov, V.Yu. Kachorovskii, and Taiichi Otsuji1, "Current Driven Plasmon Instabilities and Terahertz Amplification in Graphene", in press (2019)"
[6] V. Yu. Kachorovskii and M. S. Shur, "Currentt-induced terahertz oscillations in plasmonic crystal", Appl.Phys. Lett., 100, 232108 (2012)

.

Hartmut Roskos

"Light-matter interaction in a 1D THz photonic crystal cavity:
Ultrastrong coupling and nonlinear optics"

Short abstract:

"

This presentation explores enhanced light-matter interaction in a high-Q dielectric cavity for THz radiation.

A first study is devoted to polaritonic coupling of THz radiation with metallic THz metamaterials at room temperature. The ultrastrong coupling manifests itself in the formation of split cavity plasmon-polariton modes with a normalized coupling strength g/omega_c (2g: Rabi splitting, omega_c: angular frequency of the cavity resonance) above 0.1, indicative for the ultrastrong coupling regime. The Rabi splitting scales with the square root of the density of the metamaterial's "quasi-atoms" in the cavity; as this density is low (as compared with typical atomic systems), the observed strong light-matter interaction is a result of a huge effective transition dipole moment of the metamaterial. While devoted to the investigation of fundamental strong-coupling phenomena, our study suggests various applications of metamaterials in THz cavities. The strong field enhancement together with the rich functionalities of metamaterials can be exploited for the development of voltage-controlled modulators and frequency filters, and ultra-sensitive chemical and biological sensors.

A second study investigates third-harmonic generation with impurity atoms in silicon at off-resonant excitation conditions (photon energy much lower than impurity transition energy). The experiments were performed at the FELBE free-electron laser. The use of a cavity enables the enhancement of the electric radiation field. The dependence of the power of the third-harmonic signal on the THz laser power is stronger than expected. This is explained with an efficient impact ionization of neutral impurity atoms by free charge carriers accelerated in the laser field.

"

- Prof. Dr. Hartmut Roskos
Physikalisches Institut
Johann Wolfgang Goethe-Universität
Max-von-Laue-Str. 1
D-60438 Frankfurt am Main
Tel. (Sekret.): +49-69-798-47215
Tel. (direkt): +49-69-798-47214
Telefax: +49-69-798-47221
Email: roskos@physik.uni-frankfurt.de
Web: http://www.uni-frankfurt.de/46358615/PI [1]

Links:
---
[1] http://www.uni-frankfurt.de/46358615/PI

Deep data processing for multilayered material characterized by terahertz spectroscopy

Q. Cassar,[1] A. Chopard,[1] F. Fauquet,[1] J.P. Guillet,[1] M. Pan,[1] J.B. Perraud,[1] M. Roux,[2] and P. Mounaix[1,3]
[1)] *University of Bordeaux, IMS UMR CNRS 5218 351 cours de la Libération, 33405 Talence, France*
[2)] *L'Atelier des Renaissances, 1 allée de Gieu, 33650 Saucats, France*
[3)] *Corresponding author: patrick.mounaix@u-bordeaux.fr*

Abstract – We report on further numerical developments for the analysis of multilayered structures and the extraction of individual layer properties. An iterative algorithm implements a connected propagation tree which denotes the occurrence of the incident pulse division. Each subpulse is individually monitored and its carried proportion of the incident power is extracted. Such a process allows to extract the specific dielectric properties of each layer but additionally permits to derive a parametric transfer function describing the whole interaction with an incident beam. The procedure was tested both for the art science and the aeronautic industry. Results on an XVIIth century painting and on aeronautics multilayered samples are reported.

Key Words: data processing, multilayered structures, terahertz spectroscopy.

I. INTRODUCTION

Terahertz radiations offer the opportunity to carry out contactless and non-destructive sensing of materials. As a consequence, the technique has legitimately been deployed to control layer thicknesses inside dielectric paint stacks for automotive and aeronautic industries and art science, for instance[1,2]. However, the wave propagation model commonly used to extract layer thicknesses computes indistinguishably the contribution of all the possible propagation routes. The number of calculated paths could be gigantic while a precise knowledge of the most contributing optical paths would awfully minimize the quantity of computed routes and clarify the involved propagation processes. Furthermore, the derivation of a parametric transfer function would drastically reduce the required computation power to minimize the objective function of an inverse electromagnetic formulation. A new algorithm monitoring the pulse subdivisions at dielectric interfaces has been developed[3]. The algorithm classifies each portion of the signal as a function of the number of encountered dielectric interfaces. Additionally, it identifies the various optical paths involved in these signal portions. The optical routes that contribute the most to the power are labeled and used to derive a parametric transfer function. The effectiveness of the algorithm is demonstrated by analyzing the principle optical paths and by deriving the appropriate parametric transfer function of a painting stack made of layers of several tens of microns.

II. RESULTS

The central principle for the algorithm is to increment, at each encountered dielectric interface, a parameter k denoting the pulse subdivision (Fig. 1). Each propagating signal is thus

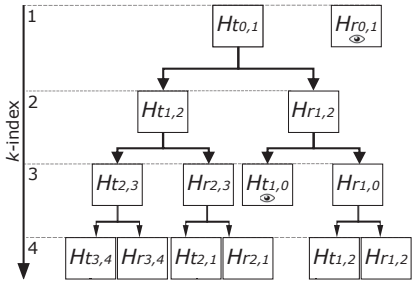

FIG. 1. Scheme of the iterative tree algorithm procedure. Each k-incrementation gives access to further possible events based on the previous ones at $k-1$. Detected pulses have been marked with an eye in the node box.

the sum of reflection and transmission processes occurring at the k-1 algorithm step, involving surrounding dielectric layers and verifying propagation continuity:

$$E^k_{r_{i,i+1}} = H_{r_{i,i+1}}(E^{k-1}_{r_{i,i-1}} + E^{k-1}_{t_{i-1,i}}) \quad (1a)$$

$$E^k_{r_{i,i-1}} = H_{r_{i,i-1}}(E^{k-1}_{r_{i,i+1}} + E^{k-1}_{t_{i+1,i}}) \quad (1b)$$

$$E^k_{t_{i,i+1}} = H_{t_{i,i+1}}(E^{k-1}_{r_{i,i-1}} + E^{k-1}_{t_{i-1,i}}) \quad (1c)$$

$$E^k_{t_{i,i-1}} = H_{t_{i,i-1}}(E^{k-1}_{r_{i,i+1}} + E^{k-1}_{t_{i+1,i}}) \quad (1d)$$

All optical paths are theoretically recorded by the detector among which, a handful is importantly contributing to the 4 layers stack signal. The numerical procedure saved a total of 33 different optical paths (Fig. 2). The correlation coefficient between the real and the optimized transfer function leading to the temporal signal measured is greater than 0.999. This new algorithm is used to understand a stratified material response by terahertz time domain characterization. The identification of the main optical paths responsible of the reflected signal led to an optimized signal reconstruction.

To achieve the simulations and the characterization, we carefully extracted the dielectric properties of each painting layer (see table 1). Both the real and the imaginary part of the dielectric function are fitted with a first order Debye relaxation model. Debye model's parameters are determined by an inverse algorithm and used to reconstruct the obtained signals.

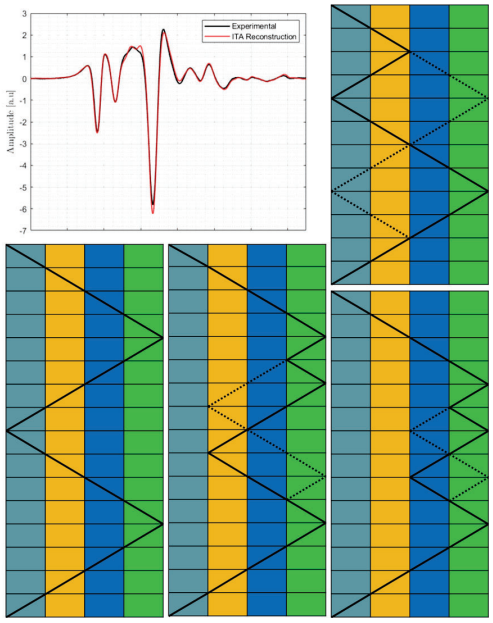

FIG. 2. Identification of some optical paths contributing to the recorded signal. The shape is mainly recovered for k-value spanning from 13 to 17. Dashed paths represent symmetric routes, providing the exact same intensity to the signal.

TABLE I. Fitting Debye parameters for the four coatings of the aeronautic painting stack extracted from a Levenberg-Marquadt algorithm.

	ε_∞	$\Delta\varepsilon$	τ [fs]	d^{IEP} [μm]	$d^{Optical}$ [μm]
Primer	3.7151	0.8461	83.038	32.2	33.1 $\pm$1
Sub-layer	3.2290	0.7095	72.074	72.7	78.6 $\pm$1
Top-layer	4.2586	0.9150	83.733	88.0	83.8 $\pm$1
Varnish	2.47834	0.3890	70.823	64.5	68.8 $\pm$1

THz pulses are generated by focusing ultrafast (100 fs) pulses of near infrared light onto the gap between two electrodes (TPS 4000 Teraview). A signal-to-noise ratio (SNR) of around 4000:1, limited by the thermal noise of the antenna, is achieved.

For the painting on copper substrate, the situation is quite different because we have only few information about the used materials and the different thicknesses. Then, THz properties of varnish layers are extracted through a specific custom-made algorithm for describing ultrathin multilayered materials. The algorithm is planned to generate a wide set of combinations between the dielectric properties and the thickness. Then, it extracts the trio minimizing the quadratic error amplitude between the simulated signal and the measured one. The Fig. 3. reports the recorded signals from the copper substrate, a pigment-copper location and a varnish-pigment-copper multi structure.

Furthermore, we extracted the thickness of the varnish by means of terahertz time-domain spectroscopy and we compared it with the data obtained by a profilometer from an area

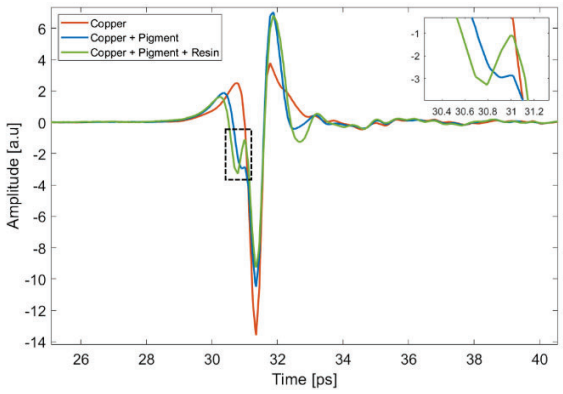

FIG. 3. THz time-domain signal for the different structures. Through these signals the dielectric properties of each layers have been extracted using a specific algorithm. A slight detection-time difference is recorded between the peak arising from the reflection on pigment and the one from the varnish.

of the sample where the varnish was partially missing. We found that the painting layer is about 40 m thick, the varnish around 20 m thick with an optical index in the range of 2.2. This information is very precious within the conservation field, considering that, once that the varnish layer has lost its optical performances, it has to be removed and replaced. The evaluation of the amount of varnish removed from a painted surface is particularly important during a cleaning operation. In fact, since this removal and replacement is not always desirable as it can lead to the damaging of the painting, it is sometime prescribed not to remove the varnish in its full thickness. Thus, the cleaning operation requires a straight control for which THz may provide a non-invasively and contactless solution.

III. CONCLUSION

We use a combination of numerical simulation to find parameters that best describe reflections from a given multilayered paint sample. The reflected terahertz time-domain waveform is simulated using a Fresnel's equations, where each paint layer is represented by a set of numerical parameters that describe both the thickness and the optical response. Numerical optimization is then employed to find a set of values for those parameters that best fits the measurements.

[1]S. Krimi, J. Klier, J. Jonuscheit, G. von Freymann, R. Urbansky, and R. Beigang, "Highly accurate thickness measurement of multi-layered automotive paints using terahertz technology," Applied Physics Letters **109**, 021105 (2016).

[2]J. Van Mechelen, A. Kuzmenko, and H. Merbold, "Stratified dispersive model for material characterization using terahertz time-domain spectroscopy," Optics letters **39**, 3853–3856 (2014).

[3]Q. Cassar, A. Chopard, F. Fauquet, J.-P. Guillet, M. Pan, J.-B. Perraud, and P. Mounaix, "Iterative tree algorithm to evaluate terahertz signal contribution of specific optical paths within multi-layered materials," IEEE Transactions on Terahertz Science and Technology (2019).

High Resolution Spectroscopy in the THz using synchrotron radiation source

O. Pirali[1,2], J.-F. Lampin[3], Z. S. Buchanan[4], S. Eliet[3], M.-A. Martin-Drumel[1], F. Hindle[5], G. Mouret[5]

[1] Institut des Sciences Moléculaires d'Orsay, ISMO, CNRS, Univ. Paris-Sud, Université Paris-Saclay, F-91405 Orsay, France

[2] AILES beamline, Synchrotron SOLEIL, L'Orme des Merisiers Saint-Aubin, 91192 Gif-sur Yvette, France

[3]Institut d'Electronique Microélectronique et Nanotechnologie (IEMN), Lille University, CNRS, Avenue Poincaré F-59652 Villeneuve d'Ascq Cedex, France

[4]Department of Chemistry, University of California, Davis, One Shields Avenue, Davis, CA 95616, USA

[5]Laboratoire de Physico-Chimie de l'Atmosphère (LPCA), Université du Littoral Côte d'Opale, Avenue Schumann F-59140 Dunkerque, France

E-mail: olivier.pirali@u-psud.fr

Abstract – Synchrotron emission extracted on the AILES beamline of SOLEIL facility is a powerful source of terahertz (THz) radiation. Using a FT commercial interferometer, various operation modes of the synchrotron machine can be used to record high resolution molecular spectra in a broadband region covering roughly the 0.5-20 THz range. More recently, important instrumental developments based on heterodyne mixing of the synchrotron radiation with various local oscillators have opened new perspectives on the beamline, in terms of broadand high resolution spectroscopy in the THz domain (< 5 THz). The capabilities of the beamline will be presented through the absorption spectra of various families of molecules.

Keywords – THz, synchrotron radiation, high resolution molecular spectroscopy

I. Introduction

The needs for both broadband and high resolution measurements of THz molecular spectra are very important in scientific communities such as astrophysics and atmospheric sciences. Many instruments have been developed in several laboratories over the world to record high resolution spectra of isolated neutral molecules, radicals, ions, molecular complexes. For these instruments, the available bandwidth often remains rather limited. In the presentation, I will describe the various experimental setup we developed on the AILES beamline of synchrotron SOLEIL which exploit the broadband and relatively intense THz/far-IR synchrotron radiation.

I. Synchrotron-based Fourier-Transform spectroscopy

On the AILES beamline at SOLEIL, the synchrotron radiation is used as a far-IR continuum source for a Bruker IFS 125 FT interferometer [1]. This instrument allows recording broadband spectra with a resolution (limited by the mechanical displacement of the moving mirror) of about 30 MHz. This ensemble, together with the development of several types of sample compartments, permits the investigation of the absorption spectra of various families of molecular species in the THz range. In particular, three different discharge cells allow to study the absorption spectra of highly reactive species such as radicals [2] and ions [3]. As an example, Fig.1 shows the high resolution absorption spectrum of KrH^+ molecular ion produced in a hollow cathode-type discharge cell. The spectrum covers the 50-300 cm^{-1} region, very difficult to access by table-top laboratory instrumentation. The resolution is 30 MHz (limited by the interferometer) and the acquisition-time was few hours. The absorption lines of KrH^+ assigned on the spectrum involve relatively high values of the rotational quantum number *J*.

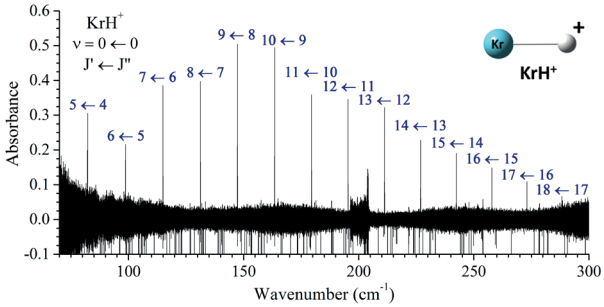

Fig. 1. Absorption spectrum of the molecular ion KrH^+ produced in a liquid-nitrogen cooled hollow cathode discharge cell. The absorption path length was set to 24m. KrH^+ was produced in a discharge of Kr and H_2 precursors. The negative lines correspond to gas phase water absorptions.

It is important to note that despite the great advantages to record broadband spectra with the FT interferometer, the rotational structure of open-shell molecules (radicals and ions) display complex internal couplings leading to fine structures which are often

difficult to resolve with a 30 MHz ultimate resolution interferometer.

A second important part of our activity is dedicated to study the high resolution spectroscopy of relatively large C-bearing molecules (Polycyclic Aromatic Hydrocarbons, diamondoids…). These species are among the largest species to be studied at high resolution (c.a. rotationally resolved) in the THz range. In most of the cases, due to high spectral congestion, the full rotational structure could not be resolved because of the ultimate instrumental resolution limited to 30 MHz [4].

III. Heterodyne Spectrometers

In order to improve the available spectral resolution on the AILES beamline of SOLEIL, we are developing new spectrometers based on heterodyne mixing of synchrotron radiation with various local oscillators (LO).

We are currently developing a new instrument aiming to record sub-MHz resolution absorption spectra in the 0.5-5 THz range. The principle of the experiment is given on Fig.2. The THz continuum extracted by the beamline is mixed with a QCL-based molecular laser LO emitting around 1.073 THz on a Hot Electron Bolometer (HEB) mixer. The 5 GHz intermediate frequency (IF) is analyzed using a XFFTS [5].

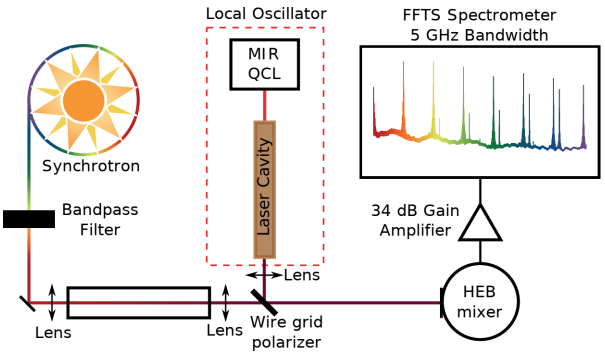

Fig. 2. Schematic representation of the heterodyne experimental set-up we developed on the AILES beamline.

To test the performances of the new instrument, we recorded several molecular absorptions in the available bandwidth. Fig.3 shows two absorption lines of H_2S located at 1 071 313 MHz and 1 072 836 MHz. These lines were recorded by injecting 20 µbar of H_2S in a 55 cm long absorption cell and the acquisition time was less than 1s. In the presentation I will discuss the performances of this new experimental set-up and the limitations we are facing. In particular the frequency jittering of the molecular laser LO together with the rapid saturation of the HEB mixer leads to relatively intense baseline fluctuations. Thanks to the availability of a large number of LO THz frequencies, this preliminary results is very encouraging and should allow sub-MHz resolution molecular spectroscopy studies in the 0.5-5 THz range.

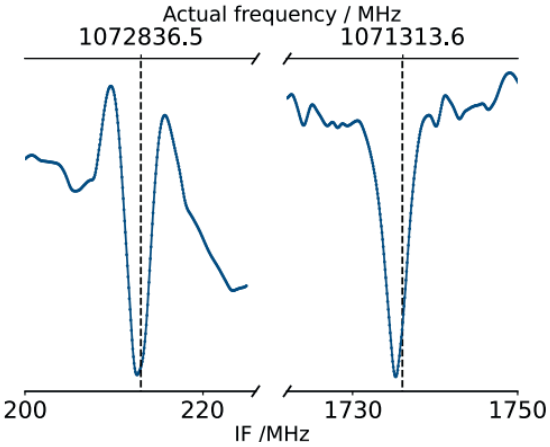

Fig. 3. Pure rotation absorption lines of H_2S within the 5 GHz bandwidth around 1 073 049 MHz LO frequency.

IV. Conclusions

I will briefly present the various high resolution spectroscopy studies which are developed on the AILES beamline of SOLEIL using a THz synchrotron-based FT interferometer. This approach provides numerous advantages in terms of broadband and sensitivity, but the limited spectral resolution hinders the studies requiring higher spectral resolution. I will present in some details the new instrumentation using heterodyne mixing of synchrotron radiation with laser-based local oscillators and discuss the performances in a context of sub-MHz resolution molecular spectroscopy in the THz range.

Acknowledgments

This work was financially supported by the Agence Nationale de la Recherche (ANR) (HEROES, ANR-16-CE30-0020-03); partial fundings from the LABoratoire d'EXcellence PALM (University Paris-Saclay) and from the SATT-Nord "TERAPOMPE" project.

References

[1] J.-B. Brubach et al., *WIRMS 2009 : 5th International Workshop on Infrared Microscopy and Spectroscopy with Accelerator Based Sources* **1214**, 81 (2010).

[2] M.-A. Martin-Drumel et al., *Review of Scientific Instrument,* **82,** 133106 (2011)

[3] S. Gruet and O. Pirali, *Molecular Physics*,**117**, 1719 (2019)

[4] S. Gruet et al., *Journal of Physical Chemistry A,* **120**, 95 (2016)

[5] J. F. Lampin et al, *Optics Letters,* accepted for publication

High-performance THz detectors in CMOS technologies

K. Ikamas[1], D. Čibiraitė[3], A. Solovjovas[1], D. But[2], A. Lisauskas[1,2]

[1] Institute of Applied Electrodynamics and Telecommunications, Vilnius University, Vilnius, Lithuania
[2] CENTERA Laboratories, High Pressure Physics Institute PAS, Warsaw, Poland
[3] Physikalisches Institut, Goethe-Universität Frankfurt, Frankfurt am Main, Germany

E-mail: alvydas.lisauskas@ff.vu.lt

Abstract –We present broadband high sensitivity terahertz (THz) detectors based on 65 nm and 90 nm CMOS technology with the state-of-the-art performance. The devices utilizes patch, bow-tie and log-spiral antenna-coupled field-effect transistors (FETs) for the detection of free-space THz radiation (TeraFETs). We report on optimized performance, which was achieved by employing a physics-based model and thorough device characterization under THz illumination at the room and liquid nitrogen temperature conditions. The implemented detector with bow-tie antenna design exhibits a nearly flat frequency response characteristic up to 1.6 THz with an optical responsivity of 45 mA/W (or 220 V/W). For this device, we have determined a minimum optical noise-equivalent power as low as 48 pW/√Hz at 0.6 THz and 70 pW/√Hz at 1.5 THz. When cooled to liquid nitrogen temperatures, the sensitivity of TerFETs increase nearly by factor of four and becomes competitive with optical performance of helium-cooled commercial bolometers.

Keywords – THz power detector, terahertz detector, broadband antenna, field-effect transistor.

I. Introduction

Sensitive detection of THz radiation (0.3-10 THz) remains a challenge for direct receivers of THz radiation. The THz power generated by the most of coherent radiation sources can be efficiently detected using room-temperature operated, antenna-coupled rectifying devices such as Schottky [1], tunneling diodes [2] and field-effect transistors (FETs) [3]. These devices can be implemented as direct power detectors or in homodyne or heterodyne coherent detection mode. In addition, THz detector arrays can be utilized for imaging purposes. One advantage of TeraFETs for THz detection is that they can be fabricated using mainstream semiconductor device technologies and hence can be realized as large area arrays.

This paper presents a physics-based circuit modelling approach which allow design and implementation of high-performance field-effect-transistor based terahertz detectors. The underlying mechanism of power detection using TeraFET is based on rectification of THz waves coupled into the channel transistor. Whereas, at frequencies lower than the standard cut-off frequency, FET-based rectifiers can be explained with standard resistive mixing approach, with rising frequency, charge-density waves in the two-dimensional gas start playing an increasingly important role and enable detection and mixing far beyond classical cut-off frequencies [4, 5]. The potential of convenient fabrication of TeraFETs by silicon CMOS foundry technologies has accelerated developments, which have already led to implementation of real-time camera [6, 7]. Although detector optimization is still ongoing, gradually leading to fundamental performance limits for room-temperature operation of the devices, cryogenic cooling allow to boost the performance to the levels comparable with optical performances of commercial, helium-cooled bolometers.

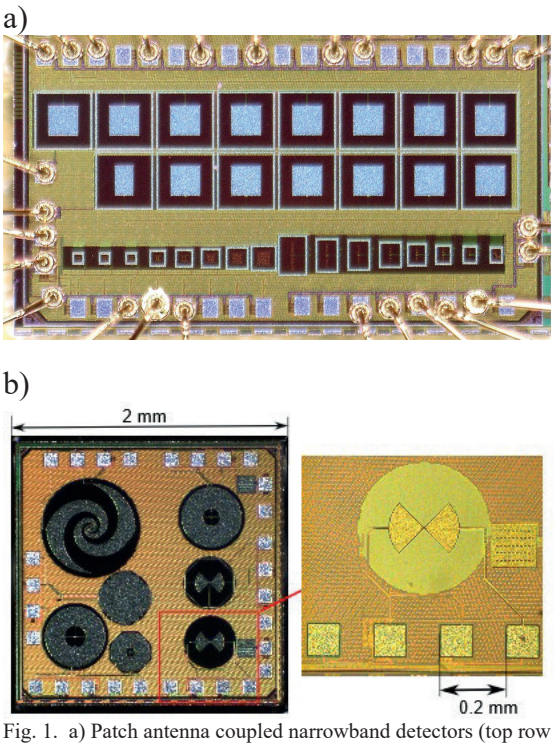

Fig. 1. a) Patch antenna coupled narrowband detectors (top row for 630 GHz, bottom row – array of devices from with resonances spanning from 1.2 to 5.6 THz). b) A micrograph of the chip with broad-band (bow-tie and log-spiral) and narrowband (slot with dipole) devices optimized for substrate-side coupling with hyper-hemispheric Si lens.

II. Section 2

Figure 1 presents the micrographs of different devices fabricated in 90-nm CMOS technology. The top panel (a) presents a series of patch-antenna coupled

devices with resonant frequencies from 630 GHz (top row) up to 5.6 THz (left corner, bottom row), whereas the lower panel (b) demonstrates the chip with broad-band and resonant devices, optimized for back-side illumination with a hyper-hemispherical silicon lens.

In order to enable the design and implementation of highly-sensitive devices, we have developed a circuit model (see Fig. 2) allowing to evaluate the role of the transistor geometry parameters such as channel length and width taking into account antenna impedance matching and the peculiarities of fabrication technology. The details on the model are given in [8, 9] Whereas the highest sensitivity is reachable for the shortest, technology defined, gate lengths, there is an optimum value for a gate width. In support of our arguments, we present implementations of several types of narrow-band and broadband detectors using a 65-nm and 90-nm CMOS technology. At 630 GHz resonant frequency, narrow-band devices reach optical responsivity of 1074 V/W and NEP of 10 pW/√Hz. From 500 GHz to 650 GHz a broad-band bow-tie antenna and hyper-hemispheric lens coupled TeraFETs demonstrate flat device responsivity (taking all available beam power) of 100 V/W with NEP of 75 pW/√Hz. When cooled down to 80 K, the sensitivity of devices gets improved by and additional factor of four.

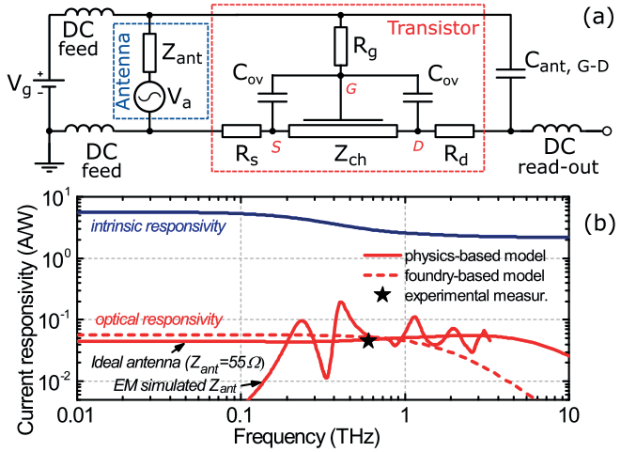

Fig. 2 (a) A simplified equivalent circuit of the TeraFET. (b) Simulated and measured current responsivity vs. radiation frequency for the TeraFET at Vg= 0.45 V. The optical responsivity was simulated separately with the foundry-based (dashed line) and the physics-based models (red solid lines). The intrinsic responsivity was simulated only with the latter model (dark blue line). The responsivity of the TeraFET with a bow-tie antenna measured at 600 GHz is denoted by a black star. Figures reproduced from [8]

III. Conclusions

In summary, the TeraFET with a bow-tie antenna exhibits a nearly flat frequency response characteristic from 0.4 THz up to 2.2 THz with an optical responsivity of 45 mA/W (or 220 V/W) at 0.6 THz. We have determined a minimum optical NEP as low as 48 pW/√Hz at 0.6 THz and 70 pW/√Hz at 1.5 THz. When cooled down to 80K there is an increased of sensitivity by an additional factor of four. The room temperature results obtained at 1.5 THz are better than the best ones reported in the literature for narrowband TeraFETs at this frequency and only up to a factor of four inferior to the results of the best narrowband devices at 0.6 THz. The log-spiral design exhibits narrower range of flat responsivity, however has higher sensitivity below 230 GHz. Furthermore, a log-spiral antenna is more suited for measurements when the polarization of a THz beam is unknown or changes in time. We conclude that characterization results of a bow-tie coupled device above 1 THz are in better agreement with the analytical model rather than with the foundry-based model predictions. Our proposed device model correctly describes the performance of the detector as it predicts the THz detection well beyond 2 THz confirmed by measurements. We are not aware of any other physical approach which could provide results of similar accuracy.

Acknowledgments

This work was supported by the Research Council of Lithuania under Contract TAP LZ-06/2015, in part by the Hessian excellence initiative LOEWE–Terahertz-Kamera für die zivile Sicherheitstechnik, in part by the EU Horizon 2020 Marie Sklodowska-Curie ITN CELTA project under Grant 675683, and in part by ESA through the THzFET Project. A.L. is thankful for the support by the Foundation for Polish Science grant IRA CENTERA.

References

[1] M. Yahyapour, N. Vieweg, A. Roggenbuck, F. Rettich, O. Cojocari, and A. Deninger, IEEE Trans. THz Sci. Technol., 6, 670 (2016).

[2] G. C. Trichopoulos, H. L. Mosbacker, D. Burdette, and K. Sertel, IEEE Trans. Antennas Propag., 61, 1733 (2013).

[3] M. Bauer, R. Venckevičius, I. Kašalynas, S. Boppel, M. Mundt, L. Minkevičius, A. Lisauskas, G. Valušis, V. Krozer, and H. G. Roskos, Opt. Express 22, 19235 (2014).

[4] M. Dyakonov and M. Shur, IEEE Trans. Electron.Dev. 43, 380 (1996).

[5] A. Lisauskas, U. Pfeiffer, E. Öjefors, P. Haring Bolívar, D. Glaab, and H. G. Roskos, J. Appl. Phys. 105, 114511 (2009).

[6] R. Al Hadi, H. Sherry, J. Grzyb, Y. Zhao, W. Förster, H. M. Keller, A. Cathelin, A. Kaiser, and U. R. Pfeiffer, IEEE J. Solid-State Circuits 47, 2999 (2012).

[7] J. Zdanevičius, M. Bauer, S. Boppel, V. Palenskis, A. Lisauskas, V. Krozer, and H. G. Roskos, J. Infrared Millim Terahertz Waves 36, 986 (2015).

[8] K. Ikamas, D. Čibiraite, A. Lisauskas, M. Bauer, V. Krozer, and H. G. Roskos, IEEE Electron Device Letters 39, 1413 (2018).

[9] J. Zdanevicius, D. Cibiraite, K. Ikamas, M. Bauer, J. Matukas, A. Lisauskas, H. Richter, T. Hagelschuer, V. Krozer, H.-W. Hubers, and H. G. Roskos, IEEE Transactions on Terahertz Science and Technology 8, 613 (2018).

Advantages of extended focus in THz imaging

L. Minkevičius[1], D. Jokubauskis[1], I. Kašalynas[1], S. Orlov[2], A. Urbas[2], and G. Valušis[1]

[1] Department of Optoelectronics, Center for Physical Sciences and Technology, Vilnius, Lithuania

[2] Department of Fundamental Research, Center for Physical Sciences and Technology, Vilnius, Lithuania

E-mail: gintaras.valusis@ftmc.lt

Abstract – **The Fibonacci (bifocal) and Bessel THz imaging are demonstrated using silicon diffractive zone plates in continuous wave mode at 0.6 THz. Spatial profiles and focal depth characteristics are investigated both theoretically and experimentally. Possibilities of application of the approaches for thick objects inspection are revealed and discussed.**

Keywords – THz imaging, Fibonacci focusing, Bessel beam

I. Introduction

Effective solutions in passive optical components in reducing dimensions of room-temperature terahertz (THz) imaging systems is one of the main topics in THz photonics.

Recently, we demonstrated that thin silicon based multilevel phase Fresnel lenses are suitable solution for optical components for the entire THz range [1]. It was shown that at least 4 and up to 8 phase quantization levels are needed for efficient diffractive element compromising the performance and fabrication complexity of phase structures.

In this communication, we demonstrate advantages of THz beam manipulation in realization of the extended focus geometry in THz imaging providing thus inspection of thick objects with small sensitivity of object position.

II. Designs and Imaging Results

The Fibonacci structure was composed so that each element of the sequence can be found as the concatenation of the two previous elements [2]. In Bessel imaging, we designed special binary axicons which are more compact and thus less lossy when compared with classical cone axicons. Silicon of 0.5 mm thickness with resistance 0.01–1 MΩ·cm and refractive index of 3.46 served as stable material for multilevel phase Fresnel lenses fabrication in the laser ablation process. The design was obtained using three-dimensional finite-difference time-domain method. The modelling was performed using spatial resolution from 0.01 mm up to 0.1 mm. To simplify the simulation, symmetry conditions of the structure were applied, and the absorbing boundary conditions were set in all the directions.

In Fibonacci imaging, THz images of various packaged objects at 0.6 THz frequency were simultaneously recorded with the spatial resolution of

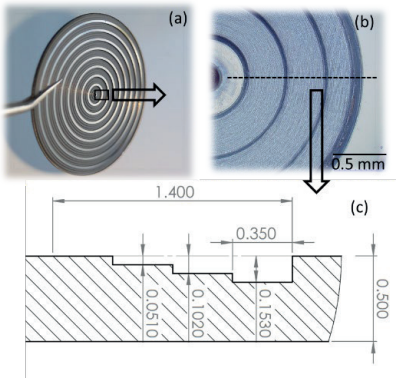

Fig. 1. The photo of thin silicon-based Bessel diffractive element for the 0.6 THz (a). Photo of the zoomed area in the center part displays ablated and polished silicon surface (b) Sample cross-section with marked dimensions of four phase quantization levels (c). (according to L. Minkevičius, et al, IRMMW-2019 abstracts [3])

wavelength in two different planes separated by 7 mm distance.

Bessel imaging was realized via fabricated Bessel zone plate of 20 mm in diameter (Fig. 1 a) Enlarged subzones of the ablated rings with detailed geometrical parameters are displayed in Fig.1 b, c. The electric field of shape like needle along the beam propagation was obtained enabling imaging of object with more than 12 mm thickness. The focusing gain up to 25 dB, focal depth of 15 mm and beam waist reaching 0.4 mm was estimated. A novel approach of THz imaging with two Bessel zone plates providing a 2×λ resolution at 0.6 THz frequency with weak dependence of object positioning between the diffractive elements was demonstrated [3]. It is worth noting that the resolution was found less sensitive to the position of the thick sample in *z* direction comparing with images using conventional zone plates.

IV. Conclusions

Imaging performances using high resistivity Fibonacci lens and Bessel zone plate are discussed and compared.

References

[1] L. Minkevičius et al, *Opt. Lett.* **42**, 1875 (2017).

[2] D. Jokubauskis et al, *Opt. Lett.* **43**, 2795 (2018).

[3] L. Minkevičius et al, in *Proc. to the* The 44d Intern. Conf. Infrared, Milli. Terahertz Waves (**IRMMW-THz 2019**), Paris, France, 1-6 September 2019, Comm. Th-PM2-1-1.

THz time-domain spectroscopy of bismuth films

A.D. Zaitsev[1], P.S. Demchenko[1], E.S.Makarova[2], A.S. Tukmakova[2], N.S. Kablukova[2], A.V. Asach[2], A.V. Novotelnova[2], M.K. Khodzitsky[1]
[1]THz biomedicine Laboratory, ITMO University, Saint Petersburg, Russia
[2]Faculty of Cryogenic Engineering, ITMO University, Saint Petersburg, Russia

E-mail: khodzitskiy@yandex.ru

Abstract – In this paper, optical properties of bismuth thin films with different thicknesses in range from 10 to 150 nm on different dielectric substrates were obtained and analyzed using THz time-domain spectroscopy.

Keywords – THz time-domain spectroscopy, bismuth films

Bismuth (Bi) is one of the most unique materials being extensively studied in condensed matter physics. This semimetal material is of such long-term research interest due to its exceptional properties deriving from low carrier effective masses ($\approx 10^{-2}$ electron masses), long mean free path (≈1 mm), and large high-frequency dielectric constant ($\approx 10^{2}$)[1]. Bismuth exhibits a very small Fermi surface and bandgap at L point of the Brillouin zone[2], quantum size effect (QSE) due to extremely long Fermi wavelength (30–40 nm)[3]. Because of QSE, the oscillation of the bismuth thin-film resistance as a function of the film thickness was reported in 1966[4]. Moreover, a semimetal-to-semiconductor transition (at 20-30 nm thickness) caused by the QSE was theoretically predicted in 1967[5]. It should be noted that up to now the carrier dynamics of the electronic states in bismuth thin films has not fully been understood[3].

In recent works, it was clearly shown that conductivity of Bi thin films strongly depends on the film thickness, but the measurements were performed only in the range of thicknesses up to 40 nm[2,6,7]. In addition, the samples of Bi in these works were placed on the surface of bulk silicon (Si) which has semiconductor properties and introduces significant errors in the measurements of carrier dynamics in pure bismuth by changing the Fermi energy of charge carriers in this semimetal.

Despite the technological interest in bismuth, its properties have been studied in the terahertz (THz) frequency range only recently[2,6]. It was shown that THz radiation interacts well with thin-film bismuth. To date, there are no works where the dependencies of the parameters of pure bismuth placed on different dielectric substrates are studied in the THz frequency range. Such research is needed to determine the true constitutive parameters of thin films of bismuth with different thicknesses and to assess the prospects for usage of this material in devices operating in the THz frequency range.

In this paper, THz properties of bismuth thin films with different thicknesses in range from 5 to 200 nm on different dielectric substrates were investigated by THz time-domain spectroscopy.

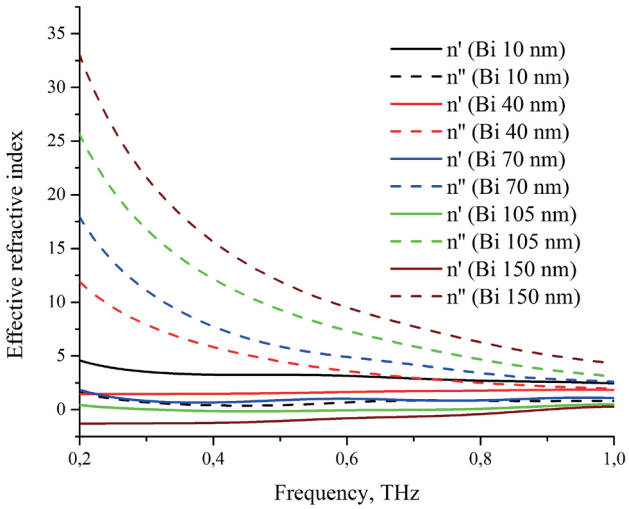

Fig.1. Effective complex refractive index of bismuth film on mica substrate for various film thicknesses.

The transmittance spectra, the complex dielectric permittivity, complex refractive index and complex sheet conductivity dispersions of bismuth thin films on the mica and polyimide substrates were obtained and analyzed (Fig.1).

ACKNOWLEDGMENTS

This work was financially supported by Russian Science Foundation (Grant №19-72-10141).

REFERENCES

[1] R. Tediosi, Physical review letters 99, 016406 (2007).
[2] I. Katayama, in Terahertz Emitters, Receivers, and Applications IX, Vol. 10756 (International Societyfor Optics and Photonics, 2018) p. 107560P.
[3] E. Rogacheva, Applied physics letters 82, 2628 (2003).
[4] Y.F. Ogrin, Soviet Journal of Experimental and Theoretical Physics Letters 3, 71 (1966).
[5] V. Sandomirskii, Sov. Phys. JETP 25, 101 (1967).
[6] K.Yokota, Applied Physics Letters 100, 251605 (2012).
[7]T. Hirahara, Applied Physics Letters 91, 202106 (2007).

A new approach for THz molecular lasers

S. Barbieri[1], J. Turut[1], A. Pagies[1], J.-F. Lampin[1]
[1] Institute of Electronics Microelectronics and Nanotechnology, UMR CNRS 8520, Lille University, Villeneuve d'Ascq, France
E-mail: jean-francois.lampin@univ-lille.fr

Abstract – Despite several progress generation of electromagnetic power in the THz range is still underdeveloped compared to the other frequency bands. Direct THz generation poses fundamental and practical problems very difficult to solve. Generating THz using sources from lower or higher frequencies is an alternative way. We will discuss our recent results about a new approach for continuous wave THz molecular lasers. Traditionally these lasers were pumped by CO_2 lasers that have several drawbacks. We have demonstrated that mid-infrared quantum cascade lasers can be used as pump lasers to invert the population of polar molecules. Here we demonstrate an efficient laser based on ammonia (NH_3).

Keywords – Terahertz, Laser, Ammonia

I. Introduction

Using optical sources for generating submillimeter or THz waves was proposed in the 1960's consecutively to the demonstration of the first optical oscillator (laser)[1]. Two approaches were investigated: the photoelectric mixing (or photomixing) and the difference frequency generation (DFG) in nonlinear crystals. But in 1970 the first optically-pumped THz laser (OPTL) was demonstrated at Bell Telephone Labs[2]. It was powerful and was adopted quickly as a replacement for the discharge-pumped molecular laser which was difficult to operate and less efficient. These sources were (and still are) the most powerful in the THz range for narrow band emission but they are also bulky and expensive. We have proposed to pump a molecular laser with a quantum cascade laser (QCL) instead of a CO_2 laser[3]. Since their demonstration in 1994 the performance of the QCLs has increased significantly and it is possible to consider their use for pumping other lasers.

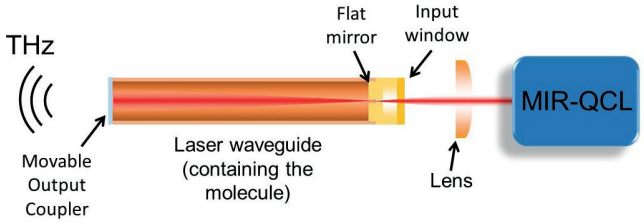

Fig. 1. Simplified schematic of the mid-IR (MIR) QCL-pumped THz molecular laser.

II. QCL-Pumped Molecular Laser

Fig. 1 displays a typical schematic of this kind of laser. The reduced size of the QCL compared to a typical CO_2 laser is welcome but the main advantage of the QCL is its continuous tunability. The tunability of CW CO_2 lasers is generally less than 1 GHz around each CO_2 line but QCLs can reach a tunability of few 100's GHz or more. The molecule and the transition can then be chosen to optimize some parameters of the molecular laser like the frequency, the gain or the efficiency.

The THz cavity is made of a hollow metallic waveguide closed by to flat mirrors. One of them has a hole in the center to allow the pumping beam to enter into the cavity. The other mirror is the output coupler and transmit partially the THz beam. This mirror is mounted on a translation and piezo stage to allow the fine adjustment of the cavity length.

We have demonstrated the first QCL-pumped molecular laser by choosing the NH_3 (ammonia) molecule. It is a light molecule that exhibits a strong permanent electric dipole and that strongly absorbs infrared. Its equilibrium configuration is a pyramidal symmetric top and the various quantum levels are dictated by the J and K quantum numbers. But this molecule has also a large amplitude internal motion due to the tunnel effect of the nitrogen atom through the potential created by the three hydrogen atoms. This effect splits the NH_3 levels in symmetric (s) and anti-symmetric levels (a). They are separated by about 0.8 cm^{-1} when the molecule is its fundamental vibrational state. Inversion of population between these levels was achieved in the first maser[7] demonstration around 24 GHz. In the first vibrational state (v_2=1), a and s levels are separated by about 36 cm^{-1} corresponding to about 1 THz. Inversion of population between these levels and CW THz oscillation are possible by pumping the molecule with a MIR-QCL[3-5].

III. Experiments

A laser such as that described in Fig. 1 was realized, filled with NH_3 and optimized.

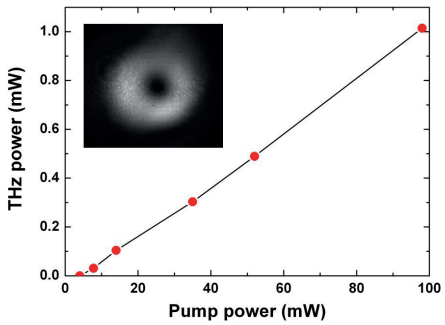

Fig. 2. THz power versus mid-IR pump power (inset: image of the beam)[9].

Fig. 2 shows the highest measured THz power at 1073 GHz versus the 10.3 µm pump power. The threshold is very low (few mW) and the conversion efficiency is close to 1 mW/W. The maximum theoretical efficiency of this kind of laser is given by: $\frac{1}{2}(\nu_{THz}/\nu_{pump})$ = 1.8 mW/W. The measured efficiency is equal to 55% of the maximum theoretical efficiency. The inset in Fig. 2 shows the beam pattern of the most powerful mode: it corresponds to the TE_{01} mode of the metallic circular waveguide which has very low losses.

The THz gain has been measured in a single pass cell[8]. The maximum measured value is 10.1 dB/m at 1073 GHz for a pumping power of 40 mW. This value is the highest measured in a CW-MIR-pumped gas in the THz range. It explains why the threshold of the laser is very low.

Fig. 3 shows the different laser transitions obtained with the QCL-pumped laser. All these laser lines are pure inversion transitions of NH_3 in the ν_2=1 excited state labelled by their (J,K) quantum numbers. The spectra were measured using a subharmonic mixer.

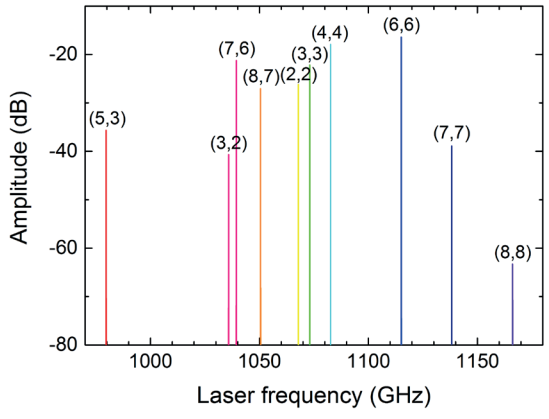

Fig. 3. Spectra of the different laser transitions obtained with the QCL-pumped NH_3 laser labelled by their (J,K) numbers.

We have also investigated recently the frequency noise of this laser[6,9]. It has been measured by beating the laser frequency with the 1080th harmonic of the repetition rate of a 1 GHz, 1560 nm frequency comb as a reference. We find a frequency noise power spectral density lower than 10 Hz^2/Hz (-95 dBc/Hz) at 100 kHz from the carrier. If we equal this value with the phase noise of a ×108 multiplied source it would require a 10 GHz oscillator with a phase noise of -135 dBc/Hz (100 kHz from the carrier) which is a low value comparable to the best commercial synthesized sources. We have also showed that the laser can be phase-locked to a frequency reference by controlling the QCL drive current down to a sub-Hz linewidth[9].

IV. Applications

We have investigated some possible applications of this kind of laser. The first application concerns the THz imaging: as showed in Fig. 2, the output power is sufficient to illuminate the sensor of a THz microbolometer camera at 25 frame/s with a good signal/noise ratio. The laser can also be used as a local oscillator. We have demonstrated that it can pump efficiently a NbN hot electron bolometer (HEB) mixer. The noise temperature was sufficiently low to detect the radiation produced around 1 THz by a Hg lamp. In a second experiment we have detected the synchrotron radiation from the AILES beamline at Soleil synchrotron[10]. Thanks to the excellent frequency resolution of this heterodyne receiver, it was possible to demonstrate molecular spectroscopy around 1 THz with MHz resolution[10]. Finally, as it was demonstrated in the past, the OPTL can also be used to build a magneto-conducted spectrometer. We have used it to investigate the effective mass of electrons in an InAs quantum well thanks to cyclotron resonance[11].

In this work we have demonstrated that a CW THz laser source can be built from a MIR QCL and a THz cavity filled with polar molecules. This source operates at room-temperature, does not need high voltage or water cooling. With ammonia its efficiency and its phase noise are comparable to state-of-the-art multiplication source at 1 THz. At higher frequencies, better efficiencies are expected. At frequencies higher than 1 THz and/or with more powerful QCL we can expect CW output powers in the 10 mW range.

Acknowledgments

We acknowledge the members of the IEMN Terahertz Photonics Group. This work has benefited from the facilities of the EQUIPEX ExCELSiOR Nanoscience Characterization Center and the RENATECH network. This work was supported by the SATT-Nord project TERAPOMPE, the ANR project HEROES (ANR-16-CE30-0020) and the LABEX Cluster of Excellence FIRST-TF (ANR-10-LABX-48-01). We also acknowledge financial support from the region Hauts-de-France and the 'Fonds Européen de Développement Régional' (FEDER) through the 'Contrat de Projets Etat Région (CPER)' "Photonics for Society".

REFERENCES

[1]. J.C. Bass, "Generation of millimetre and submillimetre waves by frequency mixing of laser beams", *Millimetre and submillimetre waves*, Ed. F. A. Benson, Chap. 8, Iliffe, London, 1969.

[2] T.Y. Chang and T.J. Bridges, "Laser action at 452, 496, and 541 μm in optically pumped CH_3F," *Optics Communications,* **1**, 423 (1970).

[3] A. Pagies, G. Ducournau, and J.-F. Lampin, "Low-threshold terahertz molecular laser optically pumped by a quantum cascade laser," *APL Photonics,* **1**, 031302 (2016).

[4] A. Pagies, G. Ducournau, and J.-F. Lampin, "Continuous wave terahertz molecular laser optically pumped by a quantum cascade laser," *41st International Conference on Infrared, Millimeter, and Terahertz waves (IRMMW-THz)*, Copenhagen, Denmark, 2016.

[5] A. Pagies, G. Ducournau, and J.-F. Lampin, "Progress in continuous wave THz molecular laser optically pumped by a quantum cascade laser," *42nd International Conference on Infrared, Millimeter, and Terahertz waves (IRMMW-THz)*, Cancun, Mexico, 2017.

[6] A. Pagies, S. Eliet, J.-F. Lampin, G. Santarelli, W. Hansel, R. Holzwarth, and S. Barbieri, "Frequency noise power spectral density of a molecular THz-laser using a fs-fibre laser comb with 1 GHz repetition rate," *43rd International Conference on Infrared, Millimeter, and Terahertz waves (IRMMW-THz)*, Nagoya, Japan, 2018.

[7] J.P. Gordon, H. J. Zeiger, and C.H. Townes, "The maser-new type of microwave amplifier, frequency standard, and spectrometer," *Physical Review,* **99**, 1264 (1955).

[8] M. Micica, S. Eliet, M. Vanwolleghem, R. Motiyenko, A. Pienkina, L. Margulès, K. Postava, J. Pistora, and J.-F. Lampin, "High-resolution THz gain measurements in optically pumped ammonia," *Optics Express,* **26**, 212242 (2018).

[9] J.-F. Lampin, A. Pagies, G. Santarelli, J. Hesler, W. Hänsel, R. Holzwarth, and S. Barbieri, "Quantum cascade laser-pumped terahertz molecular lasers: frequency noise and stabilization using a 1560 nm frequency comb," submitted.

[10] J.-F. Lampin, O. Pirali, Z.S. Buchanan, S. Eliet, M.-A. Martin-Drumel, J. Turut, P. Roy, F. Hindle, and G. Mouret, "Broadband terahertz heterodyne spectrometer exploiting synchrotron radiation at megahertz resolution," Optics Letters, in press.

[11] J.-F. Lampin, A. Pagies, S. Barbieri, L. Desplanque, X. Wallart, J. Hesler, O. Drachenko, and J. Leotin, "Terahertz pulsed-field magneto-spectrometer at room-temperature," *44th International Conference on Infrared, Millimeter, and Terahertz waves (IRMMW-THz)*, Paris, France, 2019.

Room-temperature terahertz quantum cascade laser sources based on intra-cavity difference frequency generation

M.A. Belkin
[1] Walter Schottky Institute and Department of Electrical and Computer Engineering, Technical University of Munich, Germany
E-mail: mikhail.belkin@wsi.tum.de

I will review the recent progress of electrically-pumped semiconductor sources of terahertz radiation based on intra-cavity difference-frequency generation (DFG) in mid-infrared quantum cascade lasers (QCLs). These devices, referred to as THz DFG-QCLs, are similar in fabrication and operation simplicity to THz QCLs, but, unlike THz QCLs, they offer room-temperature operation with narrow emission linewidth and broadband spectral tuning in the entire 1-6 THz range.

Keywords – quantum cascade lasers, difference-frequency generation, terahertz

Conical vs Gaussian Terahertz Emission from Two-Color Laser-Induced Air Plasma Filaments

Ch. B. Sørensen[1], L. Guiramand[2], J. Degert[2], M. Tondusson[2], E. Skovsen[1], E. Freysz[2], E. Abraham[2]
[1] Department of Materials and Production, Aalborg University, Denmark
[2] CNRS LOMA, UMR 5798, Université de Bordeaux, Talence, France

E-mail: jerome.degert@u-bordeaux.fr

Abstract – We demonstrate that terahertz generation in a two-color laser filament can exhibit conical or Gaussian far-field distribution depending on the experimental conditions. By measuring the spatial distribution of the THz electric field in the 0-3 THz spectral range, we have shown that the conical emission is likely due to photo-induced carriers in the silicon filter used to block the remaining pump laser pulses. However, the terahertz generation can retrieve a Gaussian spatial distribution by replacing the silicon filter by a ceramic one in which the photo-excitation of charge carrier does not occur.

Keywords – terahertz, plasma filament, conical emission

I. Introduction

Generation of intense terahertz (THz) pulses from two-color air plasma filaments has been used successfully for broadband time-domain spectroscopy and nonlinear THz optics. However, the exact mechanism for THz emission, including the characterization of the electric field spatial distribution, has been the subject of ongoing debate. Especially, ring and uni-modal THz emissions were described with good agreement between models and experimental results[1-3]. However, most of these previous works, performed with incoherent and broadband detectors (e.g. pyrometers and Golay cells), were done in the wide frequency range up to 15 THz and few results have described the angular beam structure below 3 THz.

In this communication, we describe the far-field spatial distribution of the THz electric field generated by two-color femtosecond laser-induced plasma filaments. We used a real-time 2D electro-optic coherent detection scheme with a 0-3 THz spectral range. We paid a specific attention to the filter used to block the high-intensity waste light that propagates beyond and from the plasma filaments. We discussed the influence of this filter on the THz beam propagation by comparing a Si filter with a ceramic one (alumina, Al_2O_3) presenting high ablation resistance and decent THz transmission[4].

II. Experiment and Results

To characterize the influence of the Si filter, we measured the THz electric field by direct 2D electro optical sampling in a large aperture <110> ZnTe crystal (Figure 1)[5]. By changing the time delay between the

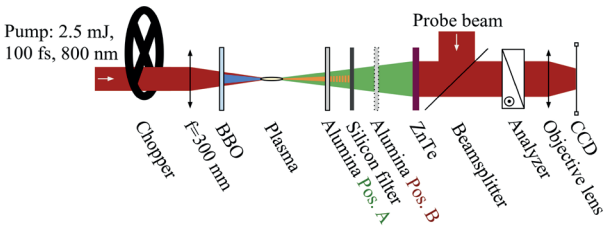

Fig. 1: Measurement setup with two possible positions for the alumina filter. For the 'Silicon first' case, position B is used, while for the 'Alumina first' the ceramic filter is in position A.

infrared probe pulse and the THz pulse, it is possible to determine the temporal evolution of the THz electric field. Then, after Fourier transformation of the temporal data, we can analyze the spatial distribution of the THz electric field from 0 to 3 THz.

Two configurations have been investigated: (i) Si filter before the alumina filter (1 mm thick, 96% Al_2O_3, CSC ltd) (alumina in position B in Fig. 1); (ii) alumina filter before the Si filter (alumina in position A in Fig. 1). With the 'alumina first' configuration, the waste light with photon energy higher than 1.11eV can excite charge carriers in the Si wafer.

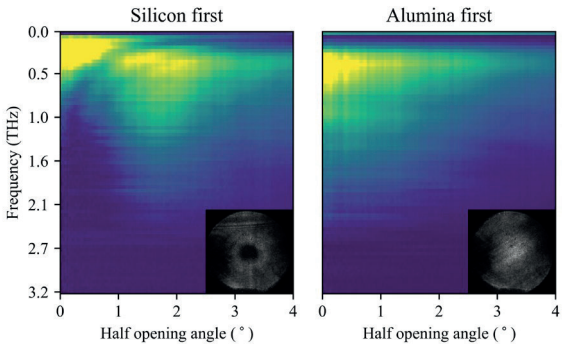

Fig. 2: THz intensity as a function of frequency and half opening angle of the THz emission. Insets: 2D spatial distribution of THz intensity at 1.5 THz.

From the 3D representation of the THz intensity (frequency and transverse spatial profile), we can plot the evolution of the THz intensity as a function of frequency and half opening angle of the THz beam at the ZnTe crystal position (Figure 2). With the 'Silicon filter first' configuration, a clear conical THz emission with 1.5° opening angle is observed beyond 0.5 THz, in agreement with previous works[1-3]. However, with the 'alumina filter

first', the THz emission exhibits a uni-modal spatial distribution for all frequencies. A complementary optical pump-THz probe experiment leads us to conclude that the conical emission observed with the Si filter is due to charge carriers photo-excitation of Si induced by the two-color femtosecond laser pulses generating the plasma.

III. Conclusions

In this communication, we have shown that the use of a Si filter to block the two-color optical pump in THz air plasma emission has a strong influence on the conical character or not of the THz beam. These results question the commonly accepted models for THz emission from a plasma filament and will motivate further theoretical and experimental investigations.

References

[1] P. Klarskov et al., New Jour. of Phys. 15(7), 075012 (2013).
[2] H. Zhong et al., Appl Phys. Lett. 88(26) 261103 (2006).
[3] A. Gorodetsky et al., Phys. Rev. A 89, 033838 (2014).
[4] K.Z. Rajab et al., J. Micro. and Elect. Pack 5, 101 (2008).
[5] M. Brossard et al., IEEE Trans. THz Sc. Technol.7(6), 741 (2017).

Higher frequency electronics and sub-terahertz diabetes detection

V. Krozer[1], G. Giacomo[1], Aldo Moreno-Oyervides[2], M. Carmen Aguilera-Morillo[3], Fernando Larcher[4], and Pablo Acedo[2]

[1] Physics Department, Goethe University Frankfurt am Main, Germany
[2] Electronics Technology Department, Universidad Carlos III de Madrid, Leganes, Spain
[3] Bioengineering Department, Universidad Carlos III de Madrid, Leganes, Spain
[4] Epithelial Biomedicine Division, CIEMAT, Madrid 28040, Spain

E-mail: krozer@physik.uni-frankfurt.de

Abstract – We demonstrate a W-band transmit receive unit with reference channel for biomedical applications, which are based on Functional Principal Component Logit Regression (FPCLoR), which enables to obtain a predictive model for sustained hyperglycemia, typically associated to diabetes. The predictions are based on transmission data from non-invasive millimeter-wave spectrometer at W-band. We show that there exist a frequency range most suitable for identification, classification, and prediction of sustained hyperglycemia. We discuss the required components of the spectroscopic instrument with the aim to obtain a compact and potentially low-cost non-invasive instrument for hyperglycemia assessment.

Keywords – keyword1, keyword2, keyword3

I. Introduction

Millimeter-wave spectroscopy has received much attention for biomedical applications, due to its spectral resolution, high sensitivity, measurement speed, and richness in information contained in the acquired spectrum. Many biomedical applications have been addressed recently utilizing millimeter-wave (mm-wave) spectroscopy [1]–[5], being diabetes detection one of the first applications envisaged for this technique. Microwave, millimeter-wave (mm-wave) and terahertz (THz) spectroscopy has been proposed for Diabetes Mellitus (DM) diagnostic associated to instantaneous glucose level measurement [6]–[10] and sustained hyperglycemia states detection [11], both relevant to the diagnostic and patient control. However, in both cases, we are still far from an operational diagnostic based on these techniques that leverages the advantages identified for such a system such as non-invasiveness, the use of non-ionizing radiation, and the potential low-cost of the developed system.

This paper proposes a mm-wave reflect/transmit setup using a multiplied source and subharmonic Schottky diode receivers and appropriate statistical spectroscopy techniques to arrive at a diagnostic tool for non-invasive control of sustained hyperglycemia state. The focus of the paper is on the discussion of the importance of using adequate statistical techniques to process the spectral data in mm-wave spectroscopy to develop biomedically relevant diagnostic systems as for example in DM diagnostic.

II. W-Band Setup

The spectral interrogation for the non-invasive assessment of sustained hyperglycemia was carried out by a spectrometer operating across the full W-band with steps of 1.5 GHz. As shown in Fig.1, generators deliver a swept signal in the Ku-band (12.5-18.5 GHz in steps of 0.25 GHz) with 0.3 MHz frequency difference between the two signals. One signal generator is connected to an Active Frequency Sixtupler (MULT), resulting in a frequency sweep within the W-band. The MULT is realized in a waveguide housing and exhibits a WR10 waveguide output. The output signal from the MULT is fed to a dual directional coupler. The coupled arms of the coupler define the reference and reflect channels, respectively, with subharmonic mixer receivers at each coupled port. The thru branch of the coupler is fed into a waveguide probe and device under test (DUT). The transmission path is measured with equivalent subharmonic mixer receivers, as in the reference and reflect ports. The outputs of the subharmonic receivers deliver an intermediate frequency of IF = 1.8 MHz and are connected to a data acquisition unit (Handyscope HS4-10, TiePie engineering, Sneek, Netherlands), which digitizes the measured signals with a sampling rate of 10 MHz. Finally, all the sampled signals are filtered and processed using LabVIEW software.

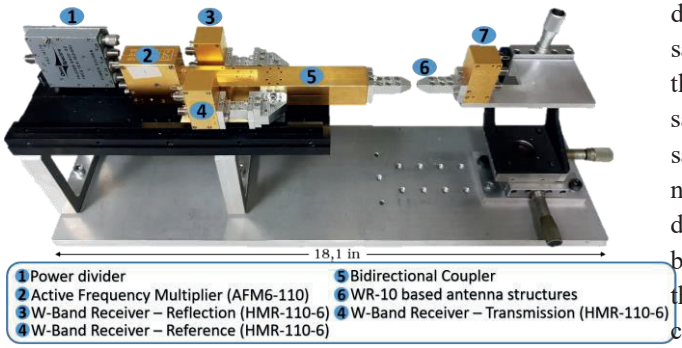

Fig.1. Mm-wave spectroscopic instrument for the non-invasive sustained hyperglycemia assessment.

It will be shown that this setup can be realized much more compact using modern MMIC techniques.

III. Sample Population

Two experiments were conducted with sixteen months elapsed between the first and second experiment, and a different sample of mice for each experiment referred to as "A" and "B". In both experiments, the sample of mice included animals with normoglycemic and hyperglycemic conditions. Healthy mice of different strains with an expected blood glucose level of 100 mg/dl were considered as normoglycemic animals. Within the hyperglycemic cases, two different types of hyperglycemia were considered: obese mice due to a genetic mutation that causes a deficiency of leptin (Lep^{ob}/ Lep^{ob}) and diabetic mice due to a genetic mutation that causes insulin resistance (Lep^{db}/ Lep^{db}).

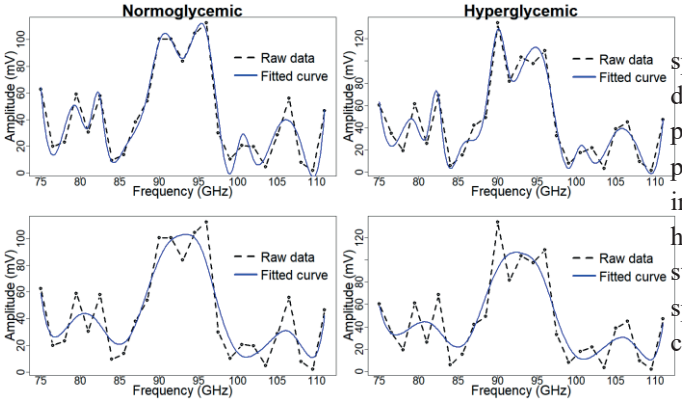

Fig. 2. Estimated and measured transmission amplitude for a normoglycemic (left panel) and a hyperglycemic mouse (right panel) by using two different approximations: regression splines (at the top) defined on 17 not equally spaced nodes and P-splines (at the bottom) defined on 17 equally spaced nodes with $\lambda = 0.11$.

The multi-test analysis showed that the diagnostic tool allows for correct diagnosis (detection) of sustained hyperglycemia in animal models with excellent and very robust results. Then, sample A, measured at a second experiment, was used to validate the consistency of the diagnostic tool to discriminate the condition in a new sample. Once again, a FPCLoR model was fitted using the 33 mice from sample B as training sample, and sample A was the test sample. As reported in TABLE I, sample A consists of 20 mice with hyperglycemia and normoglycemia proportionately distributed. Functional data from both, sample A and sample B were estimated by using P-splines defined on 17 equally spaced points in the spectrum, as shown in Fig.4 (bottom). The ROC curve corresponding to the fitted model is shown in Fig. 6 with the AUC = 0.95. Testing the prediction capabilities of the fitted FPCLoR model on the test sample, we obtain a 100% on the new observations correctly classified (CCR). These results validate the consistency of the measured spectral response for sustained hyperglycemia, and consequently, supports the reliability of the spectroscopy instrument.

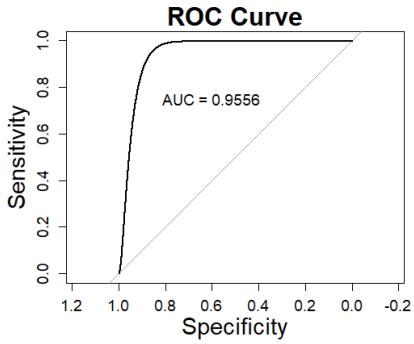

Fig. 3. ROC Curve estimated for the FPCLoR model.

IV. Conclusions

This paper demonstrates the suitability of mm-wave spectroscopy in the W-band for diabetes diagnostics and discrimination using advanced statistical methods. The paper also shows that the model developed here is predictive and provides excellent results across several independent tests. The results obtained for sustained hyperglycemia discrimination and prediction, which is strongly related to diabetes condition, were based on spectral data from the transmission reflection setup covering the full W-band.

The spectral data employed in this work are based on transmission amplitude data only, demonstrating that the amplitude spectrum contains the major information, leading to the conclusion that transmission through the skinfold is important. An advantage of this technique is its inherent insensitivity to skin reflectivity. Moreover, no previous calibration by a reference response from spectrometer has to be performed to the measured amplitude prior the statistical analysis. These results

simplify the overall spectroscopy system resulting in a simple transmission type spectrometer with limited frequency bandwidth of operation. We also show that interpreting the FPCLoR model allows to detect the most contributing frequencies for discrimination, so that, spectral interrogation can be optimized by selecting a substantially narrower frequency band enough for discrimination.

REFERENCES

[1] G. G. Hernandez-Cardoso *et al.*, "Terahertz imaging for early screening of diabetic foot syndrome: A proof of concept," *Sci. Rep.*, vol. 7, no. 42124, 2017.

[2] J. Y. Sim, C.-G. Ahn, E.-J. Jeong, and B. Kyu kim, "In vivo microscopic photoacoustic spectroscopy for non-invasive glucose monitoring invulnerable to skin secretion products," *Sci. Rep.*, vol. 8, no. 1059, 2018.

[3] Y. Nikawa and T. Michiyama, "Non-invasive measurement of blood-sugar level by reflection of millimeter-waves," in *Asia-Pacific Microwave Conference*, 2006.

[4] P. H. Siegel, A. Tang, G. Virbila, Y. Kim, M. C. Frank Chang, and V. Pikov, "Compact non-invasive millimeter-wave glucose sensor," in *40th International Conference on Infrared, Millimeter, and Terahertz waves (IRMMW-THz)*, 2015.

[5] B. M. Garin, V. V. Meriakri, E. E. Chigrai, M. P. Parkhomenko, and M. G. Akat'eva, "Dielectric properties of water solutions with small content of glucose in the millimeter - wave band and the determination of glucose in blood," *PIERS online*, vol. 7, pp. 555–558, 2011.

[6] P. H. Siegel, Y. Lee, and V. Pikov, "Millimeter-wave non-invasive monitoring of glucose in anesthetized rats," in *39th International Conference on Infrared, Millimeter, and Terahertz waves (IRMMW-THz)*, 2014.

[7] S. F. Clarke and J. R. Foster, "A history of blood glucose meters and their role in self-monitoring of diabetes mellitus," *Br. J. Biomed. Sci.*, vol. 69, no. 2, pp. 83–93, Jan. 2012.

[8] W.-C. Shih, K. L. Bechtel, and M. V. Rebec, "Noninvasive glucose sensing by transcutaneous Raman spectroscopy," *J. Biomed. Opt.*, vol. 20, no. 5, p. 051036, Feb. 2015.

[9] S. Liakat, K. A. Bors, L. Xu, C. M. Woods, J. Doyle, and C. F. Gmachl, "Noninvasive in vivo glucose sensing on human subjects using mid-infrared light," *Biomed. Opt. Express*, vol. 5, no. 7, p. 2397, Jul. 2014.

[10] E. Ryckeboer, R. Bockstaele, M. Vanslembrouck, and R. Baets, "Glucose sensing by waveguide-based absorption spectroscopy on a silicon chip," *Biomed. Opt. Express*, vol. 5, no. 5, p. 1636, May 2014.

[11] P. Martín-Mateos *et al.*, "In-vivo, non-invasive detection of hyperglycemic states in animal models using mm-wave spectroscopy," *Sci. Rep.*, vol. 6, no. 34035, 2016.

Abdel El-Fatimy

(Centrale Casablanca, Morocco. CEITEC, Brno University, Brno, Czech Republic)

Title: _Defect-induced cooling effect on graphene hot-electron bolometers._

Abstract: We report on the hot-electron cooling mechanism in graphene bolometers where the defect density can be controlled with the fabrication process. We show that the devices with high defect density exhibit the cubic power law and the defect-induced cooling produce a slower increase of the thermal conductance with increasing temperature, thereby greatly enhancing the device responsivity compared to devices with lower defect density and operating with normal-collision cooling [1].

[1] A El Fatimy et al, Carbon, Volume 154 [2], December 2019, Pages 497-502, https://doi.org/10.1016/j.carbon.2019.08.019 [3]

Detection Of Terahertz Radiation With Graphene-Based Field Effect Transistors.

Fedorov G.E.[1*], D. Svintsov[1], D. Bandurin[1,2], I. Gayduchenko[3], G. Goltsman[3]
[1] Moscow Institute of Physics and Technology (State University), Russia
[2] School of Physics, University of Manchester, United Kingdom
[3] Physics Department, Moscow State University of Education (MSPU), Russian Federation
E-mail: gefedorov@mail.ru

An overview of experimental work aimed at disentangling different mechanism of rectification of terahertz radiation in field effect transistors having gate electrode coupled to the radiation is provided. Response of a realistic device is in most cases an interplay between rectification at p-n junction, thermopower and hydrodynamical nonlinearity in the channel.

Keywords – terahertz detectors, graphene, FET

I. Introduction

An elegant proposal of terahertz radiation (THz) detector was put forward several decades ago by Dyakonov and Shur [1]. In their structure, radiation is coupled between source and gate of a high-mobility field-effect transistor with a quasi 2D channel, while photovoltage is read out between source and drain. The origin of asymmetry required for finite photocurrent is asymmetry of AC signal feeding (which is between source and gate) and asymmetry of boundary conditions - no ac current is flowing into the drain. While real structures are more sophisticated than predicted by the original toy model of plasmon launching by source-gate pair, they have proved to be among the most efficient THz rectifiers benefiting from zero-bias operation, low noise, and compatibility with CMOS technology [2]. In this talk I will discuss our resent results that provide insight into different mechanism of rectification in such structures with a conduction channel formed by graphene. Our results may be used for further optimization of nanocarbon based THz detectors.

II. Results

First we use device based on monolayer graphene combined experimental and theoretical studies of sub-THz response in graphene field-effect transistors analyzed at different temperatures. This temperature-dependent study allowed us to reveal the role of the photothermoelectric effect[3], p-n junction rectification [4], and plasmonic rectification in the sub-THz photoresponse of graphene FETs.

Next we show how to improve the performance of our detectors, taking advantage of BLG's gate-tunable band structure and fabricated a dual-gated device (top and bottom insets of Fig. 1. The idea is that when an electric field is applied perpendicular to the channel it induces a band gap in BLG that leads to a steeper dependence of the FET resistance R2pt on the gate voltage [5].

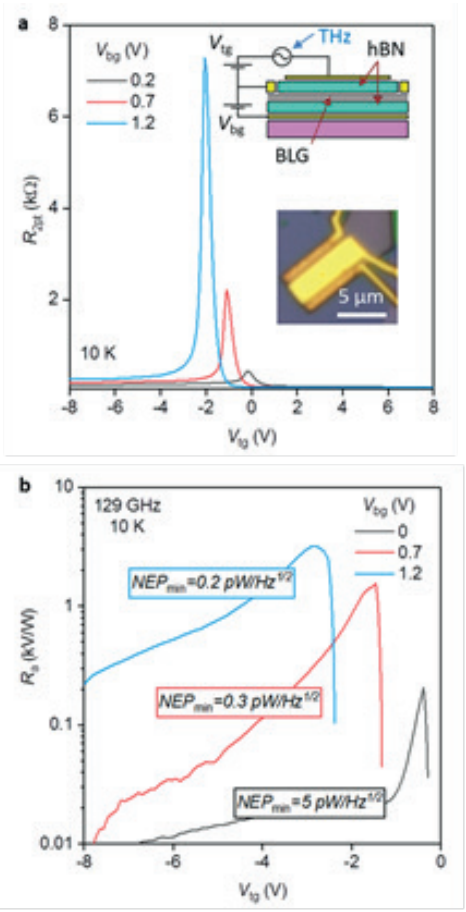

Fig. 1. Photoresponse of a dual-gated BLG detector. a, Two-terminal resistance as a function of Vtg measured in a dual-gated BLG FET for different Vbg. Top inset: Schematic of a dual-gated THz detector. Bottom inset: Optical photographs of the device. b, Responsivity as a function of Vtg for different Vbg measured at given f and T.

In another set of experiments we explore the idea of shifting the top gate position with respect to the source. The response of the detector at any detection mechanism is proportional to the difference between the squared

amplitudes of the high-frequency potential at the source and drain. The shift of the top gate near the source will lead to the attenuation of the wave that came to the drain, and increase the amplitude of the wave that came to the source.

ACKNOWLEDGMENTS

This work was financially supported by the Russian Foundation for Basic Research under the proj. 18-29-20116-mk.

REFERENCES

[1] Dyakonov, M., & Shur, M. IEEE transactions on electron devices, 43(3), 380-387. (1996).

[2] Knap, W., Dyakonov, et al., Journal of Infrared, Millimeter, and Terahertz Waves, 30(12), 1319-1337. (2009)

[3] D Bandirun, I Gayduchenko, et al., Appl. Phys. Lett., 112, 141101, (2018)

[4] I A Gayduchenko, G E Fedorov, et al.,, Nanotechnology, 29, 245204 (2018)

[5] D. Bandurin, D. Svintsov, I. Gayduchenko, et al., Nature Communications, 9, 5392 (2018)

Graphene in FET THz detectors

A. A. Generalov[1,2], A. Vorobiev[3], J. Stake[3], and Z. Sun[1,2]
[1] Department of Electronics and Nanoengineering, Aalto University, FI-00076, Aalto, Finland
[2] QTF Centre of Excellence, Department of Applied Physics, Aalto University, FI-00076, Aalto, Finland
[3] Department of Microtechnology and Nanoscience - MC2, Chalmers University of Technology, SE-41296 Göteborg, Sweden

E-mail: andrey.generalov@aalto.fi

Abstract – Field effect transistors (FETs) are excellent candidates for inexpensive room temperature THz detectors. Implementation of graphene in FET THz detectors can potentially bring their performance higher and help to overcome the limits of FET THz detectors in Si, GaN and other technologies. This contribution shows the dependence of GFET THz detector responsivity on graphene quality and discusses the important figures of merit for these detectors.

Keywords – graphene, THz detector, FET

I. Introduction

Many applications such as bio sensing, medical diagnostics and security screening significantly benefit from THz imaging technologies. However, state of the art THz detectors are typically based on cryogenically cooled systems which are expensive and inconvenient in real-life applications. An attractive solution to cost-effective and scalable room temperature THz detectors is the field effect transistor (FET). With certain boundary conditions the THz radiation induces charge density oscillations in a two-dimensional electron gas in the transistor channel which rectifies as a DC current between the source and drain terminals.

The FET THz detectors were demonstrated experimentally in various materials, such as Si [1], InP [2], GaN [3], graphene [4-8], and others. Of these materials, graphene is one of the most promising one in terms of fundamental mobility limit. On the other hand, the graphene technology has been significantly pushed, offering large scale devices with its relatively simple, flexible and cost-effective fabrication and integration technologies.

The graphene FET (GFET) THz detectors were first presented in 2012 and since then their performance is constantly growing as the methods of fabrication are developing and the quality of graphene is improving. GFET THz detectors have demonstrated noise equivalent power (NEP) from 2000 pW/Hz$^{1/2}$ in 2012 [4], to 512 pW/Hz$^{1/2}$ in 2014 [5], and 130 pW/Hz$^{1/2}$ in 2017 [6], which is close to compete with other materials-based THz detectors.

This abstract is concentrated on application of graphene in FET THz detectors and discussing the graphene fabrication process influence on the THz detection performance.

II. Fabrication process and THz responsivity

The relation between a dc transfer curve of GFET and the gate bias dependent THz responsivity was introduced and experimentally verified in [4-6]. It can be described with the following expression:

$$\Delta U \propto \frac{1}{\sigma}\frac{\partial \sigma}{\partial V_g}, \qquad (1)$$

where ΔU is a rectified dc voltage, σ is a channel conductivity, and V_g is a difference between gate voltage and Dirac voltage. As a consequence from (1) it was demonstrated in [6] that the THz responsivity is inversely proportional to residual carrier concentration n_0 in graphene, which is determined by the defects and contamination in graphene layer. Therefore the fabrication process of the GFET THz detectors was tailored to minimize the contamination of graphene layer during the process.

The GFET THz detectors are fabricated on the high-resistivity Si substrate with a 300 nm SiO_2 layer. The substrate is covered with a single-layer CVD graphene which is supplied commercially by Graphenea. To prevent any liquids processes on the graphene in the FET channel the graphene layer is covered with an Al_2O_3 gate dielectric. This allows for a cleaner gate dielectric/graphene interface with lower n_0.

Next, the Al_2O_3 outside the transistor channel is etched with a buffered oxide etch (BOE), and the graphene is patterned with a reactive ion plasma etching before the deposition source and drain contacts. Finally the gate electrode is deposited on top of the Al_2O_3 gate dielectric.

The process described in [6] allowed to achieve a record THz detection responsivity of 74 V/W at room temperature with the graphene mobility of μ_e = 3100 cm^2/Vs, n_0 = 4.5·10^{15} m^{-2}. However, the additional lithography steps of graphene etching and Al_2O_3 etching resulted in a high specific contact resistance of 4000 Ω·μm. Further improved process used in [9] allowed for extremely low graphene/metal specific contact resistivity as low as 90 Ω·μm [9], while still protecting the graphene from the contamination in the transistor channel. The combination of these techniques in GFET THz detectors is to bring their performance forward towards the real life application THz detectors.

IV. Conclusions

Graphene is an ideal candidate for the room temperature THz detectors. The responsivity of GFET detector depends on graphene quality and fabrication process. The developments in GFET fabrication methods allow for further GFET sensitivity improvement and approach the state of the art values for other technologies.

Acknowledgments

This work was financially supported by Academy of Finland, by Chalmers Area of Advance, and by the Knut and Alice Wallenberg Foundation.

References

[1] S. Boppel *et al.*, "CMOS integrated antenna-coupled field-effect transistors for the detection of radiation from 0.2 to 4.3 THz," *IEEE Trans. Microw. Theory Techn.*, **60**, 3834–3843 (2012).

[2] T. Watanabe *et al.*, "InP- and GaAs-based plasmonic high-electron-mobility transistors for room-temperature ultrahigh-sensitive terahertz sensing and imaging," *IEEE Sensors Journal*, **13**, 89–99 (2013).

[3] S. Boppel *et al.*, "0.25-µm GaN TeraFETs optimized as THz power detectors and intensity-gradient sensors," *IEEE Trans. THz Sci. Technol.*, **6**, 348–350 (2016).

[4] L. Vicarelli *et al*., "Graphene field-effect transistors as room-temperature terahertz detectors," *Nature Materials*, **11**, 865–871 (2012).

[5] A. Zak et al., "Antenna-integrated 0.6 THz FET direct detectors based on CVD graphene," *Nano Letters*, **14**, 5834–5838 (2014).

[6] A. A. Generalov, M. A. Andersson, X. Yang, A. Vorobiev, and Jan Stake, "A 400-GHz graphene FET detector," *IEEE Transactions on Terahertz Science and Technology*, **7**, 614–616 (2017).

[7] A. A. Generalov, M. A. Andersson, X. Yang, A. Vorobiev, and Jan Stake, "A heterodyne graphene FET detector at 400 GHz," *Proceeding of the 42nd International Conference on Infrared, Millimeter, and Terahertz Waves*, Cancun, Mexico, 27 Aug - 1 Sep 2017.

[8] X. Yang, A. Vorobiev, A. A. Generalov, M. Andersson, and J. Stake, "A flexible graphene terahertz detector," *Applied Physics Letters*, **111**, 021102 (2017).

[9] M. Bonmann, M. Asad, X. Yang, A. Generalov, A. Vorobiev, L. Banszerus, C. Stampfer, M. Otto, D. Neumaier, and J. Stake, "Graphene field-effect transistors with high extrinsic f_T and f_{max}," *IEEE Electron Device Letters*, **40**, 131–134 (2019).

AlGaN/GaN Heterostructures for Plasma Wave Detection and Emission in THz Regime

M. Sakowicz[1], P. Sai[2,3], D. B. But[2,3], G. Cywiński[1,4], M. Dub[1], I. Kasalynas[5], P. Prystawko[1], S. Rumyantsev[2] and W. Knap[2,4,6]

[1] Institute of High Pressure Physics "Unipress", PAS, Warsaw, Poland

[2] Center for Terahertz Research and Applications (CENTERA), Institute of High Pressure Physics "Unipress", PAS, Warsaw, Poland

[3] V. Ye. Lashkaryov Institute of Semiconductor Physics NAS of Ukraine, ISP NASU Kyiv, Ukraine

[4] CEZAMAT, Warsaw University of Technology, Warsaw, Poland

[5] Center for Physical Sciences and Technology, CPST, Vilnius, Lithuania

[6] Laboratoire Charles Coulomb, University of Montpellier and CNRS UMR 5221, 34950 Montpellier, France

E-mail: sakowicz@unipress.waw.pl

Abstract – We report on the investigations of the fin-shaped GaN/AlGaN field effect transistors with two lateral Schottky barrier gates exactly placed on the edges of the fin-shaped transistor channel. This kind FinFET modification (EdgeFET) allowed us to efficiently control the current flow in two-dimensional electron gas (2DEG) conduction channel. We present experimental data of sub-THz detection by EdgeFETs. We describe also how it is beneficial for observation of resonant plasma wave THz detection and emission.

Keywords – GaN, plasma waves, THz, detection, emission

I. Introduction

At the beginning of 90's Dyakonov and Shur proposed plasma excitations in nanometer field effect transistors for THz detection and emission [1,2]. They have shown that the channel of a field effect transistor (FET) can act as a resonator for plasma waves with a typical wave velocity $s \approx 10^8$ cm/s. The fundamental frequency f of this resonator depends on its dimensions and for the gate length L of a micron or less, can reach the terahertz (THz) range, since $f \sim s/L$. It was predicted also [1,2] that a steady current flow in an asymmetric FET channel can lead to instability against the spontaneous generation of plasma waves. This can in turn produce narrow band and tunable by the external gate voltage emission of electromagnetic waves in the THz frequency range.

Similar to emission, resonant plasma detection can be very interesting because it also can be narrowband and tuneable by the gate voltage. Both resonant THz emission [3-6] and detection [7,8] were observed experimentally, clearly demonstrating effects related to the excitation of plasma waves. However all observed resonant phenomena were much broader than theoretically predicted. Also in many cases the observed emission was not resonant and not voltage tunable [3].

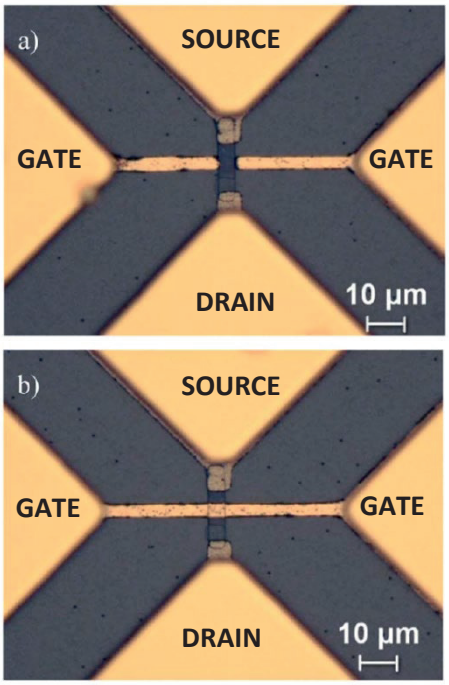

Fig. 1. Nomarski contrast microscope photos of GaN/AlGaN EdgeFET (a) and FinFET (b).

Polish-Lithuanian Funding Initiative DAINA based project "Terahertz Plasma Wave Instabilities in GaN/AlGaN Nanowires" aims to solve three problems which limit plasma wave instabilities generation in AlGaN/GaN high-electron-mobility transistor (HEMT) structures: (i) Coexistence of concurrent oblique modes; (ii) Shallow impurities emission; (iii) Blackbody (BB) radiation caused by Joule heating of biased HEMT channels. In this work we proposed the solutions based on new designs of narrow channel (nanowire) HEMT (EdgeFET), an original control of the residual impurities via THz electroluminescence spectroscopy, and a specific cooling of the plasmonic channel and investigation of the BB radiation efficiency of GaN/AlGaN HEMT structures grown on different (SiC and Al_2O_3) substrates [9-12].

II. Experimental Details

GaN/AlGaN heterostructure with two-dimension electron (2DEG) gas was used for FET fabrication, since gallium nitride (GaN) provides the highest electron saturation velocity, has a high breakdown voltage and operates in a wide range of temperatures [13,14]. Thus, this material has the huge frequency-power performance potential among commonly used semiconductors. GaN based devices have been already demonstrated as terahertz detectors by several groups [5,8,15,16]

The measurements were performed at room temperature on wafer using a probe station. The high frequency properties were studied using a radiation source operating at 110-170 GHz. The linear polarized radiation was focused on the devices using parabolic mirrors.

III. Results

The transfer current-voltage characteristic of EdgeFET (Fig. 2 b) indicate that this transistor can be pinched off by two lateral Schottky barriers even in the case of the micrometer dimension width of FET channel, that is $W = 4$ µm. Threshold voltage of both, FinFETs and EdgeFETs was in the range from -0.9 V to -1.2 V.

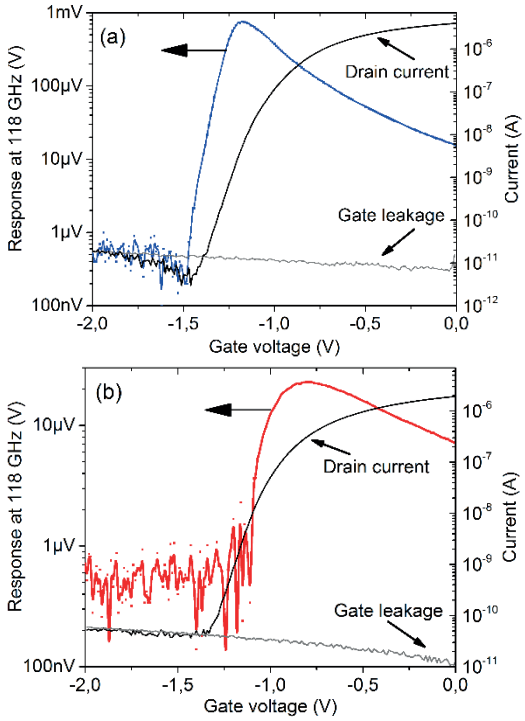

Fig. 2. Response measurements and transfer current-voltage characteristics of FinFET (a) and EdgeFET (b).

Figure 2 shows results of room temperature experiments on non-resonant detection at sub-THz (110-170 GHz) frequencies by EdgeFETs in comparison with the detection by FinFETs. As shown in the current figure, the signal peak for FinFET is near its threshold voltage and there is slight shift to lower voltage range of signal maximum in case of EdgeFET.

IV. Conclusions

We have proposed, fabricated and investigated the modification of fin-shaped GaN/AlGaN field effect transistors, called EdgeFET, with two gates based on lateral Schottky barrier contact directly to the 2DEG. We demonstrated that the transfer current-voltage characteristics of EdgeFET are similar to those of the conventional FinFET. EdgeFET transistors can be used as non-resonant detector in sub-THz range. Control of the side gates allows changing the width of two-dimensional electron gas and forming a wire, as we expect should be beneficial for observation of terahertz plasma wave resonances. This paves the way towards future terahertz detectors and emitters using high-quality factor plasma wave resonances, for which it is necessary to eliminate oblique modes.

Acknowledgments

The work at CENTERA was supported by the Center for Terahertz Research and Applications project carried out within the International Research Agendas program of the Foundation for Polish Science co-financed by the European Union under the European Regional Development Fund, by the Foundation for Polish Science through the grant TEAM/2016-3/25 and by the National Science Centre, Poland allocated on the basis of the decisions No. UMO-2017/25/N/ST3/00408 and No. UMO-2017/27/L/ST7/03283.

References

[1] M. I. Dyakonov, M. S. Shur, Phys. Rev. Lett. 71, p.2465 (1993).

[2] M. I. Dyakonov, M. S. Shur, IEEE Trans. Electron Devices 43, p.380 (1996).

[3] W. Knap, et al., Appl. Phys. Lett. 84, 3523 (2004).

[4] N. Dyakonova, et al., J. Appl. Phys. 97, 4313 (2005).

[5] N. Dyakonova, et al., Appl. Phys. Lett. 88, 141906 (2006).

[6] A. El Fatimy, et al., J. of Appl. Phys. 107, 024504 (2010).

[7] El Fatimy, et al., Appl. Phys. Lett. 89,13 (2006).

[8] El Fatimy, et al., Electronics Letters 42(23), 1342-1344 (2006).

[9] G. Cywiński et al., Appl. Phys. Lett. 112, 133502 (2018);

[10] V. Janonis et al., Physica Status Solidi (b) 255, art. no. 1700498 (2018).

[11] I Grigelionis et al., Materials Science in Semiconductor Processing 93, p.280 (2019).

[12] P. Sai et al., submitted to Appl. Phys. Lett. (2019).

[13] M. Shur and R. F. Davis, GaN-based materials and devices: growth, fabrication, characterization and performance vol. 11: World Scientific (2004).

[14] M. Shur, "GaN and related materials for high power applications," MRS Online Proceedings Library Archive, vol. 483 (1997).

[15] D. Čibiraitė, M. Bauer, A. Rämer, S. Chevtchenko, A. Lisauskas, J. Matukas, et al., "Enhanced performance of AlGaN/GaN HEMT-Based THz detectors at room temperature and at low temperature," in Infrared, Millimeter, and Terahertz Waves (IRMMW-THz), 2017 42nd International Conference on, 2017, pp. 1-2.

[16] T. Tanigawa, T. Onishi, S. Takigawa, and T. Otsuji, "Enhanced responsivity in a novel AlGaN/GaN plasmon-resonant terahertz detector using gate-dipole antenna with parasitic elements," in Device Research Conference (DRC), pp. 167-168 (2010)

Point-contact spectroscopy of topological materials

Tomasz Dietl[1, 2]

[1]*International Research Centre MagTop, Institute of Physics, Polish Academy of Sciences, PL-02268 Warsaw, Poland*

[2]*WPI-Advanced Institute for Materials Research, Tohoku University, Sendai 980-0845, Japan*

(Email: dietl@MagTop.ifpan.edu.pl)

Abstract: The rise of magnetic quantum materials opens for magnetic semiconductors a new chapter involving: (i) functionalities of spin polarized topological boundary states; (ii) magnetic proximity effects, and (iii) the control of magnetism by gating and by a number of layers in van der Waals heterostructures [1]. Importantly, by detaching few-layer thick epitaxial films from substrates, the "lego" method can be extended to virtually any magnetic semiconductor [2]. In this context, I will address the question on whether it is possible to extend the functionalities of magnetic quantum materials to above room temperature. Encouraging examples of compounds in which the *p-d* Zener mechanism on the one hand and the superexchange on the other lead to magnetic order persisting up to high temperatures will be discussed. The issue of d^0 ferromagnetism will be touched upon bringing up the case of organic semiconductors and bilayer graphene [3], in which spin order appears with no magnetic impurities, albeit so far only at helium temperatures. In the main body of the talk, I will discuss a superconductivity-like behavior discovered at interfaces of metals and topological materials by point-contact spectroscopy, and will show corresponding data for magnetic topological crystalline insulators serving to elucidate a possible origin of the phenomenon [4].

References

[1] T Dietl, A Bonanni, T Dietl. Families of magnetic semiconductors -- an overview. J. Semicond. 2019, 40(8): 080301, and references therein.

[2] K Yuan, X Yao, H Wang, B Han, P Gao, K Watanabe, T Taniguchi, L Dai, J Zhao, Y Ye. Peeling off Nanometer-Thick Ferromagnetic Layers and Their van der Waals Heterostructures. Adv. Electron. Mater. 2019, 1900345.

[3] A L Sharpe, E J Fox, A W Barnard, J Finney, K Watanabe, T Taniguchi, M A Kastner, D Goldhaber-Gordon. Emergent ferromagnetism near three-quarters filling in twisted bilayer graphene. Science 2019, 365: 605.

[4] G P Mazur, K Dybko, A Szczerbakow, J Z Domagala, A Kazakov, M Zgirski, E Lusakowska, S Kret, J Korczak, T Story, M Sawicki, T Dietl. Experimental search for the origin of low-energy modes in topological materials. Phys. Rev. B 2019, 100: 041408(R).

Quantum Hall states in HgTe topological quantum wells probed by transconductance fluctuations

B. Jouault[1], S. Mantion[1], S. Nanot[1], C. Consejo[1], Sandra Ruffenach[1], S. Krishtopenko[1], S. V. Morozov[2], N. N. Mikhailov[3,4], S. A. Dvoretskii[3,4], Wojciech Knap[1], F. Teppe[1]

[1] Laboratoire Charles Coulomb, UMR 5221 Centre National de la Recherche Scientifique, University of Montpellier, F-34095 Montpellier, France

[2] Institute for Physics of Microstructures RAS, GSP-105, Nizhni Novgorod 603950, Russia

[3] Institute of Semiconductor Physics, Siberian Branch, Russian Academy of Sciences, Prospekt Akademika Lavrent'eva 13, 630090 Novosibirsk, Russia

[4] Novosibirsk State University, Pirogova Street 2, 630090 Novosibirsk, Russia

e-mail: benoit.jouault@umontpellier.fr

Abstract – We have investigated quantum Hall states in a CdTe/HgTe/CdTe quantum well using transconductance fluctuation (TF) measurements. On the electron side, several integer QH states are observed, corresponding to filling factor ν = 1, 2, 3, 4. For magnetic fields above 2 Teslas, QH states ν = 0 are also observed in the normal gap. These observations are in perfect agreement with what is observed in previous studies on GaAs-based 2D quantum and graphene. These observations confirm that the observed TFs reflect charge localization phenomena. On the hole side, surprisingly, TFs corresponding to anomalous *positive* filling factor ν are also clearly observed. We attribute the emergence of TFs to localized states of the hole side maxima. A semi-phenomenological model confirms that the population of these side maxima may induce unusual transconductance fluctuations of anomalous slope.

Keywords – Quantum Hall effect, two-dimensional topological insulator, transconductance

I. Introduction

It is well established that HgTe-based quantum wells (QW) can act either as a band insulator (BI) or as a less trivial topological insulator (TI), depending on the quantum well thickness[1,2] and temperature.[3] Under a magnetic field, a significant way of discriminating the TI phase from the BI phase presenting the chiral edge states of the ordinary quantum Hall effect (QHE) is to probe the dispersion of the Landau levels (LLs), and more particularly the behaviour of a particular pair of LLs called the zero-mode LLs. The most powerful experimental methods to perform these analyses are magnetoabsorption and magnetotransport measurements. The last method has also specific advantage as it can scan both edges states and bulk of the 2DEG or reveal fragile many-body states. However, transport measurements in large devices are usually blurred by disorder and this limits the use of this method.

Here, our work is motivated by recent studies[4-6] which demonstrate that transconductance measurements may reveal microscopic information on two-dimensional electron systems (2DEGs), even when macroscopic devices are measured. We present detailed measurements of the transconductance as a function of both carrier concentration and magnetic field in a HgTe quantum well and demonstrate that local charging effects are indeed detected.

II. Experimental details

The sample was grown by molecular beam epitaxy (MBE) on semi-insulating GaAs(013) substrate. A CdTe buffer, followed by an indium doped 40-nm Cd0:71Hg:29Te barrier and the 6.6 nm HgTe QW, were grown one by one. Then, for the top barrier, a 35-nm indium doped $Cd_{71}Hg_{29}Te$ layer, followed by a 40-nm CdTe cap layer were grown above the QW. The barriers from both sides of the QW are selectively doped with indium, in order to form a 2D electron gas in the QW with

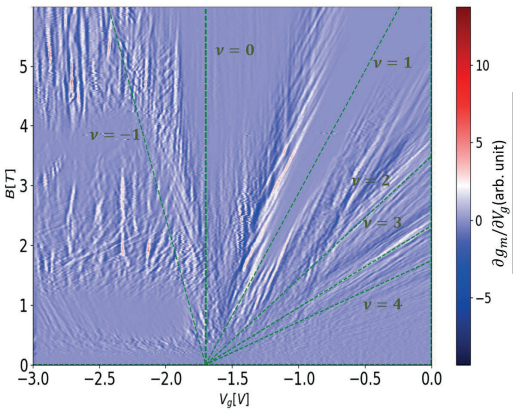

Fig. 1. Colour map of the derivative of the transconductance dg_m/dV_g in the (V_g, B) plane. The green dashed lines are guides for the eyes and correspond to slopes of filling factor $\nu = -1, 0, 1, 2, 3, 4$.

concentration of a few 10^{11} cm^{-2} at low temperatures. After MBE growth, 100-nm SiO_2 and 200-nm Si_3N_4 dielectric layers are deposited on top of the structure by a plasmochemical method. The investigated Hall bar has a total length of 650 µm and a total width of 50 µm.

The measurements were performed in a two-probe configuration at a base temperature of 280 mK. A constant dc-bias voltage $V_{sd} \simeq 0.1$ mV was applied between the source and the drain. A small ac voltage of 2 mV (corresponding to a carrier density variation of $\simeq 2$ electrons per micrometre square) and frequency 71 Hz was superimposed to a chosen dc gate voltage and the corresponding current δI_{V_g} was detected at fixed V_g with a lock-in amplifier. Then the transconductance $g_m = \delta I_{V_g}/\delta V_g$ was measured while the gate voltage Vg was swept between -3 V and 0 V and the magnetic field B between 0 and 3.2 T.

Figure 1 displays a colour map of the derivative transconductance $\partial g_m(V_g, B)/\partial V_g$. We plot the derivative of g_m rather than g_m in order to enhance the visibility of the fluctuations in Fig. 1. The charge neutrality point (corresponding to the topological gap) is at $V_g \simeq$ -1.65 V. In the conduction band ($V_g > -1.7$ V), distinct sets of parallel lines are clearly distinguished, which emerge roughly from the point ($V_g \simeq -1.7$ V, $B \simeq$0 T). A detailed analysis (using histograms of the correlation function between pairs of transconductance points) shows that these slopes are quantized and correspond to positive filling factor $\nu =$ 0,1, 2, 3 and 4. This result is in accordance with what was observed in other 2DEGs, like GaAs-based quantum wells, monolayer and bilayer graphene[4-6]. The rough quantization of the slope cannot be explained in a single particle picture. This quantization is usually attributed to non-linear screening and charge localization, which takes place when a LL is incompletely filled. In this regime, compressible dots are formed and separated by an incompressible sea in the 2DEG plane. Coulomb blockade in the dots then takes place and the discrete nature of the charge comes into play. If the charge remains constant in the partly populated LL when V_g or B are modified, then the screening remains the same and hence the screened disorder potential and the conductivity do not change. By contrast, if charge is added in some dots during a given modification of B or V_g, then the screened disorder potential and hence the conductivity are altered. Each conductance lines in the (B, V_g) plane can be attributed to specific charge density and disorder potential in the last and partly populated LL. More formally, the average charge n of the 2DEG is given by:

$$n = n_{LLL} + N(\frac{eB}{h}), \quad (1)$$

where n_{LLL} is the charge of the last (and partly occupied) LL and N is an integer corresponding to the number of completely filled LLs. As the charge is given by the gate voltage $ne = C\,V_g$, it immediately follows from Eq. (1) that all isocharge lines for n_{LLL} have a slope corresponding to $\nu = N$. In other words, the TFs are associated to some specific isocharge lines for the partly populated LL.

This model is expected to break down if several LLs are partly populated simultaneously, as it is the case in the valence band of CdTe/HgTe/CdTe QWs, where side maxima are present. Our experimental observation indeed confirms that the model as given by Eq. (1) is not valid. In Fig. 1, we observe sets of roughly parallel line when the Fermi energy is tuned in the valence band ($V_g < -1.7$ V) but the slope of these lines roughly correspond to $\nu = -1$ at low field $B < 1.2$ T (which is expected) and to $\nu \simeq 0$ and $\nu \sim 3 - 4$ at higher field (which is totally unexpected). Similar results were reproduced for three pairs of contacts in the same device.

We have calculated the LL dispersion of the LL as a function of B. Our calculations show that the energy separation between the LLs of these maxima is much smaller than the expected linewidth of the LL themselves. Moreover, these side maxima having a high mass, they have a large density of states and act as charge reservoir. We have also evaluated self-consistently the position of the Fermi energy E_F as a function of (V_g, B). We have recalculated the isolines of charge carrier density for each partly populated LL, for both valence and conduction band. The main result is that the isocharge lines of the LLs in the valence band indeed follow a complex behaviour, with unusual slopes in the (V_g, B) plane. The slope can be even positive for some magnetic field intervals, as indeed observed experimentally.

IV. Conclusions

We conducted transconductance measurements on a Hall bar made from a topological HgTe quantum well. We observed pronounced and reproducible transconductance fluctuations in the (B, V_g) plane, which we attribute to screening and charge localization. In the conduction band, the slopes of these TFs follow lines of positive integer filling factor, as already observed in other 2DEGs. On the hole side, we observe a completely new behaviour and unexpected slopes are observed. We attribute the appearance of these new lines to charge localization in the side maxima of the valence band, which act as a charge reservoir.

Acknowledgments

This work was supported by the CNRS via the LIA "TeraMIR," by MIPS department of Montpellier University through the "Occitanie Terahertz Platform" and by the French Agence Nationale pour la Recherche (Dirac3D project).

References

[1] B. A. Bernevig, T. L. Hughes, and S. C. Zhang, Science **314**, 1757 (2006).

[2] B. Buttner, C. X. Liu, G. Tkachov, E. G. Novik, C. Brune, H. Buhmann, E. M. Hankiewicz, P. Recher, B. Trauzettel, S. C. Zhang et al., Nat. Phys. **7**, 418 (2011).

[3] A. M. Kadykov, S. S. Krishtopenko, B. Jouault, W. Desrat, W. Knap, S. Ruffenach, C. Consejo, J. Torres, S. V. Morozov, N. N. Mikhailov, S. A. Dvoretskii, and F. Teppe, Phys. Rev. Lett. **120**, 086401 (2018).

[4] Youngwook Kim, Dong Su Lee, Suyong Jung Viera Skákalová, T. Taniguchi, K. Watanabe, Jun Sung Kim, and Jurgen H. Smet, NanoLetters **15**, 7445 (2015).

[5] Dong Su Lee, Viera Sk´akalov´a R. Thomas Weitz, Klaus von Klitzing, and Jurgen H. Smet, Phys. Rev. Lett. **109**, 056602 (2012).

[6] Manohar Kumar and Antti Laitinen and Pertti Hakonen, Nat. Commun. **9**, 2776 (2018).

Topological phase transition in HgTe quantum wells induced by hydrostatic pressure

I. Yahniuk[1], S. S. Krishtopenko[2], M. Majewicz[3], T. Dietl[3,4], S. A. Dvoretsky[5], N. N. Mikhailov[5], G. Cywiński[1], V. I. Gavrilenko[6], G. Grabecki[3], J. Wróbel[3], A. Kazakov[4], F. Teppe[2], J. Przybytek[1], and Knap[1,2]

[1] CENTERA Laboratories, Institute of High Pressure Physics, Polish Academy of Sciences, Warsaw, Poland
[2] Laboratoire Charles Coulomb (L2C), UMR CNRS 5221, University of Montpellier, F-34095 Montpellier, France
[3] Institute of Physics PAS, al. Lotników 32/46, PL 02-668 Warsaw, Poland
[4] International Research Centre MagTop, al. Lotników 32/46, PL 02-668 Warsaw, Poland
[5] Rzhanov Institute of Semiconductor Physics SB of RAS, 630090 Novosibirsk, Russia
[6] Institute for Physics of Microstructures RAS, GSP-105, 603950, N. Novgorod, Russia

E-mail: *ivan.yahniuk@unipress.waw.pl*

Abstract – We report on the first clear observation of topological phase transition in HgTe quantum wells induced by hydrostatic pressure. By using gated Hall bar devices, we investigate the pressure evolution of a peculiar pair of "*zero-mode*" Landau levels, whose crossing at a critical magnetic field B_c is a characteristic of inverted band structure in the quantum well. Accurate values of B_c and a pressure phase diagram are extracted from magneto-transport measurements. By following the pressure dependence of B_c, we define a critical pressure P_c, at which the bulk band gap vanishes, and the topological phase transition occurs.

Keywords – HgTe QWs, Topological insulators, Phase Transitions, Pressure

I. Introduction

HgTe quantum wells (QWs) with an inverted band structure, i.e., the QW electric subbands derived from the Γ_8 band are above the subbands originating from the Γ_6 band forming two dimensional topological insulator (2D TI) characterized by gapless helical edge states., is realized provided that the band structure is inverted. This occurs if the QW thickness d is larger than a critical value $d_c \sim$ 6.3 nm[1,2] and the magnitude of the magnetic field B is smaller than a critical value B_c at which the QW uppermost Landau level derived from Γ_6 band becomes higher in energy than the lowest Landau level originating from the Γ_8 band[3,4]. The existence of such a topological phase transition has been shown as a function of the QW thickness[2] and temperature[4] that reduces a distance between the Γ_8 and Γ_6 bands. In this work, we report on the first clear observation of topological phase transition in HgTe QWs induced by hydrostatic pressure. Accurate values of B_c and a pressure phase diagram have been extracted from magnetotransport measurements. By following the pressure dependence of B_c, we define a critical pressure P_c, corresponding to the topological phase transition between trivial insulator and 2D TI.

II. Theory

Figure 1 shows a pressure evolution of the electron-like (*E1*) and hole-like (*H1*) subbands at zero quasimomentum in the 8 nm wide HgTe/$Cd_{0.62}Hg_{0.38}$Te QW grown on CdTe buffer. At small hydrostatic pressure, the QW has inverted band ordering with the *H1* subband lying above the *E1* level. When pressure increases, the band gap vanishes and the system passes through phase transition at critical pressure value denoted as P_c. At the critical pressure, the HgTe QW hosts a gapless state with single-valley massless Dirac fermions. Further increasing of the pressure yields the opening of the trivial gap, corresponding to the normal band ordering in the QW.

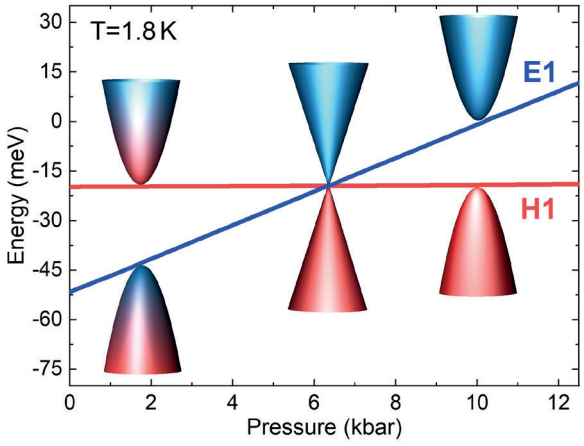

Fig. 1. The evolution of the *E1* and *H1* subbands at zero quasimomentum as a function of hydrostatic pressure in the 8 nm wide HgTe/$Cd_{0.62}Hg_{0.38}$Te QW grown on CdTe buffer. Blue and red colors correspond to the *E1* and *H1* subbands, respectively. All the calculations are performed at T = 1.8 K [5].

II. Discussion

The two QW samples studied in this work were grown by molecular beam epitaxy (MBE) on a [013]-oriented semi-insulating GaAs substrate with a relaxed CdTe buffer[6] with the QW width d of 8 nm (sample S1) and 7.1 nm (sample S2) patterned to a Hall bar geometry with ratio L:W = 2:1. A gate electrode completed the structure. In the gate voltage region, in which charge transport proceeds via edge states, we observe strong reduced of local resistivity in a critical magnetic field B_c defining the boundary of the topological phase. With increasing hydrostatic pressure, B_c decreases and eventually vanishes at the critical pressure P_c.

One of the efficient methods to obtain experimental values of B_c is the measurements of the transverse conductivity σ_{xy} in the samples with gated Hall bars. In magnetic fields, derivative of the transverse conductivity from gate voltage $d\sigma_{xy}/dV_G$ show conspicuous peaks with maxima positions, corresponding the crossing of the Fermi level and Landau levels. Plotting the $d\sigma_{xy}/dV_G$ *versus* magnetic field allows to perform a magnetotransport mapping of the LLs and to define the critical magnetic field B_c, representing the band ordering[4,7].

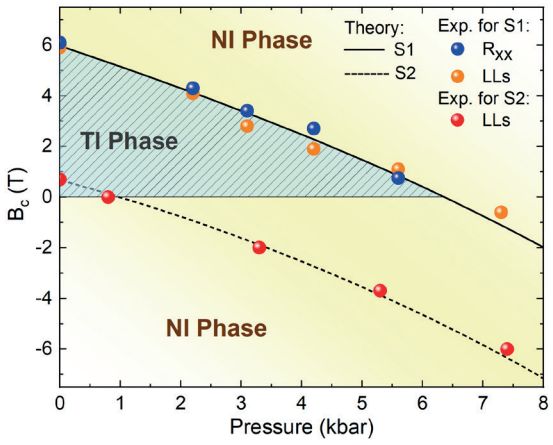

Fig. 2. Theoretically (solid- & dash- curves) and experimentally obtained Bc for samples S1 & S2 as a function of pressure. Black and blue symbols represent value of magnetic field at which longitudinal resistance are rapidly reduced. Orange and red ones extracted from LL fan charts. Blue- and light orange- regions correspond to non-trivial (inverted) and trivial band ordering, respectively.

The band inversion at the Γ point of the Brillouin zone suggests the existence of nontrivial topological insulator phase. As mentioned above, an external magnetic field gives rise to the crossing of the zero-mode LLs at finite B_c. Thus, to clarify the pressure induced transition, we compare theoretical and experimental results of the critical magnetic field as a function of pressure, as shown in Fig. 2. The plot presents a good agreement between the values of B_c derived from the analysis experimental results and theoretical calculations.

III. Conclusions

To summarize, we have reported on the first clear observation of topological phase transition in HgTe QWs induced by hydrostatic pressure. Accurate values of B_c and a pressure phase diagram have been extracted from magnetotransport measurements. By following the pressure dependence of B_c, we define a critical pressure P_c, corresponding to the topological phase transition between trivial insulator and 2D TI. Our experimental results are in good agreement with band structure calculations[5].

Acknowledgments

This work was supported by the Foundation for Polish Science through the IRA Program financed by EU within SG OP Program, by the National Science Centre of Poland allocated on the basis of the decision Nos UMO-2017/25/N/ST3/00408. Research in France was partially supported by MIPS department of Montpellier University through the "Occitanie Terahertz Platform", by the Languedoc-Roussillon region via the "Gepeto Terahertz platform", by CNRS through LIA "TeraMIR" and by the French Agence Nationale pour la Recherche

References

[1] B.A. Bernevig, T.L. Hughes, S.C. Zhang. *Science* **314**, 1757 (2006).
[2] M. König, S. Wiedmann, C. Brüne, A. Roth, H. Buhmann, L.W. Molenkamp, X.L. Qi, S.C. Zhang. *Science* **318**, 766 (2007).
[3] B. Scharf, A. Matos-Abiague, J. Fabian. *Phys. Rev. B* **86**, 075418 (2012).
[4] A. M. Kadykov et al. *Phys. Rev. Lett.* **120**, 086401 (2008).
[5] S. S. Krishtopenko et al. *Phys. Rev. B* **94**, 245402 (2016).
[6] S. Dvoretsky et al. *J. Electron. Mater*. **39**, 918 (2010).
[7] B. Buttner et al. *Nat. Phys.* **7**, 418 (2011).

Fingerprints of topological Anderson insulator in HgTe quantum well

S.S. Krishtopenko[1], I. Yahniuk[2], G. Grabecki[3], S. Kret[3], T. Dietl[3], N.N. Mikhailov[4], S.A. Dvoretskii[4], F. Teppe[1] and W. Knap[2]

[1]*Laboratoire Charles Coulomb (L2C), UMR CNRS 5221, GIS-TERALAB, Université de Montpellier, 34095, Montpellier, France*

[2]*Institute of High Pressure Physics PAS, 29/37 Sokolowska, Warsaw, Poland*

[3]*Institute of Physics PAS, al. Lotnikow, Warsaw, Poland*

[4]*Institute of Semiconductor Physics, Siberian Branch, Russian Academy of Sciences, pr. Akademika Lavrent'eva 13, Novosibirsk, 630090 Russia*

(e-mail: sergey.krishtopenko@umontpellier.fr)

We report on pressure-dependent transport measurements in HgTe quantum well with artificially introduced point defects. A stable disorder due to point defects in our sample is confirmed by X-ray diffraction and high-resolution transmission electron microscopy. After disordering the *n*-type quantum well, we observe a strong non-local resistance vanishing at certain magnetic field, when the Fermi level lies far from the bottom of conduction band. To describe experimental data, we evaluate renormalization of the gap, chemical potential and mobility drop within the continuous Bernevig-Hughes-Zhang model with spatially correlated disorder in the self-consistent Born approximation. We find out that our experimental results may be interpreted as the fingerprints of topological Anderson insulator if the correlation length of the disorder is of several monolayers. The latter is consistent with the disorder potential formed by the point defects.

THz resonant-tunneling diodes

M. Feiginov[1]
[1] ET/IT Department, TU Wien (Vienna University of Technology), Gusshausstrasse 25/354, 1040 Vienna, Austria

E-mail: michael.feiginov@tuwien.ac.at

Abstract – Recent progress in the development of resonant-tunneling diodes (RTDs) and THz RTD oscillators is described. Strategies and concepts to increase their operating frequencies are pointed out, different types of fundamental RTD oscillators and novel oscillator concepts are outlined.

Keywords – resonant-tunnelling diodes; THz oscillators; tunnel relaxation time; tunnel lifetime; travelling-wave oscillators

I. INTRODUCTION

Resonant-tunneling diodes (RTDs) have reemerged in the last years as a promising and viable technology for sub-THz and THz radiation sources. RTD oscillators working above 1 THz have been demonstrated for the first time in 2010-2011 [1,2]. Presently, their operating frequencies are getting close to 2 THz [3,4]. The contemporary RTD oscillators can deliver ~0.5 mW at sub-THz frequencies and ~10 μW at THz frequencies [1-5]. It was demonstrated that RTD oscillators could be as small as a fraction of mm^2 [2], they consume low DC power and operate at room temperature. RTD oscillators have been used in high-speed wireless data-transmission experiments recently [6,7]. In meanwhile [8], we understand better the physics of RTD limitations at very high frequencies, we could find the ways, how to overcome the limitations and suggested novel types of RTD oscillators.

II. RESULTS

We were concerned with inherent limitations and relaxation tunnel processes (described by a time constant τ_{rel}) inside RTDs. We have predicted that τ_{rel} is not limited by the tunnel lifetime (τ) of electrons in the quantum well of RTDs [9,10]. It turns out, that the relaxation processes could be much faster, as well as much slower than τ, depending on the operating regime of RTDs [9,10]. We have also predicted that RTDs with unusually highly-doped collector should exhibit negative differential conductance at frequencies far beyond limitations due to τ and τ_{rel}, i.e., when $\tau\omega>>1$ and $\tau_{rel}\omega>>1$ [10,11]. The effects are proved experimentally up to ~600 GHz [12-14]. Following further along this line of development – relying on RTDs with heavily doped collector and rather low current density - we could demonstrate oscillators working at ~1.1 THz in the regime $\tau_{rel}\omega\approx1$ [2]. The analysis of the oscillators suggests that multi-THz frequencies should be achievable with RTD oscillators and the RTD oscillators have much room for further optimization [2,3,14]. We have also shown that dynamic nonlinear characteristics of RTDs are strongly influenced by the Coulomb-interaction effects and relaxation processes [15]. The calculated output power is in good agreement with the measurement results for RTD oscillators working in the high-frequency ($\tau_{rel}\omega>>1$) regime [15].

Further on, we have brought the concept of an RTD with heavily doped collector to its logical limit: we have increased the collector doping to the extend, that the lowest quantum-well subband of the RTD stays immersed under collector Fermi level. In such RTDs, the electrons are injected into the quantum well not only from the emitter side (which is usual for RTDs), but also from the collector. The oscillators with such RTDs were demonstrated to be working up to ~1.5 THz [3].

We have also analyzed theoretically the travelling-wave microstrip RTD oscillators [16]. Such oscillators could be seen conceptually similar to THz quantum-cascade lasers (QCLs) with the metal-metal waveguide and with a single cascade period (an RTD) as their active core. However, contrary to THz QCLs, microstrip RTDs should be working at room temperature. Assuming realistic parameters of RTD layers (we took them from our past experimental studies) we show that microstrip RTD oscillators could be working up to ~1.5 THz [16]. We expect that RTD layers specifically optimized for microstrip oscillators should extend the operating frequency even further.

IV. CONCLUSIONS

In conclusion, there is much room for further development of RTDs and RTD oscillators, that should enable operation of RTD oscillators at multi-THz frequencies and increase their output power. RTD oscillators have potential to evolve into enabling technology for real-world THz applications.

REFERENCES

[1] S. Suzuki, *et al.*, Appl. Phys. Lett., **97**, 242102 (2010).
[2] M. Feiginov, *et al.*, Appl. Phys. Lett., **99**, 233506 (2011).
[3] M. Feiginov, *et al.*, Appl. Phys. Lett., **104**, 243509 (2014).
[4] T. Maekawa, *et al.*, Appl. Phys. Expr., **9**, 024101 (2016).
[5] S. Suzuki, *et al.*, IEEE J. Sel. Top. Quant. Electron., **19**, 8500108 (2013).
[6] N. Oshima, *et al.*, Electron. Lett., **52**, 1897 (2016).
[7] T. Shiode, *et al.*, in Asia-Pac. Microwave Conf. 2011, December 2011, pp. 1122–1125.

[8] M. Feiginov, Int. J. Infrared and Millimeter Waves, **40**, 365 (2019).
[9] M. Feiginov, Appl. Phys. Lett., **76**, 2904 (2000).
[10] M. Feiginov, Nanotechnology, **11**, 359 (2000).
[11] M. Feiginov, Appl. Phys. Lett., **78**, 3301 (2001).
[12] M. Feiginov and D. Roy Chowdhury, Appl. Phys. Lett., **91**, 203501 (2007).
[13] M. Feiginov, *et al.*, EPL, **94**, 48007 (2011).
[14] M. Feiginov, *et al.*, EPL, **97**, 58006 (2012).
[15] M. Feiginov, *et al.*, Appl. Phys. Lett., **99**, 133501 (2011).
[16] M. Feiginov, Appl. Phys. Lett., **107**, 123504 (2015).

V.I. Gavrilenko
Title: "Long wavelength stimulated emission from HgCdTe quantum wells: overcoming the Auger recombination"

Abstract:
Stimulated emission (SE) at wavelengths up to 31 um (9.7 THz) and is demonstrated from HgCdTe quantum well (QW) heterostructures. Non-radiative Auger recombination is show to be mitigated due to relativistic energy spectrum. Pump-probe carrier lifetime measurements show that further increase in SE wavelength is feasible up to 60 um (5 THz).

The growth and characterization HgTe/CdHgTe quantum wells

N.N. Mikhailov[1,2], S.A. Dvoretsky[1,3], D.G. Ikusov, V. G. Remesnik[1], V.A. Shvets[1,2], I.N. Uzhakov[1]

[1] ISP SB RAN, 630090, Ave. Lavrentiev, 13, Novosibirsk, Russia
[2] NSU, 630090, st. Pirogova 2, Novosibirsk, Russia
[3] NR TSU, 634050, Ave. Lenina 36, Tomsk, Russia

E-mail: mikhailov@isp.nsc.ru

Abstract – The growth of multiple HgTe quantum wells (QW) structures on (013) CdTe/ZnTe/GaAs substrate by molecular beam epitaxy with ellipsometric control *in-situ* is presented. The model of the "effective" substrate for reconstructing of the composition distribution profile in HgTe QWs using ellipsometric parameters measurements is at growth is developed and used to describe the experimental results. A nondestructive method for determining of the size quantization energy level in grown multiple HgTe QW structures is developed by measuring of absorption and photoconductivity spectra. The dependence of size quantization energy level on the HgTe QW thickness at 298 K and 77 K was determined.

Keywords – HgTe, quantum wells, growth, size quantization energy level

I. INTRODUCTION

The nanostructures based on solid solutions of mercury cadmium tellurides are of great interest for fundamental studies of physical phenomena in low-dimensional systems (2D and 3D topological insulators), double and multiple quantum wells (QWs) and laser structures. The results of scientific research can be used for practical applications, such as lasers and photodetectors operating in the infrared and terahertz ranges. The laser structures based on HgCdTe should have waveguide layers of constant composition and active emitting elements in the form of built-in HgTe QWs. The structures for infrared photodetectors based on multiple HgTe QW can be alternative to the layers of solid solutions. Theoretical calculations showed the possibility of creating effective photodetectors based on structures with multiple HgTe QWs for which the spectral characteristics are determined by the composition of the $Hg_{1-x}Cd_xTe$ spacers (where x is CdTe molar fraction) and the thickness of HgTe layer.

The theoretical calculations of physical phenomena are used the representation of HgCdTe QW with rectangular profile of composition. For HgTe QW with large layer thicknesses more than 15 -20 nm may be this assumption is quite justified, since the possible transition regions at the HgCdTe/HgTe boundaries apparently do not affected on common physical picture. However, during the growth of HgTe QWs, the formation of transition layers at boundaries between spacers and HgTe layers is possible, which at small thicknesses can significantly affect the overall picture of physical phenomena and should be taken into account in theoretical calculations. For HgTe QWs, there is exist the critical thickness of 6.3 nm, at which a transition from a direct band to inverse band structure occurs. Therefore, for QWs with thicknesses close to critical, the transition layers noticeably affect both the position of the size quantization levels and the spectral characteristics of lasers or photodetectors.

We have developed the method for precision reconstruction of the composition distribution profile from in situ measured ellipsometry measurements at growth of multiple HgTe QWs. This method is based on the replacement of a variable-composition layer by a constant-composition substrate with "effective" optical constants [1]. This method allows one to restore with high accuracy the distribution of the composition over the thickness in consequentially grown HgTe QWs.

II. EXPERIMENTAL RESULTS

The structures with multiple of HgTe QWs were grown by molecular beam epitaxy with ellipsometric control *in situ*. The structures were grown on the molecular beam epitaxy unit "Ob-M". To interrupt the Cd flow, a mechanical valve was used located between the annular flow former (which allowed the spatial distribution of the flow to be preserved) and the cadmium source. The amount of HgTe QWs varied from 5 to 200, and the thickness of the HgTe layers varied from 3 to 18 nm. The composition of the barriers was $X_{CdTe} \geq 0.6 \div 0.75$, the thickness of the $Hg_{1-x}C_xdTe$ barriers was ~30nm.

The adsorption and photoconductivity spectra of such structures are presented. The precise composition distribution of the grown HgTe QWs was reconstructed using the model of "effective" substrate. The position of the size quantization energy levels and the long-wavelength cut-off of photoconductivity were determined from the absorption and photoconductivity spectra.

Figure 1 shows typical profiles of the composition distribution in the structure with 50 HgTe QWs. This composition distribution composition was obtained using the developed method of the "effective" substrate [1]. It can be seen that a reproducible composition distribution

is observed in the all grown HgTe QWs. The average statistical scatter for a fixed coordinate was δX_{CdTe} ~□0.02 molar fractions.

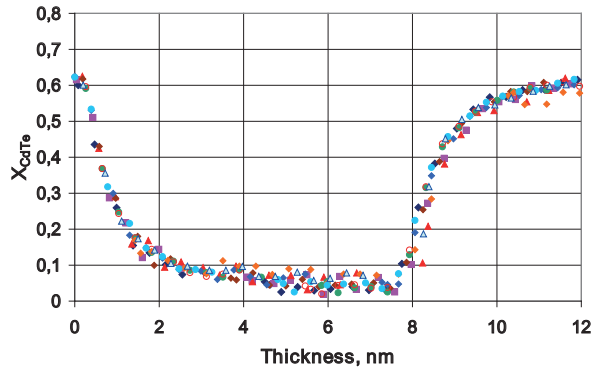

Fig. 1. Typical profiles of the composition distribution in the structure with 50 HgTe

The position of size quantization energy level and the long wavelength cut-off is determined from absorption and photoconductivity spectra.

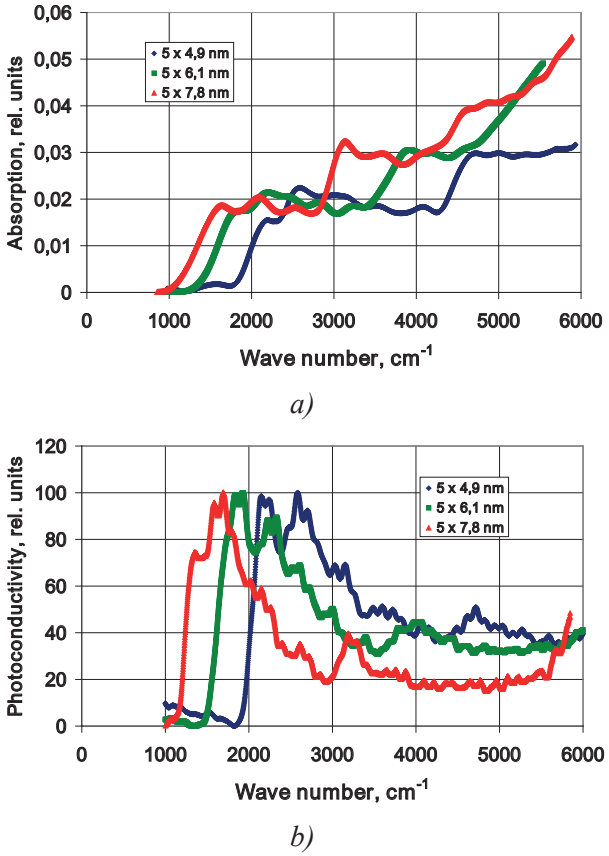

Fig. 2. Absorption spectra - a) and photoconductivity spectra –b) for HgTe QW structures with 5 HgTe layers of different thicknesses

Figure 2a shows the absorption spectra for HgTe QW structures with 5 HgTe layers of different thicknesses. The plateaus are corresponding to the transitions between size quantization energy levels. Figure 2b shows the photoconductivity spectra of the same structures. It can be seen that the long wavelength cut-off depends on the thickness of the HgTe layer in HgTe QW. As the thickness increases, the long wavelength cut-off is shifted toward the longer wavelength range with the increasing the HgTe layer thickness. The additional peaks of the photoconductivity spectra are corresponding to transitions from size quantization energy levels. The data on the photoconductivity spectra are in good agreement with the results obtained from the absorption spectra.

For structures with multiple HgTe QWs, the dependence of the long wavelength cut-off has been studied at 300 K and at 77 K. The shift of the long wavelength cut-off with HgTe thickness decreasing into longer wavelength is observed.

There were fabricated photoconductors on the basis of multiple HgTe QWs. It was shown that V-W response is comparable with bulk material ones at analogous long wavelength cut-off.

III. Conclusions

It was shown that “effective” substrate method allows to reconstruct of the distribution profile in HgTe QWs with nanometric thicknesses. A good reproducibility of the composition distribution profile was demonstrated at reconstruction for structures up to 50 HgTe QWs.

A non-destructive method is proposed for determining the position of size quantization levels in HgTe QWs from measuring absorption spectra. The comparison of the obtained results with measurements of the photoconductivity spectra showed that the proposed method can be used to characterize the position of size quantization energy level.

The experimental dependences of size quantization energy level position on the thickness of the HgTe QW at temperatures of 298 and 77 K is obtained.

Acknowledgments

This work was partially supported by the Russian Foundation for Basic Research (project No. 18-29-20053).

References

[1] V.A. Shvets, N. N. Mikhailov, D.G. Ikusov, I.N. Uzhakov, S.A. Dvoretskii, Determining the compositional profile of HgTe/$Hg_{1-x}Cd_xTe$ quantum wells by Single-Wavelength Ellipsometry, *Optics and Spectroscopy* **127**, 2, p. 340–346 (2019)

Nonlocal Terahertz Photoconductivity in the Topological Phase of $Hg_{1-x}Cd_xTe$ Semiconductors

A. S. Kazakov[1], A. V. Galeeva[1], A. I. Artamkin[1], S. A. Dvoretsky[2], N. N. Mikhailov[2], M. I. Bannikov[3], S. N. Danilov[4], L. I. Ryabova[5], D. R. Khokhlov[1,3]

[1] Physics Department, M.V. Lomonosov Moscow state University, Moscow, Russia
[2] A.V. Rzhanov Institute of Semiconductor Physics, Syberian Branch of RAS, Novosibirsk, Russia
[3] P.N. Lebedev Physical Institute of RAS, Moscow, Russia
[4] Faculty of Physics, University of Regensburg, Regensburg, Germany
[5] Chemistry Department, M.V. Lomonosov Moscow State University, Moscow, Russia

E-mail: khokhlov@mig.phys.msu.ru

Abstract – We present results on non-local terahertz photoconductivity in $Hg_{1-x}Cd_xTe$ thick epitaxial films with the inverted energy spectrum (x<~0.16). We show that the phototransport features observed in magnetic field indicate realization of the nonlocal electron transport regime which is inherent to 2D topological insulators. We discuss the results in terms of a qualitative model that takes into account coexistence of the bulk transport and boundary conductive channels.

Keywords – terahertz radiation,photoconductivity, topological phase

I. Introduction

Electron transport properties of materials exhibiting a topological phase transition attract a great deal of attention of both experimentalists and theorists. $Hg_{1-x}Cd_xTe$ solid solutions reveal a composition-driven transition from the trivial semiconductor ($x > 0.16$ at $T = 4.2$ K), characterized by the direct energy spectrum, to the topological phase ($x < 0.16$ at $T = 4.2$ K) with the inverted energy band structure. The topological phase is featured by formation of edge or surface conductive states with high-mobility massless charge carriers. Study of photoelectric effects under terahertz laser excitation may provide an experimental observation of topological conductive states in $Hg_{1-x}Cd_xTe$ solid solutions characterized by relatively low bulk carrier concentration. Previously, we studied photoconductivity in $Hg_{1-x}Cd_xTe$ solid solutions with both inverted and direct spectrum in the standard Hall bar geometry, discussed bulk- and interface-related non-equilibrium processes, which may contribute to the terahertz photoconductivity in $Hg_{1-x}Cd_xTe$ epitaxial layers,[1,2]. In this paper, we focus on discrimination of the edge component of the terahertz phototransport in $Hg_{1-x}Cd_xTe$ structures with the inverted energy spectrum. We use a nonlocal configuration for phototransport measurements implying spatial separation of current and potential probes and thus providing an opportunity to vary the bulk contribution to the net photoresponse.

II. Experimental

4 μm thick $Hg_{1-x}Cd_xTe$ films ($0.12<x<0.16$) were synthesized on a semi-insulating GaAs [013] substrate with ZnTe and CdTe buffer layers by molecular beam epitaxy. Transport properties of the structures were studied in the 4.2 - 300 K temperature range in magnetic fields up to 4 T. All the samples were of the *n*-type. The typical concentration of electrons in the film bulk was ~ 10^{14} cm^{-3} at $T = 4.2$ K. Photoconductivity induced by the terahertz laser pulses was studied in the Faraday geometry at the 2 THz frequency in magnetic fields up to 4 T at $T = 4.2$ K. All samples were prepared by photolithography. Measurements were performed for both the standard Hall bar sample geometry and the nonlocal H-bar-like geometry (see inset in the fig.1) with a variable distance between pairs of current and potential probes. The typical sample length was ~ 5 mm, the width was varied from 0.5 to 2.5 mm.

III. Results

The response induced by terahertz radiation has been studied in all samples upon application of a bias voltage. No photoresponse has been observed at the zero bias. In the absence of a magnetic field, the response is relatively small and corresponds to the bulk transport of the excited carriers. The magnetic field applied leads to a qualitative change in both magnitude and kinetics of the photoresponse. Typical kinetics of the photoresponse measured using different pairs of potential probes in magnetic field are shown in the Fig. 1. The electric measurement circuit and a typical sample geometry (hereinafter referred as nonlocal geometry) are shown in the inset.

One can see that the photoresponse measured in the nonlocal configuration almost does not depend on the distance between pairs of potential (2-7, 3-6 or 4-5 in the inset in fig. 1) and current (1-8 in the inset) probes within the typical sample length. It should be stressed, that at the

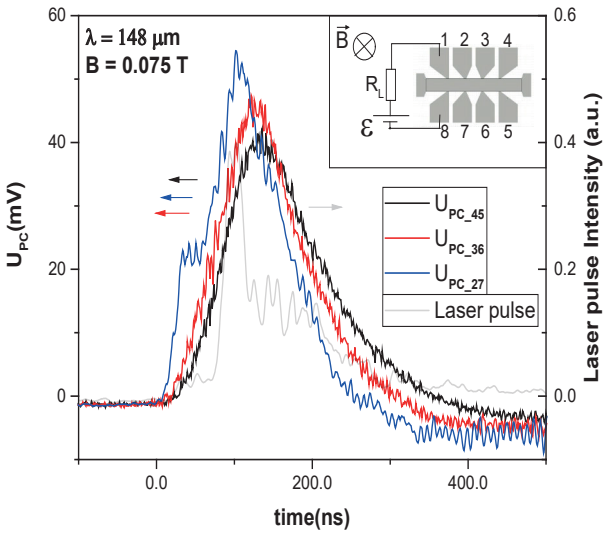

Fig. 1. Kinetics of the photoresponse measured in the sample with the composition x = 0.13 under terahertz photoexcitation with the wavelength λ=148 μm in magnetic field B = 0.075 T. Blue, red and black curves correspond to the photoresponse kinetics measured using 2-7, 3-6, and 4-5 pairs of potential probes, respectively. The grey curve corresponds to the laser pulse time profile. The inset shows schematically the sample geometry and the electric measurement circuit.

same time, the potential drop measured in the absence of the laser illumination decreases exponentially as the distance between the potential and the current probes increases. Moreover, the potential drop totally vanishes between the most distant pair of potential probes. Therefore, it is reasonable to assume that the response observed at the most distant probes mainly does not correspond to the bulk transport. Instead, the photoresponse may be attributed to another transport channel formation. One can expect that the effect described may be mainly related to existence of the edge photocurrent induced by combined effect of terahertz radiation, magnetic field and bias voltage applied.

Let us now turn to the experimental result, which gives us one extra argument for the statement above. We apply the bias voltage to 3-6 probes (see the inset in fig. 2, a) and measure the photoresponse to the right and to the left from the 3-6 probe pair line (fig. 2, a – d).

It should be stressed that for photoresponse kinetics measured at the same pair of potential probes (e.g. 4-5) with the same polarity of the battery, reversal of the magnetic field direction leads to photoresponse sign inversion (see fig. 2 a and b). Also, for kinetics measured in a given magnetic field direction, switching a pair of potential probes to another mirror-opposite pair (from 2-7 to 4-5) again leads to the reversal of the photoresponse sign.

The nonlocal photoresponse behavior in external magnetic field provides an argument for the edge non-equilibrium transport channel formation. The nonlocal photoresponse sign depends on the potential probe position and the magnetic field direction indicating the chirality of the non-equilibrium transport induced.

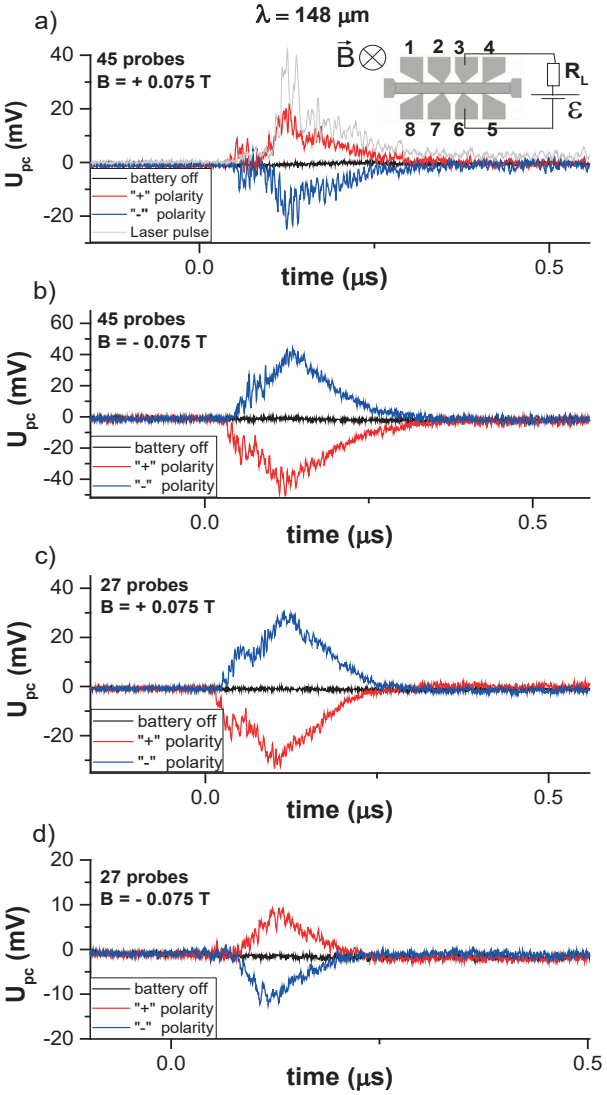

Fig. 2. Kinetics of the photoresponse induced by terahertz radiation with λ=148 μm with bias voltage at 3-6 probes measured from different pairs of potential probes (a, b - 4-5; c, d - 2-7) in magnetic field B = ±0.075 T. The sample with the width 0.5 mm. The insets shows schematically the geometry of the sample and the experimental measurement circuit.

III. Summary

In summary, we have directly demonstrated existence of the nonlocal component of the terahertz photoresponse in the $Hg_{1-x}Cd_xTe$ thick epitaxial films in magnetic field. The observed nontrivial features of the phototransport may be interpreted as manifestation of a chiral edge conductive channel formation in the topological phase of $Hg_{1-x}Cd_xTe$ ternary alloys.

The research described in this paper was supported by the grant of the Russian Science Foundation # 19-12-00034.

References

[1] A. V. Galeeva, A. I. Artamkin, A. S. Kazakov et al. *Beilstein J. Nanotechnol.* **9**, 1035 (2018).

[2] A. V. Galeeva, A. I. Artamkin, N. N. Mikhailov et al. *JETP Lett.* **106**, 162 (2017).

THz magnetospectroscopy of a HgCdTe epitaxial layer under hydrostatic pressure

D. Yavorskiy[1,2] , D. But[2], M. Szoła[2], V. I. Gavrilenko[3] , W. Knap[2] and J. Łusakowski[1]
[1] Faculty of Physics, University of Warsaw, Pasteura 5, 02-093 Warsaw, Poland
[2] Center for Terahertz Research and Applications, Institute of High Pressure Physics PAS, Sokołowska 29/37, 01-142 Warsaw, Poland
[3] Institute for Physics of Microstructures, RAS, GSP-105, 603950 N. Novgorod, Russia

E-mail: dmitriy.yavorskiy@fuw.edu.pl

A HgCdTe epitaxial layer was studied in magnetotransmission experiments in THz range. Measurements were carried out under hydrostatic pressures equal to 0.0 kbar, 1.63 kbar, 2.96 kbar, 3.83 kbar and at temperature equal to 2K. In order to understand and interpret obtained magnetotransmission spectra, Kane model was applied. Based on the fitted values obtained of the energy gap, it is shown that the energy gap has increased with pressure from -36 meV to -13 meV.

Keywords – HgCdTe, THz, magnetospectroscopy, topological insulator, phase transition

I. Introduction

Since the discovery of topological insulator phase a lot of semiconductng materials are coming back to favor after decades of oblivion. One of those intensively studied materials is mixed crystal - mercury cadmium telluride.

One of the properties of HgCdTe is that its energy gap can be driven by cadmium content, temperature or pressure from inverted to normal band structure through gapless state. Recently, it was showed [1] that such transitions induced by temperature are possible. There are also of works (see e.g., [2], [3], [4]) in which authors showed evolution of energy band structure under a hydrostatic pressure. The main motivation behind this work was to see whether phase transition can be monitored with magnetooptical studies, since the earlier works concentrated only magnetotransport measurements.

II. Experimental setup

The studied sample was a 3.2 μm - thick MBE-grown HgCdTe epitaxial layer with Cd content of 15%. The sample was placed inside the pressure cell, wherein the liquid was a mixture of oil and gasoline. In order to determine the hydrostatic pressure, an InSb manometer was used. Pressure cell with the sample inside was placed in a liquid helium cryostat with a superconducting coil. A molecular laser, VDI and BWO generators were used as sources of THz radiation. The THz radiation was guided to the sample through a stainless steel waveguide and then through the 5 mm thick sapphire window into the pressure cell. Transmitted THz signal was registered by a carbon bolometer placed under the sample.

III. Results

From magnetotransmission experiments four sets of data were obtained at different hydrostatic pressures - 0.0 kbar, 1.63 kbar, 2.96 kbar, 3.83 kbar. Each set consists of seven transmission spectra acquired for different photon energies: 2.73 meV, 3.71 meV, 6.67 meV, 7.61 meV, 10.44 meV, 12.85 meV and 17.56 meV. An exemplary evolution of magnetotransmission spectra measured at a monochromatic 10.44 meV radiation at different hydrostatic pressures is shown in Fig. 1. Each spectrum consists of three lines. It is easy to notice that with the increase of the hydrostatic pressure the position of each line shifts to the smaller magnetic fields.

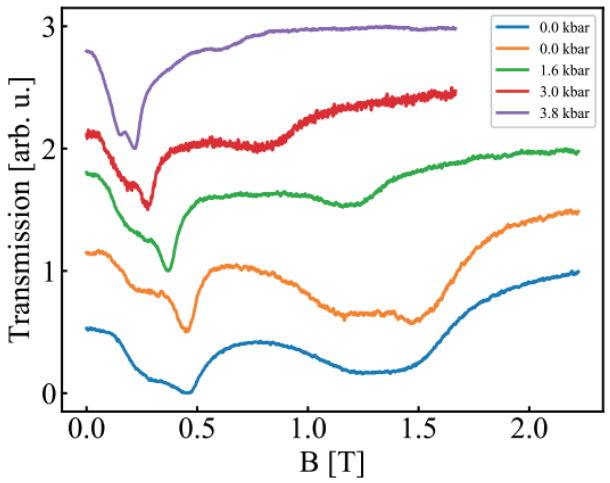

Fig.1 Magnetotransmission measurements of 10.44 meV radiation through the sample.

Based on the Kane model mentioned in the article of F. Teppe et. al. [1] and the selection rules of allowed optical transition fittings of LL spectrum for each set were performed. This procedure let us to receive values

of energy band-gap for each hydrostatic pressure and recognise Landau levels between which optical transition occured. Taking into account results of fitting, we propose that observed three lines are related to transitions between Landau levels in the conduction band.

It was also found the energy gap also chanes from -36 meV to -13 meV while the pressure increases from 0 kbar to almost 4 kbar.

IV. Conclusions

To conclude, we performed magnetotransmission experiments on a HgCdte epitaxial layer under hydrostatic pressure. Based on the obtained results we showed that dependence of the energy gap on the hydrostatic pressure is given by:

$$\frac{\partial E}{\partial P}\Big|_{\Gamma} = 6.3 \frac{meV}{kbar}$$

This value is consistent with the results obtained by other authors, as can be inferred from table below.

Table 1: Values of $\frac{\partial E}{\partial P}\Big|_{\Gamma}$ in literature data.

Reference	Cd compound[%]	Experimental techniques	$\frac{\partial E}{\partial P}\Big\|_{\Gamma}$ [meV]
[2]	27/28	Transport measurements	10
[3]	15	Transport measurements	3
[4]	0/10/15/20/28	Transport measurements	12

Acknowledgments

This work was financially supported by Center for Terahertz Research and Applications (CENTERA)" project is carried out within the 'International Research Agendas' programme of the Foundation for Polish Science co-financed by the European Union under the European Regional Development Fund

References

[1] Teppe, F. et al. Temperature-driven massless Kane fermions in HgCdTe crystals. Nat. Commun. 7, 12576 (2016).

[2] Characterisation under hydrostatic pressure of narrow-gap Hg1−xCdxTe and Hg1−xZnxTe. JCGonthier, ARaymond, JLRobert,RTribouletandJPFaurie,Sernicond.Sci.Technol. 5 (1990) S217-S22019

[3] Three-Band Model Applied to Narrow-Gap HgCdTe C. Fau J. F. Dame M. de Carvalho J. Calas M. Averous B. A. Lombos, phys. stat. sol. (b) 125, 831 (1984)

[4] Structure de bandes des alliages HgTe-CdTe C. Verie: phys. stat. sol. 17, 889 (1966)

Fine study of zero-mode Landau levels in HgTe quantum wells

Frederic Teppe

Laboratoire Charles Coulomb (L2C), UMR CNRS 5221, GIS-TERALAB, Université de Montpellier, 34095, Montpellier, France

(e-mail: frederic.teppe@umontpellier.fr)

The most efficient way to discriminate trivial and inverted band ordering in HgTe/CdHgTe QWs is to probe evolution of a particular pair of zero-mode Landau levels (LLs) under applied magnetic field [1]. These zero-mode LLs split from the edges of $E1$ and $H1$ subbands and have pure electron-like and hole-like origin, respectively. The electron-like LL always tends toward high energies, while the energy of the zero-mode LL from the $H1$ subband decreases with magnetic field. In inverted HgTe QWs, the zero-mode LLs cross at a critical magnetic field B_c, above which the inverted band ordering transforms into the trivial one [1].

The presence of bulk inversion asymmetry (BIA) [2] in the unit cell of zinc-blend materials and interface inversion asymmetry (IIA) at the HgTe/CdHgTe heterojunction [3] induces the anticrossing of zero-mode LLs in the vicinity of B_c. So far, experimental values of anticrossing gap Δ arising in the vicinity of B_c obtained by different techniques differ significantly from each others. Particularly, the measurements of magnetotransport [4,5] performed with the gated Hall bars show that the anticrossing gap is small. On the contrary, far-infrared magnetospectroscopy reveals a fine structure of the strong absorption lines, corresponding to the α and β transitions from the zero-mode LLs [6,7]. Analysis of this fine structure in the vicinity of B_c within the Dirac-like model including BIA and IIA gives Δ~5 meV for the joint effect. Thus, the controversial experimental values of the anticrossing gap obtained in magnetotransport and magnetospectroscopy produce a lot of speculations on the actual strength of BIA and IIA in HgTe QWs.

In my talk, I will present recent experimental results obtained by far-infrared magnetospectroscopy in Montpellier. Particularly, we focused on the evolution of optical transitions from the zero-mode LLs in inverted HgTe QWs at different electron concentration varied by persistent photoconductivity effect. By fitting the difference in the transition energies in the vicinity of critical magnetic field B_c with an analytical expression including BIA and IIA, we extract the band-gap and anticrossing gap Δ from our experimental data. Unexpected strong dependence of the band-gap and Δ on the electron concentration clearly evidences that electron-electron interaction affects the LL transitions beyond the single-particle picture. This paves the way towards clarifying the key reason for controversial conclusions on the strength of BIA and IIA in HgTe QWs obtained by magnetotransport and magnetospectroscopy.

[1] M. Konig et al., Science **318**, 766 (2007).

[2] C. Liu et al., Phys. Rev. Lett. **100**, 236601 (2008).

[3] M. V. Durnev and S. A. Tarasenko, Phys. Rev. B **93**, 075434 (2016).

[4] B. Buttner et al., Nat. Phys. **7**, 418 (2011).

[5] A. M. Kadykov et al., Phys. Rev. Lett. **120**, 086401 (2018).
[6] M. Orlita et al., Phys. Rev. B **83**, 115307 (2011).
[7] M. Zholudev et al., Phys. Rev. B **86**, 205420 (2012).

Author index

Giacomo G.	Fri-C-3
Gianesello F.	Thu-A-2
Gidel G.	Thu-A-2
Gloria D.	Thu-A-2
Goltsman G.	Fri-D-2
Gorbenko I. V.	Thu-A-4
Grabecki G.	Fri-E-3, Fri-E-5
Guillet J.P.	Wed-G-2, Thu-B-2
Guiramand L.	Fri-C-2
Herault E.	Tue-B-1
Hindle F.	Wed-E-3, Thu-B-3
Huang Z.	Thu-A-3
Ikamas K.	Thu-B-4
Ikusov D. G.	Sat-F-2
Jeannin M.	Wed-E-1
Jokubauskis D.	Thu-B-5
Jorudas J.	Tue-B-5
Jouault B.	Fri-E-2
Kablukova N. S.	Thu-B-6
Kachorovskii V. Yu.	Thu-A-4
Karpisz T.	Wed-F-5
Kašalynas I.	Thu-B-5, Fri-D-4
Kazakov A.	Fri-E-3
Kazakov A. S.	Sat-F-3
Khodzitsky M. K.	Thu-B-6
Khokhlov D. R.	Sat-F-3
Knap W.	Tue-B-4, Tue-B-5, Wed-C-1, Thu-A-4, Fri-D-4, Fri-E-2, Fri-E-3, Fri-E-5, Sat-F-4
Kołaciński C.	Tue-A-2, Tue-A-4
Komorowski P.	Wed-D-4
Kopyt P.	Tue-A-4, Wed-F-5
Krawczyk P.	Wed-C-3
Kret S.	Fri-E-5
Krishtopenko S. S.	Tue-B-3, Fri-E-2, Fri-E-3, Fri-E-5
Krozer V.	Fri-C-3
Krupka J.	Wed-F-5
Lacombe E.	Thu-A-2
Lampin J-F.	Wed-F-2, Thu-A-2, Thu-B-3
Larcher F.	Fri-C-3
Latzel P.	Thu-A-2
Lepilliet S.	Tue-A-5, Wed-F-2
Lesueur J.	Wed-F-4
Li H.	Wed-F-2
Li L.	Wed-E-1
Li Z.	Wed-F-2, Thu-A-3
Linfield E.	Wed-E-1
Lisauskas A.	Thu-B-4
Locquet A.	Wed-G-3
Lorkiewicz J.	Wed-C-3
Luxey C.	Thu-A-2
Łusakowski J.	Tue-B-2, Sat-F-4
Łusakowski J.	Sat-F-4
Majewicz M.	Fri-E-3
Makarova E. S.	Thu-B-6
Mangeney J.	Wed-C-4
Mantion S.	Fri-E-2
Marczewski J.	Tue-A-4
Martin-Drumel M.-A.	Wed-E-3, Thu-B-3
Michailov N. N.	Tue-B-3, Fri-E-2, Fri-E-3, Fri-E-5, Sat-F-2, Sat-F-3
Minkevičius L.	Thu-B-5
Monroy I. T.	Tue-A-1
Moreno-Oyervides A.	Fri-C-3
Morozov S. V.	Fri-E-2

Mounaix P.	Wed-G-2, Thu-B-2
Mouret G.	Wed-E-3, Thu-B-3
Nanot S.	Fri-E-2
Nietubyć R.	Wed-C-3
Novotelnova A. V.	Thu-B-6
Obrebski D.	Tue-A-4
Orlita M.	Fri-E-4
Orlov S.	Thu-B-5
Pagies A.	Wed-F-1
Pałka N.	Wed-C-3, Wed-D-5
Pan M.	Wed-G-2, Thu-B-2
Perraud J.B.	Wed-G-2, Thu-B-2
Peytavit E.	Thu-A-2
Pirali O.	Wed-E-3, Thu-B-3
Pitchappa P.	Wed-F-4
Prystawko P.	Tue-B-4, Tue-B-5, Fri-D-4
Przybytek J.	Fri-E-3
Recoba-Pawlowski E.	Wed-F-4
Remesnik V. G.	Sat-F-2
Roskos H.	Thu-B-1
Roux M.	Wed-G-2, Thu-B-2
Roy P.	Wed-E-3
Ruffenach S.	Fri-E-2
Rumyantsev S.	Tue-B-2, Tue-B-4, Tue-B-5, Fri-D-4
Ryabova L. I.	Sat-F-3
Sai P.	Tue-B-4, Tue-B-5, Fri-D-4
Sakowicz M.	Tue-B-5, Tue-B-4, Fri-D-4
Salski B.	Wed-F-5
Samnouni M.	Tue-A-5
Sekutowicz J.	Wed-C-3
Shvets V. A.	Sat-F-2
Siemion A.	Wed-D-4

Singh R.	Wed-F-4
Sirtori C.	Wed-E-1
Skovsen E.	Fri-C-2
Sobotka P.	Wed-D-4
Solovjovas A.	Thu-B-4
Sørensen Ch. B.	Fri-C-2
Srivastava Y.	Wed-F-4
Stake J.	Fri-D-3
Staszczak M.	Wed-C-3
Story T.	Wed-C-2
Sun Z.	Fri-D-3
Surma M.	Wed-D-4
Svintsov D.	Fri-D-2
Sypek M.	Wed-D-4
Szamota- Leandersson K.	Wed-C-3
Szewiński J.	Wed-C-3
Szoła M.	Sat-F-4
Szriftgiser P.	Thu-A-2
Teppe F.	Tue-B-3, Wed-D-1, Fri-E-2, Fri-E-3, Fri-E-5, Sat-F-5
Todorov Y.	Wed-E-1
Tondusson M.	Fri-C-2
Torres J.	Wed-D-2
Tukmakova A. S.	Thu-B-6
Turut J.	Wed-E-3, Wed-F-1
Ulysse C.	Wed-F-4
Urbas A.	Thu-B-5
Uzhakov I. N.	Sat-F-2
Valušis G.	Thu-B-5
Vasanelli A.	Wed-E-1
Vorobiev A.	Fri-D-3
Walczakowski M.	Wed-D-4
Wallart X.	Tue-A-5, Thu-A-2

Wan W.	Wed-F-2
Wang X.	Thu-A-3
Wichmann N.	Tue-A-5
Wiśniewski A.	Wed-C-2
Wojciechowski M.	Tue-A-3
Wojtowicz T.	Wed-C-2
Wróbel J.	Fri-E-3
Yahniuk I.	Tue-B-2, Fri-E-3, Fri-E-5
Yan W.	Thu-A-3
Yang F.	Thu-A-3
Yashchyshyn Y.	Wed-D-3
Yavorskiy D.	Sat-F-4
Zagrajek P.	Tue-A-4, Wed-C-3
Zaitsev A. D.	Thu-B-6
Zaknoune M.	Thu-A-2
Zégaoui M.	Thu-A-2
Zhai M.	Wed-G-3
Zhang B.	Thu-A-3